

INVESTIGATION OF PRODUCTIVITY OF HEAVY OIL CARBONATE  
RESERVOIRS AND OIL SHALES USING ELECTRICAL HEATING METHODS

A THESIS SUBMITTED TO  
THE GRADUATE SCHOOL OF NATURAL AND APPLIED SCIENCES  
OF  
MIDDLE EAST TECHNICAL UNIVERSITY

BY

BERNA HASÇAKIR

IN PARTIAL FULFILLMENT OF THE REQUIREMENTS  
FOR  
THE DEGREE OF DOCTOR OF PHILOSOPHY  
IN  
PETROLEUM AND NATURAL GAS ENGINEERING

AUGUST 2008

Approval of the thesis:

**INVESTIGATION OF PRODUCTIVITY OF HEAVY OIL CARBONATE  
RESERVOIRS AND OIL SHALES USING ELECTRICAL HEATING METHODS**

submitted by **BERNA HASÇAKIR** in partial fulfillment of the requirements for the degree of **Doctor of Philosophy in Petroleum and Natural Gas Engineering Department, Middle East Technical University** by,

Prof. Dr. Canan Özgen \_\_\_\_\_  
Dean, Graduate School of **Natural and Applied Sciences**

Prof. Dr. Mahmut Parlaktuna \_\_\_\_\_  
Head of Department, **Petroleum & Natural Gas Engineering**

Prof. Dr. Serhat Akın \_\_\_\_\_  
Supervisor, **Petroleum & Natural Gas Engineering Dept., METU**

**Examining Committee Members:**

Prof. Dr. Nurkan Karahanoğlu \_\_\_\_\_  
Geological Engineering Dept., METU

Prof. Dr. Serhat Akın \_\_\_\_\_  
Petroleum and Natural Gas Engineering Dept., METU

Prof. Dr. Birol Demiral \_\_\_\_\_  
Geoscience and Petroleum Engineering Dept., UTP

Prof. Dr. Mahmut Parlaktuna \_\_\_\_\_  
Petroleum and Natural Gas Engineering Dept., METU

Prof. Dr. Mustafa Verşan Kök \_\_\_\_\_  
Petroleum and Natural Gas Engineering Dept., METU

**Date: 29.08.2008**

**I hereby declare that all information in this document has been obtained and presented in accordance with academic rules and ethical conduct. I also declare that, as required by these rules and conduct, I have fully cited and referenced all material and results that are not original to this work.**

Name, Last name: Berna Haşçakır

Signature:

## ABSTRACT

### INVESTIGATION OF PRODUCTIVITY OF HEAVY OIL CARBONATE RESERVOIRS AND OIL SHALES USING ELECTRICAL HEATING METHODS

Hasçakır, Berna

Ph.D., Department of Petroleum and Natural Gas Engineering

Supervisor: Prof. Dr. Serhat Akin

August 2008, 229 pages

The recovery characteristics of Bolu-Himmetođlu, Bolu-Hatıldıđ, Kütahya-Seyitömer, and Niđe-Ulukıřla oil shale samples and Batı Raman, Çamurlu, and Garzan crude oil samples were tested experimentally using retort and microwave heating techniques. Many parameters like heating time, porosity, water saturation were studied. To enhance the efficiency of the processes three different iron powders (i.e.; Fe, Fe<sub>2</sub>O<sub>3</sub>, and FeCl<sub>3</sub>) were added to the samples and the doses of the iron powders were optimized. While crude oil viscosities were measured to explain the fluid rheologies, since it is impossible to measure the shale oil viscosity at the laboratory conditions due to its very high viscosity, shale oil viscosities were obtained numerically by using the electrical heating option of a reservoir simulator (CMG, STARS 2007) by matching between the laboratory and numerical oil production and temperature distribution results. Then the field scale simulations for retorting of oil shale and crude oil fields were conducted. Since the microwave heating cannot be simulated by CMG, STARS, microwave heating was modeled analytically. In order to explain the feasibility of heating processes, an economic evaluation was carried out. The experimental, numerical, and analytical results show that field scale oil recovery from oil shales and heavy crude oils by electrical and electromagnetic heating could be economically viable.

While microwave heating is advantageous from an operational point of view, retorting is advantageous if the technical feasibility of the study is considered.

Keywords: Oil Shale, Crude Oil, Thermal EOR Methods, Crude Oil Rheology, Numerical and Analytical Models.

## ÖZ

### AĞIR PETROL İÇEREN KARBONAT REZERVUARLARININ VE BITÜMLÜ ŞİSTLERİN ELEKTRİKSEL ISITMA YÖNTEMLERİYLE ÜRETİLEBİLİRLİĞİNİN ARAŞTIRILMASI

Hasçakır, Berna

Doktora, Petrol ve Doğal Gaz Mühendisliği Bölümü

Tez Yöneticisi: Prof. Dr. Serhat Akin

Ağustos 2008, 229 sayfa

Retort ve mikrodalga teknikleri kullanılarak, Bolu-Himmetoğlu, Bolu-Hatıldağ, Kütahya-Seyitömer, ve Niğde-Ulukışla bitümlü şist örneklerinin ve Batı Raman, Çamurlu, ve Garzan petrol örneklerinin üretilebilirliği, retort ve mikrodalga ısıtma teknikleri kullanılarak, deneysel olarak test edilmiştir. Isıtma süresi, gözeneklilik, su doygunluğu gibi birçok parametre çalışılmıştır. Süreçlerin verimliliğini artırma amacıyla üç değişik demir tozu (Fe, Fe<sub>2</sub>O<sub>3</sub>, and FeCl<sub>3</sub>) örneklere eklenmiş ve demir tozlarının dozları optimize edilmiştir. Ham petrol numunelerinin akışkanlıkları, akış özelliklerini belirleyebilmek için ölçülebilirken, bitümlü şisten elde edilen petrolün viskozitesinin, çok ağır özellik taşmasından dolayı, laboratuvar koşullarında ölçülmesi mümkün olmadığından, viskozite değerleri bir sayısal rezervuar modeli olan CMG, STARS 2007 modelinin elektiriksel ısıtma opsiyonu kullanılarak, petrol üretim ve sıcaklık dağılım sonuçlarını laboratuvar ve numerik model değerleri ile karşılaştırarak elde edilmiştir. Daha sonra bitümlü şist ve ham petrol sahalarının retort işlemi, saha ölçeğinde modellenmiştir. Mikrodalga ile ısıtma, CMG, STARS modeli ile modellenemediğinden, mikrodalga ısıtma analitik olarak modellenmiştir. Isıtma süreçlerinin uygulanabilirliğini ortaya koyabilmek için, çalışmanın ekonomik değerlendirilmesi yapılmıştır. Deneysel, sayısal ve analitik sonuçlar, bitümlü şist ve ham petrolden, petrol kurtarımının,

elektrik ve elektromagnetik ısıtma yöntemleri ile ekonomik olarak uygulanabilirliğini göstermektedir. İşletimsel bakış açısıyla, mikrodalga ısıtma avantajlı iken, retort teknik olarak uygulanabilirliği düşünüldüğünde avantajlıdır.

Anahtar Kelimeler: Bitümlü Şist, Ham Petrol, Termal İleri Petrol Kurtarım Yöntemleri, Ham Petrol Reolojisi, Sayısal ve Analitik Modeller.

*To my nephews;  
Umut A. Kahraman  
and  
Yağız Sancaklı*

## ACKNOWLEDGEMENTS

I would like to express my sincere thanks to my supervisor Prof. Dr. Serhat AKIN for his scientific and academic guidance, suggestions, comments, encouragement, motivation and help during the course of this research. Also, I am thankful to him because of his kindly attitude not only related with the thesis but also in every occasion throughout this study.

I also would like to thank Prof. Dr. Tayfun BABADAĞLI for his respect to me even before knowing me. His comments, friendly attitude and the opportunities he gave, provided a great support during my study at University of Alberta.

I am also thankful to Assist. Prof. Dr. Evren ÖZBAYOĞLU his guidance during the interpretation of the fluid rheologies.

I am also thankful to Dr. Kemal BEHLÜLGİL for sharing his knowledge about the usage of Haake Viscometer.

I would like to thank to Naci DOGRU for his help and contribution during the experiments and in the construction of the experimental set-up.

I express my deepest thanks to Songül APARI, Yılmaz ERTAŞ, Hatice BOLATA, and Gülsün BEHLÜLGİL to behave very sincere. The conversation made while drinking coffee won't be forgotten.

I also would like to thank my friends Dr. Nuray ATEŞ, Ayten KOÇ, Tülay AKBEY, Tülin İNKAYA, Betül YAYAN for always being with me, for their encouragement, and friendship especially the last periods of my PhD.

I would like to express my thanks to Ufuk ATILMIŞ, İsa ÖZTAŞ, and Chantsalmaa DALKHAA who help me overcome the problems about computer.

İnönü University is gratefully acknowledged for providing opportunity to me to conduct my PhD at METU by OYP program.

Prof. Dr. Kemal KARTAL, Prof. Dr. Fatih HİLMİOĞLU and Research Assistant Hasan DUDU are kindly acknowledged for their guidance to help me get the required permissions for the postdoctoral studies at Stanford University.

The Scientific and Research Council of Turkey (TUBITAK) is kindly acknowledged for the project 104M 181 and for the financial support during the studies conducted at the University of Alberta.

I express my deepest thanks to Günay BOZADA, Muzaffer BOZADA, S. Ceren BOZADA, İ. Can BOZADA, and Zerrin ALP who help me overcome any kind of problem whenever I need.

I wish to express my greatest thanks to my family, especially my mother Zühal HASÇAKIR, who helps me create my self-confidence.

I wish to express my deepest gratified to Mustafa Kemal ATATÜRK who is the reason of all of my belongings.

## TABLE OF CONTENTS

PLAGIARISM.....	iii
ABSTRACT .....	iv
ÖZ .....	vi
ACKNOWLEDGEMENTS .....	ix
TABLE OF CONTENTS.....	xi
LIST OF TABLES .....	xiii
LIST OF FIGURES .....	xv
NOMENCLATURE.....	xx
CHAPTER	
1. INTRODUCTION .....	1
2. LITERATURE REVIEW .....	4
2.1. Enhanced Oil Recovery Methods.....	4
2.1.1. Current Status of EOR .....	5
2.1.2. EOR Methods .....	7
2.2. Unconventional Fossil Fuel Sources .....	16
2.2.1. Oil Shales.....	16
2.2.2. Heavy Oil .....	30
3. STATEMENT OF THE PROBLEM.....	39
4. MATERIALS & METHODS .....	41
4.1. Oil shale and crude oil samples.....	41
4.2. Experimental Setup and Procedure.....	43
4.2.1. Viscosity Experiments .....	43
4.2.2. Retort Experiments .....	44
4.2.3. Microwave Experiment .....	46
4.2.4. Enhancement of the Processes.....	47
4.2.5. Numerical Simulation .....	47
5. THEORY.....	50
5.1. Heat Transfer Mechanisms .....	50
5.2. Numerical Simulation .....	53
5.1.1. Current Continuity Equation .....	54

5.1.2. Heat Generation from Ohmic Losses .....	56
5.1.3. Mathematical Model Used by STARS .....	56
5.3. Catalytic Cracking .....	61
5.2.1. Catalysis and reaction energetic .....	64
5.2.2. Factors that affect catalytic rates.....	66
5.2.3. Catalysts Examples.....	71
5.4. Fluid Rheology .....	73
5.3.1. Definitions .....	73
5.3.2. Fluid Rheology Models.....	76
6. RESULTS AND DISCUSSION.....	80
6.1. Rheology of the crude oils.....	80
6.1.1. Determination of rheological parameters for crude oil samples .....	80
6.2. Microwave Experiments .....	92
6.2.1. Effect of porosity, water saturation, wettability and permeability .....	93
6.2.2. Recovery of oil shales under microwave irradiation.....	102
6.3. Retort Experiments .....	109
6.4. Numerical Simulation .....	114
6.4.1. Numerical Simulation Retorting of Oil Shales .....	115
6.4.2. Numerical Simulation Retorting of Crude Oils .....	126
6.5. Analytical Model.....	132
6.5.1. Modeling of Crude Oil Samples.....	132
6.5.2. Modeling of Oil Shale Samples .....	136
6.6. Economical Evaluation of the Study .....	137
6.6.1. Economical evaluation of microwave heating for crude oil samples.....	137
6.6.2. Economical evaluation of retort technique .....	139
7. CONCLUSIONS .....	142
8. RECOMMENDATIONS.....	146
REFERENCES .....	147
APPENDIES	
A. FLUID RHEOLOGY.....	156
B. TEMPERATURE DISTRIBUTIONS AND GAS EMISSIONS.....	190
C. NUMERICAL SIMULATIONS .....	202
D. ANALYTICAL MODEL.....	210
E. ECONOMIC EVALUATION OF THE STUDY .....	224

## LIST OF TABLES

### TABLES

Table 2.1 General property of kerogen types .....	18
Table 2.2 Properties of Some Important Oil Shale Deposits .....	23
Table 2.3 Main oil shale reserves in Turkey .....	24
Table 2.4 Characteristics of the Major Oil Shale Deposits in Turkey .....	25
Table 2.5 Field characterization of heavy oil reserves in Turkey .....	34
Table 4.1 Oil shale properties used in this study .....	41
Table 4.2 Reservoir properties of crude oils used in this thesis .....	42
Table 5.1 LH and ER models comparison .....	70
Table 5.2 Best catalysts for some reactions .....	72
Table 6.1 Rheological parameters for Batı Raman crude oil .....	82
Table 6.2 Rheological parameters for Çamurlu crude oil.....	85
Table 6.3 Rheological parameters for Garzan crude oil .....	87
Table 6.4 Optimization of microwave heating period .....	90
Table 6.5 Effect of microwave on the rheology of crude oil samples at 70 °C ....	91
Table 6.6 Porosity effect of microwave .....	94
Table 6.7 Permeability variations with mesh size .....	95
Table 6.8 Wettability effect under the microwave irradiation .....	96
Table 6.9 Microwave experiment summary for Himmetoğlu oil shale.....	104
Table 6.10 Microwave experiment summary for Hatıldağ oil shale.....	105
Table 6.11 Microwave experiment summary for Seyitömer oil shale.....	107
Table 6.12 Microwave experiment summary for Niğde-Ulukışla oil shale.....	109
Table 6.13 Determination of optimum heating period for retort experiments ...	110
Table 6.14 Summary for gas emissions and productions for oil shale samples	113
Table 6.15 Density and API gravity of oil shales .....	114
Table 6.16 Data used for the simulation of laboratory and field cases .....	118
Table 6.17 Analytical model results for Batı Raman Crude oil.....	133
Table 6.18 Analytical model results for Çamurlu Crude oil .....	133

Table 6.19 Analytical model results for Garzan Crude oil.....	134
Table 6.20 Optimized Electric Field Absorption Coefficient Values .	135
Table 6.21 Analytical model results for oil shale samples .....	136
Table 6.22 Economic evaluation of the study.....	140
Table E 1 Economic evaluation of microwave heating for water wet condition .	224
Table E 2 Economic Evaluation of microwave heating.....	225

## LIST OF FIGURES

### FIGURES

Figure 2.1 EOR target for different hydrocarbons .....	5
Figure 2.2 Current EOR production from contributing countries .....	6
Figure 2.3 Major EOR projects and production worldwide .....	6
Figure 2.5 Schematic Form of In-Situ Oil Retorting from Oil Shales .....	11
Figure 2.6 Differences in the temperature-time profiles for conventional and microwave dielectric heating .....	12
Figure 2.7 General compositions of oil shales .....	17
Figure 2.8 Location of main oil shale reserves .....	25
Figure 2.9 World oil sands and heavy oil resources, in billions of cubic meters..	32
Figure 2.10 Location of crude oil fields used in this study. ....	35
Figure 4.1 Haake viscometer .....	44
Figure 4.2 Retort set-up.....	45
Figure 4.3 Microwave set-up.....	46
Figure 4.4 Scales used for the simulation of laboratory results and fields .....	48
Figure 5.1 Diagrammatic example of the catalytic cracking of petroleum hydrocarbons .....	62
Figure 5.2 Catalytic cycle for conversion of A and B into C .....	64
Figure 5.3 Generic potential energy diagram .....	65
Figure 5.4 Langmuir-Hinshelwood mechanism for unimolecular reactions .....	68
Figure 5.5 LH model for bimolecular reaction .....	69
Figure 5.6 ER model for bimolecular reaction [94]. ....	70
Figure 5.7 Comparison of Eley-Rideal and Langmuir-Hinshelwood models [94].	71
Figure 5.8 Basic shear diagram .....	75
Figure 6.3 Periodic Heating Results .....	101
Figure 6.4 Optimization of iron powders for Himmetoğlu oil shale.....	103
Figure 6.5 Optimization of iron powders for Hatıldağ oil shale.....	105
Figure 6.6 Optimization of iron powders for Seyitömer oil shale.....	107

Figure 6.7 Optimization of iron powders for Niğde-Ulukışla oil shale.....	108
Figure 6.8 Temperature profile for the optimum operation periods .....	111
Figure 6.9 Retort experiment results for oil shale samples .....	112
Figure 6.10 Grid sizes used in simulations .....	115
Figure 6.11 Water-oil relative permeability curves used in simulation for oil shale samples .....	117
Figure 6.12 Gas-liquid relative permeability curves used in simulation for oil shale samples .....	117
Figure 6.13 Temperature match for all oil shales .....	119
Figure 6.14 Production match for all oil shales .....	119
Figure 6.15 Viscosity variations of all shale oils .....	120
Figure 6.16 Temperature matches for all oil shale after the addition of optimum doses of iron powders .....	121
Figure 6.17 Production matches for all oil shale after the addition of optimum doses of iron powders .....	121
Figure 6.18 Viscosity variations for all oil shale after the addition of optimum doses of iron powders .....	122
Figure 6.19 Simulation results for Himmetoğlu (OS1) (field case).....	123
Figure 6.20 Simulation results for Hatıldığ (OS2) (field case).....	124
Figure 6. 21 Simulation results for Seyitömer (OS3) (field case).....	125
Figure 6. 22 Simulation results for Ulukışla (OS4) (field case) .....	125
Figure 6.23 Oil viscosities for Batı Raman crude oil.....	127
Figure 6.24 Oil viscosities for Çamurlu crude oil .....	127
Figure 6.25 Oil viscosities for Garzan crude oil.....	128
Figure 6.26 Water-Oil relative permeability curves used in the simulation for heavy oil samples .....	129
Figure 6.27 Simulation Results for B. Raman Crude Oil.....	130
Figure 6.28 Simulation Results for Camurlu Crude Oil.....	130
Figure 6.29 Simulation Results for Garzan Crude Oil.....	131
Figure 6.30 Economic Evaluation of microwave heating for crude oil samples and water wet conditions .....	138
Figure 6.31 Economic Evaluation of microwave heating for crude oil samples and water wet conditions .....	138

Figure 6. 32 Economic Evaluation of microwave heating for crude oil samples and mixed wet conditions.....	139
Figure 6.33 Cumulative oil production results for the optimum operation conditions of oil shales.....	141
Figure A 1 Rheology of tap water for the correction of Haake viscometer.....	156
Figure A 2 Rheology of Dead Batı Raman Crude Oil.....	157
Figure A 3 Rheology of Batı Raman Crude oil after the addition of 0.1% Fe....	158
Figure A 4 Rheology of Batı Raman Crude oil after the addition of 0.5% Fe....	159
Figure A 5 Rheology of Batı Raman Crude oil after the addition of 1% Fe.....	160
Figure A 6 Rheology of Batı Raman Crude oil after the addition of 0.1% Fe <sub>2</sub> O <sub>3</sub>	161
Figure A 7 Rheology of Batı Raman Crude oil after the addition of 0.5% Fe <sub>2</sub> O <sub>3</sub>	162
Figure A 8 Rheology of Batı Raman Crude oil after the addition of 1 % Fe <sub>2</sub> O <sub>3</sub> .	163
Figure A 9 Rheology of Batı Raman Crude oil after the addition of 0.1% FeCl <sub>3</sub>	164
Figure A 10 Rheology of Batı Raman Crude oil after addition of 0.5% FeCl <sub>3</sub> ...	165
Figure A 11 Rheology of Batı Raman Crude oil after the addition of 1% FeCl <sub>3</sub> .	166
Figure A 12 Rheology of Dead Çamurlu Crude oil.....	167
Figure A 13 Rheology of Çamurlu Crude oil after the addition of 0.1% Fe.....	168
Figure A 14 Rheology of Çamurlu Crude oil after the addition of 0.5% Fe.....	169
Figure A 15 Rheology of Çamurlu Crude oil after the addition of 1% Fe.....	170
Figure A 16 Rheology of Çamurlu Crude oil after the addition of 0.1 % Fe <sub>2</sub> O <sub>3</sub> .	171
Figure A 17 Rheology of Çamurlu Crude oil after the addition of 0.5 % Fe <sub>2</sub> O <sub>3</sub> .	172
Figure A 18 Rheology of Çamurlu Crude oil after the addition of 1 % Fe <sub>2</sub> O <sub>3</sub> ....	173
Figure A 19 Rheology of Çamurlu Crude oil after the addition of 0.1 % FeCl <sub>3</sub> ..	174
Figure A 20 Rheology of Çamurlu Crude oil after the addition of 0.5 % FeCl <sub>3</sub> ..	175
Figure A 21 Rheology of Çamurlu Crude oil after the addition of 1 % FeCl <sub>3</sub> .....	176
Figure A 22 Rheology of Dead Garzan Crude oil.....	177
Figure A 23 Rheology of Garzan Crude oil after the addition of 0.1 % Fe.....	178
Figure A 24 Rheology of Garzan Crude oil after the addition of 0.5 % Fe.....	179
Figure A 25 Rheology of Garzan Crude oil after the addition of 1 % Fe.....	180
Figure A 26 Rheology of Garzan Crude oil after the addition of 0.1 % Fe <sub>2</sub> O <sub>3</sub> ...	181
Figure A 27 Rheology of Garzan Crude oil after the addition of 0.5 % Fe <sub>2</sub> O <sub>3</sub> ...	182
Figure A 28 Rheology of Garzan Crude oil after the addition of 1 % Fe <sub>2</sub> O <sub>3</sub> .....	183
Figure A 29 Rheology of Garzan Crude oil after the addition of 0.1 % FeCl <sub>3</sub> ....	184
Figure A 30 Rheology of Garzan Crude oil after the addition of 0.5 % FeCl <sub>3</sub> ....	185

Figure A 31 Rheology of Garzan Crude oil after the addition of 1 % FeCl <sub>3</sub> .....	186
Figure A 32 Rheology of Batı Raman Crude oil after microwave irradiation .....	187
Figure A 33 Rheology of Çamurlu Crude oil after microwave irradiation .....	188
Figure A 34 Rheology of Garzan Crude oil after microwave irradiation .....	189
Figure B 1 Temperature distribution of Himmetoglu Oil Shale.....	190
Figure B 2 Temperature distribution of Hatıldağ Oil Shale .....	191
Figure B 3 Temperature distribution of Seyitömer Oil Shale.....	191
Figure B 4 Temperature distribution of Ulukışla Oil Shale .....	192
Figure B 5 Gas emissions for Himmetoglu oil shale (OS1) after electromagnetic heating.....	194
Figure B 6 Gas emissions for Hatıldağ oil shale (OS2) after electromagnetic heating.....	195
Figure B 7 Gas emissions for Seyitömer oil shale (OS3) after electromagnetic heating.....	196
Figure B 8 Gas emissions for Ulukışla oil shale (OS4) after electromagnetic heating.....	197
Figure B 9 Temperature distribution for Himmetoğlu oil shale .....	198
Figure B 10 Temperature distribution for Hatıldağ oil shale.....	198
Figure B 11 Temperature distribution for Seyitömer oil shale.....	199
Figure B 12 Temperature distribution for Niğde-Ulukışla oil shale.....	199
Figure B 13 Gas emissions for Himmetoğlu oil shale .....	200
Figure B 14 Gas emissions for Hatıldağ oil shale.....	200
Figure B 15 Gas emissions for Seyitömer oil shale .....	201
Figure B 16 Gas emissions for Ulukışla oil shale .....	201
Figure C 1 Temperature distribution for Himmetoglu oil shale.....	202
Figure C 2 Temperature distribution for Himmetoglu oil shale + 0.1% Fe.....	203
Figure C 3 Temperature distribution for Hatıldağ oil shale .....	204
Figure C 4 Temperature distribution for Hatıldağ oil shale + 0.1 % Fe <sub>2</sub> O <sub>3</sub> .....	205
Figure C 5 Temperature distribution for Seyitömer oil shale.....	206
Figure C 6 Temperature distribution for Seyitömer oil shale +0.5 % Fe .....	207
Figure C 7 Temperature distribution for Niğde-Ulukışla oil shale.....	208
Figure C 8 Temperature distribution for Seyitömer oil shale + 0.1 % Fe <sub>2</sub> O <sub>3</sub> .....	209
Figure D 11 Analytical modeling results for Himmetoğlu oil shale .....	220
Figure D 12 Analytical modeling results for Hatıldağ oil shale.....	221

Figure D 13 Analytical modeling results for Seyitömeroil shale .....	222
Figure D 14 Analytical modeling results for Ulukışla oil shale .....	223

## NOMENCLATURE

### Roman Symbols

A	Diffusive Energy
B	Heat generation
A, B	Reactants, the concentration of a given A, B in mol/liter (molarity)
A, B, C	Continuous heating periods
C	Energy used in internal evaporation
$\dot{C}$	Represents the catalyst,
$c_i$	Concentration of component i
$c_s$	Sum of all the $c_i$ .
$c_p$	Specific heat of the medium at constant pressure, J/kg. K
$c_{pf}$	Specific heat capacity of the fluid phase
D	Rate of energy accumulation
$D_p$	Particle diameter, (m)
E	Convective energy flow
E	Magnitude of the electric field.
$\vec{E}$	Electric field
$E_a$	Activation energy (J/mol <sup>-1</sup> )
f	Microwave frequency,
h	Distance between the two parallel faces that are experiencing the shear
$h$	Height of a cylinder
$h_{fg, i}$	Latent heat of vaporization, J/kg,
I, II, III	Soaking periods
I	Experimental Studies Results.
II	Numerical Studies Results
k	Thermal conductivity, W/mK,
k (T)	Reaction rate coefficient or rate constant
k	Permeability (m <sup>2</sup> ).

K	Consistency index, Pa,s <sup>n</sup>
n	Flow behavior index, dimensionless
<i>n</i> and <i>m</i>	Reaction orders
<i>P</i>	Electromagnetic dissipated power per unit of volume
<i>P<sub>d</sub></i>	Power density
<i>P(r)</i>	Total power radiated across the radius <i>r</i>
<i>P<sub>res</sub></i>	Reservoir pressure
<i>q</i>	Electrical source term
<i>q</i> *	Rate of energy generation per unit volume, W/m <sup>3</sup>
R	Universal gas constant (8.314 x 10 <sup>-3</sup> kJ mol <sup>-1</sup> K <sup>-1</sup> )
<i>R<sub>i</sub></i>	Resistance
<i>S<sub>w</sub></i>	Water saturation
<i>S<sub>wi</sub></i>	Initial Water Saturation
<i>S<sub>o</sub></i>	Oil saturation
<i>S<sub>or</sub></i>	Residual oil saturation
T	Temperature, °C
<i>T<sub>res</sub></i>	Reservoir temperature
<i>u</i>	Velocity, m/s,
<i>u, v</i>	Velocity of the fluid along the fluid boundary, m/s
$\vec{v}_f$	Superficial velocity of the fluid phase
Y	Height of the fluid boundary.
<i>w<sub>i</sub></i>	Water mole fraction
1	Dead Crude Oil.
2	Crude oil containing 0.5% Fe

### Greek Symbols

$\epsilon_0$	Permittivity of free space (8.85×10 <sup>-12</sup> F/m),
$\epsilon''$	Relative dielectric loss factor
$\epsilon'$	Dielectric constant
tan $\delta$	Loss tangent
$\alpha$	Thermal diffusivity, m <sup>2</sup> /s
$\alpha$	Power absorption coefficient or attenuation constant (cm <sup>-1</sup> )

$\rho$	Mass density of the medium, kg/m <sup>3</sup> ,
$\gamma$	Specific gravity
$\dot{\gamma}$	Shear Rate, s <sup>-1</sup>
$\mu$	Kinematic viscosity
$\mu$	Permeability (H/meter)
$\lambda_{\chi}$	Thermal conductivity of the medium
$\rho_f$	Density of the fluid phase
$\sigma$	Effective conductivity of the medium, conductivity (mho/meter)
$\sigma_{w,p}(T)$	Electrical conductivity for water phase,
$\sigma_{o,p}(T)$	Electrical conductivity for oil phase,
$\sigma_{s,p}(T)$	Electrical conductivity for solid phase and
$\sigma_{r,p}(T)$	Electrical conductivity for rock/matrix
$\sigma_{w,i,p}(T)$	Electrical conductivity of aqueous component i.
$\sigma_{s,i,p}(T)$	Electrical conductivity of solid component I
$\sigma_I$	Bulk conductivity
$\sigma_{oc}=(K_{oc})^2$	Casson yield stress, Pa
$\sigma_o$	Yield Stress, Pa
$\Phi(r)$	Power density (watts/cm <sup>2</sup> )
$\phi$	Porosity
$\phi_f$	Fluid porosity
$\phi_v$	Void porosity
$\eta, \eta_a$	Dynamic viscosity of the fluid, apparent viscosity, Pa.s
$\eta_{ca}=(K_c)^2$	Casson viscosity, Pa.s
$\eta'$	Bingham Plastic viscosity, Pa.s
$\eta_{\infty}$	Infinite shear viscosity
$\omega$	Angular frequency ( $2\pi$ x frequency).
$\psi$	Electric potential

### Abbreviations

EOR	Enhanced Oil Recovery
CSS	Cyclic Steam Stimulation

SAGD	Steam Assisted Gravity Drainage
SAGP	Steam and Gas Push
THAI	Toe-To-Heel Air Injection
MEOR	Microbial EOR
OOIP	Original Oil in Place
H/C	Hydrogen / Carbon ratio
O/C	Oxygen / Carbon ratio
OC	Organic Carbon
OY	Oil Yield
EGOS	Economic Grade Oil Shale
FWS	Formation water salinity
L	Limestone
DL	Dolomitic Limestone
GOR	Gas Oil Ratio
RTC	Rock Thermal Conductivity
RHC	Rock Heat Capacity
BHP	Bottom Hole Pressure
CMG	Computer Modeling Group
STARS	Steam, Thermal, and Advanced Processes Reservoir Simulator
LH	Langmuir-Hinshelwood mechanism
ER	Eley-Rideal mechanism
RDS	Rate Determining Step
WW	Water Wet
OW	Oil Wet
MW	Mixed Wet, Molecular Weight
TEDAS	Turkish Electric Distribution Incorporated Company
GC-MS	Gas Chromatography-Mass Spectrometry
OS1	Oil Shale 1- Himmetoğlu
OS2	Oil Shale 2- Hatıldağ
OS3	Oil Shale 3- Seyitömer
OS4	Oil Shale 4- Ulukışla

## CHAPTER 1

### INTRODUCTION

Increased levels of human comfort generally encourage increasing the dependence on external energy sources. Therefore, energy development needs the ongoing effort to provide sufficient primary energy sources and secondary energy forms to power the world economy. It involves both installation of established technologies and research and development to create new energy-related technologies [1, 2].

Since the beginning of the industrial revolution, the worldwide energy consumption has been growing steadily. In 1890 the consumption of fossil fuels roughly equaled the amount of biomass fuel burned by households and industry. In 1900, global energy consumption equaled 0.7 TW ( $0.7 \times 10^{12}$  watts) [3]. In 2005, total worldwide energy consumption was 500 EJ (=  $5 \times 10^{20}$  J) (or 138,900 TWh) with 86.5% derived from the combustion of fossil fuels. This is equivalent to an average energy consumption rate of 15 TW (=  $1.5 \times 10^{13}$  W) [3].

As Turkey is a developing country, the need for energy is much higher than the developed countries, so, the rapid growth of energy consumption is predicted to continue for the next 15 years. The national conventional energy sources of Turkey cover 51% of the energy need for Turkey and remaining part is provided by importing. Because the oil and natural gas reserves in Turkey are of minor scale, the big portion of the importing energy belongs to petroleum with 80% [4, 5]. Oil shale and heavy oil resources are the second largest fossil fuel potential of Turkey after coal [6].

Oil shale is a general term used for the fine-grained sedimentary rocks that yield significant amounts of oil through pyrolysis and the oil has API gravity between 10 to 25 is defined as heavy oil [7, 8]. It is predicted that there are 1.6 billion tons

oil shale reserves and 30 oil fields produced heavy oil in Turkey [9, 10]., it is important to investigate alternative fossil fuel reserves which become economically reasonable because of the strong and steadily increase need for petroleum and in order to reduce the dependency to the energy exporting countries [11].

In order to produce oil from these resources, oil viscosity reduction should be accomplished. This can be best achieved by heating these resources up to 500°C which is known as the pyrolysis temperature [8, 12]. According to the characteristics of oil shale resources, oil retorting can be said as the most effective method for the recovery of oil from oil shale [13]. However, oil retorting can be also used for the recovery of heavy oil [8, 14]. Electromagnetic heating method is also used as a new and an alternative method for the recovery of unconventional reserves due to low processing times [15]. Microwave irradiation has been proposed to reduce the viscosity of heavy oil and for the recovery of oil shales and oil sands [16, 17].

To enhance the efficiency of the processes some chemicals can be used, so while the oil production is increased, also, the process time can be decreased. Some metallic additives are used for this purpose by considering the thermal and catalytic properties of these additives. Because of the composition of the fossil fuels, various crude oils are affected differently by different additives [15].

Thus, in this study, the recovery characteristics of four different oil shales and three different crude oil samples were tested experimentally by using retort and microwave techniques. In order to enhance the oil production by reducing oil viscosity and achieving the effective temperature distribution, three different iron powders (i.e.; Fe, Fe<sub>2</sub>O<sub>3</sub>, and FeCl<sub>3</sub>) and their three different doses (i.e.; 0.1 wt%, 0.5 wt%, and 1 wt%) were used. The retort experimental results were simulated for oil shale samples by using electrical heating option of a commercial reservoir simulator; STARS (Steam Thermal and Advanced Processes Reservoir Simulator) (CMG, 2007), coupling with optimization of parameters such as viscosity-temperature variation, molecular weight, and relative permeabilities of the oil shales needed in the simulation of the oil recovery from oil shales by

matching temperature and oil production. The accuracy of the simulation results, however, strongly depends on these parameters. These parameters are highly difficult to obtain (or not practically measurable) at the laboratory conditions, unlike conventional reservoirs. Experimental verifications and supports are critical in this regard and a new approach in the field scale simulation of the process based on the lab scale modeling of the process experimentally and numerically was introduced. This would provide realistic data needed for simulation and therefore, increase the accuracy of modeling studies. The same parameters apart from viscosity variations with temperature, which were measured experimentally, are easy to obtain by using literature data for crude oil samples.

Finally, field scale application of electrical heating was simulated for both oil shale and crude oil samples and a technical and economic evaluation of the applicability of the method was presented.

## CHAPTER 2

### LITERATURE REVIEW

#### 2.1. Enhanced Oil Recovery Methods

According to American Petroleum Institute, approximately two-thirds of the oil discovered will remain in an average reservoir after primary and secondary production. This inefficiency of oil recovery processes has long been known and the knowledge has stimulated laboratory and field testing of new processes for more than 50 years. Processes that inject fluids other than natural gas and water to augment a reservoir's ability to produce oil have been designated "improved," "tertiary," and "enhanced" oil recovery processes. The term used in this assessment is enhanced oil recovery (EOR) [18].

The target of EOR varies considerably for different types of hydrocarbons. Figure 2.1 shows the fluid saturations and the target of EOR for typical light and heavy oil reservoirs and tar sands. For light oil reservoirs, EOR is usually applicable after secondary recovery operations, and the EOR target is ~45% original oil in place (OOIP). Heavy oils and tar sands respond poorly to primary and secondary recovery methods, and the bulk of the production from such reservoirs come from EOR methods [19].

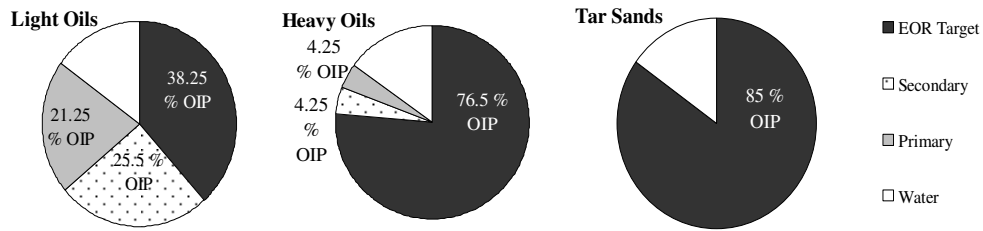


Figure 2.1 EOR target for different hydrocarbons [19]

EOR implies a reduction in oil saturation below the residual oil saturation ( $S_{or}$ ). Recovery of oils retained due to capillary forces (after a waterflood in light oil reservoirs), and oils that are immobile or nearly immobile due to high viscosity (heavy oils and tar sands) can be achieved only by lowering the oil saturation below  $S_{or}$ . Miscible processes, chemical floods and steam based methods are effective in reducing residual oil saturation [19].

### 2.1.1. Current Status of EOR

The total world oil production today (including condensate and natural gas liquids) is 84.5 million bbl/day. EOR production worldwide is about  $2.5 \times 10^6$  bbl/day, and almost all of it comes from USA, Mexico, Venezuela, Canada, Indonesia and China, as seen in Figure 2.2. Figure 2.3 shows the breakdown of the production from the contributing countries [19].

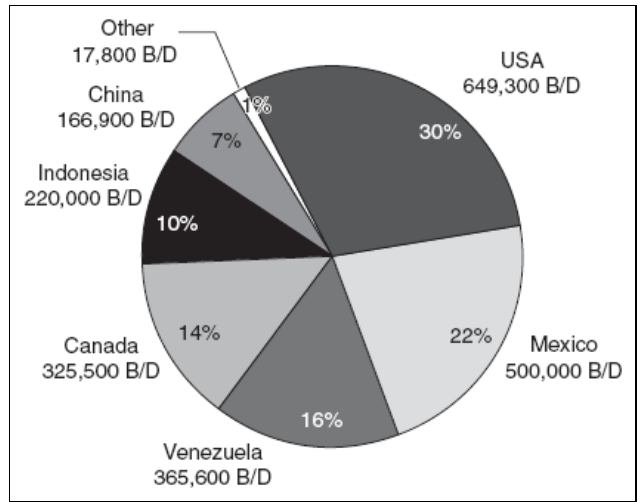


Figure 2.2 Current EOR production from contributing countries [19].

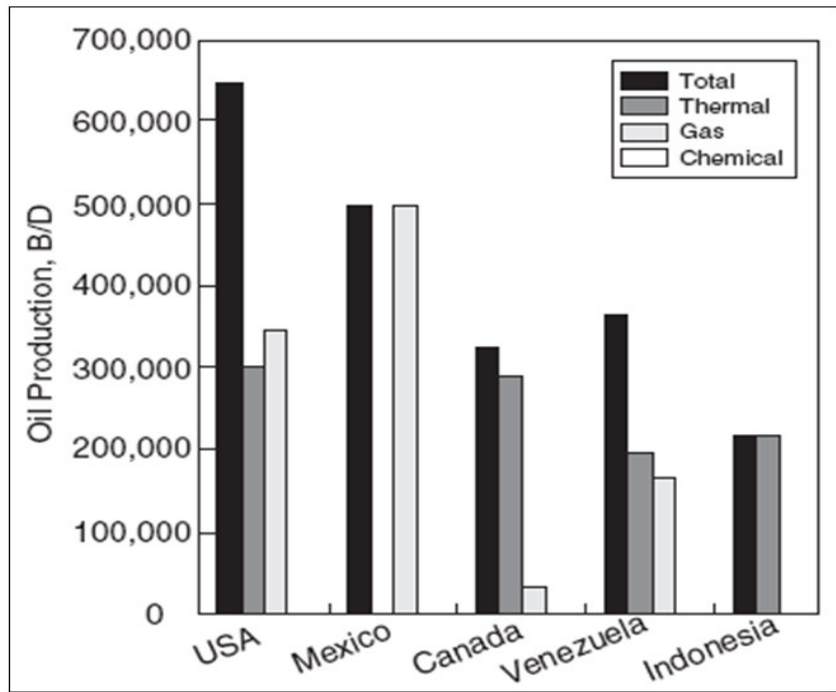


Figure 2.3 Major EOR projects and production worldwide [19].

Thermal methods are dominant in five countries. Chemical floods are active in China, the total production being 200,000 bbl / day in 2006. Most of the EOR activity took place in USA in the past, and the bulk of the production came from that country [19].

Recent advancements in technology and the current economic climate have resulted in a renewed interest in EOR. Future growth of EOR will depend on both technology and oil price. Long term commitments in capital and human resources are essential for success in EOR practice. While EOR screening methods are useful tools, recovery methods that are considered unattractive in most reservoirs can be applicable in specific situations. Also, proven EOR methods may be adapted to adverse conditions, as experienced in Canada. Considering the widening gap between demand and supply of energy, EOR will continue to play a significant role in improving recovery factors [20].

#### 2.1.2. EOR Methods

Many EOR methods have been used in the past, with varying degrees of success, for the recovery of light and heavy oils, as well as tar sands. A general classification of these methods is shown in Figure 2.4. Thermal methods are primarily intended for heavy oils and tar sands, although they are applicable to light oils in special cases. Non-thermal methods are normally used for light oils. Some of these methods have been tested for heavy oils, however, have had limited success in the field. Above all, reservoir geology and fluid properties determine the suitability of a process for a given reservoir. Among thermal methods, steam-based methods have been more successful commercially than others [19].

Among non-thermal methods, miscible flooding has been remarkably successful, however applicability is limited by the availability and cost of solvents on a commercial scale. Chemical methods have generally been uneconomic in the past, but they hold promise for the future. Among immiscible gas injection

methods, CO<sub>2</sub> floods have been relatively more successful than others for heavy oils [19].

Since two of the thermal methods were used in this study, from now on, detailed information about the thermal methods, electrical heating and electromagnetic heating methods will be given.

Thermal methods have been tested since 1950's, and they are the most advanced among EOR methods, as far as field experience and technology are concerned. They are best suited for heavy oils (10-20° API) and tar sands ( $\leq 10^\circ$  API). Thermal methods supply heat to the reservoir, and vaporize some of the oil. The major mechanisms include a large reduction in viscosity, and hence mobility ratio. Other mechanisms, such as rock and fluid expansion, compaction, steam distillation and visbreaking (viscosity reduction or breaking) may also be present. Thermal methods have been highly successful in Canada, USA, Venezuela, Indonesia and other countries [19].

Cyclic Steam Stimulation (CSS), steam flooding (Steam Assisted Gravity Drainage (SAGD)), and in situ combustion are the most widely used methods among the thermal methods [19].

Electrical heating and electromagnetic heating are the alternative methods and they are still seemed marginal applications. Due to the increasing oil prices, oil production from alternative resources by using these methods can be considered reasonable.

Hereafter, the topic will be concentrated on the electrical heating method; retort and electromagnetizing heating method; microwave which are also used in this study.

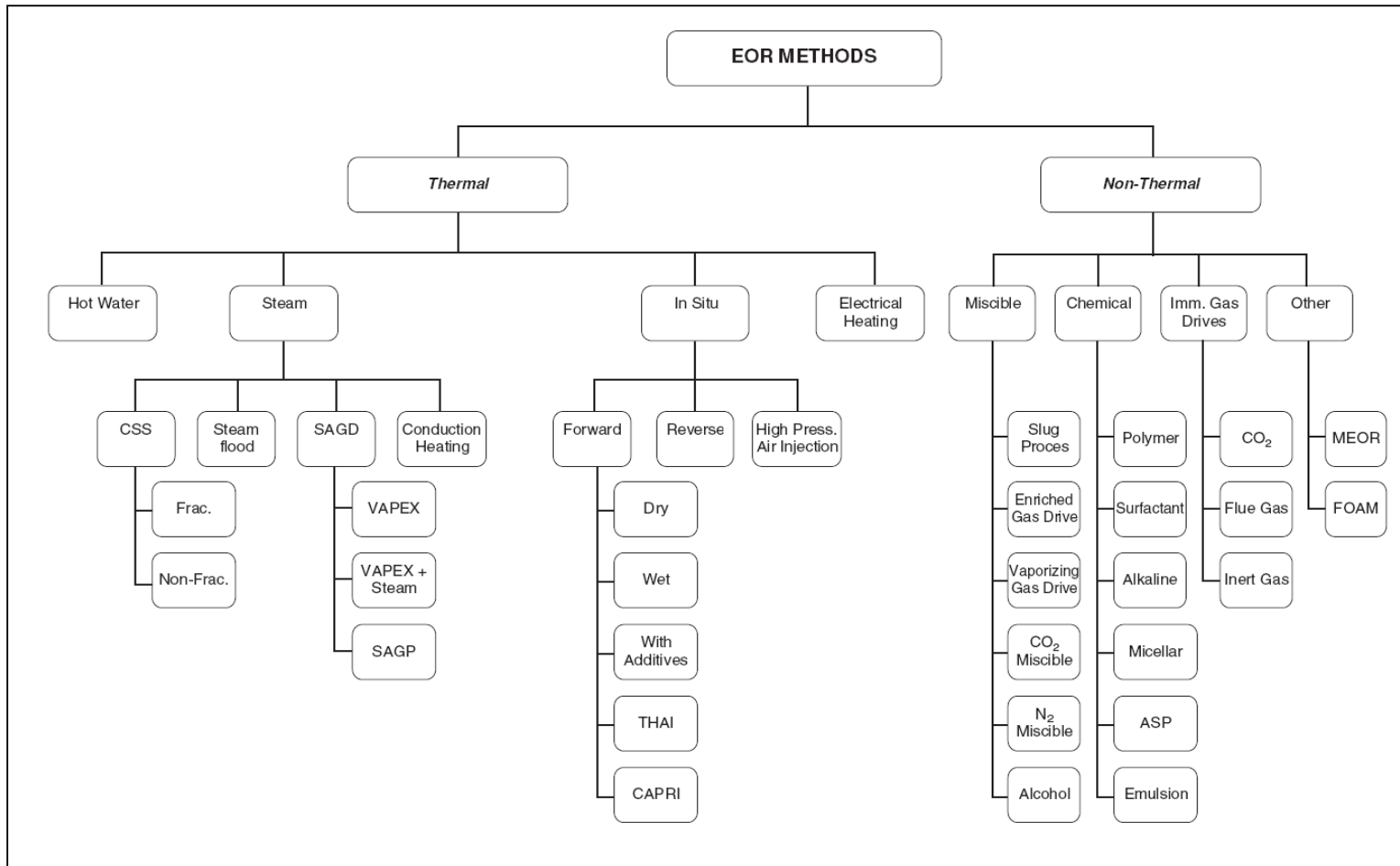


Figure 2.4 Classification of EOR methods [19].

#### 2.1.2.1. Retort Method

Retort technology is divided into two major categories as surface retorting and in-situ methods. The basic retorting sequence for both groups is the same, where kerogen undergoes a chemical conversion (pyrolysis) after the application of heat and the unconventional fossil fuel resources are converted into crude oil, gas, carbon, water and waste portions.

##### 2.1.2.1.1. Surface Retorting Technologies

In its simplest explanation, a surface retort is a closed, large metal vessel in the form of a closed reactor. Surface retorting is mostly a continuous process in which the raw unconventional oil source; such as oil shale or tar sand, undergoes pyrolysis under the effect of heating and oil and waste products are obtained. In these processes, heat can be applied directly (e.g. burning of residual carbon within oil shale inside the retort), indirectly (i.e. carbon or gas is burned outside and injected into the retort) or as their combination. The way of heat application affects the retorting results. Less oil is obtained with direct heating, as the process may result in further combustion of crude part, too. However, direct heating is economically advantageous. The most important surface retorting technologies developed are NTU Retorting Process, Lurgi Process, TOSCO II Process, UNION B Process, and Paraho Process, although there are other methods of minor importance [21].

##### 2.1.2.1.2. In-Situ Retorting Technologies

Unlike surface retorting techniques, in-situ retorting requires no or very little extraction of the unconventional oil resources. The process uses the natural strata of the reserve as the reaction zone to yield crude oil. In other words, reserve is heated within the ore body and the produced crude oil is transported to

the surface by different means. Thus, the whole ore body acts like a huge, natural retort, including all the reaction zones in a logical sequence (Figure 2.5).

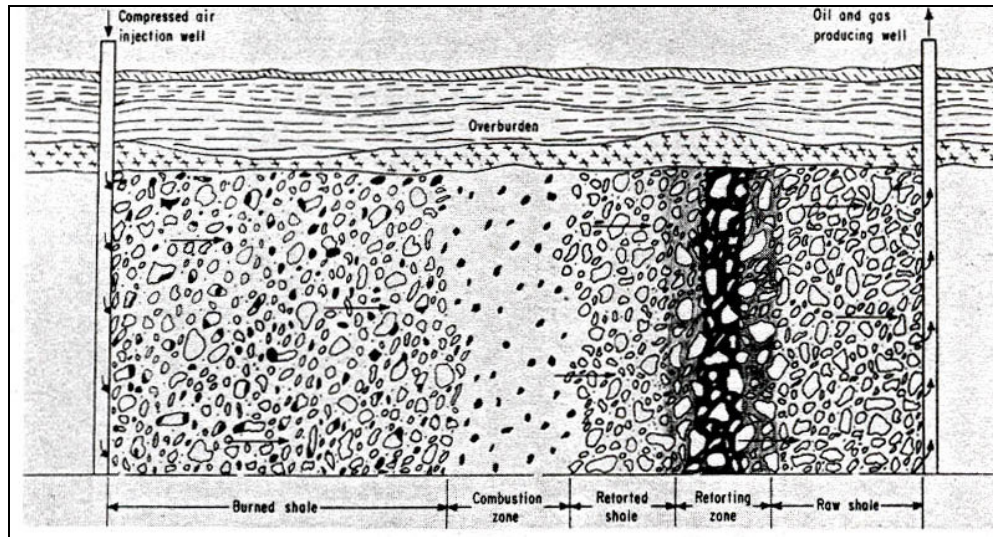


Figure 2.5 Schematic Form of In-Situ Oil Retorting from Oil Shales [22]

Once the oil shale formation in an underground retort is sufficiently fragmented, some part of the retort is initially ignited. Then, the combustion process, which supplies heat for pyrolysis in the adjacent zones, is maintained by the burning of the carbon residue on the oil shale fragments. Combustion continues from one end towards the other and pyrolysis occurs just ahead of the zone in which residual carbon burns. Water condenses and oil flow takes place at the furthest part from the burning zone. Also, spent shale behind, which remains hot, heats the injected combustion-supporting air. In a favorable in-situ retorting process, combustion and pyrolysis zones should be distinctively separated. The interference of the combustion into pyrolysis zone will result in the consumption of the valuable gas and oil. Compared to surface retorting, in-situ processes are less controlled and less advanced. Most important in-situ retorting processes are LETC (Laramie Energy Technology Center) Process, Geokinetics In-Situ and OXY Modified In-Situ processes [21, 22].

### 2.1.2.2. Microwave Method

The microwave region of the electromagnetic spectrum covers the wavelengths between 1 cm to 1 m (300 GHz to 300 MHz) and the frequencies between 2.45 GHz (12.2 cm) to 900 MHz (33.3 cm) are only for dielectric heating [23].

While the energy is transferred by conduction, convection and radiation in conventional thermal processing, molecular interactions with an electromagnetic field are the main energy transfer mechanism of microwave energy. The internal temperature distribution of a material subject to conventional heating is limited by its thermal conductivity, whereas microwave heating results in all individual elements of the material being heated individually. Accordingly, heating times using microwaves can often be reduced to less than 1% of those required using conventional heating methods (Figure 2.6) [24].

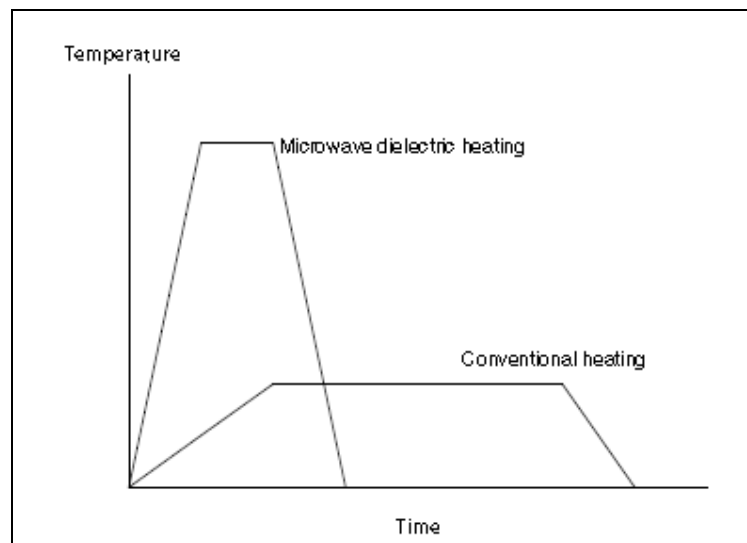


Figure 2.6 Differences in the temperature-time profiles for conventional and microwave dielectric heating [23].

There are three general classifications for the behavior of materials upon interaction with a microwave field:

1. Transparent (low-dielectric-loss materials)—microwaves pass through the material with little absorption.
2. Opaque (conductors)—microwaves are reflected by the material and do not penetrate.
3. Absorbing (high-dielectric-loss materials)—microwave energy is absorbed based on the electric field strength and the dielectric loss factor.

Microwave processing has distinct advantages in the treatment of materials which contain a mixture of absorbers and transparent components. Microwave energy is absorbed by the substances with a high dielectric loss even as passing through the low-loss transparent material, resulting in selective heating. In this case, significant energy savings are possible since the dielectric material can be heated without heating the entire matrix [25].

The power absorbed per unit volume of material, known as power density ( $P_d$ ), is dependent on the dielectric properties of the material and can be represented by

$$P_d = 2\pi f \epsilon_0 \epsilon'' |E|^2, \quad (2.1)$$

where  $f$  is the microwave frequency,  $\epsilon_0$  the permittivity of free space ( $8.85 \times 10^{-12}$  F/m),  $\epsilon''$  the relative dielectric loss factor and  $|E|$  the magnitude of the electric field. A number of heating mechanisms may occur depending on the dipolar nature of the material and whether any free electrons or ions are present. From Equation (2.1) it is evident that the microwave energy absorbed by a dielectric material is proportional to the square of the electric field strength. The design of the microwave cavity is critical in that it can allow very well-defined electric fields in a relatively small volume (single-mode cavity), or can permit the electric fields to encompass a much larger volume, albeit with a compromise in the field definition (multimode cavity). With single-mode cavities the high electric field

strength results from superposition of reflected waves, hence the geometry of the cavity is dependent on the microwave frequency [25].

The conversion of the electromagnetic radiation to thermal energy can be explained at the molecular level. There are two principle mechanisms proposed for microwave interaction with matter: dipolar polarization and ionic conduction [25].

Polar molecules tend to align them and oscillate in step with the oscillating electric field of the microwaves and during this realignment energy is lost in the form of heat through molecular friction and dielectric loss. The more polar a molecule, the more effectively the molecule will couple with the microwave field. On the other hand, ions are charged species that can couple with the oscillating electrical field of the microwaves. The effectiveness or rate of microwave heating of an ionic solution is a function of the concentration of ions in solution. Therefore, rapid heating in a microwave field is caused by the ability of absorption of the radiation by a material that is placed in the field. The frequency of the applied field affects the amount of heat generated which is directly related to the ability of the matrix to align. If the dipole does not have enough time to realign, or reorients too quickly with the applied field, no heating occurs. But for the commercial systems where 2.45 GHz frequency is applied, such extreme cases have not been seen and it provides the molecular dipole time to align in the field [26].

In the gas phase, the interaction of the small molecules with permanent dipole moments with microwave energy shows a well-defined spectrum that may be used to define the moment of inertia of the molecule. As long as the molecule has a permanent dipole moment, in this phase the rotation of molecules is quantized and the transition between the energy levels may be observed as sharp lines in the microwave spectrum. In liquids, the continuum of rotational states resulted in frequently interacting molecules and so the phenomenon loses its identity as a quantum mechanical description and rotational motions become less distinguishable from translational processes. The rotations at one center will influence the translational and rotational motions of neighboring molecules via

intermolecular interactions. The intermolecular perturbations will be greatest when the intermolecular forces arise from hydrogen bonding and strong dipole-dipole interactions. It is important to emphasize that microwave dielectric heating is not a quantum mechanical phenomenon localized at one molecular center, but is a collective property that occurs in a semi-classical manner and involves aggregates of molecules [23].

There are several important parameters related to microwave heating, such as dielectric loss, dielectric constant and penetration depth. The conversion capabilities for electromagnetic energy into heat of the materials at a given frequency and temperature are determined by their loss factors (loss tangent,  $\tan\delta$ ). Also an important parameter in deciding the extent of interaction between microwave radiation and a particular solvent is the average rotational frequency or its inverse, the average relaxation time. This relaxation time depends on the size of the molecule and the nature of the intermolecular forces. A dielectric material is one that contains permanent or induced dipoles, which when placed between two electrodes the whole assembly acts as a capacitor, that is if the electrodes are connected by a circuit the material allows charge to be stored and after the charging no D.C. conductivity is observed. The polarization of dielectrics results from the finite displacement of charges or rotation of dipoles in an electric field and must not be confused with conduction, which results from the translational motion of electric charges when a field is applied. At the molecular level, polarization may be associated either with a distortion of the distribution of the electron cloud of the molecule or the physical rotation dipoles. Dielectric heating in microwave region is strongly connected with the latter case. The permittivity of a material,  $\epsilon'$ , is the property that defines the charge-storing ability of that material irrespective of the sample's dimensions. The dielectric constant or relative permittivity of a material is the permittivity of the material relative to free space. The angle  $\delta$  represents the angle between the vector for the magnitude of the total current and the charging current. In other words loss tangent represents the phase difference between the electric field and the polarization of the material. The loss tangent can be given by the equation as follows:

$$\tan \delta = \epsilon''/\epsilon' \quad (2.2)$$

where  $\epsilon''$  and  $\epsilon'$  represents the loss factor and dielectric constant, respectively [27]. The higher the loss tangent is the better the conversion of electromagnetic energy into heat.

## **2.2. Unconventional Fossil Fuel Sources**

### **2.2.1. Oil Shales**

The term “oil shale” does not have a definite geological definition nor a specific chemical formula, but is a general expression usually used for a fine-grained sedimentary rock, containing significant amounts of kerogen (a solid mixture of organic chemical compounds), from which liquid hydrocarbons can be manufactured [7, 28].

Oil shale can also be described as any compact laminated sedimentary rock with more than 33% ash, which is capable of yielding significant amount of oil under a suitable process [29]. The average oil that can be extracted from oil shale deposits vary from 4% up to 50 % of the weight of the source rock [22].

Oil shales usually deposit in a wide variety of environments such as freshwater to saline ponds and lakes, epicontinental marine basins and subdial shelves, shallow ponds or lakes and coastal swamp depositional environments. Because of the wide range of depositional environments, oil shales spread many regions of the world. The oil shales are classified according to the depositional environments and the differentiation of organic components with the aid of ultraviolet / blue fluorescent microscopy [28].

Lithologically, oil shale covers a broad range of rocks from shales to marl and carbonates, which forms a mixture of tightly bound organic and inorganic materials. The general composition of oil shales is given in Figure 2.7 [22]. According to the depositional conditions and the characteristics of the host rock, the composition and the amount of the inorganic materials differ. For example,

true shales contain primarily clay minerals, while the well-known Green River shale is mainly carbonate associated with quartz and feldspars. Therefore, inorganic associations can be said as one of the most important criteria to classify oil shales lithologically, so based on mineral composition, oil shales can be categorized as carbonate-rich shale, siliceous shale and cannel shale.

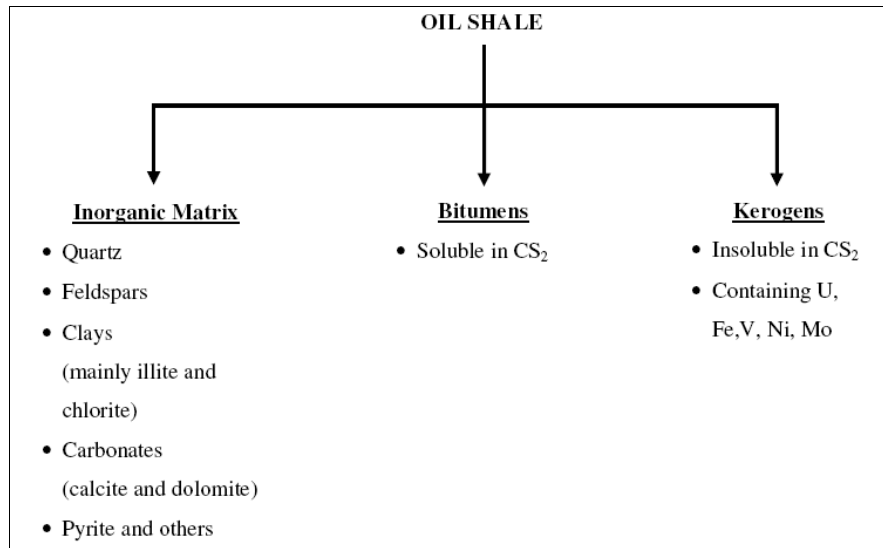


Figure 2.7 General compositions of oil shales [22]

Kerogen is a mixture of organic chemical compounds that make up a portion of the organic matter in sedimentary rocks. Because kerogen has huge molecular weight of its component compounds; upwards of 1000, it is insoluble in normal organic solvents. Bitumen and/or prebitumen which are known as soluble portion of kerogen may also exist but in relatively lower amounts. If it is heated to the right temperatures in the Earth's crust, some types of kerogen release oil or gas, collectively known as hydrocarbons (fossil fuels). If such kerogens are present in high concentration in rocks such as shale, and have not been heated to a sufficient temperature to release their hydrocarbons, they may form oil shale deposits [21].

According to ultimate production kerogen can be categorized into three. While labile kerogen breaks down to form heavy hydrocarbons (i.e. oils), refractory kerogen breaks down to form light hydrocarbons (i.e. gases), and inert kerogen forms graphite. Kerogen types are summarized in Table 2.1.

Table 2.1 General property of kerogen types [30]

Kerogen Types	H/C	O/C	Chemical Structure
Type I	>1.25	<0.15	mainly proteins and lipids, few cyclic or aromatic
Type II	<1.25	0.03-0.18	naphthenic rings, aliphatic chains
Type III	<1	0.03-0.3	extensive ring and aromatic
Type IV	<0.5		polycyclic aromatic hydrocarbons

Type 1 oil shales yield larger amount of volatile or extractable compounds than other types upon pyrolysis. Hence, from the theoretical view, Type 1 kerogen oil shales provide the highest yield of oil and are the most promising deposits in terms of conventional oil retorting [7].

Type II kerogen is common in many oil shale deposits. It is based on marine organic materials, which are formed in reducing environments. Sulphur is found in substantial amounts in the associated bitumen and generally higher than the sulphur content of Type I or III. Although pyrolysis of Type II kerogen yields less oil than Type I, the amount acquired is still sufficient to consider Type II bearing rocks as potential oil sources [7].

Type III kerogen involving rocks are found to be the least productive upon pyrolysis and probably the least favorable deposits for oil generation [7].

Type IV kerogen contains mostly decomposed organic matter in the form of polycyclic aromatic hydrocarbons. They have no potential to produce hydrocarbons [31].

### 2.2.1.1. Oil Shale History in the World

Oil shale has been used since ancient times. In 1596, the personal physician of Duke Frederick of Württemberg noted that a mineral oil distilled from oil shale could be used in healing [32]. In 1637, Swedish alum shale of Cambrian and Ordovician age was used for extracting potassium aluminum sulfate [33].

The modern industrial use of oil shale for oil extraction dates to the mid-19th century. In 1837 oil shale mining began in Autun, France. In 1847 the Scottish chemist James Young prepared "lighting oil," lubricating oil and wax from torbanite. In 1850 he patented the process of cracking oil [34]. The commercial oil extraction in Scotland started in 1857, and approximately at the same time the development of oil shale industry took-off in Germany. At the second half of the 19th century the shale oil extraction started also in Sweden, Australia, Brazil, New Zealand, Canada and the United States [35]. The first oil shale retort was constructed in the United States in 1855, but because of crude oil discovery in Pennsylvania, the United States' and Canada's oil shale industries were shut down by 1861 [33].

The second wave of oil shale industry started just before the World War I. The Office of Naval Petroleum and Oil Shale Reserves of the United States were established in 1912. The reserves were seen as a possible emergency source of fuel for the military, particularly the Navy [33]. In 1915 the oil shale industry started in Switzerland and in 1918 in Estonia. Between the World Wars oil shale industry also took off in Spain, China, Russia and South Africa, and restarted in Brazil and for a short period in Canada [33, 36].

After the World War II, the oil shale industry was phased-out in several countries because of high processing costs and the discovery of large supplies of easily accessible crude oil. The low cost of conventional oil made shale oil production uneconomic. In 1950s-1960s, the industry was closed in France, Australia, New Zealand, Spain, Scotland and South Africa, while in Germany only Rohrbach Zement in Dotternhausen continued using oil shale for cement, power and thermal energy production, and in Sweden the extraction of alum shale for

uranium and vanadium production remained until 1989 [33, 34, 37]. At the same time, the oil shale production in Estonia, Russia and China continued to grow. After World War II, Estonian-produced oil shale gas was used in Leningrad and the cities in North Estonia as a substitute for natural gas. The world's two largest oil shale-fired power stations were opened correspondingly in 1965 and in 1973. Estonian oil shale production peaked in 1980 at 31.35 million tones [35, 38, 39, 40, 41]. The United States Bureau of Mines opened a demonstration mine at Anvils Point, just west of Rifle, Colorado, which operated at a small-scale. In the early sixties, TOSCO (The Oil Shale Corporation) opened an underground mine and built an experimental plant near Parachute, Colorado. It was closed in 1972 because the price of production exceeded the cost of imported crude oil [35, 42, 43].

After the 1973 oil crisis, oil shale industry restarted in several countries. In 1974 the United States Department of the Interior announced an oil shale leasing program in the oil shale regions of Colorado and Utah on. By the early 1980s, almost all of the major oil companies had established oil shale pilot projects. The United States oil shale industry collapsed, when on 2 May 1982, known as "Black Sunday", Exxon announced the termination of its Colony Oil Shale Project near Parachute [44]. In 1980s the oil shale production decreased also in Estonia due the reduced oil shale demand by power generation industry. Most of Russian oil shale mines were closed on 1990s and the production continued only on a small-scale basis [33].

The global oil shale industry started to increase slightly in mid of 1990s. In 1992 the commercial shale oil production started in Brazil using Petrosix technology. Estonian oil shale production has continuously increased since 1995 [33]. In Australia, a demonstration-scale processing plant at the Stuart Deposit near Gladstone, Queensland produced over 1.5 million barrels of oil in 2000-2004. The facility is now on care-and-maintenance in an operable condition and the operator of the plant—Queensland Energy Resources—is conducting research and design studies for the next phase of its oil shale operations [45]. The Energy Policy Act of 2005 introduced a commercial leasing program for oil shale and tar sands

resources on public lands with an emphasis on the most geologically prospective lands within each of the states of Colorado, Utah, and Wyoming [46].

#### 2.2.1.2. Oil Shale Potential in the World

Though information about many oil shale deposits is rudimentary and much exploratory drilling and analytical work needs to be done, the potential resources of oil shale in the world are enormous.

Some deposits have been fairly well explored by drilling and analyses. The Green River oil shale in western United States, the Tertiary deposits in Queensland, Australia, the deposits in Sweden and Estonia, the El-Lajjun deposit in Jordan, perhaps those in France, Germany and Brazil, and possibly several in Russia are the examples of fairly well explored deposits. It can be assumed that the deposits will yield at least 40 liters of shale oil per tone of shale by Fischer assay. The remaining deposits are poorly known and further study and analysis are needed to adequately determine their resource potential [33]. Table 2.2 presents some characteristics of several well-known oil shale deposits in the world [47].

The United States has the largest oil shale resources in the world. The total amount is 3340 billion tons, which accounts for 62 % of the world's known oil shale potential [43, 48]. The largest known deposit is the Green River oil shale in the western United States, which contains a total estimated resource of nearly 1.5 trillion barrels. In Colorado alone, the total resource reaches 1 trillion barrels of oil. The Devonian black shales of the eastern United States are estimated at 189 billion barrels [33].

Brazil follows United States, having the world's second largest oil shale resource, the Irati shale in Sao Mateus do Sul, Parana. According to the reports of the Brazilian Ministry of Mines and Energy in 1999, the amount of proven oil shale reserves was 445.1 million m<sup>3</sup>, whereas the probable reserve potential was around 9402 m<sup>3</sup> [47].

China has an important oil shale potential, in Manchuria and particularly near Fushun, a city which is also known as the coal capital of the country. The oil shale reserves in Fushun region were reported to be around 3.6 billion tons and the total oil shale potential of the country approximates to 4.4 billion tons. The oil yield from the deposits varies between 79-89 liters per ton of shale, depending on the ore quality [47].

Oil shale reserves in the Kukersite deposit in Estonia are estimated to be 21 billion tons, which would yield a total of 3.5 billion tons of shale oil [47].

Other important deposits include those of Australia, Jordan, and Morocco. The total world resource of shale oil is estimated at 2.8 trillion barrels. This figure is considered to be conservative in view of the fact that oil shale resources of some countries are not reported and other deposits have not been fully investigated. On the other hand, several deposits, such as those of the Heath and Phosphoria Formations and portions of the Swedish alum oil shale, have been degraded by geothermal heating. Therefore, the resources reported for such deposits are probably too high and somewhat misleading [33].

Table 2.2 Properties of Some Important Oil Shale Deposits [7]

Location	Oil Shale			Retorting		Shale Oil		
	OC* (%)	H/C*	O/C*	OY (%)	$\rho_o$ (g/cc)	H/C*	N (%)	S (%)
GlenDavis	40	1.6	0.03	31	0.89	1.7	0.5	0.6
Tasmania	81	1.5	0.09	75.0				
Irati	1.2	0.05	7.4	0.94	0.8	1.0	–	1.7
Tremembe-Taubate	13–16.5	1.6	6.8–11.5	45–59	1.7	1.1	0.7	
NovaScotia	8–26	1.2	3.6–19.0	40–60				
Fushun	7.9	3	33	0.92				
Estonia Deposit	77	1.4–1.5	0.160–0.20	22	0.97	1.4	0.1	1.1
Autun, St.Hilarie	8–22	1.4–1.5	0.03	5–10	0.89–0.93	1.6	0.6–0.9	0.5–0.6
Crevenay, Severac	5–10	1.3	0.08–0.10	4–5	0.91–0.95	1.4–1.5	0.5–1.0	3.0–3.5
Ermelo	44–52	1.35	18–35	34–60	1.6	0.6		
Puertollano	26	1.4	18	57	0.7	0.4		
Kvarntop	19	6	26	0.98	0.7	1.7		
Scotland	12	1.5	0.05	8	0.88	0.8	0.4	
Alaska	25–55	1.6	0.10	0.4–0.5	0.80			
Colorado	11–16	1.55	0.05–0.10	9–13	0.90–0.94	1.65	1.8–2.1	0.6–0.8

\* $\rho_o$  at 15 °C, H/C and O/C are the atomic ratios, OC: Organic Carbon, OY: Oil yield

### 2.2.1.3. Oil Shale in Turkey

The oil shale resources in Turkey are distributed mainly in middle and western Anatolia. Generally, marl, clay and carbonates are the host rocks and organic matter is found in disseminated form [47].

Main oil shale deposits in Turkey are shown in Table 2.3 and Figure 2.8 with their geological and possible reserve amounts [49, 50].

Table 2.3 Main oil shale reserves in Turkey [50].

Name of the Deposit	Proven Reserve (x 10 <sup>3</sup> tons)	Probable Reserve (x 10 <sup>3</sup> tons)	Minable Reserve (x 10 <sup>3</sup> tons)	Total Reserve (x 10 <sup>3</sup> tons)
Bey pazarı	327684	-	205970	327.684
Burhaniye	-	15600	-	15600
Himmetođlu	65968	-	-	65968
Mengen	-	50000	-	50000
Hatıldıđ	78372	281587	-	359959
Bahçecik	-	42000	-	42000
Seyitömer	83320	38850	63292	122170
Ulukısla	-	130000	-	130000
Sarıcakaya	-	300000	-	300000
Dodurga	-	138000	-	138000
Çelteđ	-	90000	-	90000
TOTAL	555344	1086037	269262	1641381

Among the potential resources, Bey pazarı (Ankara), Seyitömer (Kütahya), Himmetođlu (Bolu) and Hatıldıđ (Bolu) deposits are of major importance in terms of quality, amount and exploitability. The characteristics of these four deposits, which constitute around 50 % of the total oil shale potential of Turkey, are given in Table 2.4 [51, 52].

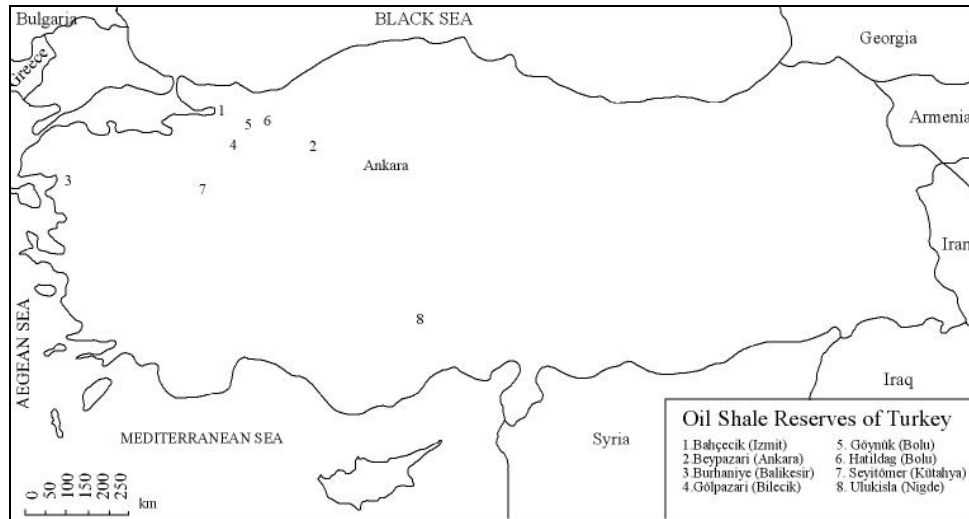


Figure 2.8 Location of main oil shale reserves [53]

Table 2.4 Characteristics of the Major Oil Shale Deposits in Turkey [51, 54, 55, 56, 57]

Deposit	Upper Calorific Value (kcal/kg)	Total Organic Carbon (%)	Oil Content (%)	Oil Content (liter)	Total Sulphur (%)	Kerogen Type
Beypazarı	812	4.8	5.4	60.0	1.4	II
Seyitömer	847	6.9	5.0	54.3	0.9	I-II
Himmetoglu	4991	30.9	43.0	482.0	2.5	I
Hatıldag	773	5.6	5.3	58.0	1.3	III

Other potential resources are in Mengen (Bolu), Ulukisla (Nigde), Bahçecik (Izmit), Burhaniye (Balıkesir), Beydili (Ankara), Dodurga (Çorum) and Demirci (Manisa) [47].

#### 2.2.1.3.1. Himmetoğlu Deposit

Himmetoğlu oil shale deposit is located in the southwestern part of Bolu province. Its location is shown as 5 in Figure 2.8. It occurs in the form of a successive, predominantly brown and brownish grey oil layers between pyroclastic outcrops. Himmetoğlu oil shale basin is of Neogene age. Volcanism and tectonic activities had considerable influences on the environmental conditions during the deposition period [58]. The deposition of the organic matter was controlled by the volcanism and the initial characteristics have been preserved without further improvement in the maturity of the organic matter. The drill-hole data shows three main zones. From top to bottom are bituminous marl (BLM), bituminous banded marl (BBM) and the major oil shale formation of Himmetoğlu (HOS) seam. Himmetoğlu Oil Shale strata overlie a lignite zone and extend throughout the deposit. The amount of the organic matter decreases from the outermost layer towards the bottom parts while the amount of zeolites increases. Himmetoğlu oil shale seam consists of more than 50 % liptinite, 20 – 50 % huminite and 0 – 20 % inertinite maceral groups and is characterized by its high organic content [58]. The origin of the organic matter is mainly algae and plants [59]. The major inorganic constituents in the organic rich zones are calcite, dolomite, silica and considerable amounts of pyrite. Economic Grade Oil Shale (EGOS) over an oil shale deposit was defined by 5 m minimum seam thickness, 750 kcal/kg minimum upper calorific value and 4 % minimum oil content [60]. The average calorific value of the EGOS zone is around 4900 kcal/kg. The in-place oil content of Himmetoğlu oil shale is 43 % by weight or approximately 482 l/ton shale. However, the average total sulphur content is high (2.5 %) due to considerable amount of pyrite. Himmetoğlu oil shale is the highest quality oil shale deposit in Turkey. Himmetoğlu oil shale zone is being excavated to exploit an underlying high quality lignite seam, utilized for domestic heating. On accounts of its high thermal quality, Himmetoğlu oil shale is an attractive alternative for thermal power generation in Turkey, which relies mostly on poor quality lignites [55, 60].

#### 2.2.1.3.2. Seyitömer Deposit

Seyitömer oil shale deposit is found in the northwest of Kütahya province. Its location is shown as 7 in Figure 2.8. The deposit overlies Seyitömer lignite basin, which supplies a 300 MW thermal power plant at the mine site. The amount of Seyitömer oil shale is around 122 million tons and more than 75% is in the form of geologically proven reserves. Seyitömer oil shale is rich in quartz, dolomite, calcite and clay minerals such as muscovite, illite and smectite [52, 57, 61]. Geochemical analysis revealed that organic content of Seyitömer oil shale was mainly derived from algae, pollen and planktonic algae as well as bacteria. Also traces of liptodetrinite and humic organic material were observed [57, 59]. Specifically, Seyitömer oil shale is characterized with its grey to green colored organic-rich zones. The EGOS in Seyitömer oil shale basin varies widely in terms of thickness and quality. The thickness ranges between 3 to 29.5 m, with an average of 12.4 m. The average upper calorific value of the EGOS is around 850 kcal / kg. The average oil content of the seam is around 5 %, corresponding to an approximate shale oil yield potential of 54 l/ton of shale. It contains a relatively high amount of ash ( $\approx 70$  %); however the total sulphur content seldom exceeds 1.5 %, with an average of less than 1 % [52, 59]. Since the oil shale seam extends over Seyitömer lignite, it is being excavated during the open-pit mining of Seyitömer lignite and stockpiled. This serves as an opportunity for the utilization of Seyitömer oil shale [47].

#### 2.2.1.3.3. Hatıldağ Deposit

Hatıldağ oil shale field is located in Hatıldağ-Bolu lacustrine basin at the south-eastern part of Göynük in Bolu province. Its location is shown as 6 in Figure 2.8. The deposit is of Paleocene- Eocene age, is in a 50 to 75 m thick limic series of calcareous bituminous rocks. The series consists of two zones, an economic grade oil shale and bituminous marl [56]. It contains around 80 % liptinite, 5 – 10 % bituminite and 5 – 10 % huminite. The high liptinitic content shows that the organic matter originated mainly from hydrogen-rich organic remains of algae and

pollen. Calcite, dolomite, quartz and smectite are the major inorganic constituents. Analcime, feldspar, chlorite and mica-illite are found in lesser amounts (5 – 10 %). The EGOS zone is in the lower part of the bituminous sequence. Average thickness and average upper calorific value of EGOS are 30.5 m and 774 kcal / kg, respectively. Hatıldağ oil shale is characterized as a poor quality deposit with a shale oil yield of 5.3 %, similar to Seyitömer deposits [47].

#### 2.2.1.3.4. Ulukışla Deposit

Ulukışla oil shale field location is shown as 8 in Figure 2.8. Ulukışla oil shale deposit underlies conglomeratic rocks and the average thickness of the oil shale bed is 13 m. The calorific value and oil content of the deposit averages 2790 kcal/kg and 13.7 %, respectively [47]. While reserves having a calorific value below 1000 kcal/kg are estimated as 600-650 million tons, calorific value above 1000 kcal/kg is estimated as 70-80 million tons or contains more than 10 % asphaltite [62].

#### 2.2.1.3.5. Other Potential Reserves in Turkey

The other potential oil shale deposits at Mengen, Beypazarı, Bahçecik, Burhaniye, Beydili, Dodurga, Demirci, Sarıcakaya and Çeltik have not been investigated in detail yet. The information about these deposits is derived from the preliminary geological borehole data and analysis. Among these deposits, Beydili and Sarıcakaya are distinguished by their huge resources. Mengen deposit is of Eocene age and located near Hatıldağ and Himmetoğlu deposits. Mengen deposit overlies a lignite seam and is 24 m thick. Bahçecik oil shale bed lies between two tuffs. The average thickness of the oil shale is 4.30 m and the shale oil yield ranges between 2 and 19 %. Demirci oil shale field is of Miocene age. The thickness of the oil shale ranges between 3 and 15.60 m. Total organic carbon content ranges from 10.40 to 22.50 % [47].

#### 2.2.1.4. Potential Use of Oil Shales

Processes for shale oil retorting mostly proved to be non-favorable due to noncompetitive cost of shale oil production. Today, large scale shale oil retorting is performed only in countries which have high-quality and big quantity oil shale reserves and lacking of petroleum and/or coal resources like Brazil, China and Estonia [47].

The vast and wide spread oil shale resources in the world offer opportunities for burning the resources as a solid fuel. Oil shale utilization is shifting towards its use as a fuel with novel combustion technologies such as fluidized beds. Carbonate minerals, which commonly dominate the inorganic content of high-ash oil shale reserves, provide a natural SO<sub>2</sub> adsorption medium during burning. This condition eliminates the cost of limestone used as a SO<sub>2</sub> retardant during combustion in fluidized beds and provides an important advantage for the utilization of low-quality oil shales over high-sulphur lignites in these systems [52, 60, 63]. Studies of pilot-scale testing of low-quality oil shale fines (-8mm, < 1158 kcal/kg) are currently continuing in Maoming, China [43, 47].

It should also be noted that most of these processes were developed in oil crisis periods and suggested as alternative oil solutions. Therefore, oil shale industry is leaning towards utilization as a direct source of energy and the recovery of by-products. This trend is predicted to continue during the near future. However, the bottom line for re-awakening of large-scale shale oil production is governed by the crude oil prices. For the long term, stimulation of shale oil production to fill the gap between demand and supply of crude oil becomes greater because of the depleting petroleum resources. If the price of petroleum remains as high as it is today, economics of shale oil production begins to look competitive. However, it will be necessary to develop more advanced and cost-effective processes to produce shale oil at affordable and competitive prices.

## 2.2.2. Heavy Oil

### 2.2.2.1. Definition and Origin of Heavy Oil

Heavy oil, sometimes referred to as low-gravity oil, is defined as oil with API gravity of  $10^0$  to  $25^0$ . Physical and chemical properties, which differentiate it from higher gravity or light oil, include viscosity, pour point, and chemical composition. They affect the producibility and the products that can be refined from it [64].

There are several hypotheses for the origin of heavy oil. According to one hypothesis, some characteristics of oil are derived from the source of the organic material and some from the physiochemistry of the aquatic basin of deposition, including the activity of microorganisms in the young sediment [7]. Heavy oil sometimes begins as high or higher gravity liquids and is altered to low-gravity material. Low-gravity oil may also be the result of generation from thermally immature source rocks [7]. The 5 percent of oil generated is immature, i.e., low gravity, while the remaining 95 percent is conventional, high-gravity petroleum that is expelled from source rocks and migrates into a trap [65]. After entrapment, a transformation from conventional to heavy oil may take place. Alteration can be affected during migration between source rock and reservoir, such as a loss of varying degrees of API gravity due to contact with formation water.

Bacteria introduced into the petroleum reservoir by infiltration of bacteria-laden circulating or connate water can be deleterious to hydrocarbon accumulations. Bacteria are the principal agent of oxidation for petroleum still in the ground [66]. Aerobic bacteria are known to survive at some shallower reservoir conditions but apparently cannot live at temperatures higher than about  $80^{\circ}\text{C}$  ( $176^{\circ}\text{F}$ ). Degradation by bacteria requires three conditions to be most effective: dissolved oxygen in the water to support the bacteria, geologic formation temperatures up to  $80^{\circ}\text{C}$  to permit growth of the bacteria, and an absence of  $\text{H}_2\text{S}$ , which is detrimental to these bacteria. Shallow accumulations often show evidence of oxidation, either from atmospheric oxygen penetrating to the reservoir or from oxygen dissolved in surface waters that contact the oil [67]. Basal tar mats are

layers of heavy oil or asphaltic tar at or just below the water/oil contacts of producing fields and are often taken as direct evidence for bacterial or water attack. Bacterial and water caused degradation of petroleum can commence, theoretically, at any stage of maturation of the oil. A number of hydrocarbon compounds and their preferential order of removal during biodegradation are listed. The end products of alteration are partially dependent on the initial composition of the petroleum and also heavily degraded oils often are difficult or impossible to produce [68].

Geological conditions for recoverability of heavy oil are comparable to those for lighter conventional oil and include: depth, presence of faults, hydrologic continuity of the reservoir rocks, clay content, trap configuration, size of the reservoir, and whether the reservoir is a single layer or lens or a set of stacked bodies.

The geologic setting for much of the production of heavy oil is within fault zones, usually at the up-dip limits of strata within a hydrocarbon province.

The majority of all heavy oil fields occur at depths of less than 5,000 ft, although deposits are exploited at depths as deep as 10,000 ft [69].

#### 2.2.2.2. Physical and Chemical Composition of Heavy Oil

The difference between heavy, low-gravity oil and light, high-gravity oil is largely a matter of chemistry; low-gravity oil is comprised of molecules with more than 15 carbon atoms (>C<sub>15</sub>; 15 is the number of carbon atoms), whereas high-gravity oil is comprised of lighter weight organic molecules (<C<sub>15</sub>) [64].

Heavy and light oil differ in viscosity and density. By definition heavy oil has a viscosity between 100 and 10,000 centipoises or a density in the range of 934-1000 kg/m<sup>3</sup> at 15.6°C (60°F) [64]. Density is influenced by chemical composition and is used to give rough estimations of the nature of petroleum and petroleum

products. Heavier, more complex molecules require more complex refining to produce gasoline, diesel, and heating oil.

Low-gravity oils contain heavy molecular components, such as asphaltenes and aromatics, and NSO (nitrogen, sulfur, and oxygen) compounds, primarily due to the selective removal of lighter compounds such as straight-chain compounds, such as normal alkanes and isoprenoids, early in the degradation process.

### 2.2.2.3. Heavy Oil Potential and Utilization in the World

World heavy oil reserves exceed those of light oil, and interestingly are concentrated in the Western Hemisphere. Yet heavy oil contributes a small fraction of world oil production. The challenge is that heavy oil is difficult and expensive to produce. Heavy oil requires massive amounts of heat to make it mobile/less viscous and able to be produced [33].

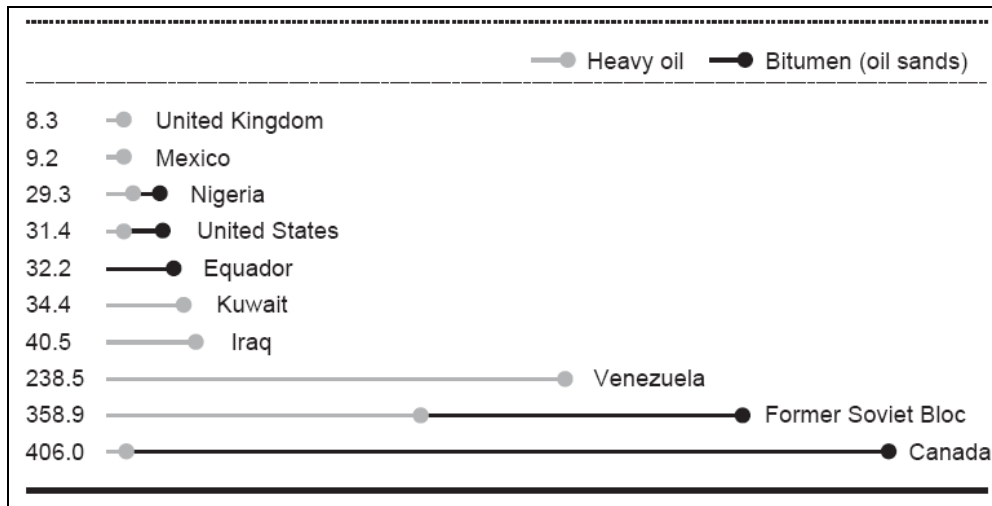


Figure 2.9 World oil sands (bitumen) and heavy oil resources, in billions of cubic meters [33].

Considerable potential heavy oil reserves are changed 500 to 1000 Gb (OIP). This amount is equivalent to 50-100% of worldwide conventional oil reserves. These heavy oil fields are mainly (80%) in North and South America (Figure 2.9).

The world's largest heavy oil and tar accumulations are the Orinoco Heavy Oil Belt of Eastern Venezuela (Tertiary/Cretaceous reservoirs) and the Athabasca and Cold Lake deposits of Alberta (Cretaceous reservoirs). These two accumulations contain 2.4 trillion barrels of oil in place which account for more than 80% of the world's heavy oil reserves [33].

#### 2.2.2.4. Heavy Oil in Turkey

There are not huge and well-known resources of heavy oil, and extra-heavy oil in Turkey. But medium and heavy oils are produced about 80 % of total oil fields in Turkey [70]. Some heavy oil fields and their characterization are given in Table 2.5.

Table 2.5 Field characterization of heavy oil reserves in Turkey [71, 72, 73, 74]

Field	Lithology	T <sub>res</sub> (°F)	P <sub>res</sub> (psia)	φ (%)	k (md)	S <sub>w</sub> (%)	°API	γ	μ (cp)	FWS (*10 <sup>4</sup> ppm)	OOIP(*10 <sup>4</sup> bbbl)
Batı Raman	L	129	1750	18	58	21	14.95	0.97	52000	4-16	1850
Raman	L	140	1300	6-22	2-50	11-19	15-19	0.94	22-35	1-7	600
Magrip	L	179	2320	6	3	31	18.5	0.94	33	0.3-1	53
Çamurlu	L	115	1700	21	40	18	12.2	0.98	700	10 <sup>-5</sup>	378
Batı Kozluca	L	132	1990	16-25	100	23	12.6	0.98	500	7	99
Güney Dinçer	DL	145	2140	14	50	27	15.5	0.96	58	2.5	54
İkiztepe	L	120	1840	15-23	50-400	12-30	10-12	0.99	936	4.5	53
Sinan	L	124	2085	25	10	25	15.7	0.96	300	0.4-21.5	53
Germik	L	160	2415	15	9	22	18.8	0.94	26	4-9.5	24
Garzan	L	160	1405-1770	10.8-12.6	4.7-15.7	20-30	26	0.94	33	0.3-1	53

\*L: Limestone, DL: Dolomitic Limestone, FWS: Formation Water Salinity, OOIP: Original Oil In Place

#### 2.2.2.4.1. Batı Raman Oil Field

Batı Raman field is the largest oil field in Turkey with estimated original oil in place of 1.75 billion STB [75]. It is located in southeast Turkey (Figure 2.10) and contains low-pressure, low-gravity (10 to 13°API) oil at an average depth of 4,300 ft. The producing formation is the Garzan Limestone, a very heterogeneous carbonate of Cretaceous age. The reservoir fluid is a very heavy crude oil, having an API gravity ranging from 9.7 to 15.1 and a viscosity ranging from 450 to 1000 centipoises at reservoir conditions [71]. Average matrix porosity is 18 %, with

mainly vugs and fissures, and secondary porosity is 1 to 2%. The typical matrix permeability by core analysis is 10 to 100 md; however, well tests show effective permeabilities in the range of 200 to 500 md, confirming the contribution of secondary porosity [72].

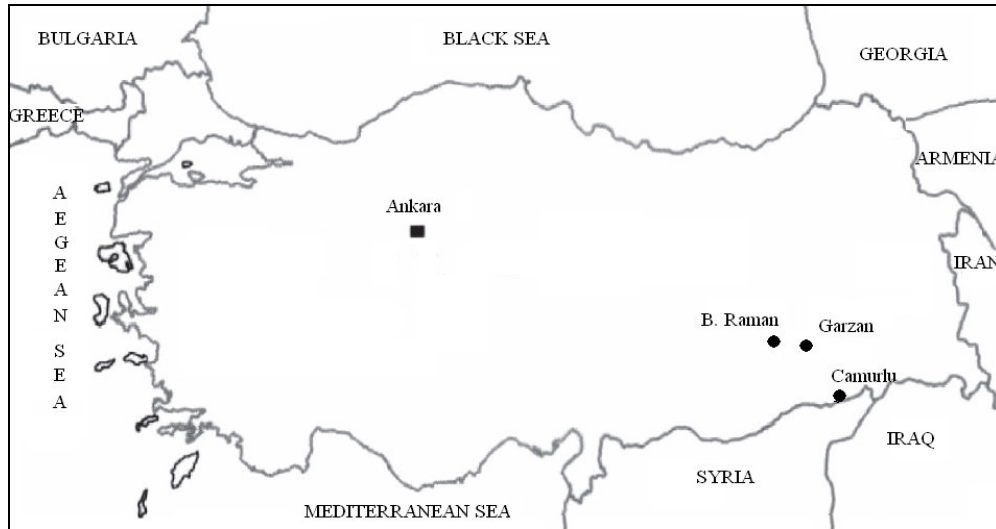


Figure 2.10 Location of crude oil fields used in this study.

The main (primary) production mechanism is rock and fluid expansion. Water drive appears to be insignificant except for a very weak aquifer influence at the central north flank wells. The solution GOR is 18 scf/STB (3.24 stb m<sup>3</sup> /stock-tank m<sup>3</sup>), resulting in a low bubble point pressure of 160 psi (1103.1 kPa). Before EOR application, the reservoir pressure did not decrease below the bubble point pressure; therefore, in practice, there had been no solution gas-drive mechanism. The original reservoir pressure was - 1,800 psi (- 12411 kPa), which dropped to an average pressure of 400 psi (2758 kPa) after cumulative production of 30 million STB (4.77 x 10 stock-tank m<sup>3</sup>) before CO<sub>2</sub> production of 30 million STB (4.77 x 10 stock-tank m<sup>3</sup>) before CO<sub>2</sub> application [73].

The field originally was developed on 62-acre/well (25-ha/well) spacing. Before the project began, 65 active producers were pumping, with a total production rate of 1,600 STB/D [254.4 stock-tank m<sup>3</sup>/d] compared with the 1969 peak rate of 9,000 STB/D (1431 stock-tank m<sup>3</sup>/d). Initially, well production rates were up to 400 STB/D (63.6 stock-tank m<sup>3</sup>/d); this decreased to an average of 25 STB/D (3.97 stock-tank m<sup>3</sup>/d) before treatment. Table 2.5 summarizes reservoir and fluid characteristics [73].

Primary recovery prospects were low because of unfavorable oil properties (such as low API gravity, low solution gas, and high viscosity), low reservoir energy, and the type of driving mechanism. It was estimated that ultimately 1.5% OOIP could be produced without an EOR application [73].

The reservoir history and unfavorable properties caused rapid declines in reservoir pressure and production which suggested the need for a suitable EOR method to increase ultimate recovery from this vast reservoir. Since 1968, several EOR pilot tests have been conducted, including steam huff 'n' puff, steamdrive, air injection, and waterflooding [73].

The results of extensive laboratory, modeling, and engineering studies; the presence of a CO<sub>2</sub> reservoir 55 miles (89 km) from Bati Raman; and economic considerations led Turkish Petroleum Cooperation (TPAO) to apply an immiscible CO<sub>2</sub> huff-'n'-puff-type EOR method to the field [73].

Through 2003, 5 % of the reserves had been produced, which is still an unexpectedly low value. Production rate has declined drastically since 2000. TPAO is seeking the most applicable methods to impede or reverse the decline [72].

#### 2.2.2.4.2. Camurlu Oil Field

The Camurlu Oil field located in the South East of Turkey close to the Syrian border has been discovered in 1975 (Figure 2.10) [76].

The producing formations are located in three separate layers:

- the shallowest one, which is about 1250 m deep, is the light-brown limestone formation of Alt Sinan. The total formation thickness is approximately 150 m including 60 m which contain a heavy viscous oil (10-12 °API) below the gas cap,
- under the Alt Sinan formation, at a depth of about 1400 m, is a dolomitic formation showing local producing capacities of heavy oil (10-12 °API) with a high watercut: Beloka,
- the deepest layer, known as Mus formation, around 2200 m deep, in the Trias, is a gas-condensate reservoir which contains 73 % CO<sub>2</sub>, it is also limestone having a good producing potential [76].

The gas cap at the top of Alt Sinan formation covers a large area. Wells producing in the oil zone of this formation have had to be shut-in due to their low oil productivity (oil viscosity is 284 cp under reservoir condition) or to the breakthrough of gas attributed to gas coning [76].

Wells completed and produced in the Beloka formation were shut in as well on account of their high watercut. For this reason the development of an EOR process has been restricted to the Alt Sinan formation [76].

Oil production started in May 1976, with average initial rate of 100 STB/day for most wells. Production rates gradually dropped to 15-20 STB/day within 2 years with a small watercut. At the end of December 1986 the cumulative oil production was 689,546 STB [74].

#### 2.2.2.4.3. Garzan Oil Field

The Garzan oil field is located in southeast-central Turkey Figure 2.10. The structure is a double plunging anticline bordered by a major reverse fault

extending along the southern flank. The age of the Garzan formation is cretaceous, comprised of carbonates of a rudist build-up complex. Oil field contains 24 degree API ( $0.91 \text{ g/cm}^3$ ) oil with a reservoir viscosity of 6.75 cp. Reservoir was initially highly undersaturated lists basic reservoir data for Garzan [77].

## CHAPTER 3

### STATEMENT OF THE PROBLEM

The world's heavy oil and oil shale resources are about 1500 billions of cubic meters [33]. When the depletion of conventional petroleum reserves and increase of hydrocarbon fuel demands are considered together, the essential of the investigation of these reserves recovery can be understood easily.

The most effective way to recover oil shale and heavy oil resources is to reduce the viscosity. Thermal methods are the best methods to achieve the viscosity reduction.

Therefore, in this study, two different thermal methods were used; retort and microwave, for the recovery of 4 different oil shale (Bolu-Himmetoğlu, Bolu-Hatıldığ, Kütahya-Seyitömer, and Niğde-Ulukışla) and 3 different crude oil (Batı Raman, Çamurlu, and Garzan) samples. While retort is a well-known heating method its applicability is restricted due to the economic reasons. Microwave is a new and quick technology.

The main objectives of this thesis are listed below:

- To determine the microwave heating efficiency both for the crude oil and oil shale samples by considering the effect of porosity, water saturation, wettability, and operation time.
- To define the retort heating efficiency for the oil shale samples by optimizing process times, heat and soak periods existing and durations.
- To investigate the rheology and oil production enhancement effects of 3 different iron powders (Fe, Fe<sub>2</sub>O<sub>3</sub>, and FeCl<sub>3</sub>) at 3 different doses (0.1%, 0.5%, and 1%) by discussing the catalytic and magnetic effects of iron powders.

- To obtain shale oil viscosities, that are believed to be impossible to obtain at the laboratory conditions, by using a reservoir simulator, CMG, STARS.
- To model the retort process for oil shale and crude oil samples for field scales by using the electrical heating option of CMG, STARS conducted with experimental techniques.
- To model microwave results analytically in order to derive the temperature distribution, that occurs during the microwave heating process.
- To evaluate the feasibility of electrical and electromagnetic heating methods.

## CHAPTER 4

### MATERIALS & METHODS

In this study, the recovery characteristics of 4 different oil shale and 3 different crude oil samples were examined, experimentally and numerically. For this purpose, the efficiency of two of the alternative thermal heating methods was compared. As oil shale samples, Bolu-Himmetođlu (OS1), Bolu-Hatıldađ (OS2), Kütahya-Seyitömer (OS3), and Niđe-Ulukıřla (OS4) oil shales and as crude oil samples Batı Raman, amurlu and Garzan crude oils, and as thermal methods electrical heating and electromagnetic heating methods were used.

#### 4.1. Oil shale and crude oil samples

The physical and chemical properties of the oil shale and crude oil samples used in this study are given in details in Table 4.1 and Table 4.2.

Table 4.1 Oil shale properties used in this study [63]

Deposit (Province)	Calorific value (kcal/cal)	Average oil yield	Total Sulfur	Oil shale resource	Shale oil resource
		Wt %		*10 <sup>6</sup> tons	
Himmetođlu (Bolu)	1390	4,6	0,9	2500	115
Hatıldađ (Bolu)	774	5,3	1,3	547	29
Seyitömer (Kütahya)	860	5,0	0,9	1000	50
Ulukıřla (Niđe)	851	-	-	130	6

Both retort and microwave heating methods were applied to the crushed form of oil shale samples.

Table 4.2 Reservoir properties of crude oils used in this thesis [8, 73, 76]

Field	Units	Bati Raman	Camurlu	Garzan
Lithology	-	Limestone	Limestone	Limestone
T <sub>res</sub>	°F	129	115	179
P <sub>res</sub>	psia	1750	1700	337
Rock Compressibility	kPa <sup>-1</sup>	5.44*10 <sup>-7</sup>	5.44*10 <sup>-7</sup>	5.44*10 <sup>-5</sup>
RHC	J/m <sup>3</sup> .°C	2315	2198	2226
RTC	J/m.day.°C	111888	111888	111888
Depth	m	1310	800	700
MW	g/mole	1342	1000	1000
BHP	psia	400	400	290
Porosity	%	18	14	6
Permeability	md	58	40	3
S <sub>wi</sub>	%	21	23	31
API Gravity	-	13	12.2	18.5
Specific Gravity	-	0,9772	0,985	0.9433
Viscosity	cp	592	700	33
FWS (*10 <sup>4</sup> )	ppm	4-16	10	0.3-1
OOIP	*10 <sup>6</sup> STB	1850	377,437	53

RHC: Rock Heat Capacity RTC: Rock Thermal Conductivity, BHP: Bottom Hole Pressure S<sub>wi</sub>: Initial Water Saturation

Crude oil samples were prepared differently for viscosity determination experiments and the experiments conducted with microwave oven. Viscosity measurements were carried out for dead crude oil samples and crude oil samples after the addition of iron powders. Sample preparation for the microwave experiments conducted with crude oils was different. Crude oil samples were mixed with crushed limestone samples at different porosities (25.86%, 34.10%, and 38.95%). In these set of experiments, different wettabilities (water wet, oil wet, and mixed wet) and water saturation values (20%, 40%, and 60%) were

tested. Water salinities were prepared according to the values given in Table 4.2 by using NaCl.

While preparing water wet conditions, limestone samples were mixed with water first, then the oil was added at predetermined saturation values. During the preparation of oil wet conditions, firstly, oil added to the limestone samples and samples were waited for one day, then water was added to the samples. Mixed wet condition is the combination of water and oil wet conditions.

Both oil shale and crude oil samples were kept at room temperature during the experimental studies.

## **4.2. Experimental Setup and Procedure**

### **4.2.1. Viscosity Experiments**

Viscosities of crude oil samples were determined by using Haake viscometer. Haake viscometer is a rotational type viscometer (Figure 4.1) which consists of three different sensors (NV, MV, and SV) for the determination of different oil viscosities. The sensor system is classified as a coaxial cylinder sensor system with two gaps for shearing the sample on the inside and on the outside of the rotor. These sensor systems inherit a temperature vessel, which is connected to an accurate thermal liquid circulator. The selection of the sensor is made according to the viscosity of the crude oil.



Figure 4.1 Haake viscometer

#### 4.2.2. Retort Experiments

Retort experiments were conducted only for oil shale samples. This set-up consists of stainless steel cylindrical body that houses the samples with inner diameter of 10 cm and height of 20 cm. The cylindrical body is wrapped with a band heater and this heater is connected to a temperature controller. A thermocouple is placed at the center of the sample holder and it is connected to the temperature controller. The sample holder is placed in another cylindrical cell which has 20 cm inner diameter and 25 cm height. In order to minimize the heat losses, the space between two cylinders is filled by a heat insulator called perlite (Figure 4.2).

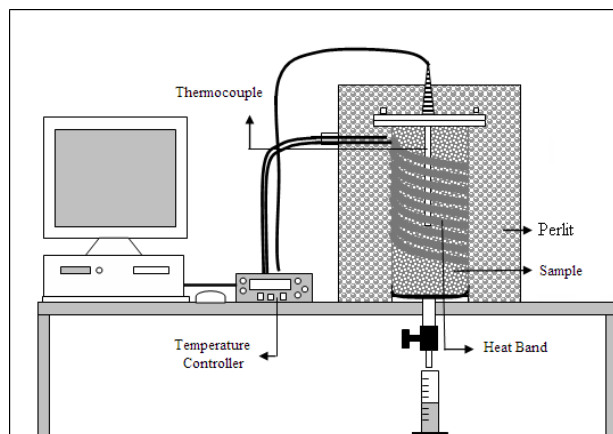


Figure 4.2 Retort set-up

A commercial software was used to record the temperature values continuously. By the help of this software and a band heater, temperature of the system could be increased to any desired temperature value.

The performance of oil shale retorting is affected by heating period, soaking period and the duration of these periods [78, 79]. Therefore, firstly, heating and soaking periods were optimized. Optimization processes were carried out only for Niğde-Ulukışla oil shale (OS4) by using eight different operation durations. The optimum operation conditions determined for Niğde-Ulukışla oil shale were used for the other oil shale samples.

During the experiments, production data in terms of oil and water production, and temperature at the center of the cell were recorded continuously. Produced oil and water are collected in a graduated cylinder. Furthermore, gas emissions were detected with a multi gas monitor (Q-RAE, Multi-Gas Monitor) in terms of  $O_2$ ,  $CO$ ,  $H_2S$ , and  $CH_4$ .

#### 4.2.3. Microwave Experiment

Microwave experiments were conducted by using two conventional kitchen microwave ovens; BOSCH HMT 72G420 and VESTEL MD-GDX23A. Experimental set-up is shown in Figure 4.3. The input and output powers of the ovens are 1400 W and 900 W, respectively. The frequency of both ovens is 2450 MHz. Two different sample holders were used during the microwave heating experiments; a glass beaker and a graphite cell. The oil shale samples were placed into 500ml beakers, and limestone-crude oil mixtures were placed into graphite cell to create a porous medium. Sample holders were put inside the oven under a glass funnel. A special thermocouple which is capable of measuring high temperatures ( $\approx 1500$  °C) was placed at the center of the samples through glass funnel. Glass funnel enabled proper collection of emitted gases by moving them to the inlet of the gas detector. This setup enabled more accurate measurements of the gas concentrations and prevented direct contact of toxic gases with magnetron of the ovens. Experimental setup was controlled with the same software that was used in retort process, such that the temperature values detected with the thermocouple could be recorded continuously.

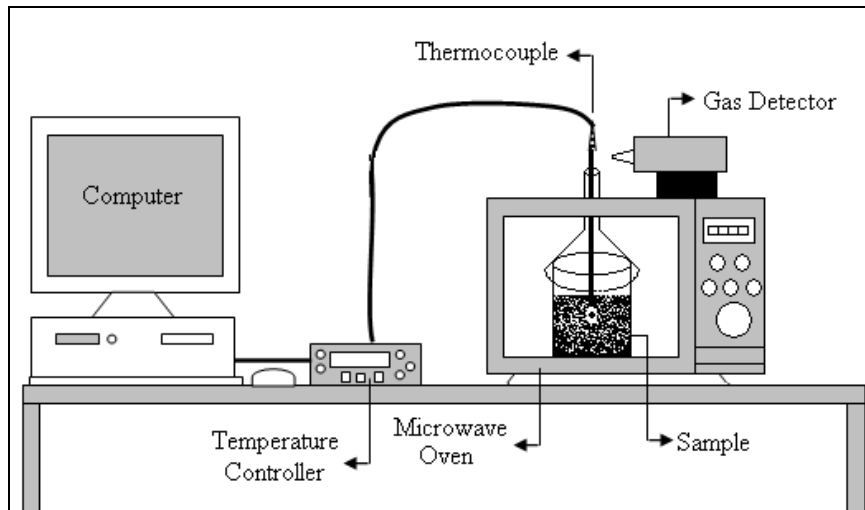


Figure 4.3 Microwave set-up

#### 4.2.4. Enhancement of the Processes

In order to enhance the efficiency of retort and microwave heating methods, some metallic additives were used. As metallic additives iron powders (i.e.; Fe, Fe<sub>2</sub>O<sub>3</sub>, and FeCl<sub>3</sub>) were used. These metallic additives were added to the samples as powdered form. Optimization of iron powders types and doses for each sample by considering oil production or viscosity reduction were conducted.

The role of iron powders to increase the oil production in microwave and retort methods are different [80, 81]. While iron powders are used to increase the thermal conductivity of the samples and to achieve catalytic cracking in retort process, they are used as microwave receptors in microwave experiments [80].

#### 4.2.5. Numerical Simulation

Numerical simulation studies were carried out for retorting of crude oil and oil shale samples. These simulation studies were performed using the electrical heating option of the commercial simulator; Steam, Thermal, and Advanced Processes Reservoir Simulator (STARS; CMG, 2007). The domain was discretized into 20x1x10, 3-D radial blocks of varying size in the radial direction and constant in the vertical direction. The dimensions of the reservoir for the laboratory and field cases are given in Figure 4.4.

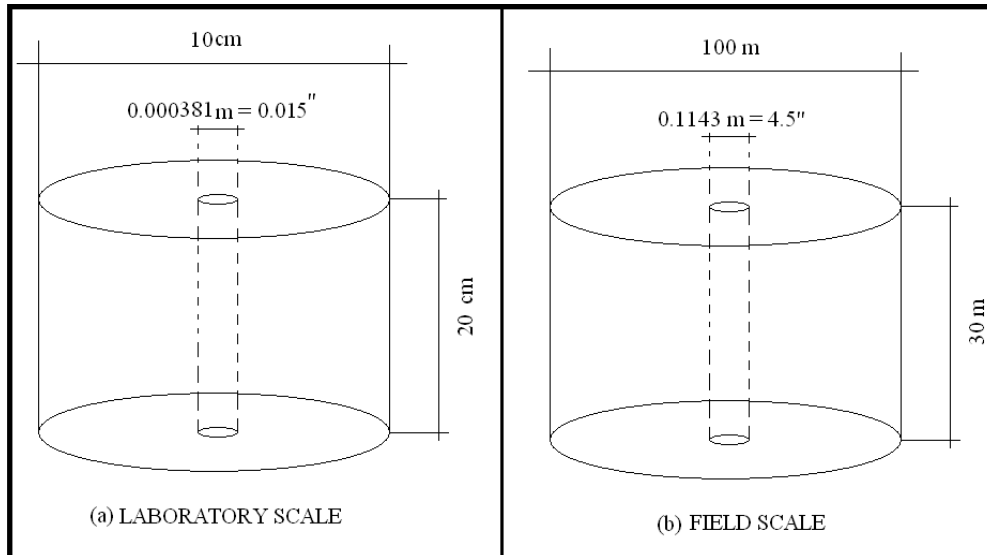


Figure 4.4 Scales used for the simulation of laboratory results and fields

In order to obtain oil production and temperature distribution data numerically, some input data are required. These input data are porosity, permeability, thermal conductivity, rock heat capacity, rock compressibility, viscosity and relative permeability values of the porous medium.

The output data in the simulation were temperature distribution and oil production. These data were also obtained experimentally at the laboratory conditions for oil shale samples. For oil shale and crude oil samples all the required input data, except from viscosity variation with temperature, were taken from literature. At the laboratory conditions, while the determination of viscosity variations with temperature is very easy for the heavy oil samples, because of high viscous characteristics of shale oils, it is very difficult to determine the viscosity of the shale oil experimentally.

In the numerical studies conducted with conceptual oil shale samples, since the output data were obtained experimentally, the temperature and oil production data were matched with the laboratory results by using the literature data and assumed viscosity-temperature data. By using the verified viscosity data, field

cases for oil shale samples were simulated to obtain oil production data. Since all input data were obtained experimentally and by the help of literature data, heavy oil reservoir data were directly simulated for field cases. During the simulation of field cases, power of the system and the number of heaters were optimized by considering both oil production and economics of the study. The calculation method is explained in detail in Chapter 5 for numerical simulation studies.

## CHAPTER 5

### THEORY

#### 5.1. Heat Transfer Mechanisms

While heating principles of these two processes have some similarities primarily, they do differ in some aspects. In order to explain the heating mechanisms of these methods, one should start with the basic heat transfer equation which can be written as [82];

$$[A] + [B] + [C] = [D] + [E] \quad (5.1)$$

Where;

A is diffusive energy, B is heat generation, C is energy used in internal evaporation, D is rate of energy accumulation, and E is convective energy flow.

For cylindrical coordinates, Equation 5.1 can be written as;

$$A = \frac{1}{r} \frac{\partial}{\partial r} \left( r \frac{\partial T}{\partial r} \right) + \frac{1}{r^2} \frac{\partial^2 T}{\partial \theta^2} + \frac{\partial^2 T}{\partial z^2} \quad B = \frac{q^*}{k} \quad C = \frac{h_{fg,i}}{k} \quad (5.2)$$
$$D = \frac{1}{\alpha} \frac{\partial T}{\partial t} \quad E = \frac{u}{\alpha} \left[ \frac{\partial T}{\partial r} + \frac{1}{r} \frac{\partial T}{\partial \theta} + \frac{\partial T}{\partial z} \right]$$

$$\alpha = \frac{k}{\rho c_p} \quad (5.3)$$

Where;

\*  $q$  is the rate of energy generation per unit volume,  $W/m^3$ ,  $\alpha$  is the thermal diffusivity,  $W/m.K$ ,  $T$  is temperature,  $K$ ,  $h_{fg, i}$  is latent heat of vaporization,  $J/kg$ ,  $k$  is thermal conductivity,  $W/mK$ ,  $u$  is velocity,  $m/s$ ,  $\rho$  is mass density,  $kg/m^3$ , and  $c_p$  is specific heat at constant pressure,  $J/kg. K$

Heating mechanism for all of the thermal processes can be explained by Equation 5.1. The only parameter different from process to process is rate of energy generation. The rate of energy generation can be explained as combustion for retort experiments and microwave heat generation for microwave experiments [83, 84, 85]. Combustion can be explained by enthalpy [83]. Microwave heat generation can be explained by Maxwell equation [84].

Heat transfer from a microwave source to a porous medium can be described with the Equations 5.4 to 5.14. Temperature distribution as a result of microwave irradiation can be then obtained by the heat equation with the following modification.

$$\rho c_p \frac{\partial T}{\partial t} + \rho_f c_{pf} \bar{v}_f \bar{\nabla} T = \bar{\nabla} \cdot (\lambda_c \bar{\nabla} T) + P \quad (5.4)$$

where  $\rho$ ,  $c_p$  and  $\lambda_c$  are the density, specific heat capacity and thermal conductivity of the medium, respectively;  $\rho_f$ ,  $c_{pf}$  and  $\bar{v}_f$  are the density, specific heat capacity and superficial velocity of the fluid phase and  $P$  is the electromagnetic dissipated power per unit of volume ( $P$ ), based in Maxwell's equations, is a function of the electric field  $\bar{E}$  and the effective conductivity ( $\sigma$ ) of the medium and it is represented by the following expression [84]:

$$P = \frac{\sigma + \omega \epsilon \tan \delta}{2} |\bar{E}|^2 \quad (5.5)$$

The energy efficiency of microwave heating is affected by the medium dielectric properties and their variations while heating. The electromagnetic heating process is directly related with the frequency employed ( $\omega=2\pi f$ ). For the low frequencies ( $\sigma \gg \omega \epsilon \tan \delta$ ), ionic heating is dominant. For high frequency cases ( $\sigma \ll \omega \epsilon \tan \delta$ ), dielectric heating is the main thermal process. In both cases the dissipated power distribution and consequently the temperature behavior, depend directly on the electric field distribution that in turn depends on the electromagnetic applicator used. For practical reasons the applicator must radiate in all directions of the hydrocarbon medium surrounding the wellbore [84].

Assuming symmetry in radial homogeneous conducting medium, no heat losses to the adjacent formations and strictly radial pressure distribution electromagnetic radiation propagation will be absorbed following Equation 5.6 [84].

$$\frac{d\Phi(r)}{dx} = -\left(\alpha + \frac{1}{r}\right)\Phi(r) \quad (5.6)$$

Where  $\Phi(r)$  is power density (watts/cm<sup>2</sup>) and  $\alpha$  is the power absorption coefficient (cm<sup>-1</sup>) that depends on the physical properties of the absorbing medium in the following manner [84].

$$\alpha = 0.02 \sqrt{\left(\frac{\omega^2 \mu \epsilon}{2}\right) \left(1 + \left(\frac{\sigma}{\omega \epsilon}\right)^2\right)^{\frac{1}{2}} - 1} \quad (5.7)$$

Where  $\sigma$  is conductivity (mho/meter),  $\mu$  is permeability (H/meter),  $\epsilon$  is permittivity (F/meter) and  $\omega$  is angular frequency ( $2\pi \times$  frequency). The total power radiated across the radius  $r$  for a cylinder of height  $h$  can be defined as Equation 5.8.

$$P(r) = 2\pi h \Phi(r) \quad (5.8)$$

Differentiating above equation by  $r$  and solving it gives

$$P(r) = P_0 e^{-\alpha(r-r_0)} \quad (5.9)$$

Combining this equation with mass balance equation due to oil moving in and out of a cylindrical element at temperature  $T(r)$  gives the following equation.

$$\frac{\partial T}{\partial t} = \frac{1}{2\pi h \rho_i S_i} \left( \frac{\alpha P_0 e^{-\alpha(r-r_0)}}{4.18} + \rho_o q_o S_o \frac{\partial T}{\partial r} \right) \quad (5.10)$$

Steady state temperature distribution due to microwave radiation is then obtained as:

$$T(r) = T_o + \frac{P_0 e^{-\alpha(r-r_0)}}{4.18 \rho_o q_o S_o} \quad (5.11)$$

Transient temperature in the case of steady flow to the wellbore is given by

$$T(r,t) = T_o + \frac{P_0 e^{\alpha r_0}}{4.18 \rho_o q_o S_o} \left( e^{-\alpha r} - e^{-\alpha \sqrt{r^2 + 2At}} \right) \quad (5.12)$$

Where

$$A = \frac{\rho_o q_o S_o}{2\pi h \rho_i S_i} \quad (5.13)$$

Finally for the no flow case taking the limit of equation 5.12 as the flow rate goes to zero gives the following result.

$$T(r,t) = T_o + \frac{\alpha P_0 e^{-\alpha(r-r_0)}}{2\pi h (4.18 \rho_o S_o)} \quad (5.14)$$

## 5.2. Numerical Simulation

In theory, the full form of Maxwell's equations, along with appropriate boundary conditions, may be solved to find the electric field for any physical configuration at

any frequency. The following simplifying assumptions are used in the CMG-STARS model to make the computations more tractable [86]:

1. For anisotropic electrical conductivity, the principal axes of the conductivity tensor are parallel to the coordinate axes. Anisotropic conductivities arise when thin silts or shales are intermixed with oil-bearing matrix. With horizontal bedding, for example, current flows through the different materials in parallel in each horizontal direction but in series in the vertical direction. The conductivity tensor assumption above is usually preferable to the expense of modeling each individual material bed with a separate grid block layer [86].

2. The electrical properties (conductivity, permittivity and magnetic permeability) do not depend on the strengths of the electric or magnetic fields [86].

3. The quasi-static approximation is used, whereby the smallest wavelength resulting from application of a single-frequency potential is much larger than the largest physical length in the reservoir. This allows us to neglect electric fields that are produced by changing magnetic fields. The wavelength of a 60 Hz field will depend on the electrical conductivity of the formations surrounding the electrodes [86].

4. Displacement current can be neglected if the potential frequency used is low enough. This allows expressing the electric field in terms of a scalar electrical potential. For oil sand this assumption is well justified below a potential frequency of 1 MHz, and so is valid at 60 Hz. In general the electrical potential may be a phasor, with real and imaginary parts [86].

#### 5.1.1. Current Continuity Equation

With the above assumptions and Ohm's Law, the electric potential may be solved from the current conservation equation [86].

$$\nabla \cdot (\sigma \nabla \psi) = q \quad (5.15)$$

The electric potential phasor  $\psi$  is  $\psi_R + \mathbf{j}\psi_I$  where  $\psi_R$  and  $\psi_I$  vary in space and  $\mathbf{j}^2 = -1$ . The electrical source term phasor  $q$  is  $q_R + \mathbf{j}q_I$ . The electrical conductivity  $\sigma$  is a diagonal tensor, with no imaginary components since the formation has no capacitance or inductance. The differential operator is real, so equation 5.15 can be decoupled into two separate equations [86].

$$\nabla \cdot (\sigma \nabla \psi_R) = q_R \quad (5.16)$$

$$\nabla \cdot (\sigma \nabla \psi_I) = q_I \quad (5.17)$$

In the case of a three-dimensional Cartesian grid, the equation for real components is;

$$\frac{\partial}{\partial x} \left[ \sigma_x \frac{\partial \psi_R}{\partial x} \right] + \frac{\partial}{\partial y} \left[ \sigma_y \frac{\partial \psi_R}{\partial y} \right] + \frac{\partial}{\partial z} \left[ \sigma_z \frac{\partial \psi_R}{\partial z} \right] = q_R \quad (5.18)$$

There is a similar equation for the imaginary components. Note that  $\sigma$  depends on temperature and phase saturations, so that  $\sigma$  and  $\psi$  may vary slowly with time. This dependence couples the current equations and hence the electrical potential to the fluid and reservoir conditions [86].

If all source terms have  $q_I = 0$  the result is  $\psi_I = 0$  everywhere, in which case equation 5.17 does not need to be solved. This applies to non-alternating as well as single-phase alternating cases. For alternating current cases  $\psi$  is the rms (root-mean-square) potential, allowing the same formulas to be used for both direct and alternating cases [86].

### 5.1.2. Heat Generation from Ohmic Losses

The heating rate due to electrical conduction is

$$Q = \sigma_x \left[ \frac{\partial \psi_R}{\partial x} \right]^2 + \sigma_y \left[ \frac{\partial \psi_R}{\partial y} \right]^2 + \sigma_z \left[ \frac{\partial \psi_R}{\partial z} \right]^2 + \sigma_x \left[ \frac{\partial \psi_I}{\partial x} \right]^2 + \sigma_y \left[ \frac{\partial \psi_I}{\partial y} \right]^2 + \sigma_z \left[ \frac{\partial \psi_I}{\partial z} \right]^2 \quad (5.19)$$

This heating rate couples the fluid and reservoir conditions to the electrical potential [86].

### 5.1.3. Mathematical Model Used by STARS

#### 5.1.3.1. Electrical Conductivity

Electrical conductivities should be defined as  $\sigma_{w,p}(T)$  for water phase,  $\sigma_{o,p}(T)$  for oil phase,  $\sigma_{s,p}(T)$  for solid phase and  $\sigma_{r,p}(T)$  for rock/matrix for each grid block in three directions ( $p=l, j, k$ ). The water phase value has possible composition dependence, which is expressed as;

$$\sigma_{w,p}(T) = \sum_i w_i \sigma_{w,i,p}(T) \quad (5.20)$$

Where  $w_i$  is water mole fraction and  $\sigma_{w,i,p}(T)$  is electrical conductivity, both of aqueous component  $i$ . The water phase value has an additional dependence on fluid porosity  $\phi_f$  and water saturation  $S_w$  from Archie equation for example,

$$\sigma_{w,p}(T, \phi_f, S_w) = \sigma_{w,p}(T) \bullet \left[ \phi_f^{1.37} \frac{S_w^2}{0.88} \right], p = i, j, k \quad (5.21)$$

The solid phase value has possible composition dependence

$$\sigma_{S,p}(T) = \sum_i (c_i / c_s) \sigma_{S,i,p}(T) \quad (5.22)$$

Where  $c_i$  is concentration and  $\sigma_{s,i,p}(T)$  is electrical conductivity, both of solid component  $i$ , and  $c_s$  is the sum of all the  $c_i$ .

The bulk electrical conductivity is obtained from volume-weighted averaging

$$\sigma_p = \sigma_{w,p}(T, \phi_f, S_w) + \sigma_{r,p}(T) \cdot (1 - \phi_v) + \sigma_{s,p}(T) \cdot (\phi_v - \phi_f) + \sigma_{o,p}(T) \cdot \phi_f \cdot S_o \quad (5.23)$$

where  $\phi_i$ , fluid porosity,  $\phi_v$ , void porosity,  $S_w$ , water saturation and  $S_o$ , oil saturation [86].

#### 5.1.3.2. Current Conservation Equation

Current flow between block  $i$  and block  $i+1$  is separated electrically by two resistances in series. From block center  $i$  to common block face  $i+(1/2)$  the geometric factor (separation divided by cross-sectional area) is  $T_i$  and the bulk conductivity is  $\sigma_i$ , so the resistance is  $R_i = T_i / \sigma_i$ . Similarly for block  $i+1$ ,  $R_{i+1} = T_{i+1} / \sigma_{i+1}$ . The current flow from block center  $i$  to block center  $i+1$  is potential drop over resistance in series [86].

$$I_{i,i+1} = (V_i - V_{i+1}) / (R_i + R_{i+1}) \quad (5.24)$$

Therefore, application of equation 5.15 to a grid block amounts to constraining to zero the sum of the current flow terms like equation 5.24 between that block and all its neighbors. The current equations for all the blocks are solved simultaneously along with the fluid flow conservation equations. Therefore, when the time step is converged the resulting potential field reflects the newest reservoir conditions. The error in current material balance usually is very small [86].

The calculations explained above are only applied to internal block faces, that is, faces between two grid blocks. For external block faces there is no current flow other than specified electric boundaries [86].

#### 5.1.3.3. Boundary Conditions

An electrical boundary is a collection of block faces that are assumed to be at the same potential, and through which current flows into and out of the reservoir. Since a grid block's potential is referenced to the geometrical center of the block, there is a potential drop between a segment of electrical boundary and its host grid block. A boundary face may be external or internal to the grid [86].

Each host block has an additional current term similar to equation 5.24, corresponding to the electrical boundary, with a similar definition for geometric term and resistance. The (real or imaginary) current flow from block center  $I$  to boundary  $b$  is

$$I_{i,b} = \frac{(v_i - v_b)}{R_i} \quad (5.25)$$

The current of each boundary segment is saved for purposes of reporting as well as detection and control of a maximum-current type constraint [86].

##### 5.1.3.3.1. Phase Modes

There are two possible simulation modes with respect to alternating current (AC) phasing. When at least one boundary has an imaginary ( $j$  component) source term, both the real and imaginary components of potential and current are calculated. In this case the model is in multi-phase mode since the imaginary components can model boundaries of different phases. On the other hand, when

there are no imaginary source terms then the j component equation 5.17 is not solved and the run is in single-phase mode. A case containing only real potentials of both signs together can be handled by single-phase mode [86].

#### 5.1.3.3.2. Heat Generation

The heat generation rate in a grid block is the sum of the rates for all the currents flowing in that block. The real current obtained in equation 5.24 for inter-block flow contributes to the heating rate Q in two grid blocks

$$Q_i = (I_{i,i+1})^2 * R_i \therefore Q_{i+1} = (I_{i,i+1})^2 * R_{i+1} \quad (5.26)$$

And the boundary-block flow in Eqn. 5.25 also contributes to the heating rate

$$Q_i = (I_{i,b})^2 * R_i \quad (5.27)$$

There are similar contributions for imaginary current components [86].

To maximize convergence stability, the electrical heating rate is kept constant after a specified Newton iteration. Typically this means that a time step's heating rate is based on the potential field resulting from the previous time step. However, when a boundary constraint is changed the new value is felt immediately in the heating rate after one fluid/heat flow iteration that establishes the new voltage field [86].

#### 5.1.3.3.3. Electrical Operating Constraints

There are four types of operating constraint: maximum potential, maximum current, maximum total heating rate and maximum no-flash heating rate. Each

boundary must have an initial potential assigned to it, but current, total heat rate and no-flash heat rate constraints are optional [86].

All boundaries start operating with their (mandatory) potential constraints, providing after one iteration a base potential field against which all other constraints types are tested. This constraint type treats  $V_b$  in equation 5.27 as known and calculates the resulting  $I_{i,b}$ .

Before it becomes the operating constraint, a current-type constraint is tested by comparing its value against the magnitude of the boundary's summed  $I_{i,b}$ ; when the value exceeds the specified maximum, that boundary is switched to operate on its current type constraint. A current constraint distributes the specified current amongst the boundary's faces according to weighting factors  $(V_i - V_b)/R_i$  and then treats  $I_{i,b}$  in equation 5.27 as known. These weighting factors depend on the last updated (and possibly lagged) resistances and potential field, but the specified total current magnitude for that boundary is honoured. When a current constraint is in effect, the calculated  $V_b$  is tested against that boundary's potential constraint. Since a current type constraint operates by adjusting  $V_b$  as a ratio of its initial value and phase, this constraint type cannot be applied to a boundary with  $V_b = 0$ . Also, a boundary's current type constraint operates best when most or all of the layers contribute current of the same sign, that is, the boundary's potential is either higher or lower than surrounding values [86].

The total heat rate (power) and no-flash constraints are global constraint types which can over-ride any other constraint. Each global constraint operates by adjusting the entire potential field by a scalar factor. This technique is possible because equation 5.15 lacks an accumulation term and resistances do not depend upon potentials, so multiplying all potentials by factor  $x$  results in local (and hence total) heating rates multiplied by  $x^2$ . This adjustment is done at the end of a time step as well as whenever the heating rate is updated. Before a global constraint becomes the operating constraint, heating rates are calculated from the existing potential field and scale factors are obtained. If the scale factor is less than one, that is, the global constraint is more restrictive, operation is switched to that constraint and the scale factor is applied to the entire potential field. A boundary

with zero potential can be used as a reference (ground) since its potential does not change when the factor is applied [86].

Combining the algorithms described above results in automatic switching between constraints depending on changing conditions, so that the most restrictive constraint is used. For example, it is common to specify maximum potentials and total heating rate. At the start the process may be running on maximum potentials, but the heating rate increases as the reservoir heats and conductivity increases. When the maximum total heating rate is reached, non-zero boundary potentials are decreased so that the total heating rate is equal to the maximum specified [86].

### **5.3. Catalytic Cracking**

Cracking is the process whereby complex organic molecules such as kerogens or heavy hydrocarbons are broken down into simpler molecules (e.g. light hydrocarbons) by the breaking of carbon-carbon bonds. Cracking is also referred to as pyrolysis. Pyrolysis can also be defined as the chemical decomposition of organic materials by heating in the absence of oxygen or any other reagents, except possibly steam [87, 88]. Pyrolysis is a special case of thermolysis which is also known as thermal decomposition. Extreme pyrolysis, which leaves only carbon as the residue, is called carbonization. Anhydrous Pyrolysis (occurs whenever solid organic material is heated strongly in absence of oxygen, under pressure and at operating temperatures above 430 °C [806 °F]), Hydrous Pyrolysis (occurs in the presence of water, such as steam cracking of oil), Vacuum Pyrolysis (organic material is heated in a vacuum in order to decrease boiling point and avoid adverse chemical reactions), and Biomass Pyrolysis (accomplished by the biomass particles) are the types of pyrolysis [87, 88].

The rate of cracking or pyrolysis and the end products are strongly dependent on the temperature and presence of any catalysts. Oil refinery cracking processes allow the production of "light" products such as LPG and gasoline from heavier crude oil distillation fractions such as gas oils and residues. Fluid Catalytic

Cracking (FCC) produces a high yield of gasoline and LPG while hydrocracking is a major source of jet fuel, diesel, naphtha and LPG. Thermal cracking is currently used to "upgrade" very heavy fractions ("upgrading", "visbreaking"), or to produce light fractions or distillates, burner fuel and/or petroleum coke. A diagrammatic example of the catalytic cracking of petroleum hydrocarbons is shown in Figure 5.1.

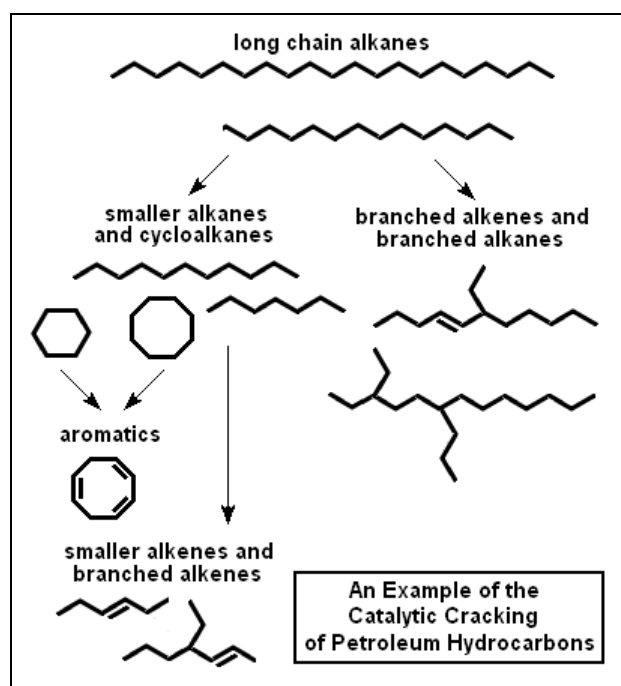


Figure 5.1 Diagrammatic example of the catalytic cracking of petroleum hydrocarbons [87]

The major elements in unconventional oil resources (oil shale and heavy oil) are C, H, N, O, S and possibly Fe from pyrite [87]. The molecular structures of the hydrocarbons make the decomposition of the compounds or changing the structures of the bonds hard.

Catalytic graphitization is one of these methods to change the structures of the bonds by addition of certain inorganic and organic additives to the carbonaceous matrix. The overall effect is to lower the temperature needed to achieve a certain degree of graphitization [88]. Although many data are available on the influence of inorganic catalysts like iron oxide and nickel oxide on the graphitizability of various forms of carbon, like needle cokes, binder pitch and coal tar pitch etc. [88] very little is known about the influence of such additives in the matrix phase during processing of C/C composites. The effect of addition of SiC and TiO<sub>2</sub> powders to non-graphitizable carbonaceous matrices such as furfuryl alcohol and furan resin, during the development carbon/carbon composites have been studied [89]. Boron has been used as catalyst in the non-graphitizable matrix, i.e. polyarylacetylene (PAA) to form PAN fiber based C/C composites. It seems that the catalysts are used to enhance the degree of graphitizability of typically non-graphitizable matrices during processing of C/C composites [90].

The catalytic effect of iron on the gasification reaction has been examined by several investigators but in most of these investigations the amount of iron, as an impurity, in carbon has been kept low (less than 1 %) [91]. The catalytic effect of iron-based catalysts on the coal liquefaction was examined and sulfur-promoted iron oxides and iron sulfides with different atomic ratios of S/Fe are considered to be a very active catalyst for coal liquefaction [92]. After the addition of sulfur-promoted iron oxide, liquefied coal amount increased 20% more than only iron based catalysts used case [92]. Iron sulfide catalysts are considered to be oxidized by water during the coal liquefaction process to convert the surface of the sulfides to surface-sulfate species [92].

In order to explain the mechanisms of both thermal and catalytic cracking simple decomposition should be considered first.

Catalysts generally react with one or more reactants to form an intermediate that subsequently give the final reaction product, in the process regenerating the catalyst [93]. The following is a typical reaction scheme, where  $\overset{\cdot}{C}$  represents the catalyst, A and B are reactants, and C is the product of the reaction:



Although the catalyst is consumed by reaction 5.28, it is subsequently produced by reaction 5.31 (Figure 5.2), so for the overall reaction [93]:

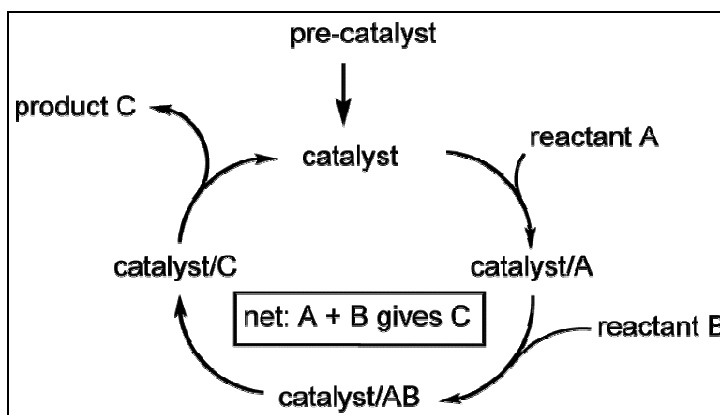


Figure 5.2 Catalytic cycle for conversion of A and B into C [93].

As a catalyst is regenerated in a reaction, often only small amounts are needed to increase the rate of the reaction. In practice, however, catalysts are sometimes consumed in secondary processes [93].

### 5.2.1. Catalysis and reaction energetic

Catalysts work by providing an (alternative) mechanism involving a different transition state and lower activation energy. The effect of this is that more

molecular collisions have the energy needed to reach the transition state. Hence, catalysts can perform reactions that, albeit thermodynamically feasible, would not run without the presence of a catalyst, or perform them much faster, more specific, or at lower temperatures. This can be observed on a Boltzmann distribution and energy profile diagram. This means that catalysts reduce the amount of energy needed to start a chemical reaction [94].

Catalysts do not change the favorableness of a reaction: they have no effect on the chemical equilibrium of a reaction because the rate of both the forward and the reverse reaction are both affected. The net free energy change of a reaction is the same whether a catalyst is used or not; the catalyst just makes it easier to activate [94].

Generic potential energy diagram (Figure 5.3) shows the effect of a catalyst in a hypothetical exothermic chemical reaction  $X + Y$  to give  $Z$ . The presence of the catalyst opens a different reaction pathway (shown in red) with lower activation energy. The final result and the overall thermodynamics are the same [94].

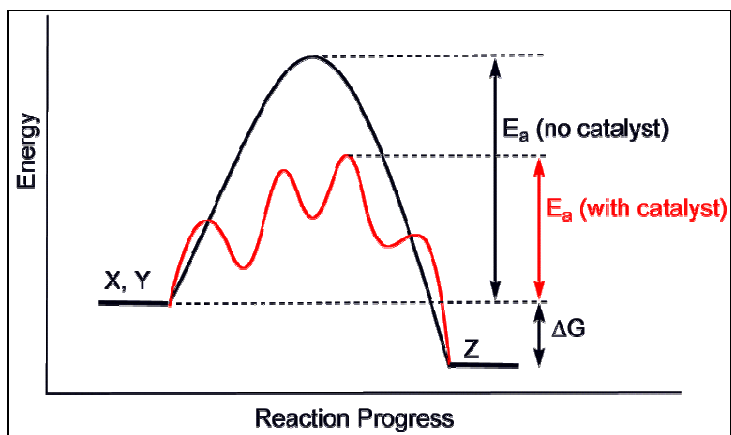


Figure 5.3 Generic potential energy diagram [94].

### 5.2.2. Factors that affect catalytic rates

Catalysis manifests itself in accelerated rates of reactions, and thus many catalytic systems are analyzed with attention to how those rates are affected, beyond the usual parameters that affect all reactions, e.g. temperature, pressure, and concentration. In autocatalysis, a reaction produces catalysts, thus the rates of reactions subject to autocatalysis accelerate with time [94].

Some molecules inhibit catalysis by competing for the active sites. The strongest inhibitors are called poisons. Many catalysts used in petrochemical applications lose activity due to poisoning. Such catalysts are regenerated and reused multiple times to save costs and energy and to reduce environmental impact from disposal of spent catalysts [94].

In order to understand the effectiveness of the catalytic reactions rate equation should be defined;

For a generic reaction Equation 5.33, the simple rate equation (as opposed to the much more common complicated rate equations) is of the form:

$$r = k(T)[A]^m[B]^n \quad (5.33)$$

In this equation,  $[X]$  expresses the concentration of a given X, usually in mol/liter (molarity). The  $k(T)$  is the reaction rate coefficient or rate constant, although it is not really a constant, as it includes everything that affects reaction rate outside concentration such as temperature but also including ionic strength, surface area of the adsorbent or light irradiation [91].

The exponent  $n$  and  $m$  are the reaction orders and depend on the reaction mechanism. The rate equation is a differential equation, and it can be integrated in order to obtain an integrated rate equation that links concentrations of reactants or products with time [91].

By using Langmuir-Hinshelwood or Eley-Rideal rate equations, the catalytic reaction mechanisms can be defined for oil shales or heavy oils [91].

While in Langmuir-Hinshelwood (LH) mechanism reaction occurs between adsorbates (both molecules adsorb and the adsorbed molecules undergo a bimolecular reaction), in Eley-Rideal (ER) mechanism reaction occurs between adsorbate and incoming molecule (only one of the molecules adsorbs and the other one reacts with it directly, without adsorbing).

### 5.2.2.1. Langmuir-Hinshelwood (LH) Mechanism

With LH model, decomposition occurs uniformly across the surface. Products are weakly bound and rapidly desorbed (Figure 5.4). The rate determining step (RDS) is the surface decomposition step.



$$\text{Rate} = r = k \Theta_A \quad (5.35)$$

For Langmuir adsorption

$$r = \frac{kK_p}{1 + K_p} \quad (5.36)$$

There are two limiting cases for LH model;

1. Low pressures/ Weak binding	2. High pressures/ Strong binding
$K_p \ll 1$	$K_p \gg 1$
Rate $\approx kK_p$	Rate $\approx k$
Rate linearly dependent on gas pressure	Rate independent of gas pressure
First order reaction	Zero order reaction
Surface coverage very low	Surface coverage almost unity

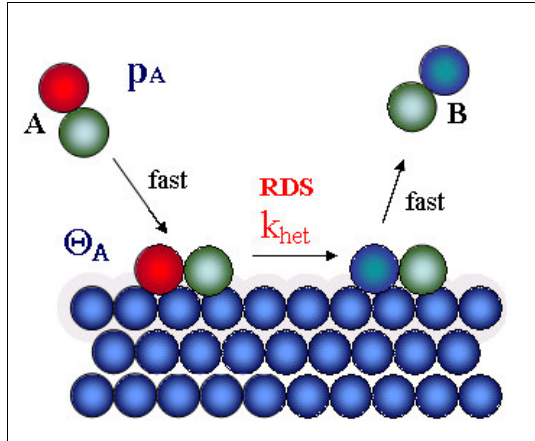
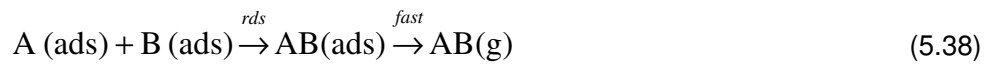


Figure 5.4 Langmuir-Hinshelwood mechanism for unimolecular reactions [94].

Langmuir-Hinshelwood reaction with surface reaction as RDS is shown in Figure 5.5.



$$Rate = r = k\theta_A\theta_B
 \tag{5.39}$$

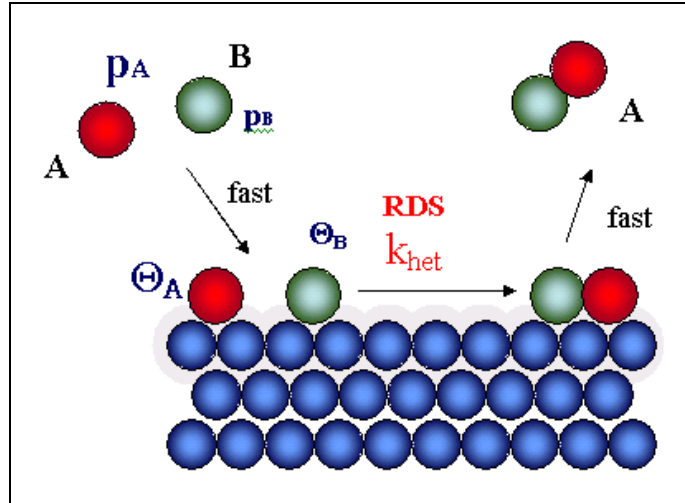


Figure 5.5 LH model for bimolecular reaction [94].

LH model for bimolecular reaction;

$$Rate = r = \frac{kK_A p_A K_B p_B}{(1 + K_A p_A + K_B p_B)^2} \quad (5.40)$$

#### 5.2.2.2. Eley-Rideal (ER) Mechanism

In Eley-Rideal bimolecular surface reactions, an adsorbed molecule may react directly with an impinging gas molecule by a collisional mechanism (Figure 5.6).

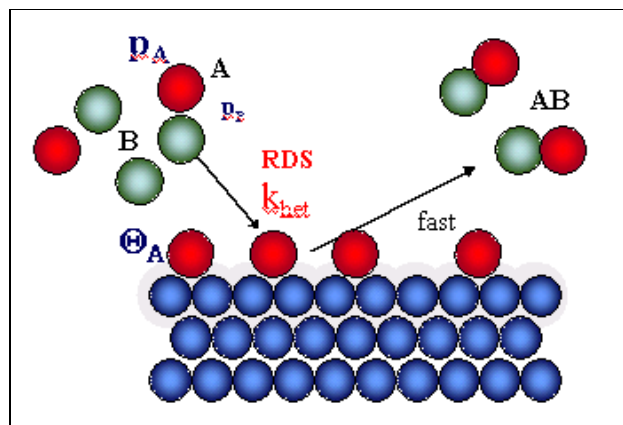


Figure 5.6 ER model for bimolecular reaction [94].

Two models can be compared with two simple examples; for the following reaction;



Table 5.1 LH and ER models comparison [94].

LH model	ER model
$A_2 + * = A_2^*$	$A_2 + * = A_2^*$
$A_2^* + * = 2A^*$	$A_2^* + * = 2A^*$
$B + * = B^*$	$A^* + B = AB + *$
$A^* + B^* = AB^* + *$	
$AB^* = AB + *$	

For the Eley-Rideal mechanism, the rate will increase with increasing coverage until the surface is completely covered by  $A^*$ .

For the Langmuir-Hinshelwood mechanism, the rate will go through a maximum and end up at zero, when the surface is completely covered by  $A^*$ . This happens because the step



cannot proceed when  $A^*$  blocks all sites.

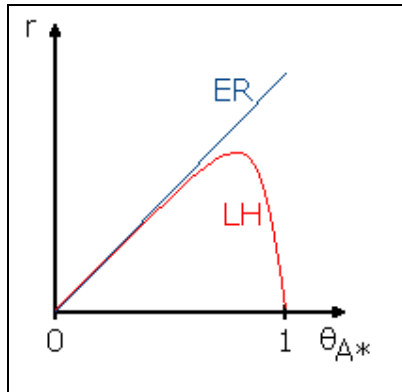


Figure 5.7 Comparison of Eley-Rideal and Langmuir-Hinshelwood models [94].

### 5.2.3. Catalysts Examples

Catalysts are used to increase the efficiency of the process and decrease the reaction time [88]. The best catalysts for the selected reactions are given in Table 5.2.

Table 5.2 Best catalysts for some reactions [94].

Reaction	Catalyst
Catalytic cracking of crude oil	Zeolites
Hydrotreating of crude oil	Co-Mo, Ni-Mo, Ni-W(sulfidicform)
Reforming of naphtha (to gasoline)	Pt, Pt-Re, Pt-Ir
Alkylation	H <sub>2</sub> SO <sub>4</sub> , HD, solid acids
Polymerization of ethylene, propylene, a.o	Cr, TiCl <sub>x</sub> / MgCl <sub>2</sub>
Ethylene epoxidation to ethylene oxide	Ag
Vinyl chloride (ethylene + Cl <sub>2</sub> )	Cu (as chloride)
Steam reforming of methane to Co + H <sub>2</sub>	Ni
Water-gas shift reaction	Fe (oxide), Cu-ZnO
Methanation	Ni
Ammonia synthesis	Fe
Ammonia oxidation to NO and HNO <sub>3</sub>	Pt-Rh
Acrylonitrile from propylene and ammonia	Bi-Mo, Fe-Sb (oxides)
Hydrogenation of vegetable oils	Ni
Sulfuric acid	V (oxide)
Oxidation of CO&hydrocarbons (car exhaust)	Pt, Pd
Reduction of NO <sub>x</sub> (in exhaust)	Rh, vanadium oxide

Iron oxide was used for the graphitization of the carbon/carbon composites as catalyst by increasing the thermal conductivity of the system [88]. Sulfur promoted iron oxide was used for the liquefaction of coal [92]. Cobalt molybdate was used for the recovery of heavy oil gas from the Athabasca bitumen [95].

The catalytic reactions of carbon can be explained by two theories: (i) oxygen transfer and (ii) electron transfer theories. According to the oxygen transfer theory the catalyst reacts with the gaseous reactant to form an intermediate compound, such as metal oxide, which then oxidizes carbon. In doing so the catalyst itself returns to its original form [91]. The following sequence of reactions as representing the mechanism of carbon-carbon dioxide reaction catalysed by iron:



Kinetics of these reactions can be explained better by Langmuir-Hinshelwood mechanism. The catalyst is thus regarded as an oxygen carrier by an oxidation-reduction cycle [91].

According to the electron transfer theory, there is a transfer of electron from carbon matrix to the catalyst which results in weakening the carbon-carbon bonds. These weakened bonds are easily broken to release the product gas. Iron accepts electrons in the oxidized state because of the non-stoichiometric character. It is also capable of accepting electrons in the metallic state because of its unfilled d-orbital. This theory can be better explained by the Eley-Rideal rate mechanism [91].

#### 5.4. Fluid Rheology

Rheology is the study of the deformation and flow of matter under the influence of an applied stress, which might be, for example, a shear stress or extensional stress. Theoretical aspects of rheology are the relation of the flow/deformation behavior of material and its internal structure (e.g. the orientation and elongation of polymer molecules), and the flow/deformation behavior of materials that cannot be described by classical fluid mechanics or elasticity. This is also often called Non-Newtonian fluid mechanics in the case of fluids [97].

##### 5.3.1. Definitions

A shear stress is denoted,  $\sigma$  is defined as a stress which is applied parallel or tangential to a face of a material, as opposed to a normal stress which is applied perpendicularly. A viscous, Newtonian fluid (including air and water) moving along a solid boundary will incur a shear stress on that boundary. The no-slip

condition dictates that the speed of the fluid at the boundary (relative to the boundary) is 0, but at some height from the boundary the flow speed must equal that of the fluid. The region between these two points is aptly named the boundary layer. The shear stress is imparted onto the boundary as a result of this loss of velocity and can be expressed as [97].

$$\sigma = \eta \left. \frac{\partial u}{\partial y} \right|_{y=0} \quad (5.45)$$

Where;

$\eta$  is the dynamic viscosity of the fluid,  
 $u$  is the velocity of the fluid along the boundary, and  
 $y$  is the height of the boundary.

Shear rate is the rate at which a shear is applied.

$$\gamma^* = \frac{v}{h} \quad (5.46)$$

Where:

$\gamma$  is the shear rate, measured in reciprocal seconds  
 $v$  is the velocity, measured in meters per second  
 $h$  is the distance between the two parallel faces that are experiencing the shear.

For a Newtonian fluid wall Shear stress ( $\sigma$ ) can be related to shear rate by,

$$\sigma = \eta \gamma^* \quad (5.47)$$

where  $\eta$  is the viscosity of the fluid. For Non-Newtonian fluids, there are different constitutive laws depending on the fluid, which relates the stress tensor to the shear rate tensor.

Viscosity: It is a measure of the resistance of a fluid which is being deformed by either shear stress or extensional stress [97]. The preferred units of viscosity are Pa s or mPa s.

Apparent viscosity: It is a rheological property calculated from rheometer readings. Additional information can be obtained from a basic shear (shear stress-shear rate) diagram (Figure 5.8). One can calculate the apparent viscosity at any given shear rate [97]. For example, the apparent viscosity at a shear rate of  $50 \text{ s}^{-1}$  is

$$\eta_{a,50} = \frac{\sigma_{50}}{\gamma_{50}} \quad (5.48)$$

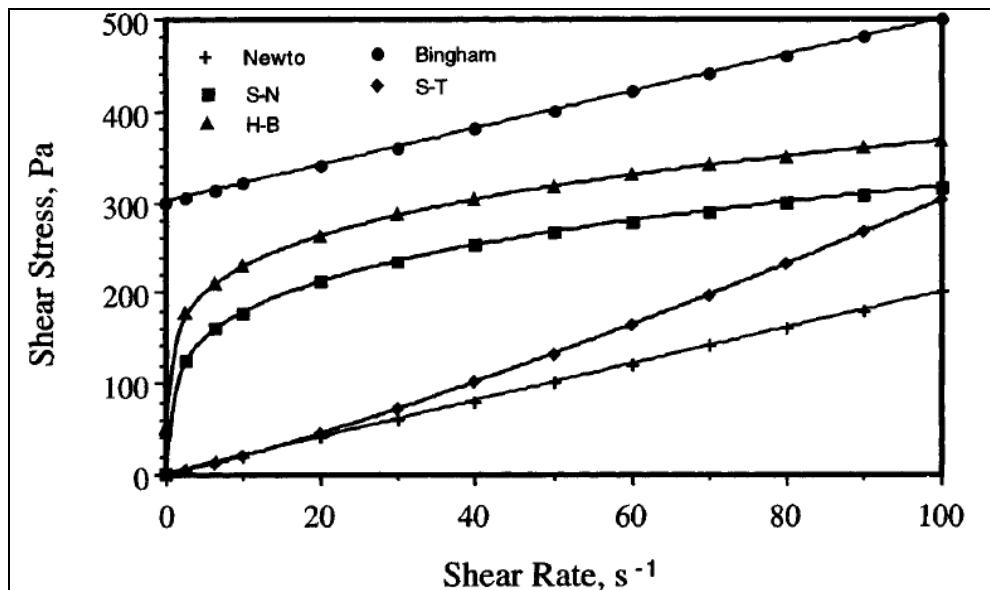


Figure 5.8 Basic shear diagram (Newto:Newtonian, S-N: Shear-Thinning, S-T: Shear Thickening, H-B: Herschel-Bulkley) [97].

Yield Stress ( $\sigma_0$ ): The yield strength or yield point of a material is defined in engineering and materials science as the stress at which a material begins to deform plastically. Prior to the yield point the material will deform elastically and will return to its original shape when the applied stress is removed [97].

### 5.3.2. Fluid Rheology Models

Viscosity is the internal friction of a fluid or its tendency to resist flow. It is denoted by the symbol  $\eta$  for Newtonian fluids, whose viscosity does not depend on the shear rate, and for non-Newtonian fluids to indicate shear rate dependence by  $\eta_a$ . Depending on the flow system and choice of shear rate and shear stress, there are several equations to calculate. Here, it is defined by the equation [97].

$$\eta_a = \frac{\text{ShearStess}}{\text{ShearRate}} = \frac{\sigma}{\dot{\gamma}} \quad (5.49)$$

#### 5.3.2.1. Newtonian Fluid Behavior

A Newtonian fluid is a fluid whose stress versus rate of stress curve is linear and passes through the origin. The constant of proportionality is known as the viscosity [97].

#### 5.3.2.2. Non-Newtonian Fluid Behavior

There are more than 30 fluid models as Non-Newtonian fluid models. The models used in this thesis are given below.

### 5.3.2.2.1. Power Law Model

Shear stress-shear rate plots of many fluids become linear when plotted on double logarithmic coordinates, and the power law model describes the data of shear- thinning and shear-thickening fluids [97].

$$\sigma = K\dot{\gamma}^n \quad (5.50)$$

where  $K$ , the consistency index ( $\text{Pa s}^n$ ), is the shear stress at a shear rate of  $1.0 \text{ s}^{-1}$  and the exponent  $n$ , the flow behavior index, is dimensionless that also reflects the closeness to Newtonian flow. For the special case of a Newtonian fluid ( $n = 1$ ), the consistency index  $K$  is identically equal to the viscosity of the fluid. When the magnitude of  $n < 1$  the fluid is shear-thinning, and when  $n > 1$  the fluid is shear-thickening in nature. Taking logarithms of both sides of Equation 5.50 [97].

$$\log \sigma = \log K + n \log \dot{\gamma} \quad (5.51)$$

The parameters  $K$  and  $n$  are determined from a plot of  $\log \sigma$  versus  $\log \dot{\gamma}$ , and the resulting straight line's intercept is  $\log K$  and the slope is  $n$ . If a large number of  $\sigma$ -  $\dot{\gamma}$  data points, for example,  $> 15$  (it is easy to obtain a large number of points with automated viscometers) is available, linear regression of  $\log \dot{\gamma}$  versus  $\log \sigma$  will provide statistically best values of  $K$  and  $n$ . Nevertheless, a plot of experimental and predicted values of  $\log \dot{\gamma}$  and  $\log \sigma$  is useful for observing trends in data and ability of the model to follow the data. Linear regression techniques also can be used for determination of the parameters of the Herschel-Bulkley (when the magnitude of the yield stress is known). Because it contains only two parameters ( $K$  and  $n$ ) that can describe shear rate-shear stress data, the power law model has been used extensively to characterize most of the fluids [97].

#### 5.3.2.2.2. Bingham Plastic Model

Bingham plastic fluid exhibits a yield stress  $\sigma_0$ , the model is

$$\sigma - \sigma_0 = \eta' \dot{\gamma} \quad (5.52)$$

where  $\eta'$  is called the Bingham plastic viscosity.

As shown in Figure 5.8, the Newtonian model and the Bingham plastic model can be illustrated by straight lines in terms of shear rate and shear stress, and the former can be described by one parameter,  $\eta$ , and the latter by two parameters,  $\eta'$  and  $\sigma_0$ , respectively. However, the shear rate-shear stress data of shear-thinning and shear-thickening fluids are curves that require more than one parameter to describe their data. Given that the equation of a straight line is simple, it is easy to understand attempts to transform shear rate-shear stress data into such lines. An additional advantage of a straight line is that it can be described by just two parameters: the slope and the intercept [97].

#### 5.3.2.2.3. Casson Model

The Casson model is a structure-based model that has been used for a number of food dispersions, although it was developed for characterizing printing inks originally [97].

$$\sigma^{0.5} = K_{0c} + K_c (\dot{\gamma})^{0.5} \quad (5.53)$$

A straight line results when the square root of shear rate,  $(\dot{\gamma})^{0.5}$ , is plotted against the square root of shear stress,  $(\sigma)^{0.5}$ , with slope  $K_c$  and intercept  $K_{0c}$ . The Casson yield stress ( $\sigma_{0c}$ ) is calculated as the square of the intercept and the Casson plastic viscosity ( $\eta_{ca}$ ) as the square of the slope [97];

$$\sigma_{Oc} = (K_{0c})^2 \quad (5.54)$$

$$\eta_{Ca} = (K_c)^2 \quad (5.55)$$

The Casson plastic viscosity can be used as the infinite shear viscosity ( $\eta_\infty$ ) of dispersions by considering the limiting viscosity at infinite shear rate [97]:

$$\left( \frac{d\sigma}{d\gamma} \right)_{\gamma \rightarrow \infty}^* = \left( \frac{d\sqrt{\sigma}}{d\gamma} \frac{d\sigma}{d\sqrt{\sigma}} \right)_{\gamma \rightarrow \infty}^* \quad (5.56)$$

Using the Casson equation, the two terms in the right-side bracket are

$$\frac{d\sqrt{\sigma}}{d\gamma} = \frac{K_c}{2\sqrt{\gamma}} \quad (5.57)$$

$$\frac{d\sigma}{d(\sqrt{\sigma})} = 2\sqrt{\sigma} \quad (5.58)$$

Combination of the equations 5.42 and 5.43 gives Casson viscosity

$$\eta_\infty = \eta_{Ca} = (K_c)^2 \quad (5.59)$$

## CHAPTER 6

### RESULTS AND DISCUSSION

#### 6.1. Rheology of the crude oils

In order to understand the fluid rheology of the crude oil samples (Batı Raman, Çamurlu and Garzan), shear stress ( $\sigma$ ) and shear rate ( $\dot{\gamma}$ ) values for each samples were interpreted by using the following fluid models [97]:

$$\sigma = \eta \dot{\gamma}, \text{ Newtonian Model} \quad (6.1)$$

$$\sigma = K \dot{\gamma}^n, \text{ Power Law Model} \quad (6.2)$$

$$\sigma - \sigma_0 = \eta \dot{\gamma}, \text{ Bingham Model} \quad (6.3)$$

$$\sigma^{0.5} = K_{oc} + K_c (\dot{\gamma})^{0.5}, \text{ Casson Model} \quad (6.4)$$

##### 6.1.1. Determination of rheological parameters for crude oil samples

###### 6.1.1.1. Effect of electrical heating

Calibration of Haake viscometer was conducted with tap water at room temperature (Figure A 1). Since these results have a consistency with literature data, viscometer was used to test the rheology of the crude oil samples [98].

Three different fluid rheology models were used to explain the flow characteristics of the crude oils. Shear stress values were measured for different shear rate values, by using Haake viscometer. Comparisons of the models were done

according to the rheological parameters of each model. Rheological parameters of Bati Raman, Çamurlu and Garzan crude oils are given in Table 6.1, Table 6.2, Table 6.3, and in Appendix A.

Bingham plastic model can be explained by interpreting the yield stress ( $\sigma_o$ ) and Bingham plastic viscosity ( $\dot{\eta}$ ), together. Once the yield stress (or "critical shear stress") is exceeded, the material flows as a Newtonian fluid with incremental shear stress and shear rate. The resistance to flow of crude oil decreases with decreasing Bingham plastic viscosity.

Power law fluid model can be explained by the consistency index (K) and the flow behavior index (n). If n is smaller than 1, the fluid is called as shear-thinning, if n is greater than 1, fluid is called as shear-thickening. If the exponent value is equal to 1 fluid is called as Newtonian. Shear-thinning fluids have a lower apparent viscosity at higher shear rates, and are usually solutions of large, polymeric molecules in a solvent with smaller molecules. It is generally supposed that the large molecular chains tumble at random and affect large volumes of fluid under low shear, but that they gradually align themselves in the direction of increasing shear and produce less resistance. Shear-thickening fluids increase in apparent viscosity at higher shear rates. They are rarely encountered, but one common example is an uncooked paste of cornstarch and water. Under high shear the water is squeezed out from between the starch molecules, which are able to interact more strongly.

Casson model is most suitable for pseudoplastic fluids with a yield value. Casson model are interpreted according to the Casson viscosity ( $\eta_{Ca}$ ) and Casson yield stress ( $\sigma_{OCa}$ ). Casson viscosity and yield stress can be evaluated same as the Bingham plastic viscosity and yield stress.

Table 6.1 Rheological parameters for Batı Raman crude oil

Sample	Temp, (oC)	Fluid Rheology								
		Bingham Model			Power Law Model			Casson Model		
		$\dot{\eta}$	$\sigma_0$	$R^2$	K	$n$	$R^2$	$\eta_{ca}$	$\sigma_{0C}$	$R^2$
Dead	20	68.52	148.41	0.92	251.64	0.29	0.95	27.21	100.86	0.98
	35	22.33	117.25	1.00	152.80	0.14	0.85	4.22	100.84	0.97
	50	6.82	116.42	1.00	127.59	0.06	0.85	0.52	109.62	0.97
	65	2.01	115.71	1.00	118.90	0.02	0.86	0.05	113.21	0.97
	75	0.24	113.87	0.98	115.96	0.01	0.84	0.01	114.19	0.95
	100	0.62	114.96	0.99	114.25	0.00	0.82	0.00	113.57	0.94
0,1% Fe	20	0.09	16.22	0.93	1.02	0.68	0.99	0.07	4.64	0.96
	35	0.09	13.04	0.94	1.07	0.66	0.99	0.08	1.59	0.88
	50	0.08	13.47	0.93	0.53	0.77	0.98	0.07	2.98	0.96
	65	0.08	15.99	0.94	0.53	0.77	0.98	0.06	4.45	0.97
	75	0.07	11.72	0.97	0.45	0.77	0.99	0.06	2.79	0.98
	100	0.06	10.30	0.95	0.38	0.77	0.99	0.05	2.28	0.97
0,5% Fe	20	0.08	12.12	0.92	0.92	0.67	0.98	0.07	1.48	0.87
	35	0.08	10.97	0.91	0.55	0.75	0.97	0.08	0.93	0.88
	50	0.08	11.33	0.91	0.55	0.75	0.97	0.08	0.51	0.86
	65	0.07	13.78	0.97	0.75	0.69	0.99	0.05	4.13	0.98
	75	0.07	11.09	0.96	0.43	0.76	0.98	0.05	2.59	0.97
	100	0.06	8.50	0.97	0.32	0.78	0.99	0.05	1.76	0.98
1% Fe	20	0.08	14.21	0.92	0.58	0.75	0.97	0.08	0.93	0.89
	50	0.07	13.12	0.93	0.62	0.72	0.98	0.07	0.95	0.89
	65	0.07	14.06	0.94	0.58	0.73	0.98	0.08	0.47	0.86
	80	0.06	12.61	0.95	0.60	0.70	0.99	0.05	3.56	0.97
	100	0.06	8.78	0.97	0.32	0.79	0.98	0.05	1.91	0.98
0,1% Fe <sub>2</sub> O <sub>3</sub>	20	0.68	38.54	0.92	26.48	0.28	0.95	0.27	26.19	0.98
	35	1.14	53.79	0.90	30.89	0.35	0.95	0.52	33.64	0.96
	50	1.07	55.61	0.94	35.47	0.31	0.95	0.48	34.35	0.98
	65	1.11	42.06	0.97	23.07	0.39	0.96	0.59	22.09	0.99
	75	0.99	29.12	0.98	7.24	0.64	0.98	0.60	12.92	0.99
	100	0.86	13.25	0.99	3.48	0.73	0.98	0.63	4.12	0.99
0,5% Fe <sub>2</sub> O <sub>3</sub>	25	1.16	25.36	0.90	10.91	0.56	0.97	0.81	9.94	0.95
	35	1.11	21.63	0.88	8.40	0.61	0.98	0.83	7.30	0.95
	50	4.25	0.41	1.00	4.51	0.98	1.00	4.19	0.01	1.00
	65	14.49	2.22	1.00	15.85	0.97	1.00	14.09	0.07	1.00
	80	4.88	0.55	1.00	5.25	0.97	1.00	4.77	0.01	1.00
1% Fe <sub>2</sub> O <sub>3</sub>	100	2.87	0.75	1.00	3.45	0.93	1.00	2.70	0.05	1.00
	20	0.09	12.26	0.95	0.62	0.75	0.99	0.073	279	0.9679
	35	0.09	11.30	0.93	0.66	0.74	0.99	0.093	1	0.9001
	50	0.09	13.47	0.97	0.71	0.73	0.99	0.071	343	0.9787
	65	0.08	13.84	0.96	0.59	0.75	0.99	0.071	324	0.9752
	80	0.07	11.03	0.97	0.49	0.75	0.99	0.073	279	0.9679
0,1% FeCl <sub>3</sub>	100	0.07	2.84	0.96	0.23	0.84	0.99	0.093	1	0.9001
	35	0.09	19.13	0.92	1.81	0.59	1.00	0.06	6.85	0.96
	50	0.09	17.22	0.92	1.38	0.63	0.99	0.06	5.66	0.96
	65	0.07	15.02	0.93	1.13	0.63	0.99	0.06	4.63	0.97
	80	0.10	12.24	0.95	0.58	0.72	0.99	0.06	3.06	0.97
0,5% FeCl <sub>3</sub>	100	0.06	9.46	0.96	0.35	0.77	0.99	0.05	2.05	0.97
	20	0.09	11.10	0.92	0.73	0.72	0.98	0.09	0.89	0.89
	35	0.08	15.96	0.92	1.06	0.67	0.99	0.07	4.72	0.96
	50	0.07	13.87	0.90	0.84	0.68	0.93	0.05	4.59	0.90
	65	0.08	15.58	0.95	0.74	0.71	0.99	0.06	4.30	0.97
	80	0.07	10.12	0.97	0.33	0.81	0.98	0.06	1.90	0.97
1% FeCl <sub>3</sub>	100	0.07	7.43	0.98	0.27	0.82	0.99	0.06	1.28	0.99
	20	0.08	16.58	0.92	1.10	0.66	0.99	0.06	5.12	0.95
	35	0.09	12.91	0.91	0.73	0.73	0.98	0.09	1.20	0.88
	50	0.08	16.82	0.94	1.01	0.67	0.98	0.06	5.41	0.95
	65	0.07	15.48	0.95	0.62	0.73	0.99	0.06	4.45	0.97
1% FeCl <sub>3</sub>	80	0.07	12.81	0.95	0.52	0.74	0.99	0.06	3.15	0.97
	100	0.06	7.66	0.96	0.25	0.83	0.99	0.06	1.21	0.98

It is clear that when the temperature increases, Bingham and Casson viscosities, Bingham and Casson yield stresses, and consistency index for Power law model are decreasing.

Power law fluid model generally well define the flow characteristics of Batu Raman crude oil with  $R^2$  values over 0.92 (Table 6.1).

For Bingham Plastic behavior, generally Bingham plastic viscosity ( $\eta'$ ) is reduced about 99% when temperature increases. Because there is no considerable changes in Bingham plastic viscosity reduction, interpretations about determination of fluid behavior was made on the basis of the reduction of yield stresses ( $\sigma_0$ ). Over 90% reduction was obtained after the addition of 1% Fe, 1 %  $Fe_2O_3$ , 0.5% Fe, and 0.5 %  $FeCl_3$ ; i.e. 90.4%, 91.7%, 91.8%, and 92.5%, respectively, at room temperature. Generally, iron addition yields better results for the Bingham plastic model at room temperature.

At 35 °C, Bingham plastic viscosity of Batu Raman crude oil is reduced over 95% after the addition of iron powders and 21% for dead crude oil sample. Efficiency of the reduction of yield stresses were calculated by comparing the Bingham plastic viscosities of the sample at 35 °C with the yield stress of dead crude oil sample at 35 °C and it has been found that highest reductions were obtained after the addition of 1 %  $Fe_2O_3$  and 0.5% Fe; i.e. 90.3% and 90.6%, respectively.

By using the same logic, at 50 °C, the highest yield stress reductions were obtained after the addition of 0.5% Fe and 0.5 %  $Fe_2O_3$ ; i.e. efficiencies are 90.3 % and 99.6%, respectively. As the temperature increases, viscosity decreases. Thus, at 50 °C the yield stress reduction for the dead sample was found as 21.5 % which is higher than the reduction at 35 °C and lower than the value at 65 °C.

At 65 °C, after the addition of 1 %  $Fe_2O_3$ , 0.5% Fe, and 0.5 %  $Fe_2O_3$ , Bingham Plastic viscosity reductions were observed as over 88%. At the temperatures between 75-80 °C, 0.5% Fe, 1 %  $Fe_2O_3$ , 1 %  $FeCl_3$ , and 0.5 %  $Fe_2O_3$  additions decreases the viscosity over 90 % and decreases the yield stress over 23%. At 100 °C most of the additives yielded good results for the reduction of yield

stresses; i.e. >90%. Vaporization of the physically bonded water and catalytic cracking reactions can occur at the same time at 100 °C. All of these reactions may help to break the weak bonds of long chained hydrocarbons which then help to reduce the viscosity of the crude oil sample.

Interpretations for power law fluid model were made on the basis of the exponent,  $n$ . Since  $n$  is smaller than 1 in Table 6.1, Batı Raman crude oil can be called as shear-thinning fluid. Shear-thinning behavior can be characterized by an apparent viscosity which decreases with increasing shear rate [96].

When the exponent approaches to 1, the fluid resistance to flow is reduced, [97]. It is observed that  $n$  is much closer to 1, after the addition of Fe and FeCl<sub>3</sub>, (i.e.; >0.6) at room temperature.

In the Casson model, the Casson viscosity and the yield stress are calculated by using the equations 5.54 and 5.55. At room temperature, and 35 °C the Casson viscosity reductions are high; > 97%, and >80%, respectively. At 50 °C, 65 °C, 80 °C and 100 °C, while high Casson viscosity reductions are calculated for some cases, most of the Casson viscosity values become greater than the dead crude oil Casson viscosity value. In order to understand the reason of this conclusion, chemical analysis should be done, before and after the addition of iron powders and after increasing the temperature. Thus, the responds of the chemical reactions to these processes can be understood well. By using the literature data, this conclusion can be explained due to the complex iron powders reactions, which can make the complex molecular structure of crude oils more complex and can form stronger bonds [93, 94]. Besides the effect of iron types, doses of this types and the temperature of the system can affect the efficiency, so iron types, doses and the temperature value should be optimized for this process. Detailed discussion is made at the end of this section, for all of the crude oil samples.

If the interpretation for all of the fluid models were conducted together by considering all of the iron powders types and doses for all of the temperature values, generally, the best viscosity and yield stress reductions are obtained after the addition of 0.5% Fe.

Table 6.2 Rheological parameters for Çamurlu crude oil

Sample	Temp. (oC)	Fluid Rheology								
		Bingham Model			Power Law Model			Casson Model		
		$\dot{\eta}$	$\sigma_0$	$R^2$	K	n	$R^2$	$\eta_{ca}$	$\sigma_{0C}$	$R^2$
Dead	30	0.44	24.72	0.92	1.40	0.87	0.97	0.39	4.66	0.95
	50	0.42	11.26	0.98	0.57	1.00	0.97	0.39	1.16	0.98
	75	0.23	4.68	0.98	0.18	1.09	0.98	0.23	0.28	0.99
	100	0.10	1.01	0.97	0.02	1.35	0.88	0.11	0.01	0.98
0.1% Fe	47	0.45	10.24	0.96	0.40	1.08	0.96	0.44	0.81	0.97
	60	0.35	3.90	0.98	0.03	1.55	0.89	0.38	0.00	0.97
	75	0.32	0.28	1.00	0.13	1.18	0.99	0.34	0.07	1.00
	100	0.09	1.76	0.96	0.07	1.11	0.93	0.08	0.36	0.97
0.5% Fe	30	0.54	20.59	0.97	1.45	0.88	0.96	0.46	4.05	0.98
	50	0.46	14.82	0.96	0.43	1.08	0.92	0.46	0.93	0.95
	75	0.41	1.75	1.00	0.52	0.97	1.00	0.39	0.15	1.00
	100	0.22	-0.46	1.00	0.16	1.06	1.00	0.23	0.02	1.00
1% Fe	30	0.44	21.22	0.97	1.26	0.86	0.96	0.39	3.36	0.97
	50	0.48	15.28	0.97	0.65	1.01	0.95	0.48	1.19	0.96
	75	0.36	5.42	0.99	0.32	1.06	0.98	0.37	0.12	0.99
	100	0.21	-0.43	1.00	0.09	1.17	0.99	0.22	0.07	1.00
0.1% Fe <sub>2</sub> O <sub>3</sub>	35	0.46	34.86	0.95	0.95	0.97	0.94	0.36	9.23	0.97
	50	0.44	14.64	0.95	0.06	1.49	0.86	0.48	0.46	0.94
	75	0.33	6.64	0.97	0.03	1.56	0.89	0.37	0.02	0.96
	100	0.17	-0.27	1.00	0.01	1.63	0.88	0.20	0.20	0.99
0.5% Fe <sub>2</sub> O <sub>3</sub>	40	0.42	36.91	0.97	1.33	0.89	0.91	0.29	13.41	0.98
	50	0.48	20.16	0.95	0.24	1.23	0.88	0.47	1.96	0.94
	75	0.47	12.13	0.94	0.04	1.53	0.93	0.57	0.02	0.92
	100	0.31	3.22	0.98	0.04	1.44	0.92	0.36	0.07	0.98
1% Fe <sub>2</sub> O <sub>3</sub>	35	0.44	37.57	0.93	0.42	1.13	0.86	0.34	10.38	0.95
	50	0.46	23.14	0.91	0.18	1.30	0.84	0.45	2.63	0.93
	75	0.43	13.55	0.97	0.25	1.18	0.92	0.43	0.86	0.95
	100	0.29	1.47	0.98	0.00	1.96	0.89	0.36	0.57	0.97
0.1% FeCl <sub>3</sub>	35	0.41	34.41	0.95	2.34	0.76	0.99	0.31	10.35	0.97
	50	0.45	11.34	0.97	0.73	0.96	0.95	0.50	0.09	0.94
	75	0.27	1.78	1.00	0.34	0.97	1.00	0.27	0.05	1.00
	100	0.16	-0.33	1.00	0.04	1.29	0.94	0.17	0.07	1.00
0.5% FeCl <sub>3</sub>	35	0.49	36.73	0.95	3.02	0.74	0.98	0.39	9.30	0.96
	50	0.50	13.74	0.97	0.72	0.99	0.96	0.49	1.09	0.97
	75	0.35	6.76	0.98	0.39	1.02	0.97	0.35	0.31	0.98
	100	0.13	1.18	0.99	0.07	1.17	0.96	0.14	0.00	0.99
1% FeCl <sub>3</sub>	30	0.46	33.76	0.95	1.17	0.92	0.96	0.36	8.78	0.97
	55	0.43	12.58	0.97	0.38	1.09	0.95	0.42	1.01	0.97
	75	0.34	6.66	0.98	0.20	1.15	0.96	0.35	0.20	0.98
	100	0.21	-0.53	1.00	0.07	1.22	0.99	0.23	0.10	1.00

The flow characteristics of Çamurlu crude oil can be explained best by Bingham plastic model (i.e.;  $R^2 > 0.93$ ) (Table 6.2).

At room temperature while power law fluid model yields the best fit among the fluid models for dead Çamurlu crude oil, for higher temperatures and after the addition of iron powders, it is observed that the fluid rheology changes.

Increasing temperature affects the reduction of Bingham plastic and Casson yield stresses more than the reduction of Bingham plastic and Casson viscosities for Çamurlu crude oil.

The flow behavior index,  $n$  is generally greater than 1 for Çamurlu crude oil, which means that the fluid is show shear-thickening behavior.

After the addition of the iron powders, the highest apparent viscosity reduction was obtained for Fe. It is observed that iron powder addition is not as effective as Batı Raman crude oil (for Çamurlu crude oil). This can be due to differences between chemical (such as composition) and physical (such as viscosity, density) properties of both crude oil samples [81, 82, 88].

Since some yield stress values are negative in Table 6.2, it demonstrates the inability of the solution methodology to provide optimal solutions in some cases.

Flow characteristic of Garzan crude oil is best explained by Power Law fluid model (Table 6.3). The reduction effectiveness of yield stresses for Bingham and Casson models are higher than the reduction effectiveness of Bingham and Casson viscosities.

Because the flow behavior index is generally smaller than 1, Garzan crude oil shows shear-thinning behavior.

Generally, iron addition has a positive effect to reduce the consistency index ( $K$ ) but this effect is not as effective as the reduction observed for Batı Raman crude oil. Due to the complex reactions of iron, for some temperature values, iron powder addition has a negative effect on the reduction of consistency index [88].

Table 6.3 Rheological parameters for Garzan crude oil

Sample	Temp. (oC)	Fluid Rheology								
		Bingham Model			Power Law Model			Casson Model		
		$\dot{\eta}$	$\sigma_0$	$R^2$	K	n	$R^2$	$\eta_{ca}$	$\sigma_{0C}$	$R^2$
Dead	25	0.011	6.37	0.80	0.17	0.70	0.95	0.01	1.83	0.88
	50	0.010	2.83	0.94	0.05	0.83	0.99	0.01	0.45	0.96
	75	0.009	0.90	1.00	0.02	0.90	1.00	0.01	0.08	1.00
	100	0.006	0.67	1.00	0.01	0.89	1.00	0.01	0.07	1.00
0.1% Fe	35	0.011	2.16	0.93	0.14	0.68	0.99	0.01	0.01	0.86
	60	0.009	1.76	0.94	0.11	0.69	0.98	0.01	0.01	0.87
	75	0.009	1.24	0.97	0.04	0.84	0.99	0.01	0.31	0.98
	100	0.007	0.61	0.98	0.01	0.97	0.97	0.01	0.18	0.99
0.5% Fe	30	0.010	1.31	0.95	0.03	0.90	0.97	0.01	0.04	0.92
	55	0.009	1.81	0.94	0.01	1.11	0.83	0.01	0.01	0.92
	75	0.008	1.42	0.97	0.01	1.09	0.96	0.01	0.20	0.96
	100	0.007	0.79	0.98	0.00	1.15	0.98	0.01	0.02	0.98
1% Fe	30	0.010	6.21	0.93	0.08	0.79	0.93	0.01	2.11	0.96
	50	0.010	3.55	0.88	0.04	0.88	0.94	0.01	0.56	0.92
	75	0.009	1.80	0.96	0.04	0.82	0.99	0.01	0.07	0.93
	100	0.007	0.97	0.99	0.04	0.78	0.99	0.01	0.16	0.99
0.1% Fe <sub>2</sub> O <sub>3</sub>	35	0.010	5.63	0.96	0.25	0.61	1.00	0.01	2.08	0.98
	50	0.009	3.83	0.94	0.18	0.63	0.99	0.01	1.27	0.97
	75	0.008	1.60	0.97	0.03	0.88	0.98	0.01	0.20	0.98
	100	0.007	0.62	0.99	0.01	1.06	0.95	0.01	0.02	0.99
0.5% Fe <sub>2</sub> O <sub>3</sub>	30	0.009	6.57	0.96	0.21	0.64	0.96	0.01	2.82	0.98
	50	0.010	2.24	0.97	0.04	0.86	0.98	0.01	0.35	0.97
	75	0.009	1.32	0.99	0.02	0.92	0.98	0.01	0.14	0.98
	100	0.008	0.32	0.99	0.00	1.18	0.94	0.01	0.01	0.98
1% Fe <sub>2</sub> O <sub>3</sub>	30	0.009	11.99	0.77	0.09	0.82	0.87	0.01	5.54	0.77
	50	0.010	2.91	0.95	0.03	0.90	0.97	0.01	0.53	0.96
	75	0.009	0.89	0.98	0.01	1.02	0.96	0.01	0.00	0.96
	100	0.007	0.53	0.99	0.01	1.01	0.98	0.01	0.00	0.97
0.1% FeCl <sub>3</sub>	35	0.011	5.01	0.95	0.01	1.11	0.78	0.01	1.36	0.97
	50	0.011	2.66	0.95	0.02	0.94	0.96	0.01	0.28	0.96
	75	0.009	1.64	0.96	0.00	1.27	0.91	0.01	0.08	0.96
	100	0.007	0.47	0.98	0.00	1.10	0.93	0.01	0.03	0.96
0.5% FeCl <sub>3</sub>	40	0.009	11.93	0.96	1.64	0.38	1.00	0.00	7.22	0.99
	50	0.011	2.10	0.94	0.03	0.91	0.97	0.01	0.03	0.93
	75	0.009	1.55	0.96	0.02	0.97	0.95	0.01	0.01	0.94
	100	0.007	0.69	0.97	0.00	1.20	0.93	0.01	0.00	0.97
1% FeCl <sub>3</sub>	35	0.010	6.03	0.93	0.05	0.85	0.97	0.01	2.04	0.96
	60	0.010	2.19	0.97	0.02	0.91	0.96	0.01	0.28	0.97
	75	0.009	1.79	0.96	0.00	1.21	0.87	0.01	0.17	0.97
	100	0.007	0.81	0.97	0.02	0.89	0.99	0.01	0.00	0.95

It can be stated that fluid behavior of viscous fluids can be explained better by using Power Law fluid model. This conclusion can be reached after the

interpretation of the experiments conducted with Batı Raman crude oil and the dead Çamurlu crude oil at room temperature.

For all of the crude oils, the effect of iron powders and temperature can be explained as follows;

Viscosity reduction for the dead crude oil samples is due to the increasing temperature known as thermal cracking. Common sense and chemical insight suggest that the higher the temperature, the faster a given chemical reaction will proceed. Quantitatively, this relationship between the rate of a reaction proceeds and its temperature is determined by the Arrhenius Equation. At higher temperatures, the probability that two molecules will collide is higher. This higher collision rate results in a higher kinetic energy, which has an effect on the activation energy of the reaction. The activation energy is the amount of energy required to ensure that a reaction happens [97].

$$k = A * \exp\left(-\frac{E_a}{RT}\right) \quad (6.5)$$

where k is the rate coefficient, A is a constant,  $E_a$  is the activation energy ( $\text{J/mol}^{-1}$ ), R is the universal gas constant ( $8.314 \times 10^{-3} \text{ kJ mol}^{-1}\text{K}^{-1}$ ), and T is the temperature (K) [97]. Increasing temperature can also increase the formation of some gases like CO,  $\text{H}_2\text{S}$  which allows more collisions and more correct geometry to reduce the viscosity [97].

Besides increasing the temperature, to increase the rate of the reactions, a catalyst can be used. Using a catalyst helps molecules achieve the correct geometry by providing a different way to react. Catalysts increase the reaction speeds by decreasing the activation energy of the reaction [81]. At higher temperatures, catalysts work better [99].

During the experimental studies, after the addition of iron powders at room temperature, good viscosity reductions were obtained. In order to explain the mechanism of the processes at room temperature, chemical reactions of iron

powders at room temperature should be considered. In the experimental studies conducted with pure iron at room temperature, iron powder is homogeneously mixed with the crude oil samples. The most well-known iron (Fe) reaction is rusting. When Fe is in contact with water and oxygen, or other strong oxidant or acids, rusting occurs. If salt is present, for example, in salt water, the metal rusts more quickly. Iron metal is relatively unaffected by pure water or by dry oxygen [100]. Furthermore, rusting is an exothermic reaction which gives heat energy to the outside. Iron may undergo some reactions with some compounds of heavy oil samples. Also due to the high salinity of the crude oil reservoirs, rusting can occur quickly and  $\text{Fe}_2\text{O}_3$  can be formed, this reaction increases the temperature of the sample, which helps to reduce the viscosity of the samples [101].

Not only rusting, but also magnetite ( $\text{FeO}\cdot\text{Fe}_2\text{O}_3$ ) and iron sulfide ( $\text{FeS}$ ) formations are also exothermic reactions [100]. Since heavy oil can contain some impurities, such as S, N, and O,  $\text{FeS}$  formation can be observed, after the addition of iron powders. These reactions may occur at the same time and further decrease the viscosity of the samples, by increasing the temperature [101].

In the experiments conducted with Iron (III) oxide ( $\text{Fe}_2\text{O}_3$ ), because of the homogeneous mixture of the iron oxide by the help of the rotor of the viscometer, magnetite ( $\text{FeO}\cdot\text{Fe}_2\text{O}_3$ ) can be formed. The heat energy exerted due to the reaction can help to decrease the viscosity of the samples at room temperature [100].

In some cases, while the iron powder doses increases, the viscosity of the samples increase as well. In these cases, the complex reactions of iron powders can cause to form more complex shaped molecules which have stronger bonds [101]. The iron reactions at higher temperature can cause to decrease oil viscosity due to the chemical cracking reactions. Also, iron compounds can form more complex compounds, such as chelate, at higher temperatures which cause to increase in oil viscosity [102].

According to experimental studies, optimum type and dose of iron powders are selected as 0.5% Fe. This optimum dose is used for all of crude oils to provide the consistency for the comparison of microwave method.

#### 6.1.1.2. Effect of electromagnetic heating

##### 6.1.1.2.1. Determination of optimum heating period

The time period necessary for utilization of effective microwave heating was determined for all of the crude oil samples and results are given in Table 6.4.

Since the temperature measurements are achieved outside the oven, at the end of each heating time, they are not the exact values that were reached in the oven. But the trend is realistic to give the optimum time period. During the optimization process both the time and the temperature values are considered together. According to Table 6.4, since the highest temperature acceleration is observed at the end of 3 minutes, 3 minute was selected as optimum process period [103].

Table 6.4 Optimization of microwave heating period [103]

Process Time (min.)	Reached Temperatures (°C)		
	Batı Raman	Çamurlu	Garzan
1	60	55	58
3	94	81	90
5	102	95	105
7	110	105	114
9	125	111	122

#### 6.1.1.2.2. Determination of rheological parameters

Crude oil samples as dead form and after the addition of 0.5% Fe, which is determined as optimum type and dose of iron powders after electrical heating, were subjected to the microwave heating for 3 minutes. Certain materials strongly absorb microwave energy and heat rapidly. These materials are called as microwave receptors [80]. 0.5% Fe was used as microwave receptor in this set of experiments. The rheological parameters of the samples subjected to the microwave heating were determined by using Haake viscometer and these parameters are given in Table 6.5 and in Appendix A.

Table 6.5 Effect of microwave on the rheology of crude oil samples at 70 °C

Fluid Rheology	Sample	Batı Raman		Çamurlu		Garzan	
	Addition	-	0.5 % Fe	-	0.5 % Fe	-	0.5 % Fe
Bingham Plastic Model	$\dot{\eta}$	0.0839	0.0764	0.5018	0.4972	0.0128	0.0108
	$\sigma_0$	9.69	8.6626	20.508	17.887	3.3019	2.3087
	$R^2$	0.9418	0.9311	0.9556	0.9649	0.9755	0.9723
Power Law Model	K	0.3398	0.23	1.7963	1.4768	0.0844	0.0287
	n	0.8411	0.891	0.8303	0.8608	0.7922	0.9092
	$R^2$	0.9752	0.9702	0.9784	0.978	0.9611	0.9599
Casson Model	$\eta_{ca}$	0.077	0.073	0.452	0.456	0.012	0.010
	$\sigma_{0C}$	1.605	1.171	3.552	2.718	0.748	0.302
	$R^2$	0.9558	0.9486	0.9648	0.9674	0.975	0.9694

The dead model viscosities determined after electrical heating are higher than the dead model viscosities after microwave heating. The effect of iron powders onto the enhancement of microwave heating is small; <8%. It can be concluded that the receptors help to reduce the viscosities of crudes but the enhancement process is not as effective as microwave irradiation.

In Power Law model  $n$  is approached to 1 which means that, these crudes don't have a strong resistance to flow after the microwave irradiation. The responds of the crude oils to the microwave irradiation is different due to the asphaltene content and composition of the asphaltene of these crude oils. The electrical properties of asphaltenes are such that they are susceptible to changes in colloidal structures of the molecules (related to colloidal properties) in the presence of electromagnetic irradiation [104]. It is proved that there is simultaneous dependence on electromagnetic treatment and asphaltene concentration such that as the power of electromagnetic treatment was increased, the viscosity at a given temperature increased as well. This dependence, however, depends on the temperature itself as well as the amount of asphaltenes [104]. When the asphaltene content of the heavy crude oils used in this study are considered, Batı Raman contains the highest amount of asphaltene (29% by weight) followed by Çamurlu and Garzan crudes [105]. Thus, the rheology of Batı Raman crude is expected to be affected more than the other crude oils. A study of the microstructure of asphaltene after treatment with electromagnetic irradiations warranted, but is beyond the scope of this thesis. One interesting feature of the crude oil viscosity is that all viscosity values converge to values that are close to each other regardless of the oil type. A higher temperature removes the effect of permanent alteration of asphaltene orientation that might have caused the alteration of the crude oil.

## **6.2. Microwave Experiments**

In the microwave experiments, 3 minutes heating time was used as heating time which is determined as optimum heating time for the electromagnetic heating of crude oil samples.

### 6.2.1. Effect of porosity, water saturation, wettability and permeability

In order to investigate the effect of porosity, water saturation, wettability and permeability on the electromagnetic heating process, crushed limestone samples at different porosities (25.86 %, 34.1%, and 38.95%) are mixed with the crude oil samples and water by using different water saturation values (60%, 40%, and 20%). The responses of 3 different wettability conditions on the electromagnetic heating were tested; i.e. water wet, oil wet, and mixed wet. Prepared samples were subjected to the microwave irradiation for 3 minutes.

Effect of porosity is given in Table 6.6. One can infer from Table 6.6 that lower the porosity yields higher recoveries. This is because of the permeability changes which makes to necessary to calculate the permeability of the limestone samples.

To calculate permeability a correlation between particle diameter and porosity was used.

$$k = \frac{\phi^3 D_p^2}{150(1 - \phi)^2} \quad (6.6)$$

Where,  $D_p$  is the particle diameter, (m),  $\phi$  is porosity,  $k$ , is permeability ( $m^2$ ). The permeability is multiplied by  $1.01325E+12$  for the unit conversion of permeability to the Darcy unit.

The particle diameters were found by using the sieve size used for the screening of limestone samples; i.e. 25.86% porosity equals to 10-20 mesh size, 38.95% porosity equals to 20-50 mesh size, 34.10% porosity equals to 80-160 mesh size. Calculated permeability variations with mesh size are given in Table 6.7.

Table 6.6 Porosity effect of microwave [106]

Sample	$S_w$ (%)	Porosity (%)	Oil production (ml)	Recovery (%)
Batı Raman	20	25.86	2.97	18.55
		34.10	0.89	5.17
		38.95	0.32	1.58
	40	25.86	3.65	28.45
		34.10	1.15	10.49
		38.95	0.88	6.05
	60	25.86	4.37	51.74
		34.10	0.83	11.91
		38.95	2.93	28.27
Çamurlu	20	25.86	2.18	14.04
		34.10	0.36	2.06
		38.95	1.21	5.77
	40	25.86	4.24	34.76
		34.10	0.39	3.25
		38.95	1.03	6.9
	60	25.86	1.66	19.69
		34.10	0.24	3.15
		38.95	0.26	2.54
Garzan	20	25.86	8.29	43.88
		34.10	0.12	0.78
		38.95	4.35	18.7
	40	25.86	10.1	81.73
		34.10	0.84	7.4
		38.95	4.03	25.68
	60	25.86	4.7	53.38
		34.10	0.24	2.51
		38.95	2.66	24.53

Highest oil recoveries were obtained for lowest porosity values. For Batı Raman crude oil highest oil production were obtained for 60% water saturation value. For Çamurlu and Garzan crude oil highest recoveris were obtained for 40% water saturation values.

Table 6.7 Permeability variations with mesh size [106]

Mesh Size	$D_p$ ( $\times 10^{-5}$ m)	$k$ ( $\times 10^{-12}$ m <sup>2</sup> )	$k$ (Darcy)
10-20	201 - 84	844.9 - 148.3	856.05 – 150.31
20-50	84 - 30	747.6 - 93.23	757.48 – 94.47
80-160	18 - 10	19.07 - 5.668	19.32 – 5.74

Table 6.6 and Table 6.7 show that high permeabilities yield better oil production values.

The effect of three different wetting conditions was tested by considering mixed wet, oil wet and water wet conditions on the microwave irradiation (Table 6.8).

Table 6.8 Wettability effect under the microwave irradiation [106]

Sample	S <sub>w</sub> (%)	Porosity (%)	Oil Production (%)		
			Mixed Wet	Oil Wet	Water Wet
Batı Raman	20	25.86	7.26	5.87	1.58
		34.10	19.56	12.19	18.55
		38.95	3.33	3.15	5.17
	40	25.86	5.17	9.27	6.05
		34.10	25.1	10.91	28.45
		38.95	7.13	2.81	10.49
	60	25.86	12.14	8.08	28.27
		34.10	11.63	20.34	51.74
		38.95	2.93	3.72	11.91
Çamurlu	20	25.86	17.51	16.42	5.77
		34.10	27.69	27.94	14.04
		38.95	0.66	10.81	2.06
	40	25.86	13.73	11.83	6.9
		34.10	32.57	13.87	34.76
		38.95	4.8	4.14	3.25
	60	25.86	11.03	16.81	2.54
		34.10	18.01	27.21	19.69
		38.95	1.88	3.44	3.15
Garzan	20	25.86	24.39	28.44	18.7
		34.10	3.97	12.3	0.78
		38.95	59.3	60.56	43.88
	40	25.86	27.64	19.47	25.68
		34.10	61.94	68.44	81.73
		38.95	4.68	2.88	7.4
	60	25.86	38.19	68.41	24.53
		34.10	49.18	63.48	53.38
		38.95	3.56	4.19	2.51

Determination of the effect of porosity, water saturation and wettability are summarized in Figure 6.1. According to this figure, effects of each parameter have to be interpreted separately.

Microwave heating efficiency is directly relevant to the composition of the material subjected to the microwave irradiation. In Figure 6.1, this relevancy is observed easily. While Batı Raman crude oil responds to the water wet condition and 60% of water saturation value, Çamurlu crude oil yields better results for oil wet condition and Garzan crude oil gives good oil production values for mixed wet condition. Thus, it can be inferred that if the crude oil is a viscous crude oil, like Batı Raman crude oil, microwave irradiation under water wet conditions will yield best oil production. When the crude oil has somewhat moderate viscosity, similar to Çamurlu crude oil, oil wet condition can yield better oil productions. Finally, as the crude oil is light enough, like Garzan crude oil, mixed wet conditions can give better results. Thus, wettability is a direct parameter that affects the microwave efficiency.

Also the saturation has a direct effect on the microwave irradiation. For Batı Raman crude oil, 60% water saturation values and for Çamurlu and Garzan crude oils, 40% water saturation values gave better oil production results.

For the entire crude oil samples, 25.86% the porosity value yielded the best oil production values. This porosity value has also the highest permeability values. Accordingly, even samples are differentiating; the effect of permeability remains the same. The oil production mechanism due to permeability seems to basically gravity drainage [19].

Since microwave heating depends on the absorption ability of the materials, it provides selective heating for different materials [25]. In order to explain the reason of the effect of crude oil viscosities on the wettability under microwave irradiation, chemical composition of crude oils should be well-defined. GC-MS (Gas chromatography-mass spectrometry) can be used to define the chemical composition and the amount of these compositions of the crude oil samples.

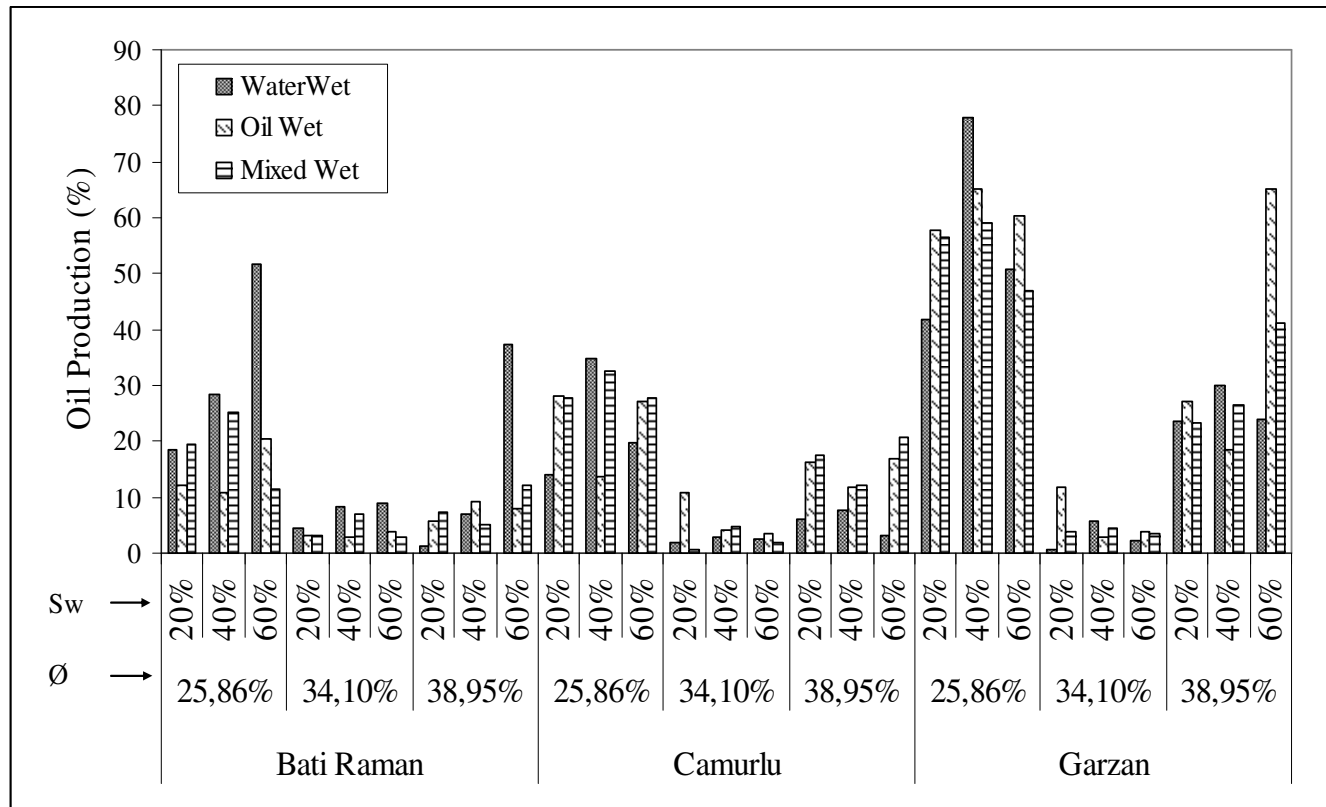


Figure 6.1 Oil production results for all samples [107]

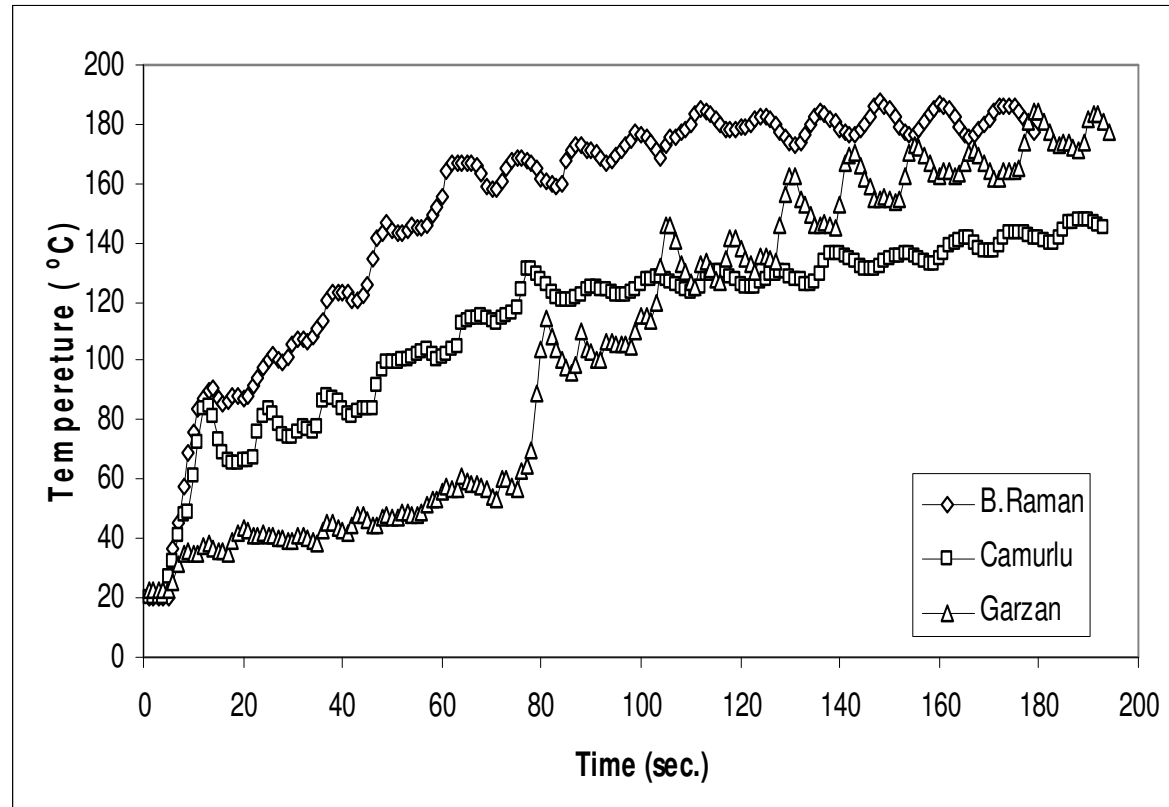


Figure 6.2 Temperature trends for best oil production values [107].

It can be seen that in all wettability cases low water saturations lead to smaller steady state temperature values. The steady state temperature in the mixed wet case was smaller than the other temperatures. It turns out that 40% water saturation case yielded the highest temperature in all cases but the water wet one. At low water and oil saturations, the dielectric permittivities of oil-wet media are lower than those of the water-wet ones [108]. This might be caused by the presence of an insulating oil film along the surface of the sand grains. Thus for a water wet medium and high water saturations the steady state temperature should be higher than the ones in oil wet and mixed wet cases. Since the steady state temperature and the viscosity are inversely proportional with each other at higher temperatures viscosity ( $\mu$ ) will be smaller and gravity drainage will be much more efficient since flow rate is proportional to square root of  $1/\mu$  [109]. Thus we expect higher production if the temperature is higher.

Besides the parameters mentioned above, temperature and heating strategy can also affect the efficiency of the microwave process (Figure 6.2, Figure 6.3).

Temperature/time plots show a steady linear climb with alternating trend up to a certain time, and then a change in slope is observed (Figure 6.2). As the temperature increases oil becomes less viscous and with the help of gravitational forces moves down to the conical production chamber. Thus voids are created making it increasingly difficult for the weaker waves to propagate. Waves with higher electromagnetic frequencies are able to overcome these “breaks” better than the weaker ones and are able to penetrate into the partially saturated porous medium and therefore, recover more oil. Since the total water present in the porous medium is different in each experiment and due to slight differences in packing flow paths (i.e. tortuosity) are somewhat different in each experiment. That’s why a different time is required to reach a slope change in temperature time plots. Moreover, since the number of liquid molecules that bump, rub, and agitate decrease as the water saturation decrease the resulting heating energy decreases. Another important observation is the presence of cyclic increase and decrease of measured temperatures during an experiment. Since a commercial microwave oven does not continuously supply microwaves cyclic increase and decrease of temperature is observed. For the microwave oven used in this study

the on/off cycle time is 12 seconds. Regarding the temperatures, the initial oil saturation is the controlling factor on the final temperature reached.

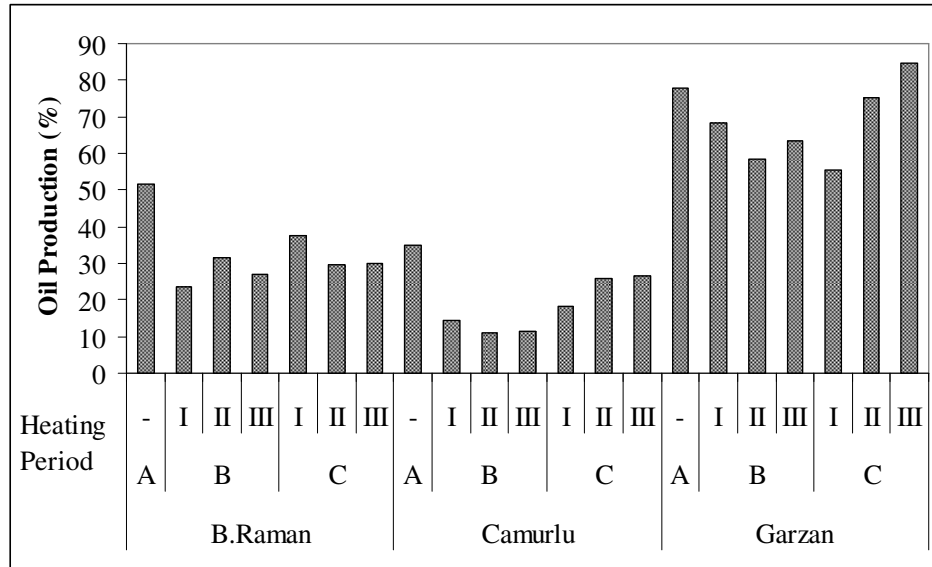


Figure 6.3 Periodic Heating Results [107]

Optimum heating strategy was investigated by changing the heating time (In Figure 6.3). To achieve this goal three cases were considered: 180, 60 and 30 seconds continuous heating (shown as A, B, and C; respectively in Figure 6.3). Furthermore, three different soaking times (I: 180, II: 240 and III: 360 seconds) were tested. It was observed that cumulative oil production was directly proportional to heating time regardless of the oil type. As the heating time increased the highest temperature reached at the end of a cycle increased and thus the production increased. While the initial production rate was not significantly affected by the operating strategy, there was an increase in the production rate at later times for runs with longer heating cycles were used. Thus the overall recovery is a strong function of temperature. In cases where longer soaking periods were applied higher oil productions compared to continuous heating were not observed due to heat losses during the long soaking periods.

Note that the microwave oven is not insulated. However, in real porous media differences between continuous heating and periodic heating might be smaller since heat losses will be somewhat smaller compared to the experiments.

#### 6.2.2. Recovery of oil shales under microwave irradiation

Effect of microwave irradiation on the recovery of oil shale was studied. In order to enhance the microwave efficiency, 3 different iron powders (Fe, Fe<sub>2</sub>O<sub>3</sub>, and FeCl<sub>3</sub>) and their three different doses (0.1%, 0.5%, and 1% by weight) were added to the samples as microwave receptors [80]. Iron powder types and doses were optimized according to the best oil production. During the experimental studies, produced oil volume, the temperature distribution and the gas emissions in terms of CO, H<sub>2</sub>S, Hydrocarbon (CH<sub>4</sub>), and O<sub>2</sub>, were recorded. Temperature and the gas emission distributions with time are given in Appendix B for each sample.

Oil and gas production results are summarized in Figure 6.4, Figure 6.5, Figure 6.6, and Figure 6.7 for all of the oil shale samples.

Because the highest oil production was obtained after the addition of 0.1% Fe, 0.1% Fe was selected as the optimum type and dose of iron powders for Himmetoğlu oil shale (Figure 6.4).

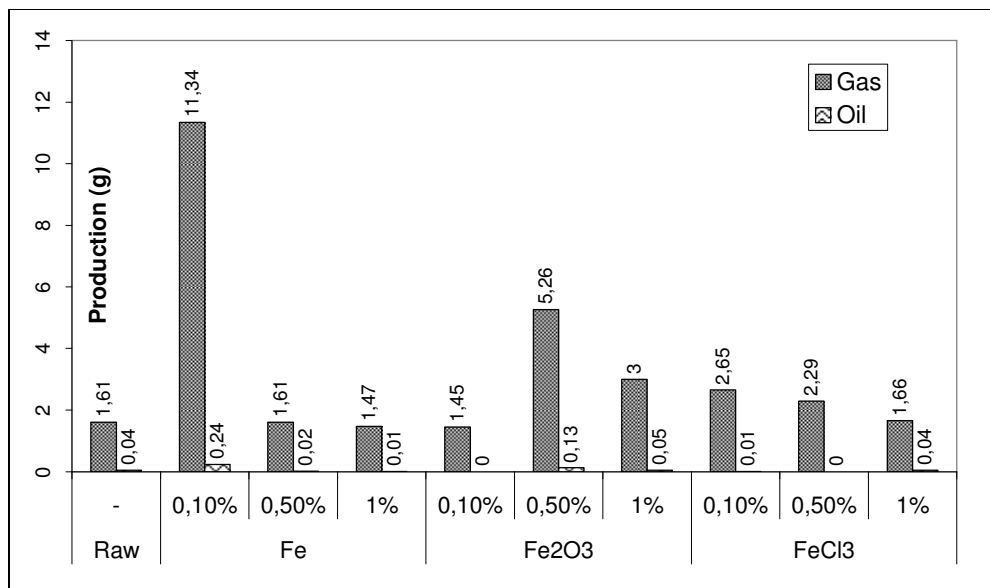


Figure 6.4 Optimization of iron powders for Himmetoğlu oil shale

The highest CO and H<sub>2</sub>S emissions were observed after the addition of 0.1% Fe (Table 6.9). Since the highest gas production is obtained after the addition of 0.1% Fe (Figure 6.4), it can be said that the most of the produced gases contain CO and H<sub>2</sub>S. Carbon monoxide is a by-product of incomplete combustion, the high amount of CO shows that during microwave heating incomplete combustion occurs. The presence of hydrogen sulfide is an evidence of occurrence of hydrodesulphurization process. Hydrodesulphurization (HDS) is a catalytic chemical process widely used to remove sulfur (S) from natural gas and from refined petroleum products such as gasoline or petrol, jet fuel, kerosene, diesel fuel, and fuel oils [110, 111]. Hydrodesulphurization is a hydrogenolysis reaction. The hydrodesulphurization reaction can be simply expressed for ethanethiol (C<sub>2</sub>H<sub>5</sub>SH) with reaction shown in equation 6.7.



Besides the ethanethiol (C<sub>2</sub>H<sub>5</sub>SH), there are numerous complex compounds contain sulfur inside the heavy oil carbonates and oil shales. The

hydrodesulphurization process helps to remove this impurity from these resources. This process also helps to decrease the oil viscosity by increasing the temperature.

Table 6.9 Microwave experiment summary for Himmetoğlu oil shale

Sample	Addition	Total Gas Emission (ppm)		Production (g)	
		CO	H <sub>2</sub> S	Gas	Oil
Raw	-	106.1	2.6	1.61	0.04
Fe	0.1%	1383.7	67.3	11.34	0.24
	0.5%	28.9	0.0	1.61	0.02
	1%	8.0	0.1	1.47	0.01
Fe <sub>2</sub> O <sub>3</sub>	0.1%	6.1	0.0	1.45	0
	0.5%	365.4	16.2	5.26	0.13
	1%	15.4	0.2	3	0.05
FeCl <sub>3</sub>	0.1%	25.3	0.1	2.65	0.01
	0.5%	27.9	0.6	2.29	0
	1%	0.0	0.0	1.66	0.04

Since the highest oil production was obtained after the addition of 0.1% Fe<sub>2</sub>O<sub>3</sub> the optimum dose for Hatıldağ oil shale was determined as 0.1% Fe<sub>2</sub>O<sub>3</sub> (Figure 6.5)

In order to understand the mechanisms occurred during the microwave heating of Hatıldağ oil shale, gas emission, oil production and gas production should be considered together. In Table 6.10 results obtained for Hatıldağ oil shale were summarized.

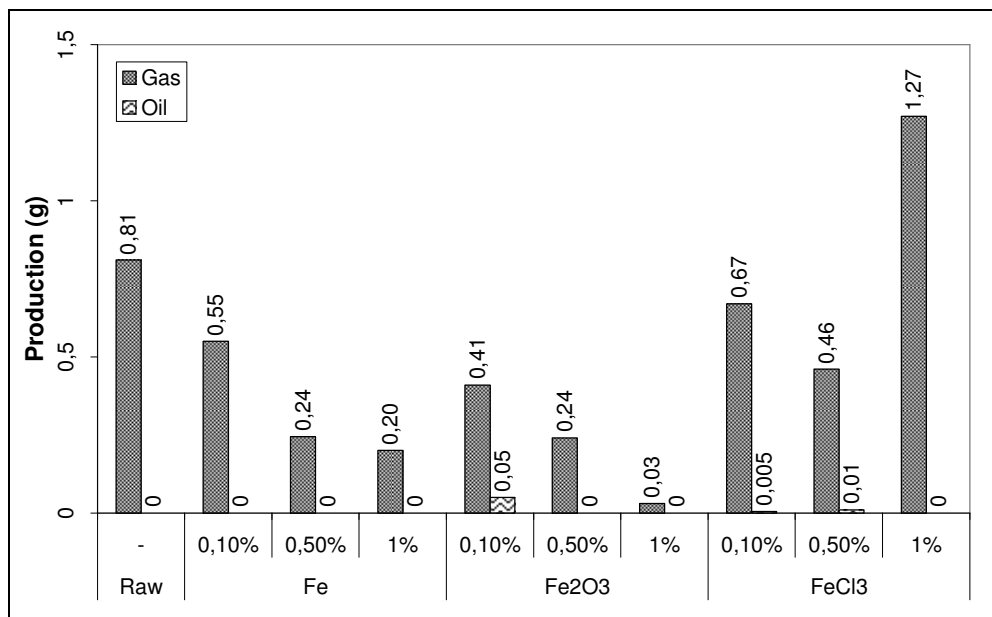


Figure 6.5 Optimization of iron powders for Hatıldağ oil shale

Table 6.10 Microwave experiment summary for Hatıldağ oil shale

Sample	Addition	Total Gas Emissions (ppm)		Production (g)	
		CO	H <sub>2</sub> S	Gas	Oil
Raw	-	12.5	0.1	0.81	0
Fe	0.1%	38	0.2	0.55	0
	0.5%	1.3	0	0.244	0
	1%	3.9	0	0.2	0
Fe <sub>2</sub> O <sub>3</sub>	0.1%	49.7	0.3	0.41	0.05
	0.5%	3.6	0	0.24	0
	1%	2.5	0	0.03	0
FeCl <sub>3</sub>	0.1%	68.7	0.8	0.67	0.005
	0.5%	0	0	0.46	0.01
	1%	100.9	0	1.27	0

After the microwave heating of raw Hatıldağ oil shale, 0.81 g gas was produced. 0.81 g gas covers the 12.5 ppm CO and 0.1 ppm H<sub>2</sub>S and the other gases exerted from the system which cannot be detected by multi gas controller device.

After the addition of 0.1% Fe, while the CO and H<sub>2</sub>S emissions are increased (volume base), and gas production (weight base) decreased. One can conclude from this result that raw oil shale process by microwave irradiation causes to form gases that cannot be detected by the multi gas controller. Also, since CO is one of the by product of pyrolysis process, the results show that after 0.1% Fe addition, pyrolysis can be accomplished better. Fe also can accelerate the incomplete combustion and/or hydrodesulphurization reaction to form CO and/or H<sub>2</sub>S; which can be another reason of increasing the CO and H<sub>2</sub>S concentration after the addition of 0.1 % Fe [112, 113]. Furthermore, it helps to remove one of the impurities (S) inside the oil shale, by helping to form more H<sub>2</sub>S. For the other doses of Fe, CO emission was not observed, so the optimum dose of Fe for Hatıldağ oil shale can be determined as 0.1%.

After the addition of Fe<sub>2</sub>O<sub>3</sub>, high CO emissions were observed and still the gas production is less than the gas production of raw sample by weight. The same discussion can be made for the 0.1% dose of Fe<sub>2</sub>O<sub>3</sub>. This dose and type also help to produce oil. Because it is the highest oil production among the other iron powders types and dose, 0.1% Fe<sub>2</sub>O<sub>3</sub> was selected as the optimum type and dose for the production of Hatıldağ oil shale.

For the 1% FeCl<sub>3</sub> addition case, while there is no oil production observed, the total gas weight and the total volume of the CO give the highest values among the other values. It is due to the temperature of the sample at the end of the process. It is the highest temperature among this set experiment with 1300 °C. At this temperature all of the light and moderate fractions and even the heaviest part of the oil are evaporated [114]. Pyrolysis, combustion, and incomplete combustion occur together. In order to understand which mechanism dominates, complete gas and ash analyses should be done.

For Seyitömer oil shale, no oil production was observed. Therefore, the optimum type and dose of the iron powder was made on the basis of the highest gas production. Thus, the optimum type and dose is selected as 0.5% Fe (Figure 6.6).

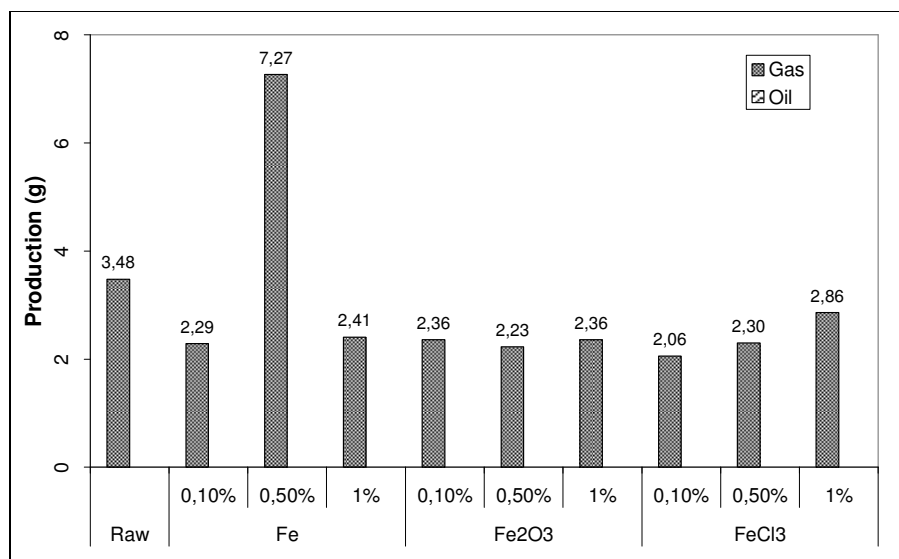


Figure 6.6 Optimization of iron powders for Seyitömer oil shale

While the highest gas production was observed after the addition of 0.5% Fe, CO and H<sub>2</sub>S emissions were not be detected for this dose of Fe (Table 6.11). The high doses of Fe and Fe<sub>2</sub>O<sub>3</sub> and all doses of FeCl<sub>3</sub> help to remove O and S as CO and H<sub>2</sub>S forms.

Table 6.11 Microwave experiment summary for Seyitömer oil shale

Sample	Addition	Total Gas Emissions (ppm)		Production (g)	
		CO	H <sub>2</sub> S	Gas	Oil
Raw	-	2.4	0.1	3.48	0.00
Fe	0.1%	0	0	2.29	0.00
	0.5%	0	0	7.27	0.00
	1%	298	1.4	2.41	0.00
Fe <sub>2</sub> O <sub>3</sub>	0.1%	0	0	2.36	0.00
	0.5%	0	0	2.23	0.00
	1%	0.2	0	2.36	0.00
FeCl <sub>3</sub>	0.1%	48.3	0.4	2.06	0.00
	0.5%	2.9	0.1	2.30	0.00
	1%	26.7	0.6	2.86	0.00

By using the same logic, the optimum doses and types of iron powders for Ulukışla oil shales were selected as 0.1% Fe<sub>2</sub>O<sub>3</sub> Figure 6.7).

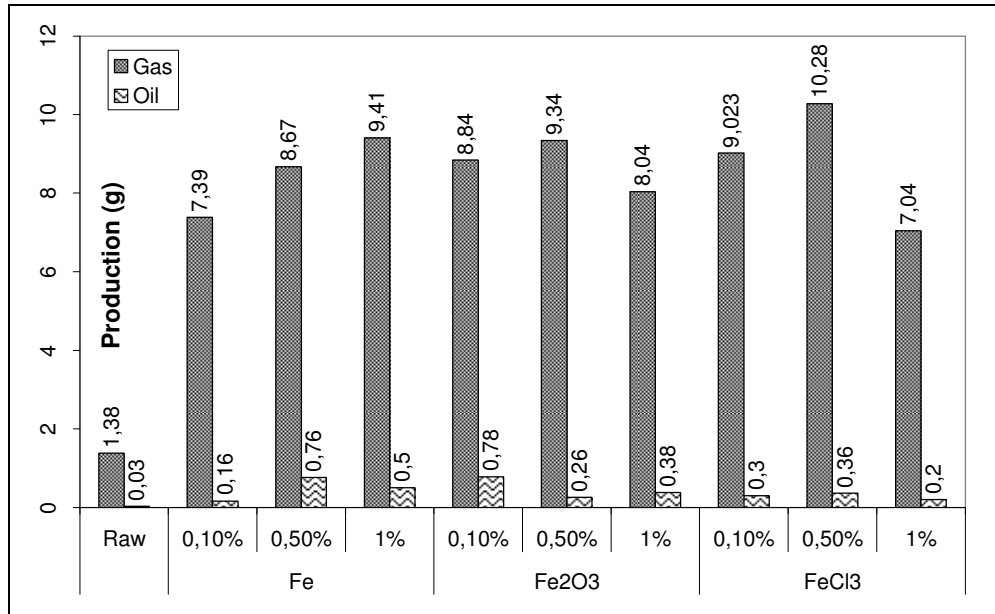


Figure 6.7 Optimization of iron powders for Niğde-Ulukışla oil shale

The total gas emissions for Ulukışla oil shales have a parallelism with the oil production values. Therefore, it can be said that most of the produced gas can be CO and H<sub>2</sub>S but after the addition of FeCl<sub>3</sub>, produced gases are different from CO and H<sub>2</sub>S. CH<sub>4</sub> was detected after the addition of 0.1% Fe<sub>2</sub>O<sub>3</sub> which means that Fe<sub>2</sub>O<sub>3</sub> helps to form lighter hydrocarbons.

Table 6.12 Microwave experiment summary for Niğde-Ulukışla oil shale

Sample	Addition	Total Gas Emissions (ppm)			Production (g)	
		CO	H <sub>2</sub> S	CH <sub>4</sub>	Gas	Oil
Raw	-	1.2	0.5	0.00	1.38	0.03
Fe	0.1%	135	17.2	0.00	7.39	0.16
	0.5%	435	8.1	0.00	8.67	0.76
	1%	393.5	11.2	0.00	9.41	0.5
Fe <sub>2</sub> O <sub>3</sub>	0.1%	1436	22.1	2.3	8.84	0.78
	0.5%	592.8	23.4	0.00	9.34	0.26
	1%	720.2	22.6	0.00	8.04	0.38
FeCl <sub>3</sub>	0.1%	9.5	0.00	0.00	9.023	0.3
	0.5%	131	0.00	0.00	10.28	0.36
	1%	187.6	0.00	0.00	7.04	0.2

Due to the compositional difference of the oil shales (Table 2.4), iron powders yielded different oil and gas production results. The produced oil and gas composition can also be different due to the oil composition and the iron reactions with the oil compounds and produced gas compounds.

### 6.3. Retort Experiments

There are two important temperatures for the pyrolysis of a fossil fuel resource (100 °C and 500 °C). 100 °C is the temperature necessary for the vaporization of the physically bonded water [98]. 500 °C is the pyrolysis temperature required for the decomposition of the kerogen. This temperature covers the boiling point of most of the hydrocarbons [114]. To achieve the vaporization of water or pyrolysis of kerogen, the only requirement is not temperature alone. Due to the complex reactions occurring during the process, reactions may also be completed within adequate time period. Therefore, besides the heating processes, also the soaking processes were applied during the retort experiments.

Firstly, the effects of soaking and heating periods were examined. Therefore, in order to determine the optimum heating periods, eight different experiments were

carried out with Niğde-Ulukişla (OS4) oil shale. Optimum heating and soaking periods were selected according to the highest oil production. These eight experiments are summarized in Table 6.13. Since thermal cracking which is also known as pyrolysis, takes place over 500 °C, 500 °C was selected as final temperature value reached to produce shale oil [15].

Table 6.13 Determination of optimum heating period for retort experiments [115]

# of Experiments	1 <sup>st</sup> Period				2 <sup>nd</sup> Period				P (cm <sup>3</sup> )
	Heating		Soaking		Heating		Soaking		
	D (s)	T (°C)	D (s)	T (°C)	D (s)	T (°C)	D (s)	T (°C)	
1	300	100	3600	100	9000	500	-	-	3
2	1800	100	3600	100	5400	500	4500	500	4
3	1200	100	2700	100	6000	500	6000	500	0,2
4	1200	100	1800	100	900	580	-	-	1
5	3600	100	-	-	6000	520	-	-	1
6	600	100	5400	100	5400	500	-	-	0,2
7	1800	100	3600	100	12600	350	-	-	0
8	-	-	6000	500	-	-	-	-	3

\*D: Duration, T: Temperature values at the end of the periods, P: Oil Production

Since the highest production obtained after the second experiment, heat and soak periods belong to this experiment were selected as optimum periods. Other experiments were tackled by using this optimum condition. Temperature profile for the optimum operation periods is given in Figure 6.8.

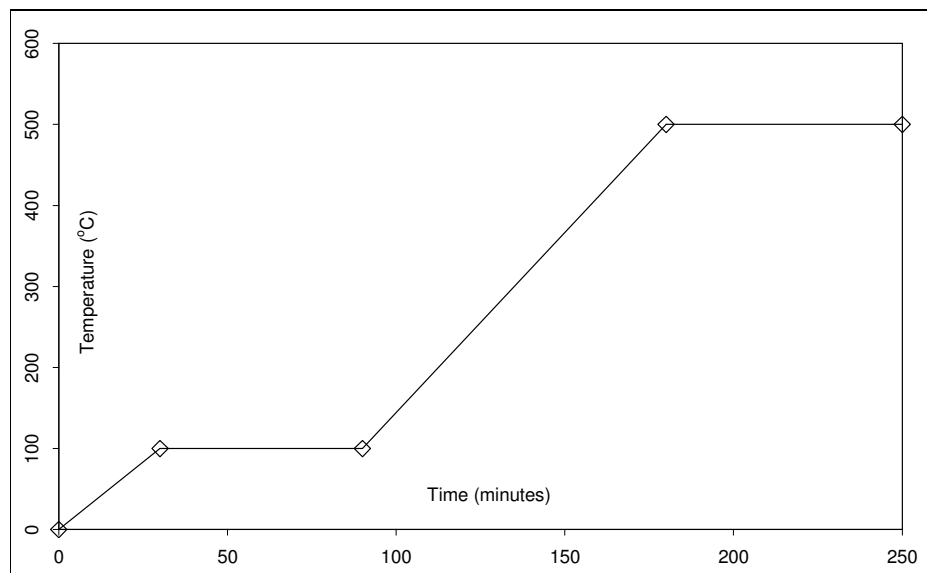


Figure 6.8 Temperature profile for the optimum operation periods [115]

One can infer from Experiment 7 that below pyrolysis temperature, it is impossible to produce oil from oil shale samples. Although it is possible to produce oil from oil shale when pyrolysis temperature is reached, the oil produced would not be much. To enhance the oil production efficiencies, effective temperature distribution and viscosity reduction of the shale oil should be accomplished together. Therefore, iron powders efficiencies on the oil production were examined by using retort setup. Since the retort experiments are time consuming when compared with the microwave experiments, the optimum doses found in microwave experiments were applied to the retort experiments. Oil production, after retorting of raw oil shale samples and after retorting of samples containing optimum types and doses of iron powders are summarized in Figure 6.9. (OS1: Himmetoğlu oil shale, OS2: Hatıldığ oil shale, OS3: Seyitömer oil shale, OS4: Ulukışla oil shale)

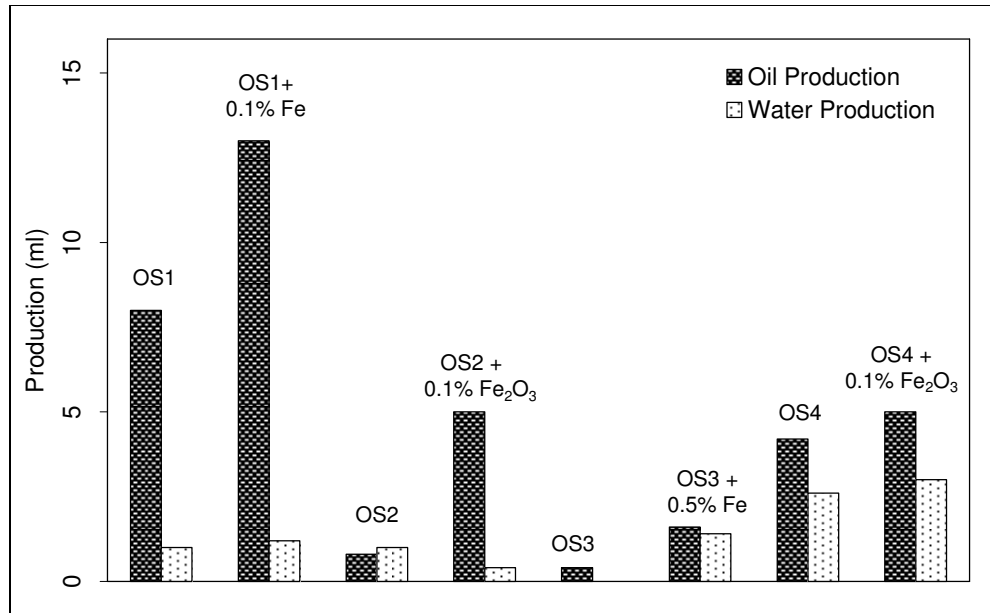


Figure 6.9 Retort experiment results for oil shale samples [116].

Because iron powders help to increase the thermal conductivity of the system, heat transfer accomplished more efficiently yielding increased oil production at laboratory conditions. Thermal cracking and catalytic cracking occur together after the addition of iron powders which help to break the chemical bonds of long chained hydrocarbons by increasing temperature and by catalysis effect of iron powders [15, 117]. Also, the magnetic effect of iron powders on the reduction of oil viscosity caused an increase in the oil production after the addition of iron powders [15, 118].

In order to understand the mechanism more clearly, gas emissions were measured during the experimental studies in terms of CO, H<sub>2</sub>S, CH<sub>4</sub> and O<sub>2</sub> (Table 6.14). After the addition of optimum doses of iron powders, CO and H<sub>2</sub>S concentrations increased for Himmetoğlu and Hatıldığ oil shales but decreased for Niğde-Ulukışla oil shale. For Seyitömer oil shale the CO concentration decreased but H<sub>2</sub>S concentration increased. It can be concluded that each oil shale has a different respond to different catalysts owing to their chemical

composition. Iron powders help to increase the thermal conductivity of the system, hence help to increase the temperature of the samples. Therefore, the temperature for the evaporation of some hydrocarbon gases can be achieved after the addition of iron powders, so the gas amount can be increased.

Yet another reason for such productions can be the catalytic cracking which helps to increase the reaction speeds [94]. Thus, within the same period of time, produced oil and gas amount due to the addition of iron powders can increase.

Table 6.14 Summary for the gas emissions and productions for oil shale samples

Sample	Addition	Total Gas Emissions (ppm)		Production (g)		
		CO	H <sub>2</sub> S	Gas	Oil	Water
Himmetoğlu	-	146.9	14.5	30.94	0.93	0
	0.1% Fe	1539.9	391.4	22.673	1.63	1.4
Hatıldağ	-	47.2	2.4	31.49	0.39	1
	0.1% Fe <sub>2</sub> O <sub>3</sub>	155.7	3.0	28.642	4.93	0.4
Seyitömer	-	319.3	0.9	79.07	7.73	1
	0.5% Fe	28.2	2.2	124.76	13.72	1.2
Ulukışla	-	5474.3	9.6	56.64	3.74	2.6
	0.1% Fe <sub>2</sub> O <sub>3</sub>	4155.8	0.8	49.502	4.61	3

Decreasing of the gas concentration can be explained by the aforementioned complex reactions of iron powders (see Chapter 5). Iron powders can react with some lighter hydrocarbon gases and at that temperature, this reaction can be at liquid phase which may help to increase oil production [82]. On the other hand, increasing oil production after the addition of iron powders can be explained as catalysis effect [88, 112].

Because the weight of produced oil was measured by the help of graduated cylinders, it is easy to find the density and API gravity of shale oils. Density and API gravities are given in Table 6.15. Density and API gravities are calculated by dividing the weight of produced oil to the volume of it. Since Table 6.15 is not

constructed by using a densitometer, the obtained data may give an idea about the densities of the shale oils which do not exist in the literature.

Table 6.15 Density and API gravity of oil shales

Sample	Addition	Oil Density (g/cm <sup>3</sup> )	API Gravity
Himmetođlu	-	0.97	14.94
	0.1% Fe	1.06	2.57
Hatıldađ	-	0.89	27.49
	0.1% Fe <sub>2</sub> O <sub>3</sub>	0.99	12.01
Seyitömer	-	1.03	5.88
	0.5% Fe	1.02	7.40
Ulukıřla	1%	0.89	27.40
	0.1% Fe <sub>2</sub> O <sub>3</sub>	0.92	21.97

#### 6.4. Numerical Simulation

All simulation studies were performed using the electrical heating option of the commercial simulator CMG-STARS, 2007 (Steam, Thermal, and Advanced Processes Reservoir Simulator). The domain was discretized into 20x1x10, 3-D radial blocks of varying size in the radial direction and constant size in the vertical direction. The dimensions of the reservoir for the field case and grid size for both laboratory and field cases are given in Figure 6.10.

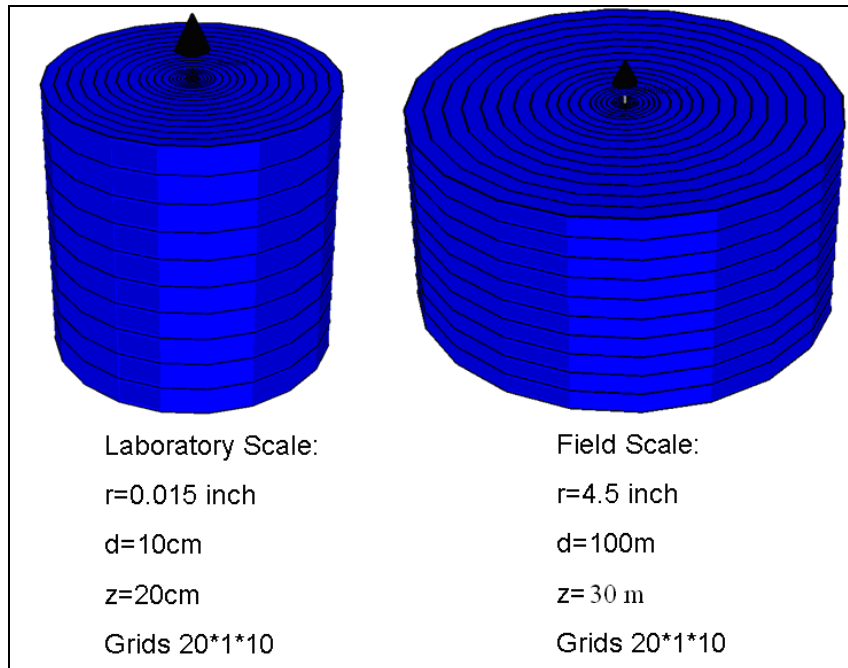


Figure 6.10 Grid sizes used in simulations [116].

Current continuity equation, heat generation from ohmic losses, and heat generation are considered together in CMG STARS model (see Chapter 5).

Because the electrical heating option of CMG, STARS cannot model the microwave heating, only the retort experiment results could be modeled by using CMG, STARS model.

#### 6.4.1. Numerical Simulation Retorting of Oil Shales

The required input data for simulation are porosity, permeability, thermal conductivity, rock heat capacity, rock compressibility, viscosity and relative permeabilities. The output data of the simulation is time dependent temperature distribution and oil production data which were also determined experimentally. All the required input data (porosity, permeability, rock properties, etc.) except

temperature-viscosity relationship were taken from the literature for the numerical simulation runs. These data were compiled from literature about the oil shales studied in this study and the common oil shale fields around the world. The viscosity-temperature relationship was obtained through matching numerically obtained temperature distributions and production data to the experimental output. Another critical parameter in addition to the viscosity-temperature data is the relative permeabilities. It was observed that the effect of relative permeabilities is trivial compared to the viscosity-temperature data. Relative permeability data used in the study were taken from another oil shale field (Figure 6.11 and Figure 6.12). Hence, relative permeabilities typically suggested for these types of simulations in the literature were adapted and used.

Because shale oil is too viscous and the amount of produced oil at the laboratory conditions is very little, it was very difficult to determine the viscosity of the shale oil experimentally. Therefore, the only way to obtain this critical data was experimental matching exercise. Another critical point that entails this type of approach is to determine the level of heating and corresponding temperature to have oil become flowable.

Using the shale oil viscosity values and literature data, the process was then simulated at field scale. In these numerical simulation studies, the power of the system, operation time and the number of heater were optimized by considering both oil production and economics of the project.

During the experiments conducted with oil shale samples, temperature data and production data were recorded continuously. As mentioned above, produced oil from oil shale is highly viscous and very little in amount at the laboratory conditions. Thus, shale oil viscosities are difficult to measure. Moreover, there is little knowledge about oil shale properties in the literature. In the simulation studies, literature data given in Table 6.16, Figure 6.11, and Figure 6.12 were used.

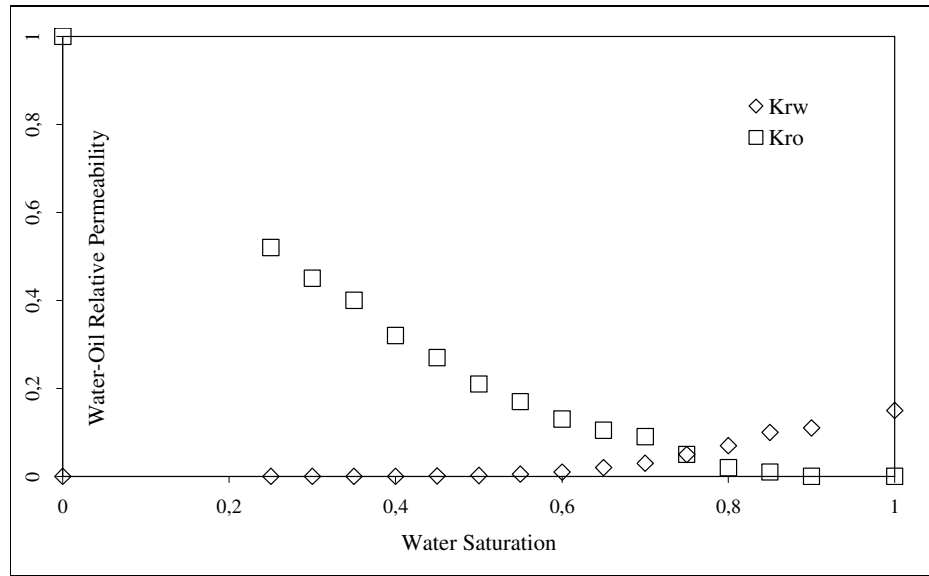


Figure 6.11 Water-oil relative permeability curves used in simulation for oil shale samples [119]

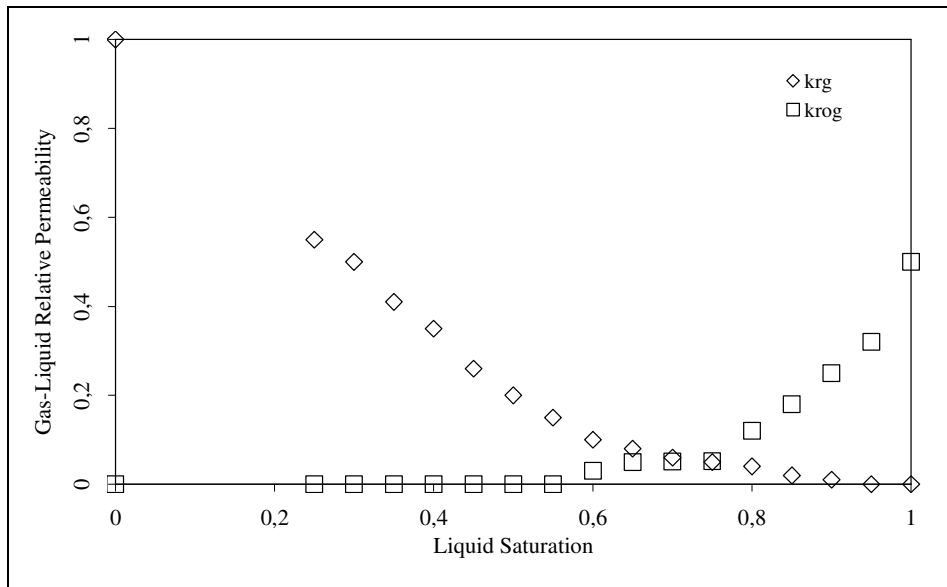


Figure 6.12 Gas-liquid relative permeability curves used in simulation for oil shale samples [119]

Table 6.16 Data used for the simulation of laboratory and field cases [120, 121]

Oil Shale Samples	Addition	Parameters		
		RHC (*10 <sup>5</sup> J/m <sup>3</sup> -C)	RTC (*10 <sup>5</sup> J/m-day-C)	MW (g/mole)
Himmetođlu (OS1)	Raw	6.4	1.44	650
	0.1 %Fe	6.53	2.06	650
Hatıldađ (OS2)	Raw	13.7	1.44	600
	0.1 %Fe <sub>2</sub> O <sub>3</sub>	12.9	2.06	600
Seyitömer (OS3)	Raw	6.5	1.7	600
	0.5 %Fe	6.9	4.5	597
Ulukıřla (OS4)	Raw	8.9	1.44	600
	0.1 % Fe <sub>2</sub> O <sub>3</sub>	9.2	2.06	600

RHC: Rock Heat Capacity, RTC: Rock Thermal Conductivity, MW: Molecular Weight

Numerical simulation conducted for laboratory studies were carried out under 101 kPa pressure and 21 °C temperature. Porosity, permeability, rock compressibility, reservoir temperature, initial water saturation and formation thickness were taken as 45%, 5000 md, 0.001 kPa<sup>-1</sup>, 50 °C, 25%, and 30 m, respectively. Sensitivity analyses were achieved for different reservoir pressures (5000-10000 kPa) and reservoir depths (500-5000 m) for the field case simulation studies [8, 13].

Using the viscosity as the adjustable parameter, the simulation outputs were matched to the experimentally obtained temperature and production data. These matches are given in Figure 6.13 and Figure 6.14. The viscosity-temperature relationship obtained through this exercise is shown in Figure 6.15.

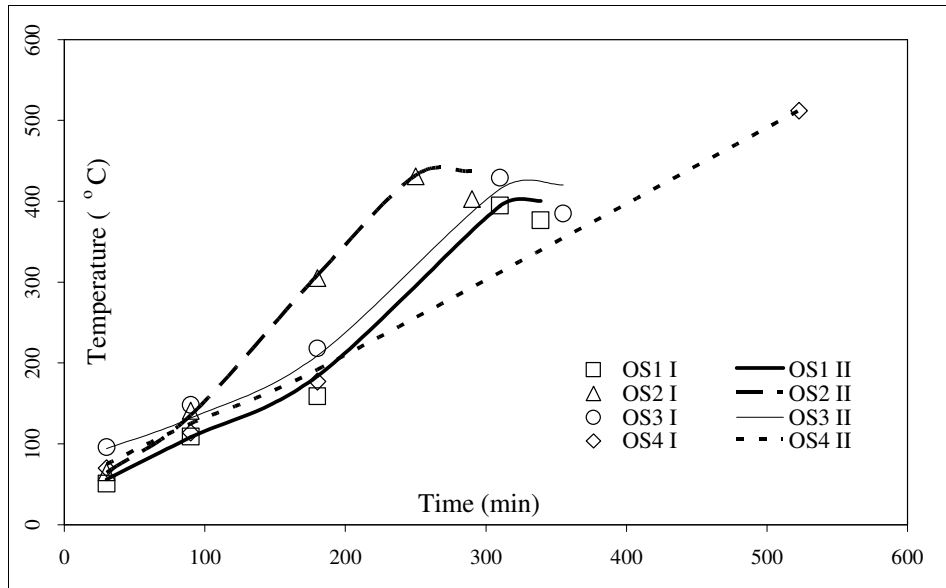


Figure 6.13 Temperature match for all oil shales (I: Experimental Studies Results, II: Numerical Studies Results)

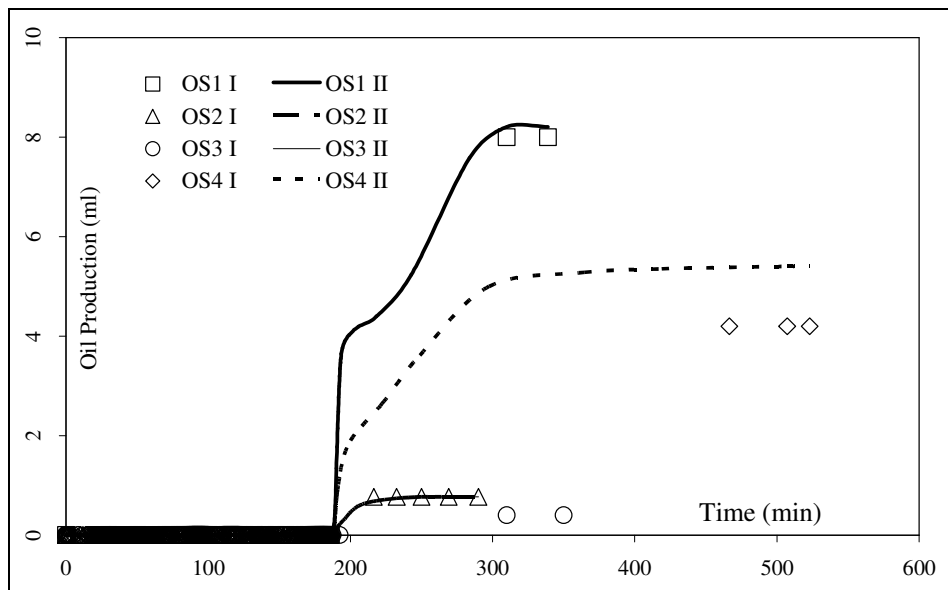


Figure 6.14 Production match for all oil shales (I: Experimental Studies Results, II: Numerical Studies Results)

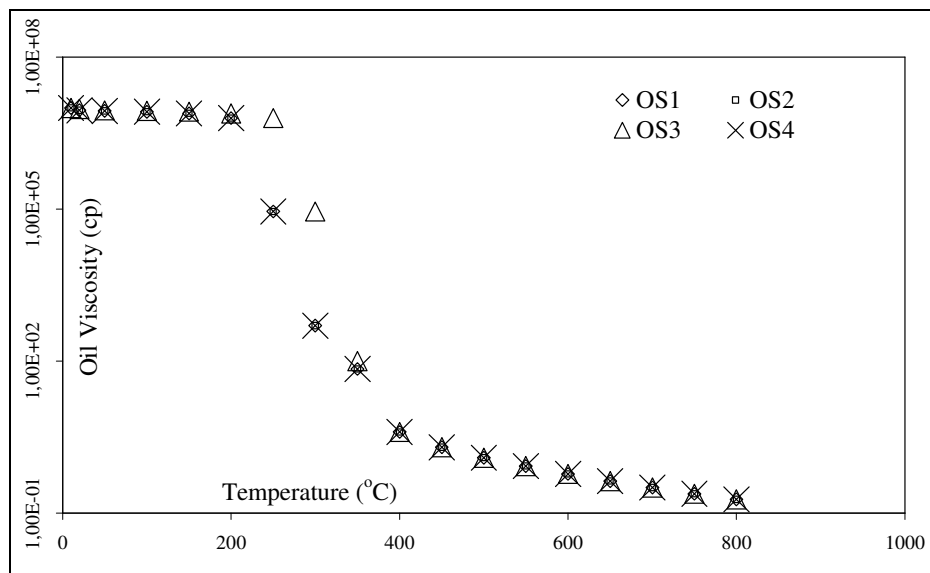


Figure 6.15 Viscosity variations of all shale oils

After 400 °C a linear relationship was observed between temperature and shale oil viscosity on a semi-log plot which means that oil starts to flow because of reaching the pyrolysis temperature. This type of trend observed after 400 °C is a typical relationship between viscosity and temperature during pyrolysis [8, 12].

Simulation studies were also performed for the verification of the experimental studies carried out after the addition of optimum iron powder types and doses. These simulation matches for all oil shales containing optimum dose and types of iron powders are given in Figure 6.16 and Figure 6.17 for temperature and production, respectively. The viscosity-temperature relationship obtained through the matching exercise is shown in Figure 6.18. As can be inferred from Figure 6.18, the iron powder addition decreases the shale oil viscosity considerably.

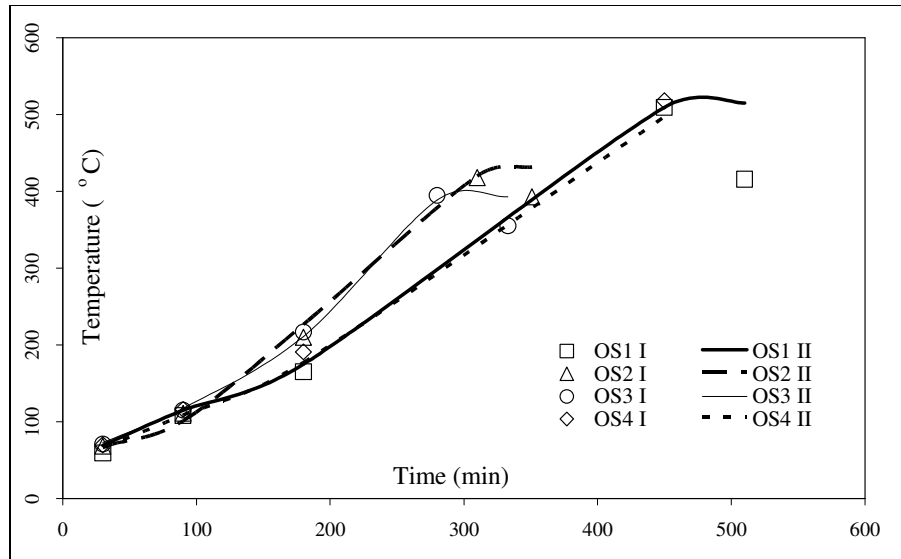


Figure 6.16 Temperature matches for all oil shale after the addition of optimum doses of iron powders (I: Experimental Studies Results, II: Numerical Studies Results)

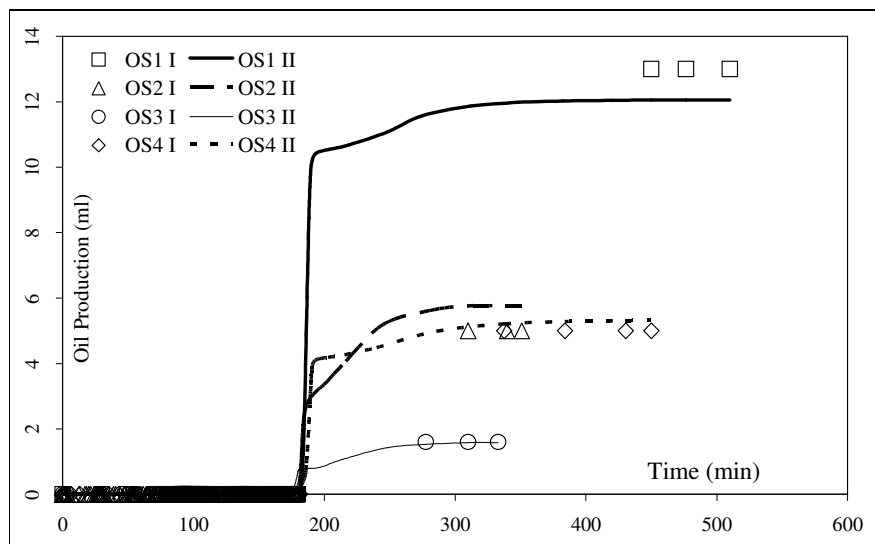


Figure 6.17 Production matches for all oil shale after the addition of optimum doses of iron powders (I: Experimental Studies Results, II: Numerical Studies Results)

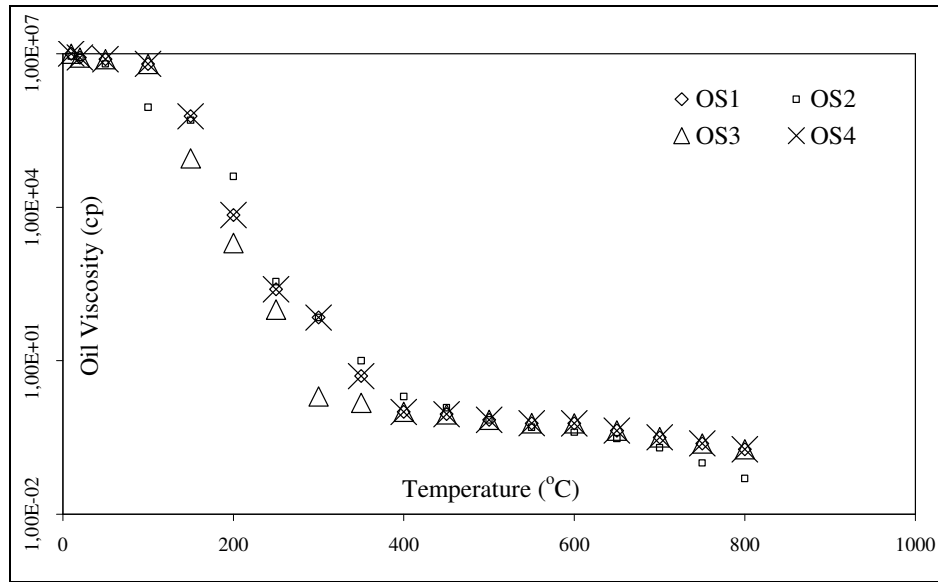


Figure 6.18 Viscosity variations for all oil shale after the addition of optimum doses of iron powders

The viscosity - temperature data obtained through matching the experimental results to the numerical output, and the porosity, permeability, rock compressibility, rock heat capacity, rock thermal conductivity and the molecular weight of oil values (as given in Table 6.16) previously used for the simulation of laboratory experiments were also used to simulate the field cases. Using the data in Table 6.16, existing as reservoir condition and some other data, also used for the laboratory simulation; the operation time, the power needed in the field application, and the number of heaters were optimized. For this purpose, an operation time of 60 and 90 days, the power values of 46296 W, 34722 W, and 23148 W, and 5 or 10 heaters were used. Furthermore, sensitivity analyses were conducted by using two different reservoir depths, i.e. 500 and 3000 m, at three different reservoir pressure values, i.e. 5000 kPa, 9000 kPa, and 10000 kPa and three different bottom hole pressures, i.e. 1000 kPa, 1800 kPa, and 2000 kPa. As the simulation results yielded very similar oil production results (given in Section 6.4.2) for different reservoir depths, pressures and bottom hole pressures (even at extreme values of those reservoir properties), it can be stated that electrical

heating of oil shale reservoirs are not critically affected by reservoir depth, pressure and bottom hole pressure values [122].

In the simulation runs, oil was produced continuously while heating the reservoir in the same well. When soaking period was applied in the simulations, it was observed that oil production did not change significantly but the operation time increased which resulted in an increase in the cost of the process.

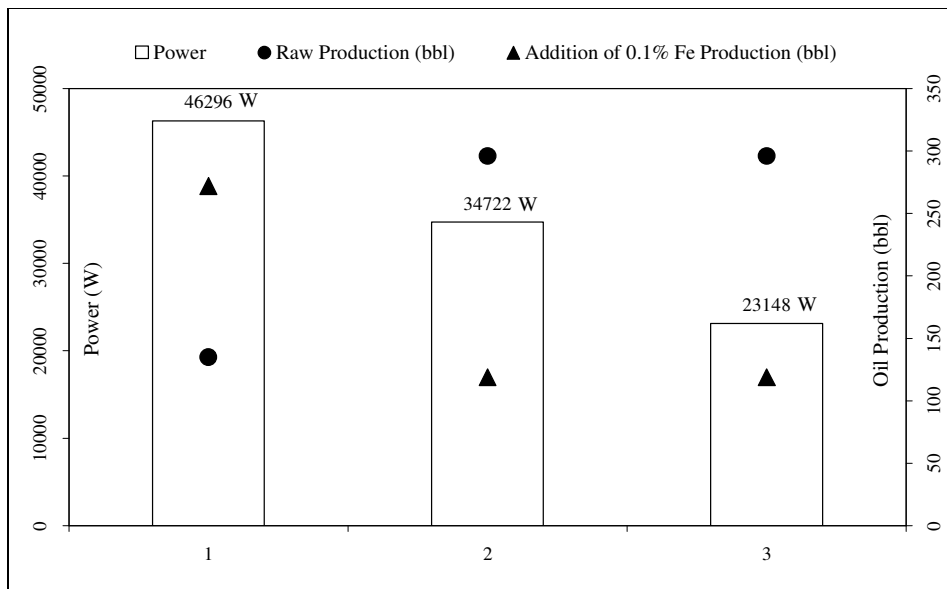


Figure 6.19 Simulation results for Himmetoğlu (OS1) (field case)

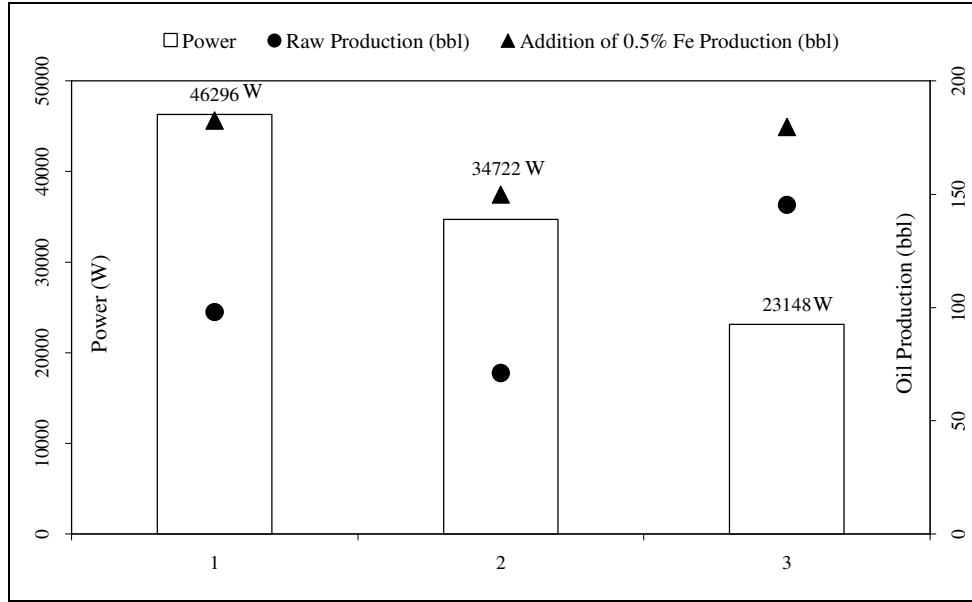


Figure 6.20 Simulation results for Hatıldağ (OS2) (field case)

For Himmetoğlu and Hatıldağ (OS1 and OS2), three different field simulations were conducted and the results were summarized in Figure 6.19 and Figure 6.20, respectively. While in the first runs the operation time was 60 days, in the second and third runs operation times were increased to 90 days. The number of heaters for the third runs was reduced from 10 to 5 so that the power exerted for these operations were decreased. For both cases, the third run yielded the optimum oil production (highest recovery/power ratio). It is observed that while the iron powder addition caused an increase in oil production for Hatıldağ oil shale (OS2), the opposite was observed for Himmetoğlu oil shale (OS1) when the power was reduced. The results for Seyitömer (OS3) are shown in Figure 6.21. It was observed that the second run gave better oil production for the raw oil shale. But after the addition of 0.5% Fe, the oil production values increased sharply because of the aforementioned effect of viscosity variation after the addition of 0.5% Fe [117, 118]. All the runs were performed for 60 days and with 10 heaters [122].

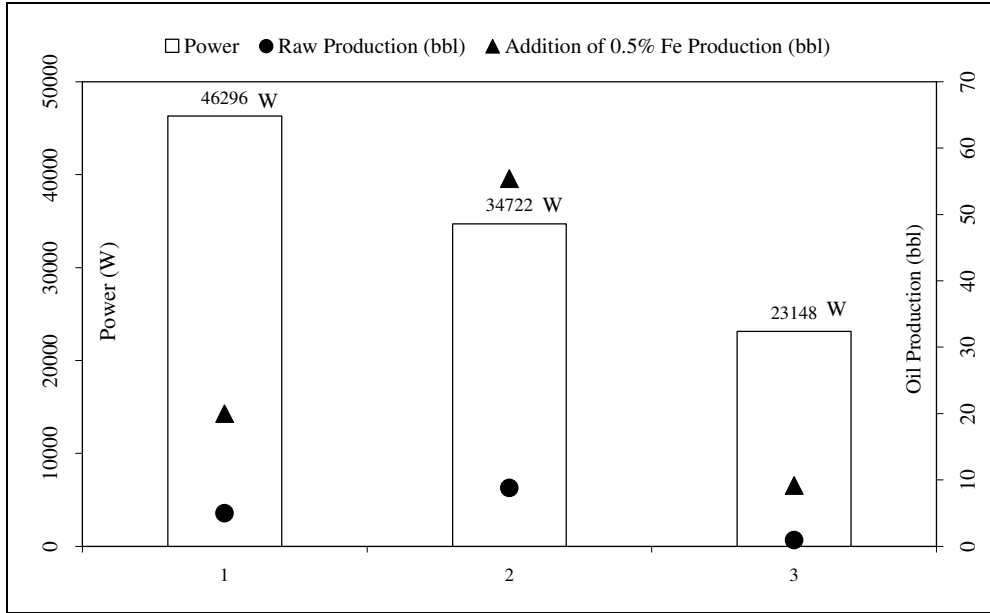


Figure 6. 21 Simulation results for Seyitömer (OS3) (field case)

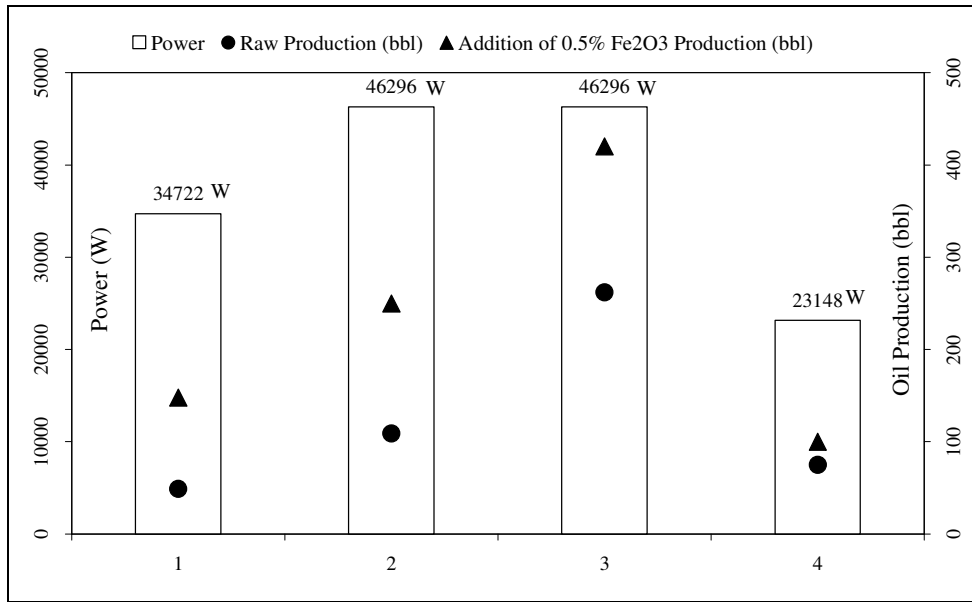


Figure 6. 22 Simulation results for Ulukışla (OS4) (field case)

For Ulukışla (OS4), four different runs were carried out and the third run yielded the highest oil production. Also the difference between the raw and 0.1%  $\text{Fe}_2\text{O}_3$  cases were very similar for the first three runs; the fourth run showed no significant change in production when  $\text{Fe}_2\text{O}_3$  is added. For the first two and fourth runs, the operation times were 60 days, it was 90 days for the third run. Ten heaters were used for the first three runs and, for the fourth run; the number of heaters was decreased to five. While keeping the number of heaters (i.e., 10) and the operation times (i.e., 60 days) constant, different powers were applied (i.e., 34722 W and 46296 W) in the first and second cases. The oil production increased from 49 bbl to 109 bbl for raw oil shale and 148 bbl to 250 bbl for additional oil shale [122].

The second and third runs compare the cases with different operation times. While the power (i.e., 46296 W) and the number of heaters (i.e., 10) were kept constant for the second and third runs, the oil production increased because of the increasing of operation time, 60 days to 90 days. The increase in the oil production for the raw production case was 240% and this value turned out to be 168% in the for the 0.5%  $\text{Fe}_2\text{O}_3$  cases.

#### 6.4.2. Numerical Simulation Retorting of Crude Oils

For crude oil samples, viscosity measurements could be determined from room temperature to 100 °C, experimentally. Therefore, in order to determine the viscosity values for the temperature values apart from these temperature ranges, viscosity measurements results were extrapolated for Bati Raman, Camurlu, and Garzan crude oils. These extrapolated data are given for the dead crude oil samples and the crude oil samples after the addition of 0.5% Fe which is optimum type and dose of iron powders for heavy oil samples in Figure 6.23, Figure 6.24, and Figure 6.25.

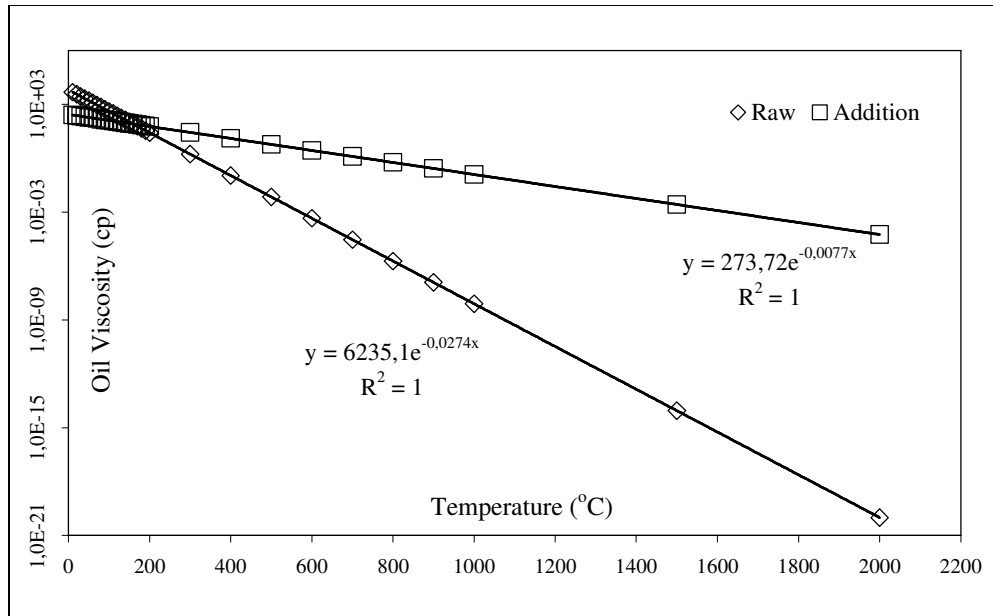


Figure 6.23 Oil viscosities for Batı Raman crude oil

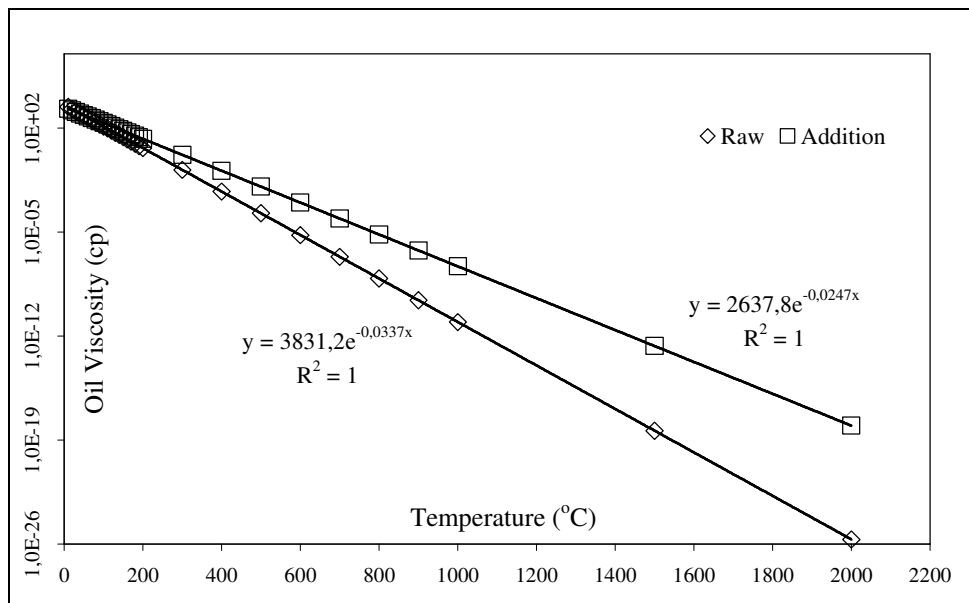


Figure 6.24 Oil viscosities for Çamurlu crude oil

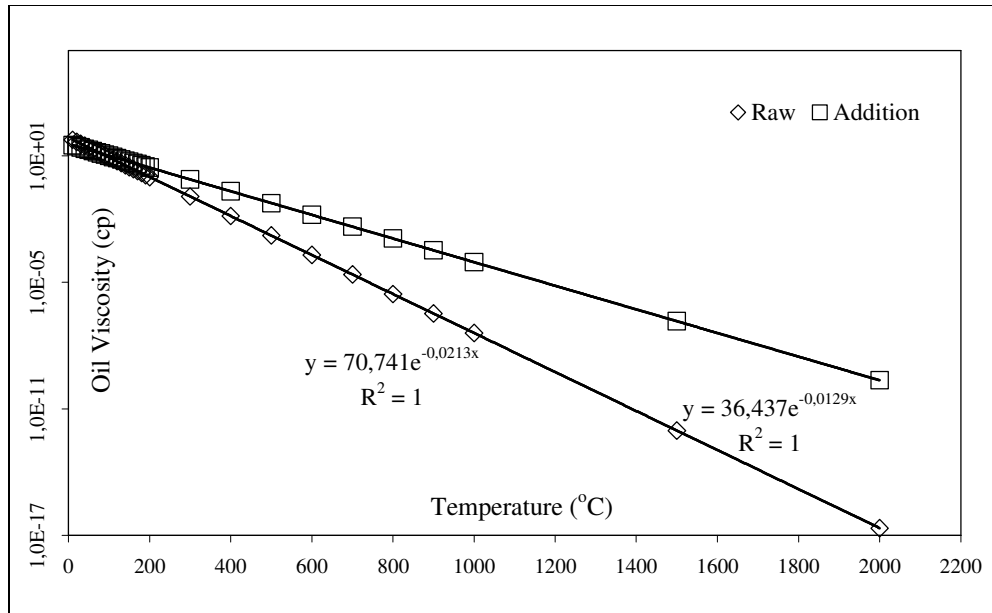


Figure 6.25 Oil viscosities for Garzan crude oil

Beside viscosity variations with temperature values, some reservoir rock and fluid properties has to be known to run the simulation. These data are taken from the literature and summarized in Table 4.2 and Figure 6.26.

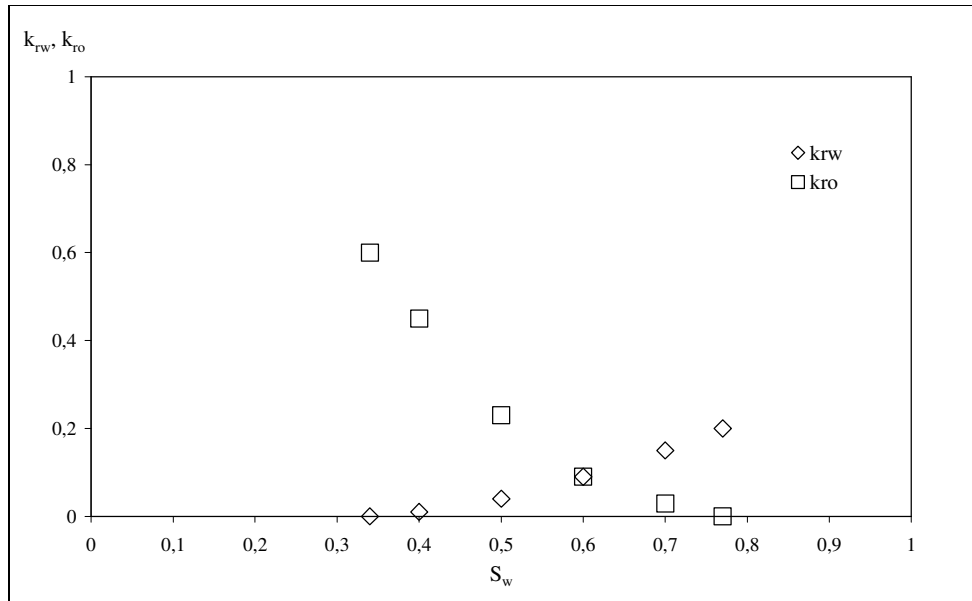


Figure 6.26 Water-Oil relative permeability curves used in the simulation for heavy oil samples [124]

Since viscosities of the crude oils were determined experimentally and the reservoir rock and fluid properties were taken from literature, by using simulation the power given to the system, number of heater used in the process and the operation times for two crude oils were tried to be optimized. Simulation results are given in Figure 6.27 and Figure 6.28.

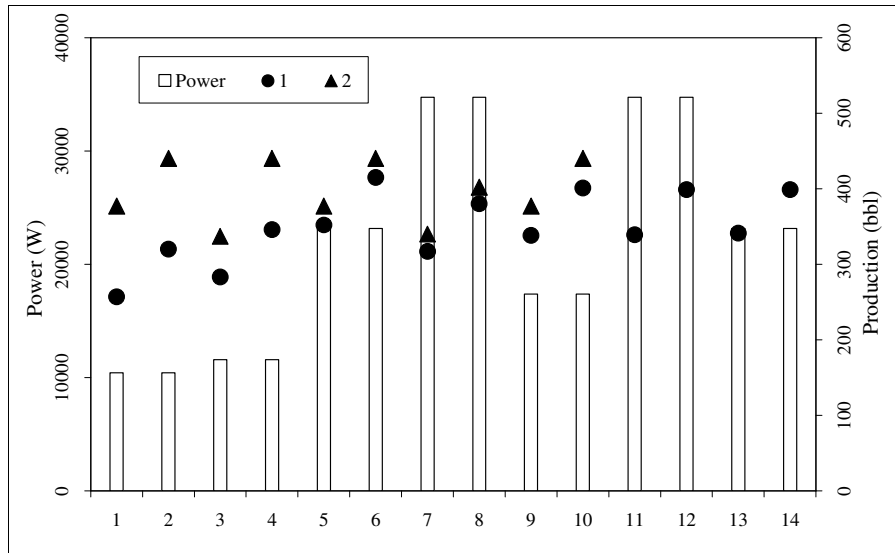


Figure 6.27 Simulation Results for B. Raman Crude Oil (1: Dead Crude Oil, 2: Crude oil containing 0.5% Fe)

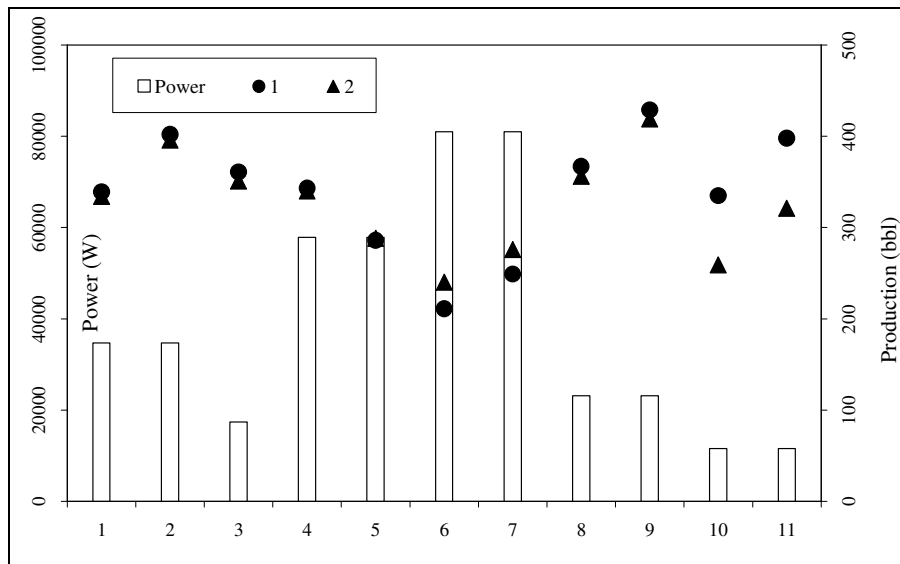


Figure 6.28 Simulation Results for Camurlu Crude Oil (1: Dead Crude Oil, 2: Crude oil containing 0.5% Fe)

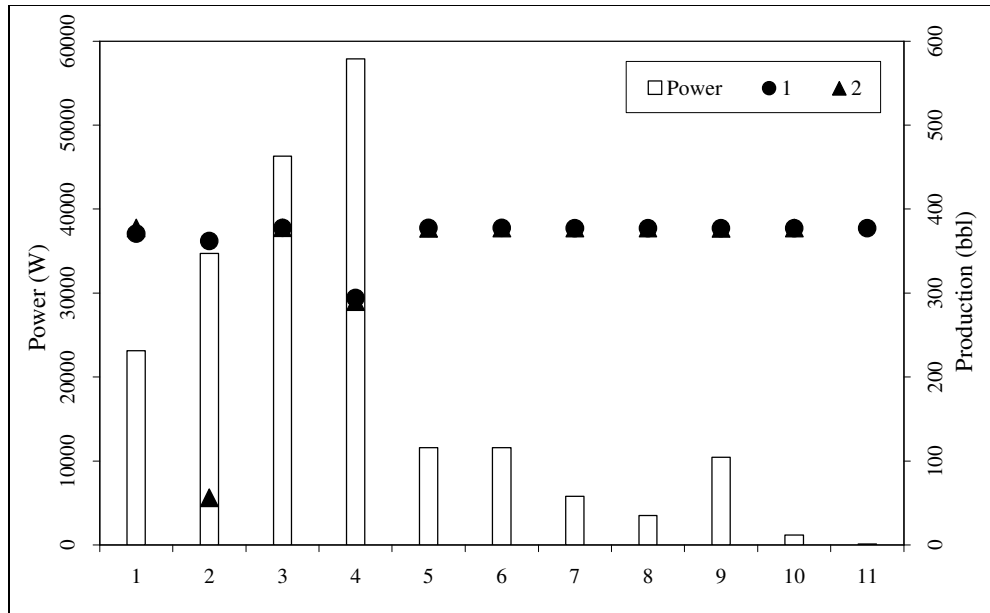


Figure 6.29 Simulation Results for Garzan Crude Oil (1: Dead Crude Oil, 2: Crude oil containing 0.5% Fe)

Optimum power, number of heaters and heating time were selecting according to the best oil production, so for Bati Raman crude oil, second run and for Camurlu crude oil ninth run (where 10 heaters at 1000 watts were used) were selected as optimum conditions. While the production increases after the addition of 0.5% Fe for Bati Raman crude oil, for the same condition the production decreases for Camurlu Crude oil.

The optimum operation times were determined as 70 days and 60 days for Bati Raman and Camurlu crude oils, respectively and the optimum number of heater was 10 for both heavy oil samples.

For Garzan crude oil, after 60 days with 10 heaters and with 1157 W total power. 377 bbl of petroleum can be produced. Therefore the conditions in 10<sup>th</sup> simulation can be selected as optimum conditions.

Because the produced oil amount doesn't relate with the power and number of heaters at reservoir conditions, it can be said that retort technique is not an effective way to recover Garzan crude oil, because of its low viscosity.

## **6.5. Analytical Model**

Since the microwave heating cannot be modeled by using CMG, STARS model, an analytical model aforementioned in Chapter 5 was used to model microwave heating.

The temperature modeling is based on Equations 5.12 and 5.14. These equations give the temperature change with respect to time, distance and some other parameters given in Equations 5.12 and 5.14. In these equations, the most critical parameter to obtain accurate temperature distribution is the power absorption coefficient (attenuation constant). The power absorption coefficient ( $\alpha$ ) may be calculated or experimentally determined for each medium. Due to the difficulties of the determination of the power adsorption coefficient at the laboratory conditions, it is calculated analytically by using the experimentally obtained temperature values for crude oil and oil shale samples. Analytical model studies were conducted for unsteady state no-flow conditions (Equation 5.14).

### **6.5.1. Modeling of Crude Oil Samples**

The power absorption coefficients ( $\alpha$ ) for Batı Raman crude oil is given in Table 6.16. There is strong correlation between the water content and power absorption coefficient ( $\alpha$ ). For high water saturation values, power absorption coefficient ( $\alpha$ ) values are smaller. For water wet and mixed wet conditions, smaller absorption coefficients were obtained. There is no relationship between the oil production and absorption coefficient. The average power absorption coefficient for Batı Raman crude oil is  $0.000074 \text{ cm}^{-1}$ . The best matches were obtained for mixed wet conditions (see in Appendix D).

Table 6.17 Analytical model results for Batı Raman Crude oil

$\phi$ (%)	$S_w$ (%)	$\alpha$		
		WW	OW	MW
25.86	20	0.0001	0.00012	0.00004
	40	0.000118	0.00011	0.000078
	60	0.0001	0.0001	0.000018
34.10	20	0.000102	0.00007	0.00013
	40	0.00004	0.00009	0.00004
	60	0.00003	0.00006	0.00005
38.95	20	0.00014	0.0002	0.00008
	40	0.000016	0.000064	0.00003
	60	0.000012	0.00005	0.000011

The power absorption coefficients ( $\alpha$ ) for Çamurlu crude oil is summarized in Table 6.18. Generally, water wet and mixed wet conditions yield small absorption coefficients for high water saturation values as Batı Raman case. Thus, this conclusion can be related with the viscosity of the crude oils. The average power adsorption coefficient was determined as  $0.000079 \text{ cm}^{-1}$ . The best matches were obtained for all saturation values of mixed wet case (see in Appendix D).

Table 6.18 Analytical model results for Çamurlu Crude oil

$\phi$ (%)	$S_w$ (%)	$\alpha$		
		WW	OW	MW
25.86	20	0.000066	0.00006	0.000058
	40	0.000056	0.000056	0.000042
	60	0.00005	0.00006	0.00003
34.10	20	0.0002	0.0002	0.000064
	40	0.000026	0.0002	0.00014
	60	0.00004	0.00004	0.000008
38.95	20	0.00018	0.00008	0.000056
	40	0.0002	0.00007	0.000032
	60	0.000036	0.00005	0.00002

The power absorption coefficients ( $\alpha$ ) for Garzan crude oil is summarized in Table 6.19. For high water saturation values, smaller absorption coefficients were calculated. The average power adsorption coefficient was determined as  $0.000079 \text{ cm}^{-1}$ . The best matches were obtained for most of the water saturation values of water wet case (see in Appendix D).

Table 6.19 Analytical model results for Garzan Crude oil

$\phi$ (%)	$S_w$ (%)	$\alpha$		
		WW	OW	MW
25.86	20	0.000066	0.000054	0.00006
	40	0.000036	0.000064	0.00008
	60	0.00006	0.000054	0.000044
34.10	20	0.000046	0.000046	0.0001
	40	0.000054	0.00007	0.000054
	60	0.000048	0.000046	0.000028
38.95	20	0.00012	0.000058	0.00004
	40	0.00004	0.00006	0.00001
	60	0.000036	0.000028	0.000006

Equation 5.12 is used for the case of unsteady state flow condition of electromagnetic heating. The results for this case are summarized in Table 6.20 for crude oil samples.

For no flow condition, magnitude of power adsorption coefficient is smaller than the flow condition case. Also the viscosity of the crude oil directly affects the magnitude of  $\alpha$ ; for high viscosity values,  $\alpha$  values are high.

Table 6.20 Optimized Electric Field Absorption Coefficient Values [106].

Sample	Porosity (%)	S <sub>w</sub> (%)	α		
			WW	OW	MW
Batı Raman	25.86	20	0.005488	0.00528	0.006652
		40	0.003114	0.003114	0.004924
		60	0.006762	0.00591	0.003442
	34.10	20	0.004264	0.004474	0.00672
		40	0.003412	0.0047	0.005832
		60	0.003404	0.004346	0.001262
	38.95	20	0.003114	0.003366	0.005216
		40	0.00169	0.00364	0.003966
		60	0.001298	0.005872	0.002106
Çamurlu	25.86	20	0.005812	0.005968	0.003442
		40	0.004626	0.003238	0.005832
		60	0.003492	0.005968	0.003442
	34.10	20	0.004492	0.005872	0.00672
		40	0.002782	0.003238	0.005832
		60	0.003782	0.003806	0.001262
	38.95	20	0.00661	0.005048	0.005216
		40	0.003114	0.004256	0.003968
		60	0.003844	0.00295	0.002106
Garzan	25.86	20	0.006376	0.006192	0.006234
		40	0.007508	0.006716	0.00671
		60	0.006714	0.003836	0.004574
	34.10	20	0.004066	0.003644	0.004736
		40	0.003114	0.003114	0.004958
		60	0.003288	0.004106	0.003106
	38.95	20	0.005038	0.006448	0.004824
		40	0.001902	0.004256	0.001872
		60	0.003114	0.003114	0.000772

Heat losses during the microwave heating of crude oils are minimized due to the thickness of graphite cell. Thus, experimental results yield good matches with model results.

### 6.5.2. Modeling of Oil Shale Samples

Analytical modeling is carried out similarly for the oil shales using unsteady state, no-flow conditions and the results are summarized in Table 6.21 and in Appendix D.

Iron addition affects the power absorption coefficient. While the same dose of  $\text{Fe}_2\text{O}_3$  made to reduce the value of power absorption coefficient, no correlation was observed for Fe. This can be due to the compositional difference of the oil shales or the reactions of iron powders.

Table 6.21 Analytical model results for oil shale samples

Oil Shale	Addition	$\alpha$
Himmetoğlu	-	0,00046
	0.1 % Fe	0,0017
Hatıldag	-	0,0014
	0.1% $\text{Fe}_2\text{O}_3$	0,0008
Seyitömer	-	0,003
	0.5% Fe	0,00034
Ulukışla	-	0,00126
	0.1% $\text{Fe}_2\text{O}_3$	0,00036

There is no direct relationship between the production (oil or gas) and the power absorption coefficient (Table 6.21, Figure 6.4, Figure 6.5, Figure 6.6, Figure 6.7)

Oil shale experiments were conducted with glass beakers. The glass beaker helps the effective temperature distribution and samples reach high temperatures within a short time periods. Since the difference between the ambient environment and the sample temperatures are so high, heat losses during the microwave heating of oil shale samples are also high. Therefore, experimental results deviate from model results.

## 6.6. Economical Evaluation of the Study

### 6.6.1. Economical evaluation of microwave heating for crude oil samples

The economics of the microwave heating method is examined with calculating the cost of the 1 bbl of oil with the current electricity price for domestic usage in Turkey [123]. The calculation gives only some idea about the economics of this operation but it seems inappropriate only considering produced amount rather than the production percentages. The microwave oven works at 900 Watt output power mode, so for 3 minutes and 45 Watt of energy is used. The cost of the power can be calculated with the price list given in [123] by dividing the produced amount cost per weight of the sample. Then it may be converted into volume units by multiplying it with density and multiplying with a conversion factor. The costs of the oil changes with the initial saturation and wettability, but the most economic ones are as follows: Batı Raman MW: 87, WW: 67, OW: 140; Çamurlu MW: 65, WW: 69, OW: 56; Garzan MW: 27, WW: 27, OW: 29 \$/bbl (see Appendix E).

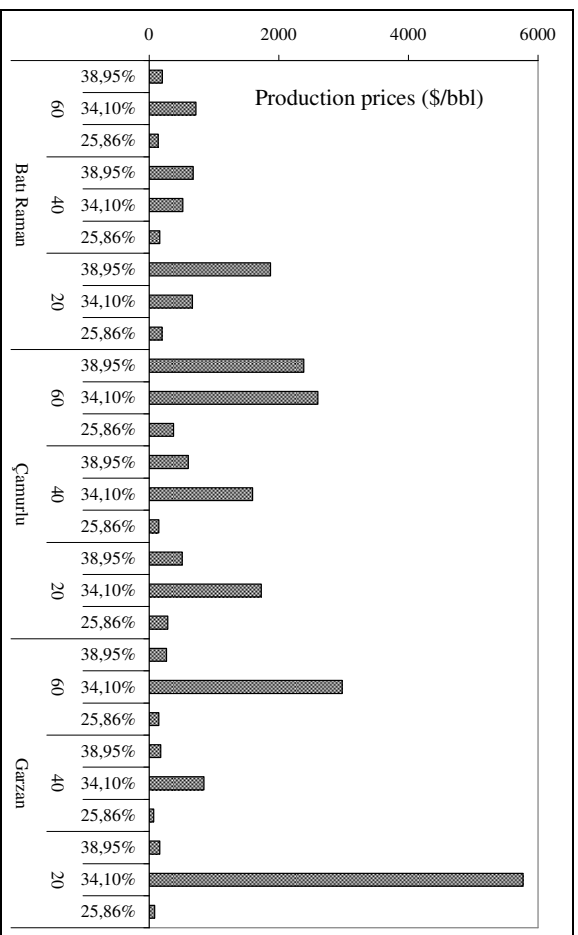


Figure 6.30 Economic evaluation of microwave heating for crude oil samples and water wet conditions

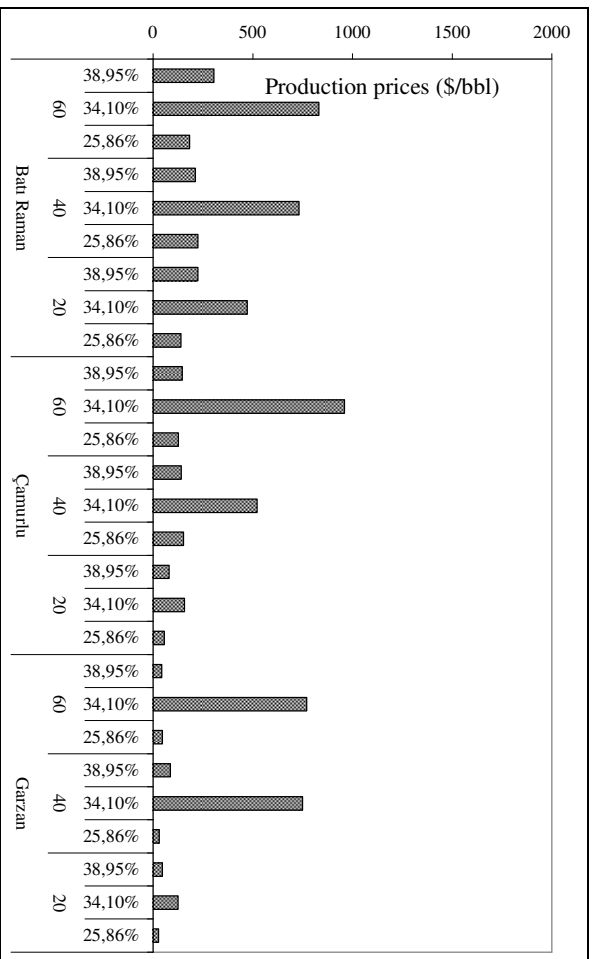


Figure 6.31 Economic evaluation of microwave heating for crude oil samples and water wet conditions

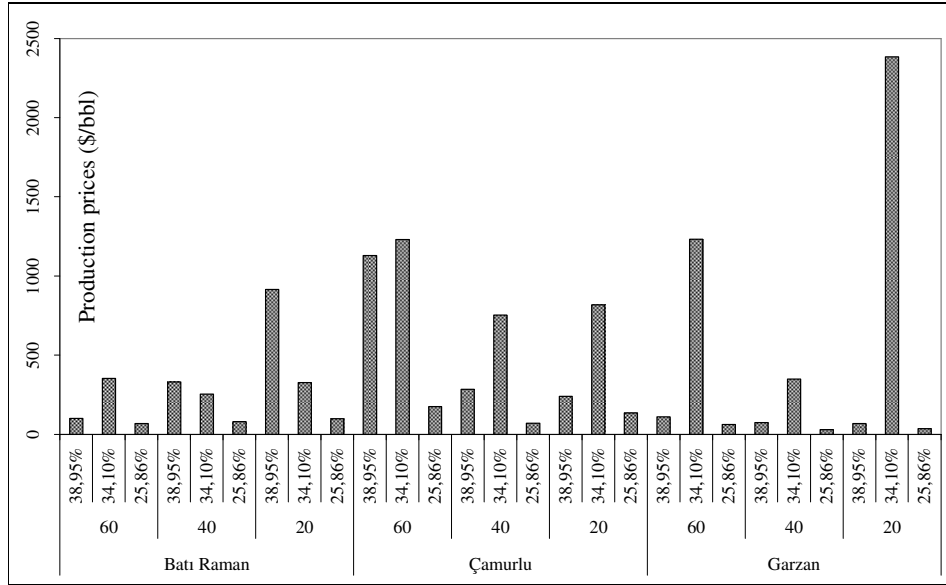


Figure 6. 32 Economic evaluation of microwave heating for crude oil samples and mixed wet conditions

#### 6.6.2. Economical evaluation of retort technique

Economic evaluation for retort technique was carried out with the numerical simulation results, by considering the cost of electricity determined by TEDAS (Turkish Electric Distribution Incorporated Company) [123]. Table 6.22 summarizes the economic evaluation of this study for only the best oil production results.

Table 6.22 Economic evaluation of the study

Sample Name	Addition	# of heater	Total operation time (days)	Oil Production (bbl)	Cost of the study (\$/bbl)
Batı Raman	-	10	70	320	4.84
	0.5% Fe	10	70	440	3.52
Çamurlu	-	10	60	429	6.88
	0.5% Fe	10	60	419	7.04
Garzan	-	10	60	377	0.39
	0.5% Fe	10	60	377	0.39
Seyitomer	-	10	60	9	502.55
	0.5% Fe	10	60	55	79.85
Hatıldag	-	5	90	145	30.46
	0.1% Fe <sub>2</sub> O <sub>3</sub>	5	90	180	24.62
Himmetoglu	-	5	90	296	15.55
	0.1% Fe	5	90	119	38.68
Ulukışla	-	10	90	262	33.78
	0.1% Fe <sub>2</sub> O <sub>3</sub>	10	90	420	21.07

\* The cost of electricity = US\$ 0.088 / 1kWh [123]

Economic evaluation shows that the recovery of oil from oil shale reserves by retort technique can be applied to three oil shale reservoirs (Himmetoğlu (OS1), Hatıldag (OS2), and Ulukışla (OS4)) but for Seyitömer oil shales this method is not an effective method (OS3).

For Batı Raman and Çamurlu crude oils, this method can be considered as an effective and cheap method, but for Garzan crude oil, because of the long operation time, other recovery methods should be tried. Note that only the heating cost was considered in this analysis and the CAPEX was not included.

Finally, Figure 6.33 shows the time dependency of the cumulative oil production for the raw oil shales and oil shales after the addition of iron powders. The best result was obtained for the Ulukışla oil shale (OS4) case with iron powder. Over the time period of investigation (90 days), the increasing trend was still obvious and the plateau region had not been reached unlike the other seven cases. It is interesting that its "raw version" also showed a similar trend but much less oil

production. Note that Ulukışla oil shale (OS4) has significantly higher rock heat capacity compared to the other three samples.

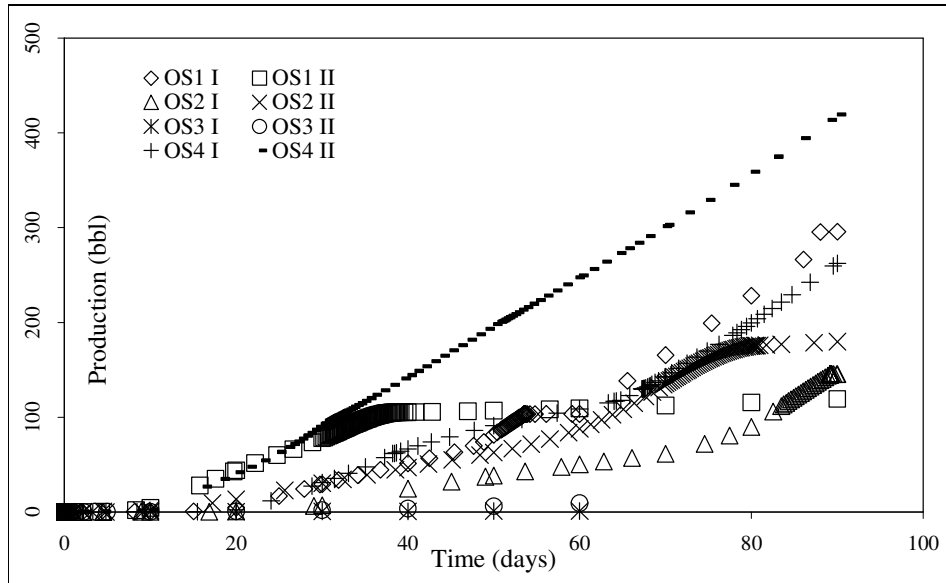


Figure 6.33 Cumulative oil production results for the optimum operation conditions of oil shales (I: Raw oil shale. II: Oil shale containing optimum types and doses of iron powders)

## CHAPTER 7

### CONCLUSIONS

In this thesis, extensive experimental, numerical and analytical studies were carried out for the recovery of Himmetoğlu, Hatıldağ, Seyitömer, and Niğde-Ulukişla oil shales and Batı Raman, Çamurlu, and Garzan crude oils by using retort and microwave techniques.

In order to determine the fluid flow behavior of Batı Raman, Çamurlu and Garzan crude oils, 3 different rheological models (Bingham, Power Law, and Casson models) were applied to experimentally obtained shear stress- shear rate values and the following conclusions were derived from experiments;

1. It is observed that for the dead crude oil, Casson Model yields the best fit to the experimental results.
2. After the addition of iron powders, yield points decrease and get closer to zero. Since the existence of yield point creates resistance to flow, decreasing yield point after the addition of iron powders can help production, transportation and the processing of produced oil.
3. Iron powders have a catalytic effect which decreases the reaction time and increases the efficiency of the reaction. Therefore, it causes to decrease the viscosity of the samples. Besides the catalytic effect, iron can react with some compounds or elements such as sulfur, nitrogen, oxygen at room temperature. These reactions can be exothermic which results the viscosity reduction even at room temperature. Furthermore, iron powders have magnetic properties which may cause to decrease the oil viscosity.

4. After the microwave heating, model viscosities reduced more than the samples that were electrically heated. Iron addition enhanced the microwave efficiency, but the enhancement was not more than 8%. More reduction was obtained when the microwave irradiation was applied alone.

During the experimental studies conducted with crude oil samples subjected to the microwave irradiation, following conclusions were derived;

5. High water saturations lead to higher oil productions regardless of the viscosity of the oil.

6. High salinity water promotes microwave assisted gravity drainage.

7. Water wet conditions must be preferred for higher oil recoveries.

8. Large porosity and permeability enhances microwave assisted gravity drainage.

9. Continuous microwave heating gives better results compared to periodic heating due to higher temperatures reached in continuous heating.

In the experimental studies that the oil shale samples were subjected to the microwave irradiation, iron types and doses were optimized and during the experimental studies gas emissions were measured in terms of CO, H<sub>2</sub>S, and CH<sub>4</sub>, subsequent conclusions about this set were done;

10. For Himmetoğlu, Hatıldağ, Seyitömer, and Niğde-Ulukışla oil shales, the optimum types and doses of iron powders were selected as 0.1% Fe, 0.1% Fe<sub>2</sub>O<sub>3</sub>, 0.5% Fe, and 0.1% Fe<sub>2</sub>O<sub>3</sub>, respectively, by considering the best oil production values.

11. The best oil production and the highest gas emissions were observed for Himmetoğlu oil shale, which has the highest shale oil amount among the oil shale samples.

During the retorting of oil shale samples, raw oil shales and the oil shales, after the addition of optimum types and doses of iron powders determined in microwave process, were subjected to the retort experiment.

12. For the effective retorting of oil shale samples, heat and soak periods should be used together and the duration of this period should be start at 100 °C and 500 °C which are the necessary temperature for the vaporization of physically bonded water and the decomposition of kerogen.

13. Because iron powder addition increases the thermal conductivity of the samples which makes the temperature distribution more effective, retort experiments must be conducted with iron powders to obtain better oil production.

The following conclusions were obtained after the numerical and analytical studies;

16. Viscosity-temperature relationship as input data to the simulator was determined as the most critical parameter

17. After 400 °C, a linear relationship between viscosity and temperature was observed on a semi-log plot.

18. All oil shales showed different recovery trends. While the highest recovery was obtained after retorting of Himmetoğlu oil shale at the laboratory conditions, the production rate and the ultimate recovery of Niğde-Ulukışla remarkably higher compared to the other three oil shales. This could be attributed to significantly higher rock heat capacity of this particular sample compared to the other three samples.

19. During the analytical modeling studies the electric field absorption coefficient which is the only unknown parameter in Abernethy's model is calculated by matching the experimental and model temperatures with least squares method and calculated as 0.0041, 0.0045, 0.0042 for water-wet, oil-wet and mixed-wet samples, respectively.

20. Analytical model studies conducted with the oil shale samples gave good matches at the beginning of the process. Due to a sudden increase in temperature that cause the deviation of the model was observed.

Finally economic evaluation of the study was done and the following conclusions were drawn;

22. The costs of the oil process change with the initial saturation and wettability, but the most economic ones are found as follows: Batı Raman MW: 87, WW: 67, OW: 140; Çamurlu MW: 65, WW: 69, OW: 56; Garzan MW: 27, WW: 27, OW: 29 \$/bbl.

23. The lowest and the highest prices for retorting crude oils were obtained as 0.39 \$/bbl and 6.88 \$/bbl for Garzan and Çamurlu crude oils, respectively. The lowest and highest electricity cost calculated for oil shale samples were 15.55 \$/bbl and 502.55 \$/bbl for Himmetoğlu and Seyitömer oil shales, respectively.

24. The technical and economic feasibility analyses showed that electrical heating is still a marginal application but the results proved that it is in an applicable range.

## CHAPTER 8

### RECOMMENDATIONS

Quantitative and qualitative analysis of oil shale and crude oil samples, before and after all of the experiments, can be helpful to understand the mechanisms of retort and microwave techniques and the responds of iron powders to these techniques. These can be accomplished by GC-MS measurements. Furthermore, this study can also be helpful to determine the reaction kinetics of the processes.

In order to explain the rheologies of the crude oils better, some statistical methods can be used.

Limestone porosities can be changed by packing and the geological properties of the limestone. Therefore, porosities can be different for the limestone samples used for experimental studies. Instead of porosities, categorization can be made according to the grain size.

Analytical studies conducted for microwave heating can also be generated for unsteady state-flow case.

## REFERENCES

1. Greene D. L., Hopson J. L., Li J., "Have we run out of oil yet? Oil peaking analysis from an optimist's perspective", Energy Policy 34 (2006) 515-531.
2. Ivanhoe L. F., "Future World Oil Supplies: There is a Limit", World Oil, November (1995) 91-94.
3. World energy Resources and Consumption <http://en.wikipedia.org/> last accessed on 20.01.2008
4. Türkiye Çevre Atlası, T.C. Çevre ve Orman Bakanlığı. ÇED ve Planlama Genel Müdürlüğü Çevre Envanteri Dairesi Başkanlığı. Ankara. 2004.
5. 21. Yüzyıla Girerken Türkiye' nin Enerji Stratejisinin Değerlendirilmesi Raporu, TÜSİAD-Türk Sanayicileri ve İş Adamları Derneği, 1998.
6. Kök M. V., "Oil shale resources in Turkey", Oil Shale. 23: 3 (2006) 209-210.
7. Tissot B. P., Welte D. H., "Petroleum formation and occurrence", Springer Verlag Germany, 1984.
8. Farouq Ali S. M., "Heavy oil – evermore mobile", Journal of Petroleum Science & Engineering 37 (2003) 5-9.
9. Madencilik Özel İhtisas Komisyonu Enerji Hammaddeleri Alt Komisyonu. Kömür Çalışma Grubu Raporu, 1996.
10. Şener M., "Neojen yaşlı Himmetoğlu (Göynük - Bolu) bitümlü şeyl sahasının litostratigrafik ve tektonik özellikleri", Türkiye Jeoloji Bülteni 36 (1993) 45-56.
11. Campbell C. J., Laherrere J. H., "The end of cheap oil", Scientific American. March (1998) 78-83.
12. Johannes I., Kruusement K., Veski R., "Evaluation of oil potential and pyrolysis kinetics of renewable fuel and shale samples by Rock-Eval analyzer", Journal of Analytical and Applied Pyrolysis 79 (2007) 183–190.
13. Altun N. E., Hicyilmaz C., Hwang J. Y., Bağcı S., "Evaluation of a Turkish low quality oil shale by flotation as a clean energy source: Material characterization and determination of flotation behavior", 87 (2006) 783-791.

14. Rangel-German E. R., Schembre J., Sandberg C., Kovscek A. R., "Electrical-heating-assisted recovery for heavy oil" *Journal of Petroleum Science and Engineering* 45 (2004) 213-231.
15. Castanier L. M., Brigham W. E., "Upgrading of crude oil via in situ combustion", *Journal of Petroleum Science and Engineering* 39 (2003) 125–136.
16. McPherson R. G., Chute F. S., Vermeulen F. E., "Recovery of Athabasca bitumen with the electromagnetic flood (EMF) process" *Journal of Canadian Petroleum Technology* 85-01-02 (1985).
17. Wadadar S. S., Islam M. R., "Numerical simulation of electromagnetic heating of Alaskan tar sands using horizontal wells" *Petroleum Society of CIM/AOSTRA Technical Conference, Banff Alberta Canada* (1991).
18. Major tar sand and heavy oil deposits of the United States, Interstate Oil Compact Commission (IOCC) Oklahoma City 272, 1984.
19. Thomas S., "Enhanced oil recovery – an overview. *Oil & Gas Science and Technology*" – Rev IFP 2007.
20. Moritis G. "Special Report – EOR/ heavy oil survey" *Oil and Gas Journal* 37 (2006) 55.
21. Weber G., Green J., "Guide to oil shale". National Conference of State Legislatures. Washington D.C. USA. p. 21, 1981.
22. Yen T. F., Chilingarian G. V. "Oil shale", Elsevier Amsterdam (1976) 1-12.
23. Tierney J. P., Lidström P., "Microwave assisted organic synthesis", CRC Press USA and Canada 2005.
24. Meredith R., "Engineers handbook of industrial microwave heating" The Institution of Electrical Engineers London, 1998.
25. Bayrakçeken, A., "Platinum and platinum-ruthenium based catalysts on various carbon supports prepared by different methods for PEM fuel cell applications", PhD Thesis, METU, Ankara, 2008.
26. Kappe O. C., "Controlled microwave heating in modern organic synthesis". *Angew. Chem. Int. Ed.* 43 (2004) 6250-6284.
27. Copson D. A., "Microwave heating: in freeze drying. electronic ovens and other applications", Westport Connecticut-USA The AVI publishing Company Inc. 1962.
28. Hutton A. C., "Petrographic classification of oil shales", *International Journal of Coal Geology* 8. (1987) 203-231.

29. Gavin J. M., "Oil shale", Washington Government Printing Office USA. (1924) 210.
30. Papoular R., "The use of kerogen data in understanding the properties and evolution of interstellar carbonaceous dust" *Astronomy and Astrophysics*. 378 (2001) 597-607.
31. Felesteen A. W., "Organic geochemical studies of some early cretaceous sediments". Abu Gharadig Basin. Western Desert. Egypt, 1998.
32. Moody R., "Oil & gas shales. Definitions & distribution in time & space", *The History of On-Shore Hydrocarbon Use in the UK*. April 20th-22nd 2007.
33. "Survey of energy resources: oil shale", World Energy Council (WEC) [http://www.worldenergy.org/publications/survey\\_of\\_energy\\_resources\\_2007/oil\\_shale/648.asp](http://www.worldenergy.org/publications/survey_of_energy_resources_2007/oil_shale/648.asp), last accessed on 25.01.2008
34. Laherrere J., "Review on oil shale data" Review of GERB (Groupe d'Etudes des Roches Bitumineuses) in the 1970s notes, 2005.
35. Prien C. H., "Survey of oil-shale research in the last three decades", Elsevier Amsterdam (1976) 235-267.
36. Liang Y., "Current status of oil shale industry in Fushun-China", *International Oil Shale Conference: Recent Trends in Oil Shale 7 -9 November 2006*. Amman. Jordan.
37. Dyni J. R., "Geology and resources of some world oil-shale deposits" U.S. Geological Survey. Scientific Investigations Report 2005-5294 2005.
38. Kattai V., Lökk U., "Historical review of the Kukersite oil shale exploration", *Oil Shale*. 15-2 (1998) 102-110.
39. Changiun D., Nuttall H. E., "The history and future of China's oil shale industry", *18th Oil Shale Symposium Proceedings*, Colorado School of Mines Press (1985) 210-215.
40. Chilin Z., "General description of Fushun oil shale retorting factory in China", *Oil Shale* 13-1 (1995) 7-11.
41. Qian J., Wang J., Li S., "Oil shale development in China", *Oil Shale* 20-3 (2003) 356-359.
42. Smith S. E., Neavel R. C., Hippo E. J., Miller R. N., "DTGA combustion of coals in the Exxon coal library", *Fuel* 60 (1981) 458-462.
43. Dyni J. R., "Geology and resources of some world oil-shale deposits", *Oil Shale* 20-3 (2003) 193-252.

44. "Oil in Colorado" Rocktalk, Division of Minerals and Geology Colorado Geological Survey 7-2. April 2004.
45. Shale Oil, AIMR Report, 2007
46. Commercial Oil Shale Leasing Program, Environmental Protection Agency (EPA), 71-165, August 25 2006.
47. Altun, N. E., "Beneficiation of Himmetođlu and Beypazari oil shales by flotation and their thermal characterization as an energy source". PhD Thesis, METU, Ankara, 2006.
48. Matthews R. D., "The Devonian-Missisipian oil shale resource of the United States", in Sixteenth Oil Shale Symposium Proceedings, 1983.
49. DPT, Sekizinci Bes Yıllık Kalkınma Planı, Madencilik Özel İhtisas Komisyonu Raporu, Enerji Hammaddeler Alt Komisyonu Kömür Çalışma Gurubu, DPT:2605 MÖİK: 616, Ankara, 2001.
50. General Directorate of Mineral Research and Exploration, "Dünyada ve Türkiye'de linyit, asfaltit, taskömürü, bitümlü şist, uranyum rezervleri", MTA Report, MTA. Ankara, 1993.
51. Güleç K., Önen A., "Turkish oil shales: reserves, characterization and utilization", Proceedings of the 1992 Eastern Oil Shale Symposium, University of Kentucky, Institute for Mining and Minerals Research, Lexington, USA (1993) 12-24.
52. Sener M., Sengüler İ., Kök M. V., "Geological considerations for the economic evaluation of oil shale deposits in Turkey", Fuel 74 (1995) 999-1003.
53. Aydođan, C., "Türkiye Asfalt Filizlerinin Deđerlendirilmesi". PhD Thesis, İTÜ, İstanbul, 1952.
54. Akkus I., Sümer A., Şengüler İ., Taka M., Pekatan R., "Beypazarı – Çayırhan bitümlü sist alanının sondaj ve yarma logları", MTA Report, MTA, Ankara, 1982.
55. Ballice L., Yüksel M., Sağlam M., Schulz H., Hanoglu C., "Application of infrared spectroscopy to the classification of kerogen types and the thermogravimetrically dericed pyrolysis kinetics of oil shales", Fuel 74-11 (1995) 1618-1623.
56. Şener M., Şengüler İ., "Geological. mineralogical. geochemical characteristics of oil shale bearing deposits in the Hatıldađ oil shale field Göynük Turkey", Fuel 77-8 (1998) 871-880.
57. Kök M.V., Şengüler İ., Hufnagel H., Sonel N., "Thermal and geochemical investigation of Seyitömer oil shale", Thermochimica Acta. 371 (2001) 111-119.

58. Şener M., Gündoğdu M. N., "Geochemical and petrographic investigation of Himmetoğlu oil shale field Göynük Turkey", Fuel 75-11 (1996) 1313-1322.
59. Putun E., Akar A., Ekinci E., Bartle K. D., "Chemistry and geochemistry of Turkish oil shale kerogens", Fuel 67 (1998) 1106-1110.
60. Hufnagel H., "Investigation of oil shale deposits in western Turkey", Technical Report Part 2, Project No. 84.2127.3, BGR Hannover, Germany, 1991.
61. Hufnagel H., "Investigation of oil shale deposits in western Turkey", Technical Report Part 1, Project No. 84.2127.3, BGR Hannover, Germany, 1989.
62. Alpan S., Bulletin of the Mineral Research and Exploration Institute of Turkey, Number: 80, April 1973.
63. Şengüler İ., "Bituminous shales: their origin, usage and importance", Bulletin of MTA Natural Resources and Economy, 3, 2007.
64. Speight J. G., "The chemistry and technology of petroleum" New York, Marcel Dekker Inc. 760, 1991.
65. Masters C. D., Root D. H., Attanasi E. D., "World resources of crude oil and natural gas", Proceedings of the 13th World Petroleum Congress, Reserves. Management, Finance and General, 4 (1992) 51-64.
66. North F. K., "Petroleum geology", Boston, Allen and Unwin, 1985
67. Winters J. C., Williams J. A., "Microbiological alteration of crude oil in the reservoir" Symposium on petroleum transformations in geologic environments: American Chemical Society Division of Petroleum Chemistry, New York, 1969.
68. Waples A., Douglas W., "Geochemistry in petroleum exploration" Boston, International Human Resources Development Corporation, 1985.
69. Meyer R. F., Duford J. M., "Resources of heavy oil and natural bitumen worldwide", The 4th UNITAR/UNDP International Conference on Heavy Crude and Tar Sands Proceedings, Geology and Chemistry 2 (1988) 277-293.
70. Baytac N., Yenilmez F., "Turkiye'de petrol sektoru", www.econturk.org, last accessed on 25.05.2008.
71. Sahin S., Kalfa U., Çelebioglu D., "Bati Raman Field immiscible CO<sub>2</sub> application: status quo and future plans", Latin American & Caribbean Petroleum Engineering Conference, Buenos Aires, Argentina, Society of Petroleum Engineers, 106575-MS, 2007.
72. Karaoguz O. K., Topguder N. N., Lane R. H., Kalfa U., Celebioglu D., "Improved sweep in Bati Raman heavy-oil CO<sub>2</sub> flood: bullhead flowing gel treatments plug natural fractures", SPE Reservoir Evaluation & Engineering, 10-2 (2007) 164-175.

73. Issever K., Pamir A. N., Tirek A., "Performance of a heavy-oil field under CO<sub>2</sub> injection, Bati Raman, Turkey", SPE Reservoir Engineering, 8-4 (1993) 256-260.
74. Gondiken S., "Camurlu field immiscible CO<sub>2</sub> huff and puff pilot project", SPE 15749, 1987.
75. Khatib A. K., Earlougher R. C., Kantar K., "CO<sub>2</sub> injection as an immiscible application for enhanced oil recovery in heavy oil reservoirs", California Regional Meeting, SPE 9928, 1981.
76. Bardon C. P., Karaoguz D., Tholance M., "Well stimulation by CO<sub>2</sub> in the heavy oil field of Camurlu in Turkey", SPE Enhanced Oil Recovery Symposium, 20-23 April 1986, Tulsa, Oklahoma, 14943-MS.
77. Warren, G. M., Memioglu, E., Bakiler, C. S., "Case study: enhanced oil recovery potential for the Garzan field, Turkey", Middle East Oil Show, 7-10 March 1987, Bahrain, 15752-MS.
78. Bilali L., Benchanaa M., El harfi K., Mokhlisse A., Outzourhit A., "A detailed study of the microwave pyrolysis of the Moroccan (Youssoufia) rock phosphate", Journal of Analytical and Applied Pyrolysis 73 (2005) 1-15.
79. El harfi K., Mokhlissea A., Chanâa M. B., Outzourhit A., "Pyrolysis of the Moroccan (Tarfaya) oil shales under microwave irradiation", Fuel 79 (2000) 733-742.
80. Jackson C., "Upgrading a heavy oil using variable frequency microwave energy", International Thermal Operations and Heavy Oil Symposium and International Horizontal Well Technology Conference, Calgary, Alberta, Canada, 2002.
81. He B., "The effect of metallic salt additives on in-situ combustion performance", MSc Thesis, Stanford University, 2004.
82. Incropera F. P., Dewitt D. P., Bergman T. L., Lavine A. S., "Fundamentals of heat and mass transfer", Sixth Edition, John Wiley & Sons, New York, 2006.
83. Ribeiro da Silvaa M. A. V., Santosa L. M. N. B. F., Schröder B., Beyer L., Dietze F., "Enthalpies of combustion of two bis (N,N-diethylthioureas)", The Journal of Chemical Thermodynamics 39-2 (2007) 279-283.
84. Abertney E. R., "Production increase of heavy oils by electromagnetic heating", Journal of Canadian Petroleum Technology, Canada, 1976.
85. Datta A. K., Anantheswaran R. C., "Handbook of microwave technology for food applications", New York, 2001.
86. Hiebert A. D., "Numerical simulation of the electrical pre-heat and steam drive bitumen recovery process for the Athabasca oil sands," PhD Thesis, University of Alberta, 1986.

87. Vandembroucke M., Largeau C., "Kerogen origin, evolution and structure", *Organic Geochemistry* 38 (2007) 719–833.
88. Dhakate S. R., Mathur R. B., Bahl O. P., "Catalytic effect of iron oxide on carbon/carbon composites during graphitization", *Carbon*. 35-12 (1997) 1753-1756.
89. Yasuda E., Hotta Y., Park S. M., *Proceeding of 22<sup>nd</sup> Biennial Conference on Carbon*, University of California, San Diego, USA, 1995.
90. Zaldivar R. J., Kobayashiand R. W., Rellick G. S., *Carbon* 29 (1991) 1145.
91. Mehrotra S. P., Sinha V. K., "Catalytic effect of iron on the carbon-carbon dioxide reaction kinetics", *Transactions* 23 (1983) 723-730.
92. Wang L., Chen P., "Mechanism study of iron-based catalysts in co-liquefaction of coal with waste plastics" *Fuel* 81 (2002) 811-815.
93. Richard I. M., "Chemical kinetics and catalysis", Wiley-Interscience. New York. 2001, ISBN 0471241970.
94. Knözinger H., Kochloefl K., "Heterogeneous catalysis and solid catalysts" *Ullmann's Encyclopedia of Industrial Chemistry*, Wiley-VCH, Weinheim, 2002.
95. Sambhi I. S., Khulbe K. C., Mann R. S., "Catalytic hydrotreatment of heavy gas oil", *Ind. Eng. Chem. Prod. Res. Dev.* 21 (1982) 575-580.
96. Chhabra R. P., Richardson J. F., "Non-Newtonian flow in the process industries: fundamentals and engineering applications", Butterworth-Heinemann, 2000.
97. Anandha Rao M., "Rheology of fluid and semisolid foods principles and applications", PhD. Thesis, Cornell University, Geneva, New York., 1999.
98. Snoeyink V. L., Jenkins D., "Water Chemistry", John Wiley & Sons, New York, 1980.
99. Cotton F. A., Wilkinson, G., "Advanced inorganic chemistry", Wiley Interscience, New York, 1988.
100. Holleman A. F., Wiberg E., "Inorganic chemistry", Academic Press, San Diego, 2001.
101. Carbon, *Encyclopædia Britannica*, <http://www.britannica.com/>, last accessed on 26.07.2008
102. Adam F. I., Hogarth G., Kabir S. E., Richards I., "Models of the iron-only hydrogenase: Synthesis and protonation of bridge and chelate complexes  $[\text{Fe}_2(\text{CO})_4\{\text{Ph}_2\text{P}(\text{CH}_2)_n\text{PPh}_2\}(\mu\text{-pdt})]$  ( $n = 2-4$ )-evidence for a terminal hydride intermediate", *Comptes Rendus Chimie*, 11-8 (2008) 890-905.

103. Hascakir B., Akin S., "Effect of metallic additives on upgrading heavy oil with microwave heating", First World Heavy Oil Conference, Beijing, China, 2006.
104. Günel O. G., Islam, M. R., "Alteration of asphaltic crude rheology with electromagnetic and ultrasonic irradiation", Journal of Petroleum Science and Engineering 26 (2000) 263-272.
105. Akin S., Bagci S., Kök M. V., Karacan C. Ö., "Oxidation of heavy oil and their SARA Fractions: Its role in modeling In-Situ combustion", SPE 63230, Proceedings of the 2000 SPE Annual Technical Conference and Exhibition held in Dallas, TX, USA, Oct. 1-4 2000.
106. Acar Ç., "Enhancing petroleum recovery from heavy oil fields by microwave heating", MSc Thesis, METU, Ankara, 2007.
107. Acar C., Hascakir B., Demiral B., Akin S., Karaca H., Kartal O. E., "Microwave heating of heavy oil reservoirs: effect of wettability", 150 Years of Petroleum Industry: Tradition & Challenges, Bucharest, Romania, October 2007.
108. Nguyen B. L., Bruining J., Slob E. C., "Effects of wettability on dielectric properties of porous media", SPE Annual Technical Conference and Exhibition held in Houston, Texas, October 3–6, 1999.
109. Akin, S., "Mathematical modeling of steam assisted gravity drainage", SPE Reservoir Evaluation & Engineering 8-5 (2005) 372-376.
110. Gary J. H., Handwerk G. E., "Petroleum refining technology and economics", 2nd Edition, Marcel Dekker, Inc. ISBN 0-8247-7150-8, 1984.
111. Yamaguchi N., "Hydrodesulfurization technologies and costs", Trans Energy Associates, William and Flora Hewlett Foundation Sulfur Workshop, Mexico City, May 29-30, 2003.
112. Douglas B., McDaniel D., Alexander J., "Concepts and models of inorganic chemistry", 3<sup>rd</sup> edition, Wiley, New York, 1993.
113. Shreve R. N., Brink J., "Kimyasal proses endüstrileri 2", 4<sup>th</sup> edition, İnkılap Kitapevi, 1995.
114. Coates J. D., Anderson R. T., Lovley D. R., "Oxidation of polycyclic aromatic hydrocarbons under sulfate-reducing conditions", Appl. Environ. Microbiol 62 (1996) 1099-1101.
115. Hascakir B., Demiral B., Akin S., "Experimental and numerical analysis of oil shale production using retort technique", 15th International Petroleum And Natural Gas Congress And Exhibition Of Turkey, Ankara, Turkey, May 2005.
116. Hascakir B., Babadagli T., Akin S., "Experimental and numerical simulation of oil recovery from oil shales by electrical heating", Energy and Fuels, Article in press, 2008.

117. Kershaw J. R., Barrass G., Gray D., "Chemical nature of coal hydrogenation oils part I: The effect of catalysts", *Fuel Processing Technology* 3-2 (1980) 115-129.
118. Odenbach S., "Ferrofluids/magnetically controlled suspensions", *Colloids and Surfaces A: Physicochem. Eng. Aspects* 217 (2003) 171-178.
119. Sarkar A. K., Sarathi P. S., "Feasibility of steam injection process in a thin. low-permeability heavy oil reservoir of Arkansas—a numerical simulation study", U.S. Department of Energy Assistant Secretary for Fossil Energy, 1993.
120. Bechtel SAIC Company, LLC, Heat Capacity Analysis Report, U.S. Department of Energy Office of Civilian Radioactive Waste Management Office of Repository Development, 2004.
121. Lide D. R., "CRC Handbook of chemistry and physics", 88<sup>th</sup> edition, 2007-2008.
122. Hascakir B., Babadagli T., Akin S., "Experimental and numerical modeling of heavy-oil recovery by electrical heating", SPE 117669, SPE International Thermal Operations and Heavy Oil Symposium held in Calgary, Alberta, Canada, 20–23 October 2008.
123. Turkish Electric Distribution Incorporated Company <http://www.tedas.gov.tr> last accessed on 01.02.2008
124. Spivak A., Karaoguz D., Issever K., Nolen J. S., "Simulation of immiscible CO<sub>2</sub> injection in a fractured carbonate reservoir, Bati Raman field, Turkey", SPE 18765, 1989.

## APPENDIX A

### FLUID RHEOLOGY

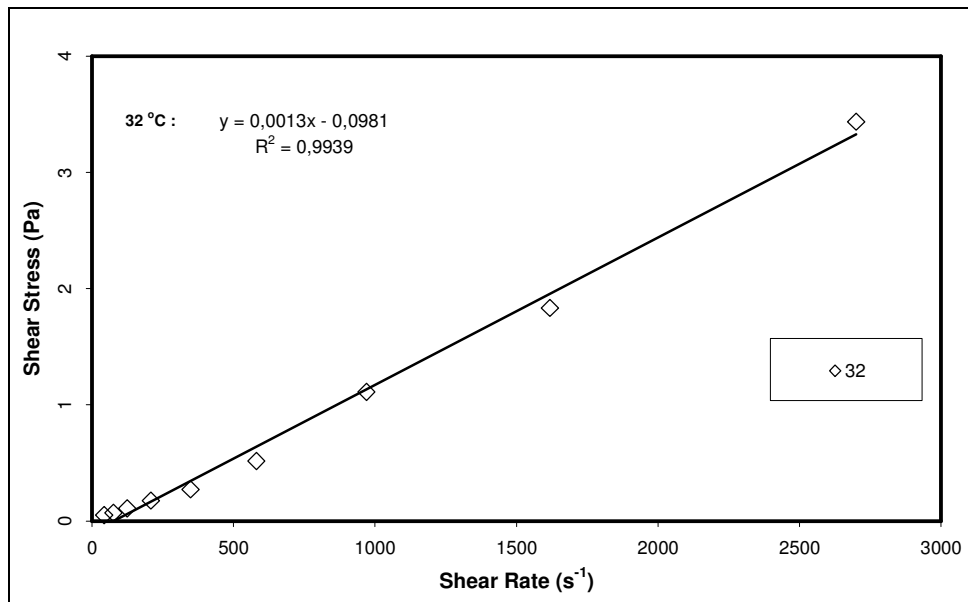


Figure A 1 Rheology of tap water for the correction of Haake viscometer

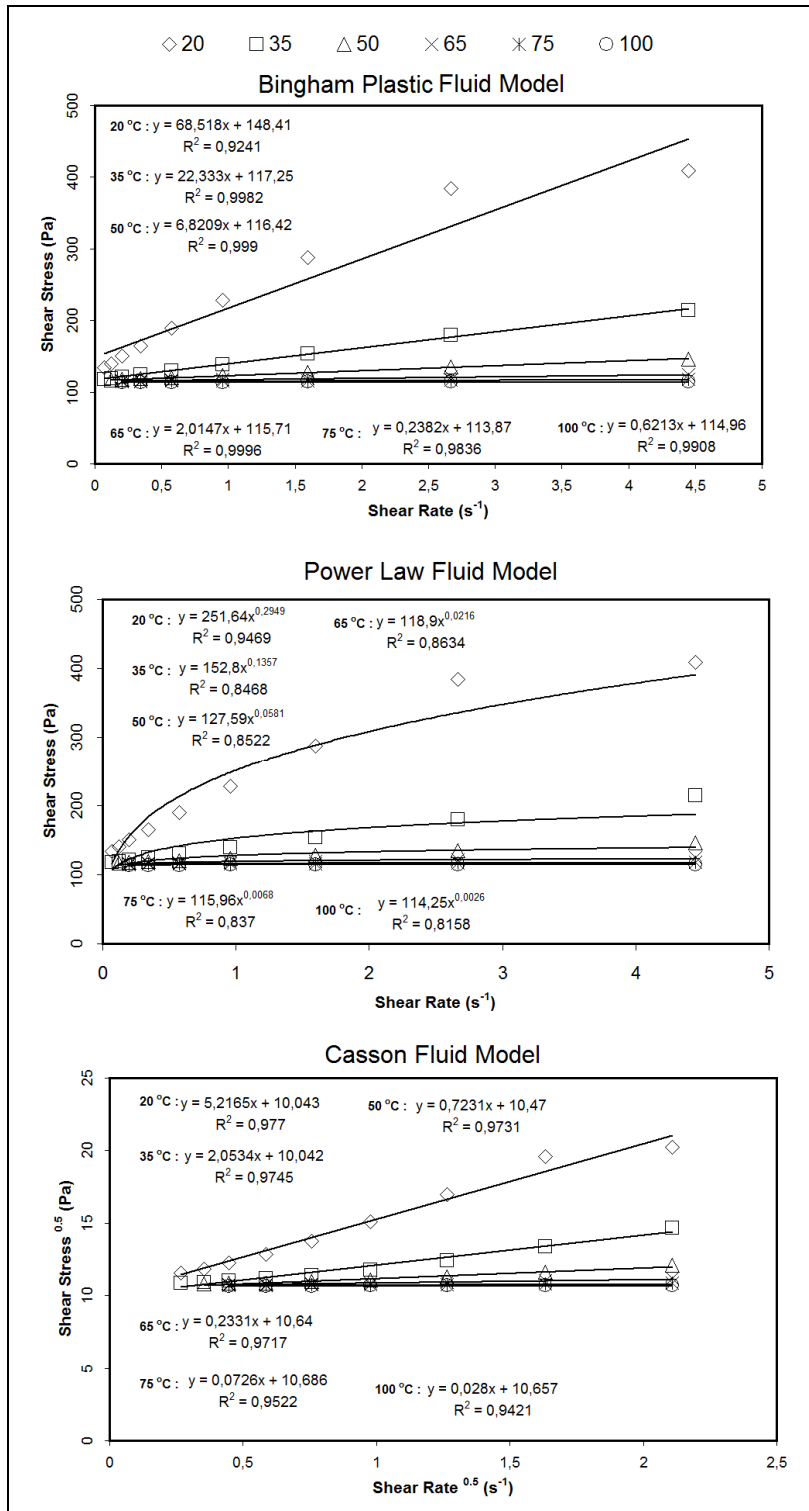


Figure A 2 Rheology of Dead Batı Raman Crude oil

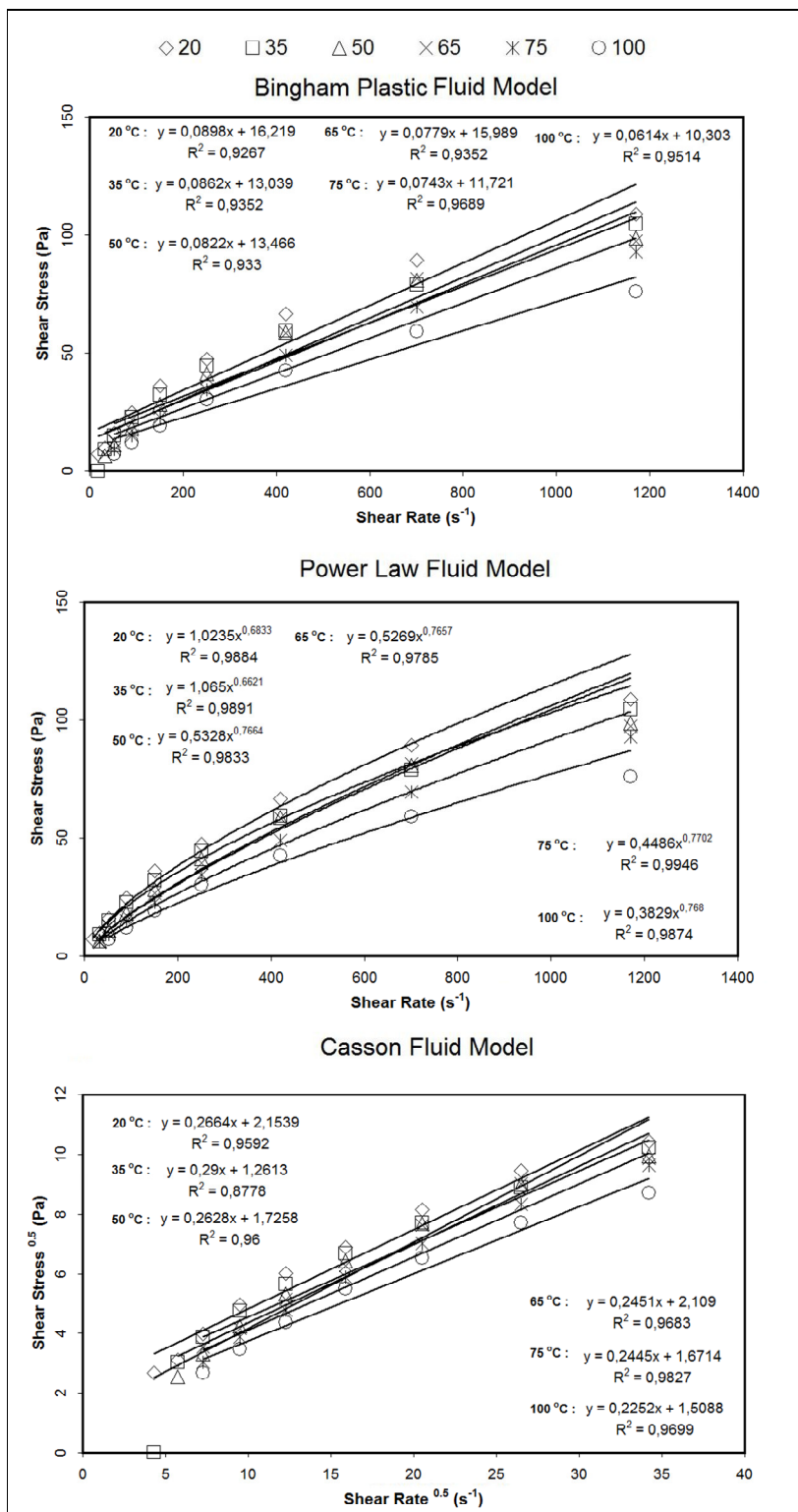


Figure A 3 Rheology of Bati Raman Crude oil after the addition of 0.1% Fe

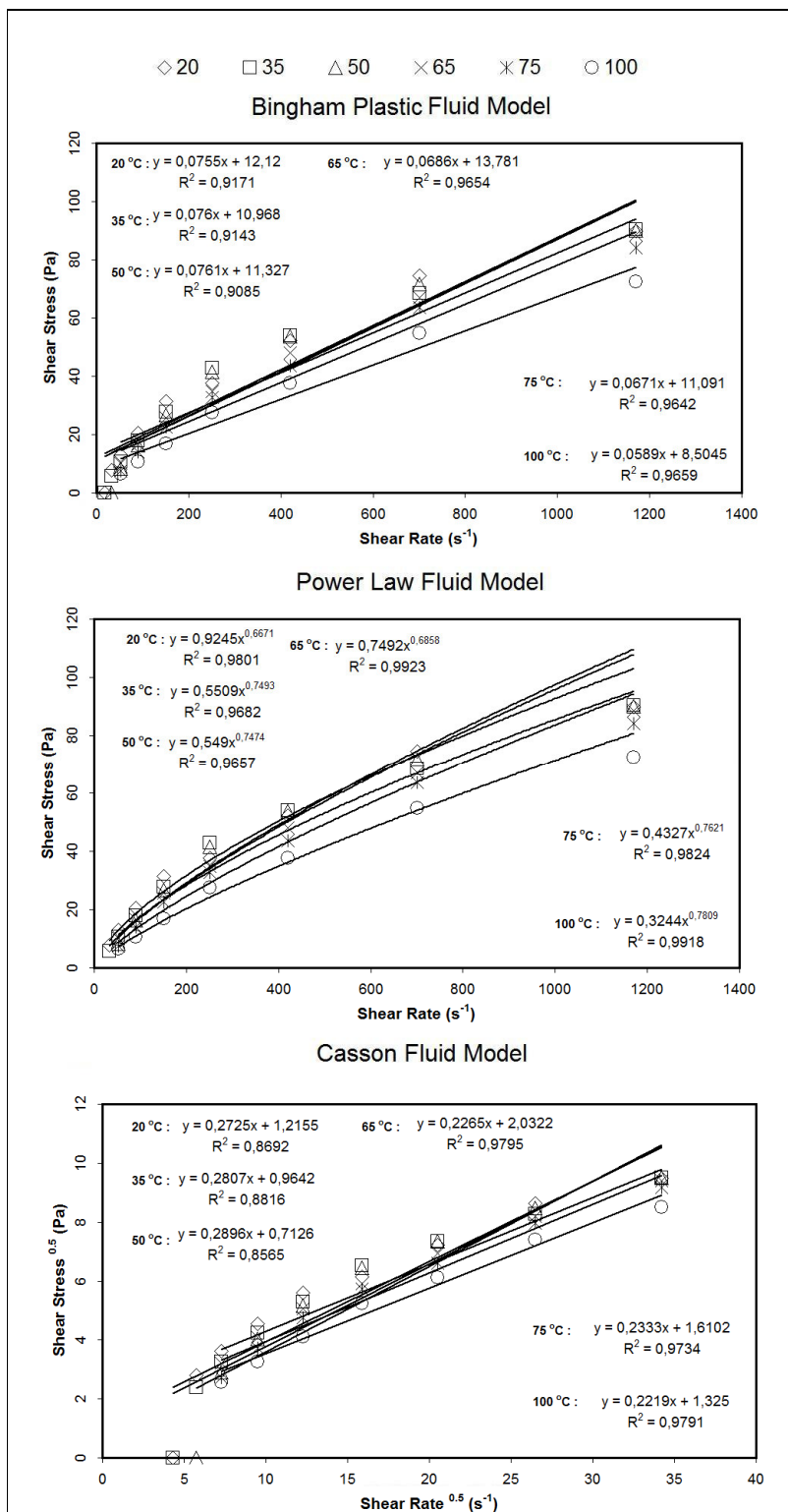


Figure A 4 Rheology of Batı Raman Crude oil after the addition of 0.5% Fe

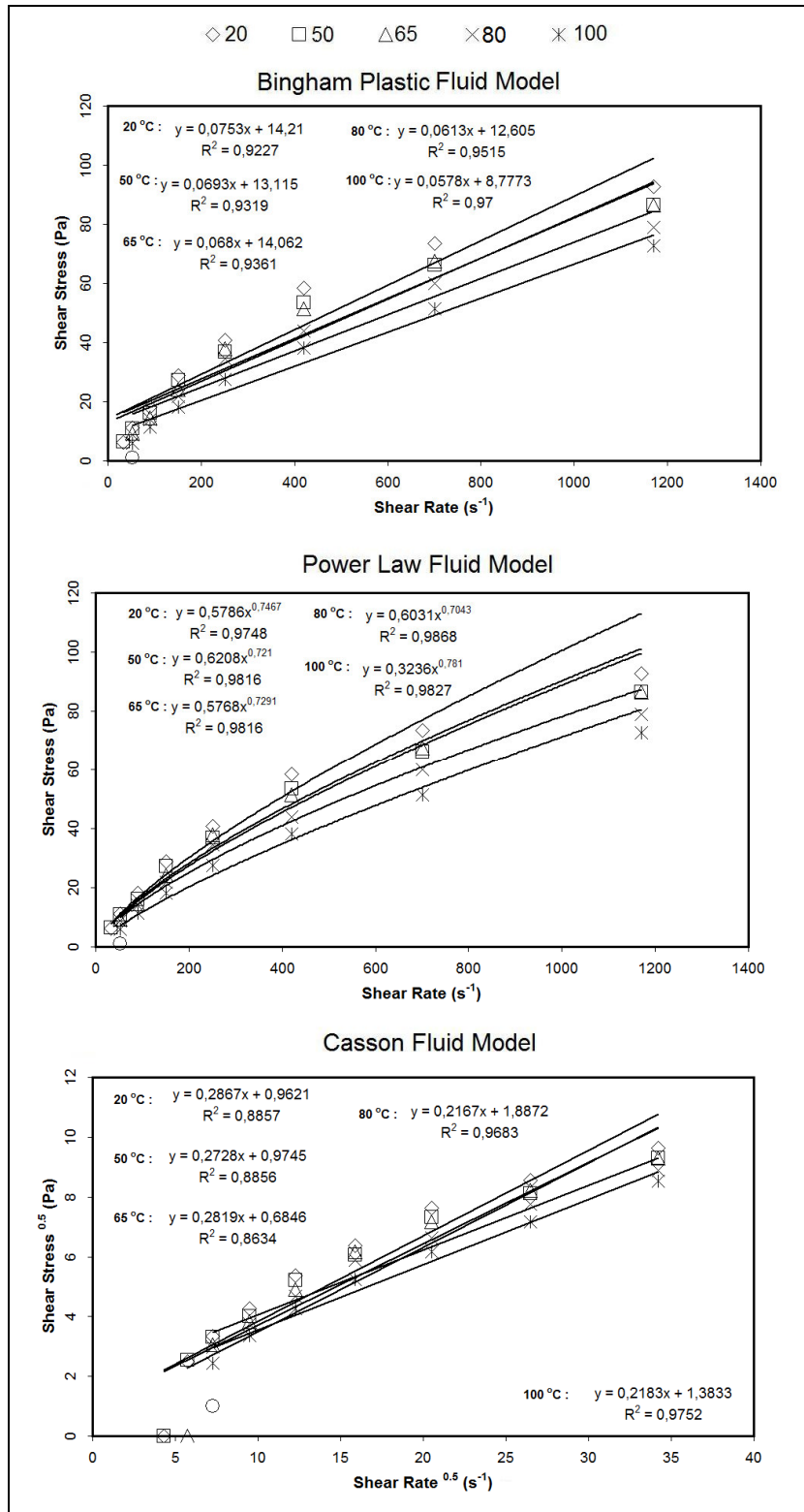


Figure A 5 Rheology of Batı Raman Crude oil after the addition of 1% Fe

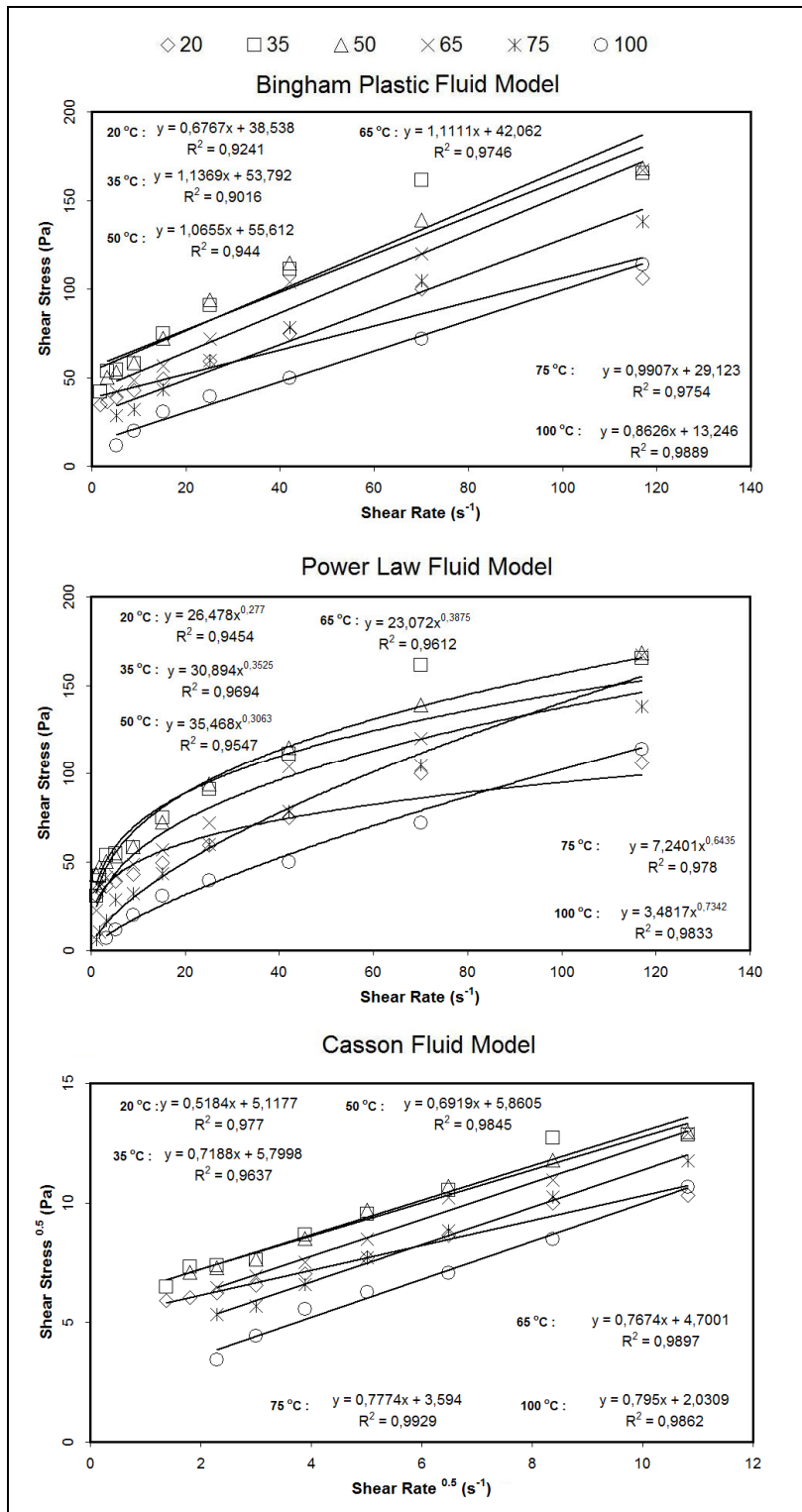


Figure A 6 Rheology of Batı Raman Crude oil after the addition of 0.1% Fe<sub>2</sub>O<sub>3</sub>

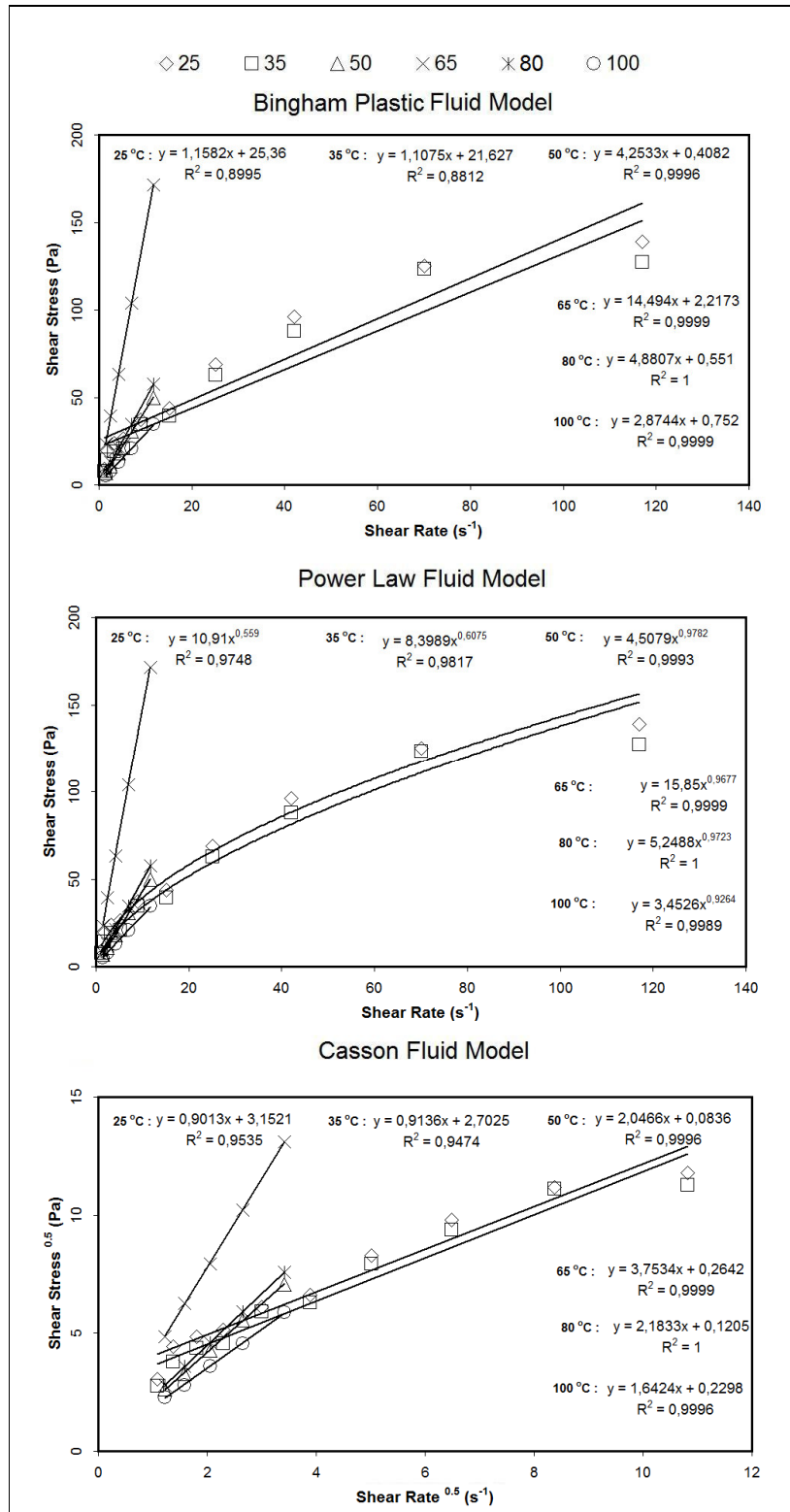


Figure A 7 Rheology of Batı Raman Crude oil after the addition of 0.5 % Fe<sub>2</sub>O<sub>3</sub>

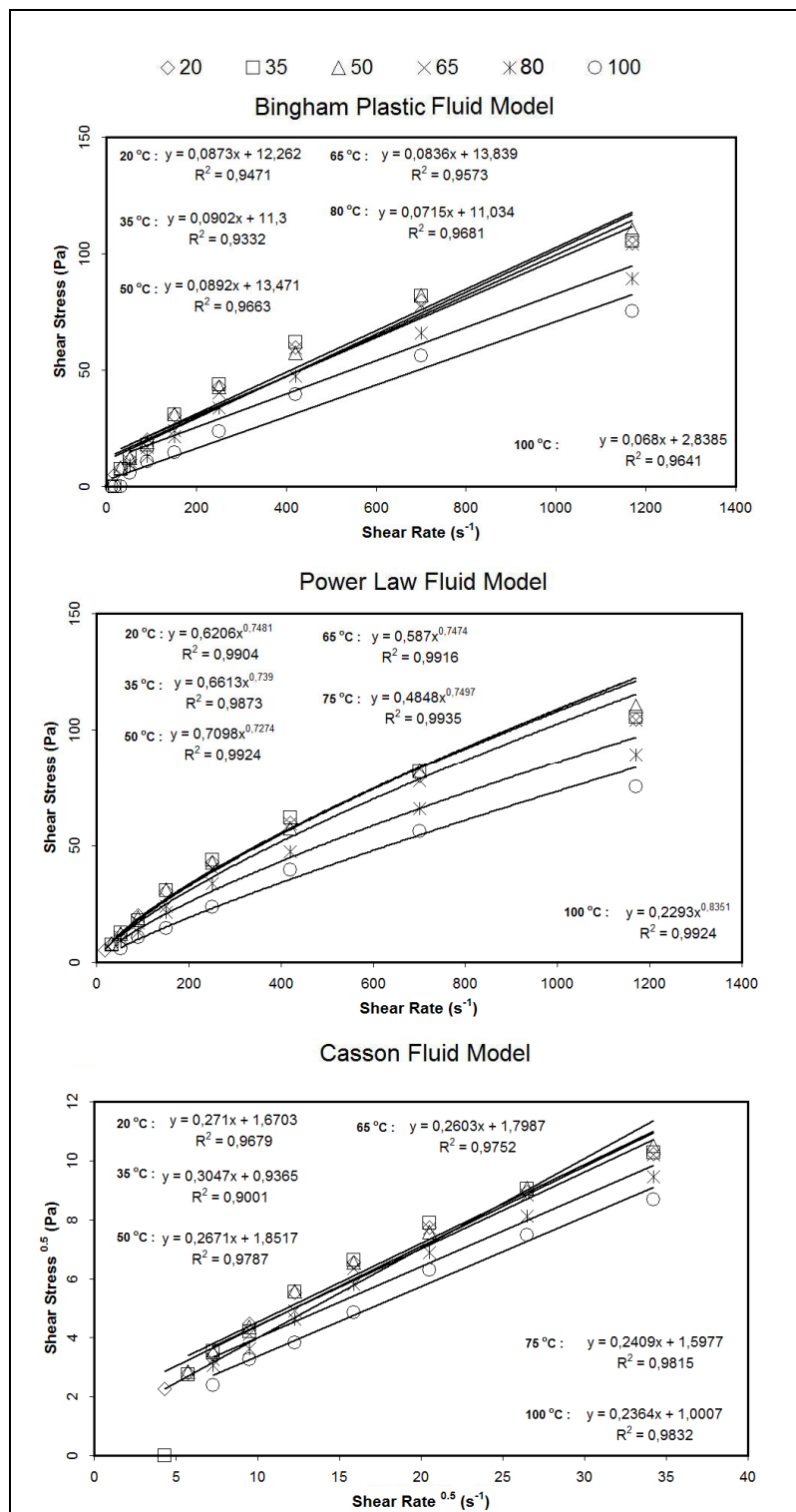


Figure A 8 Rheology of Bati Raman Crude oil after the addition of 1 %  $Fe_2O_3$

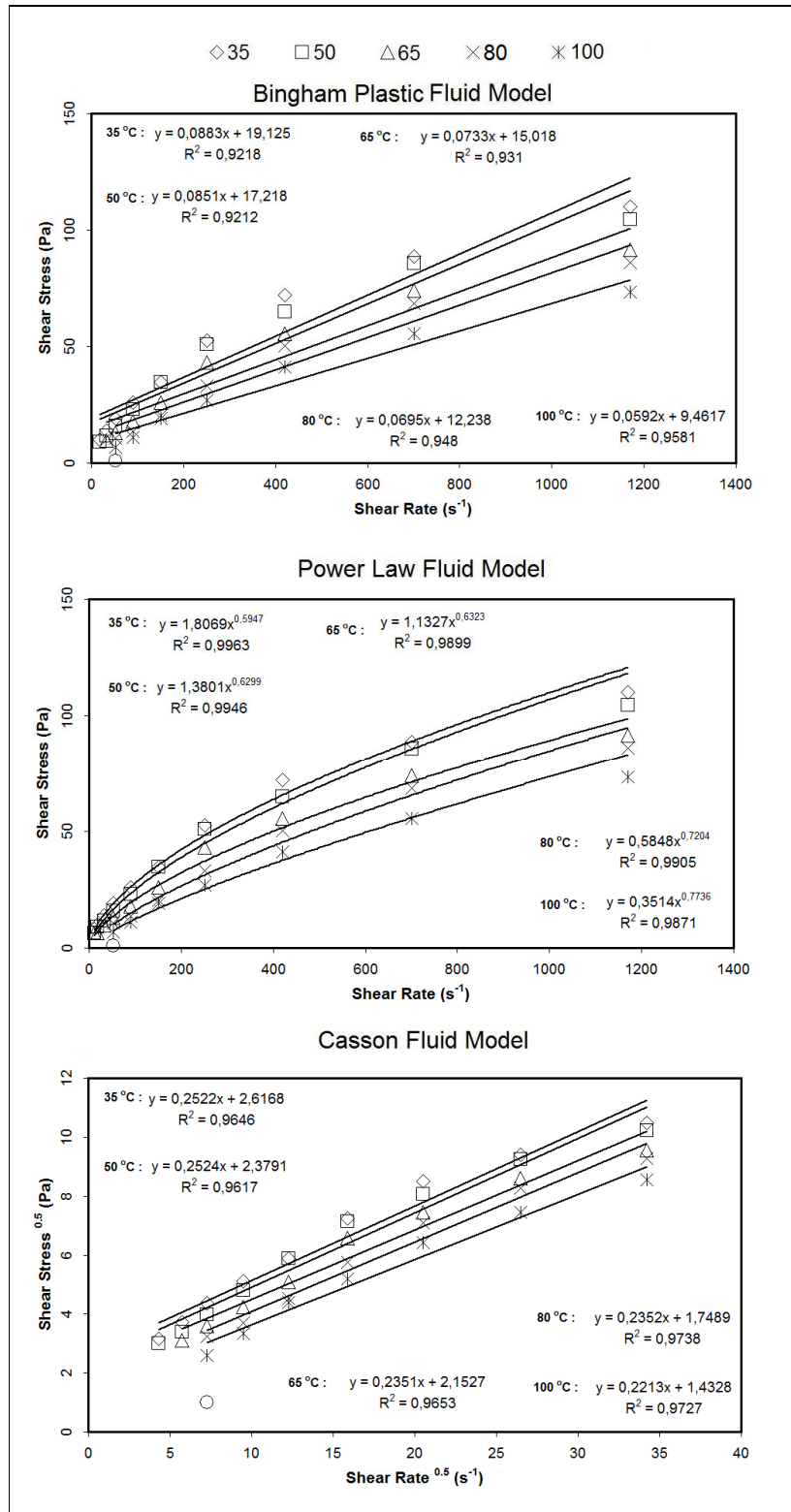


Figure A 9 Rheology of Bati Raman Crude oil after the addition of 0.1% FeCl<sub>3</sub>

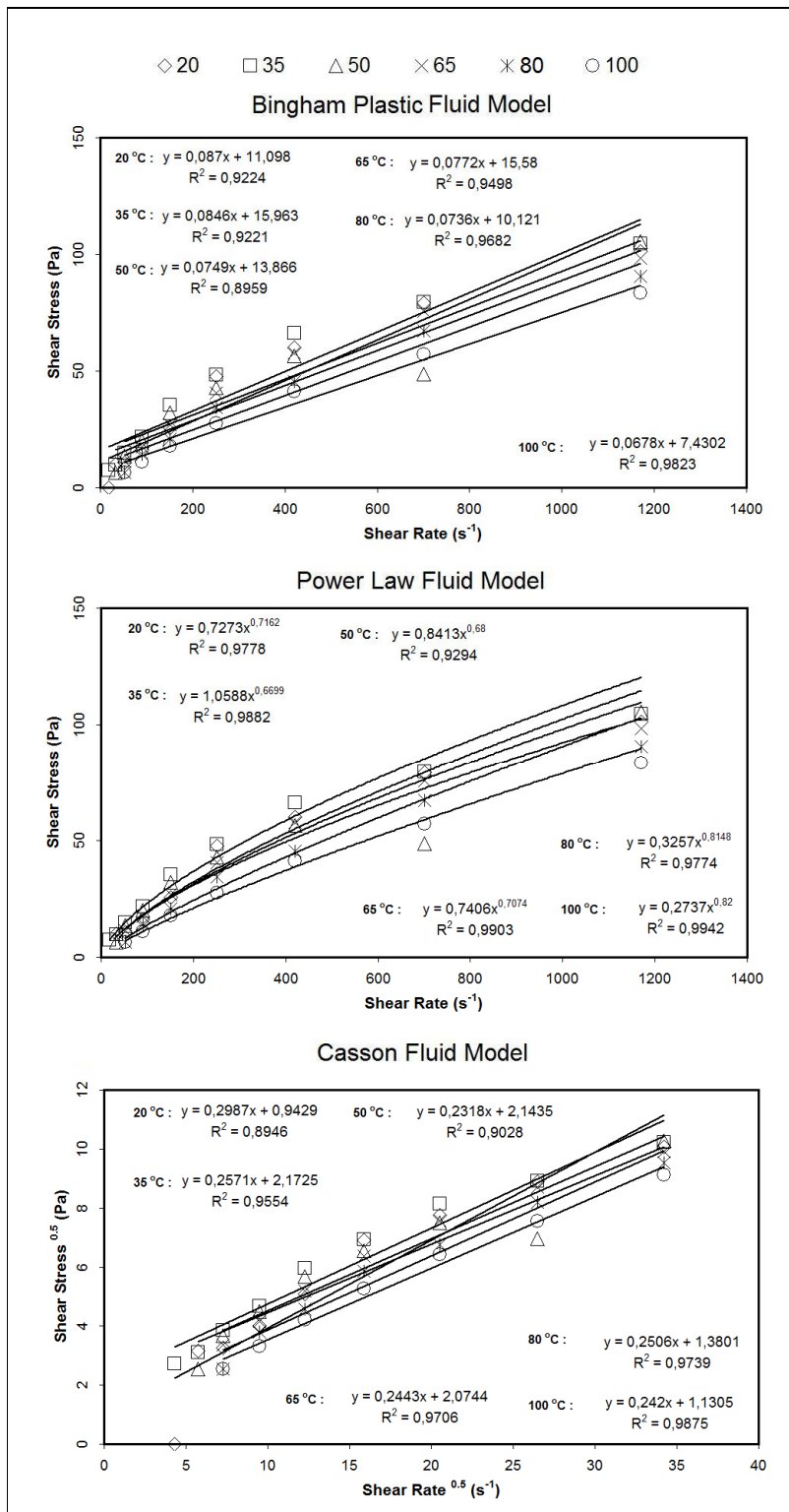


Figure A 10 Rheology of Bati Raman Crude oil after the addition of 0.5% FeCl<sub>3</sub>

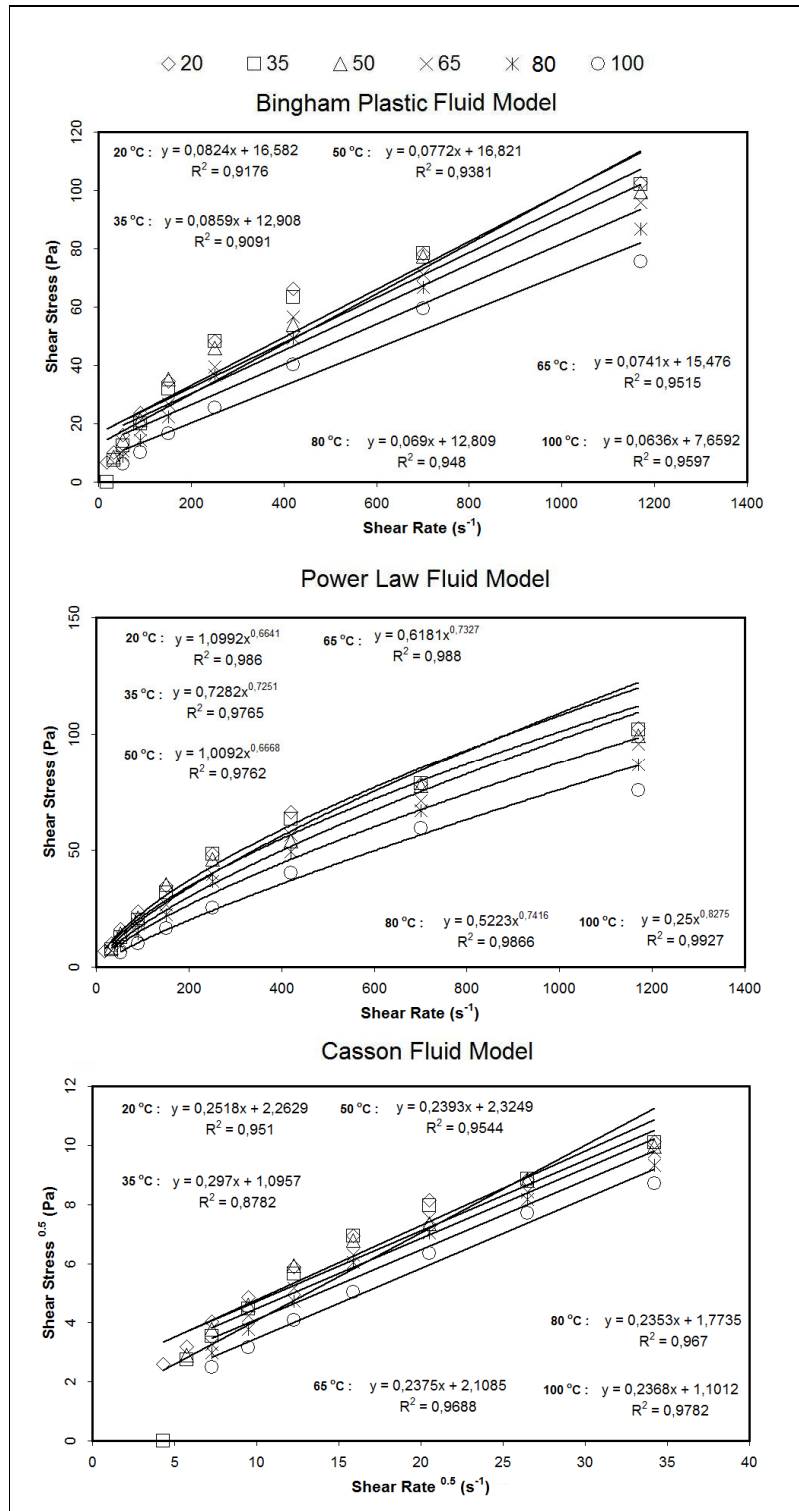


Figure A 11 Rheology of Bati Raman Crude oil after the addition of 1% FeCl<sub>3</sub>

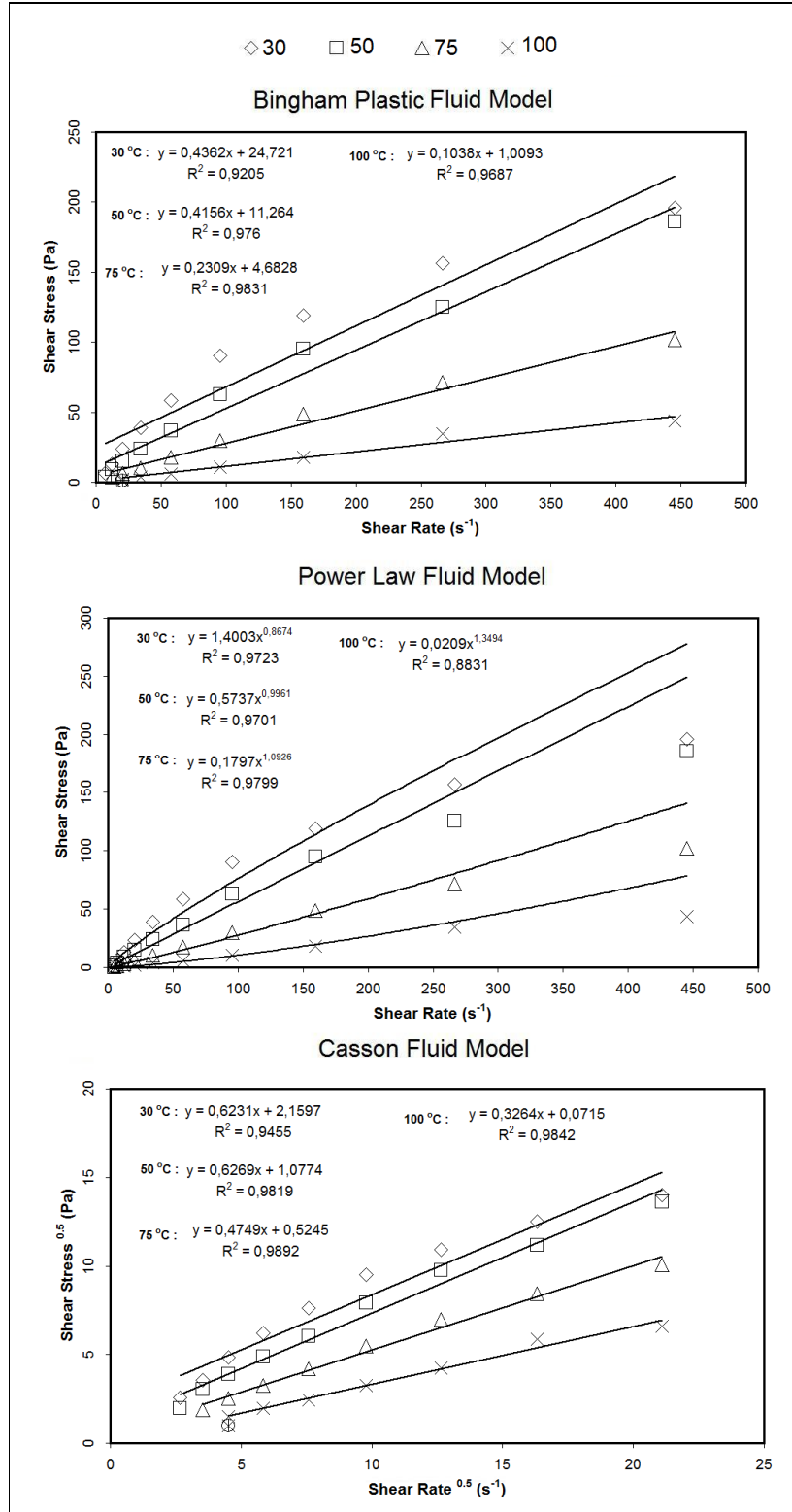


Figure A 12 Rheology of Dead Çamurlu Crude oil

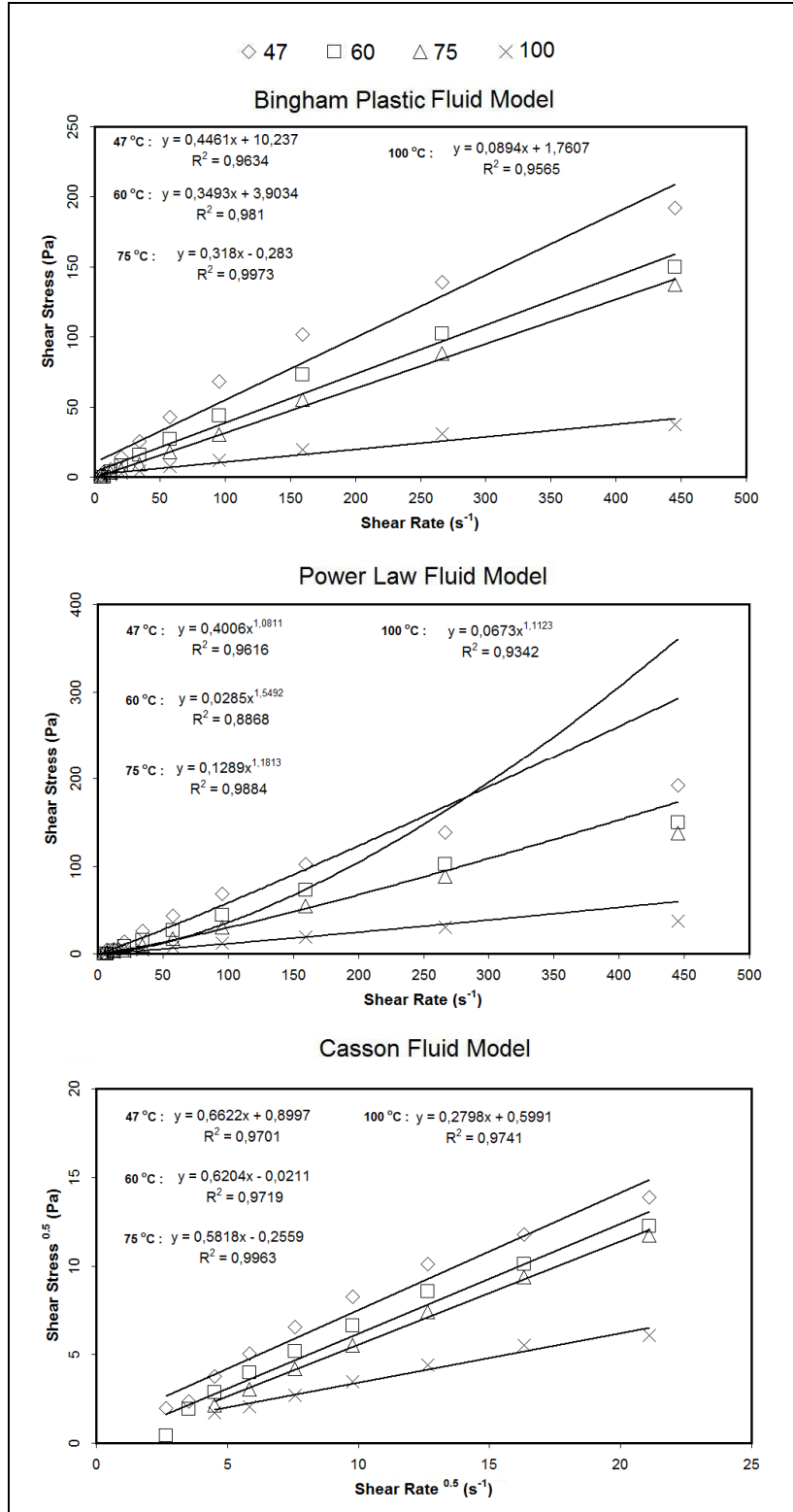


Figure A 13 Rheology of Çamurlu Crude oil after the addition of 0.1% Fe

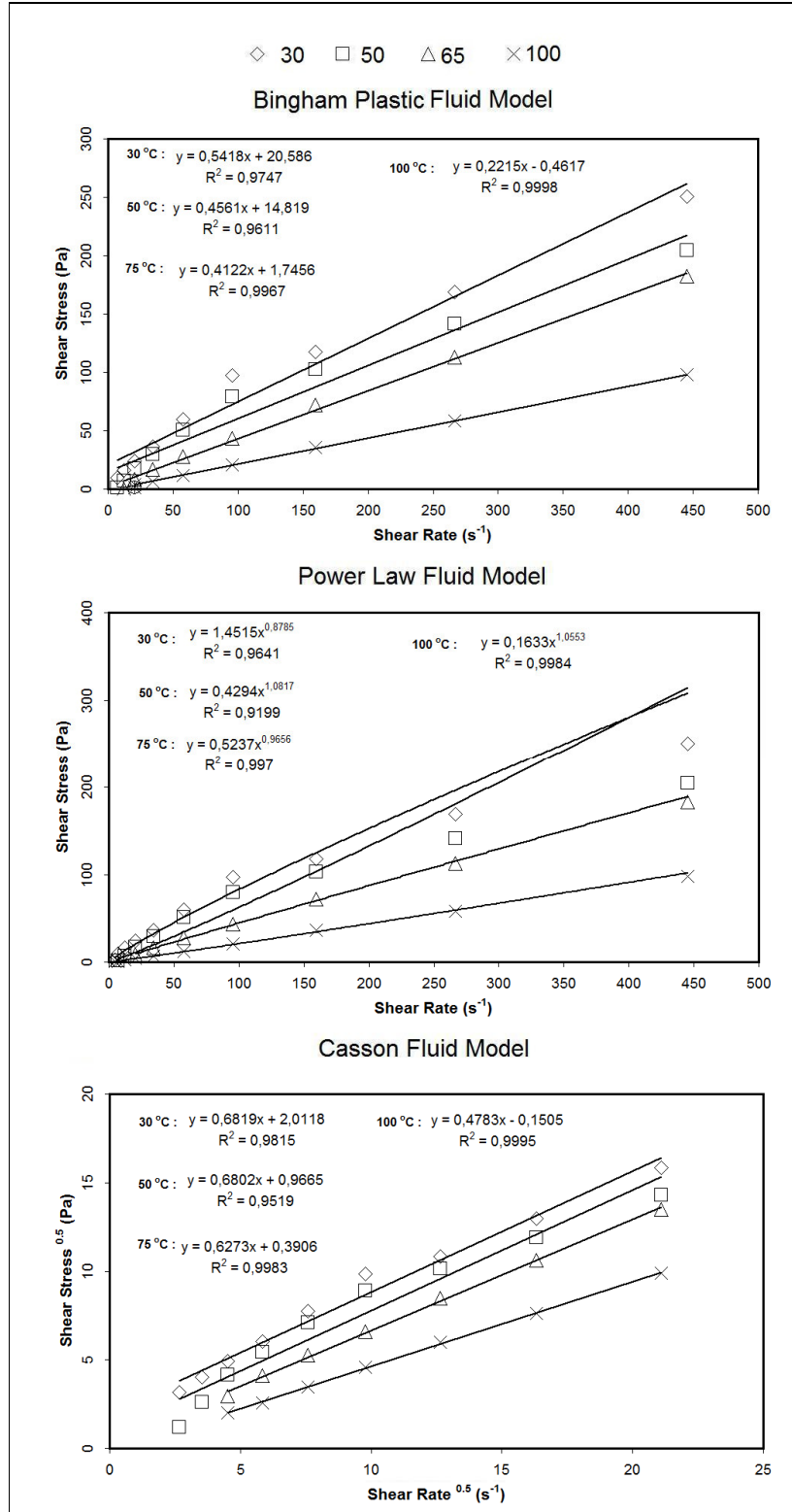


Figure A 14 Rheology of Çamurlu Crude oil after the addition of 0.5% Fe

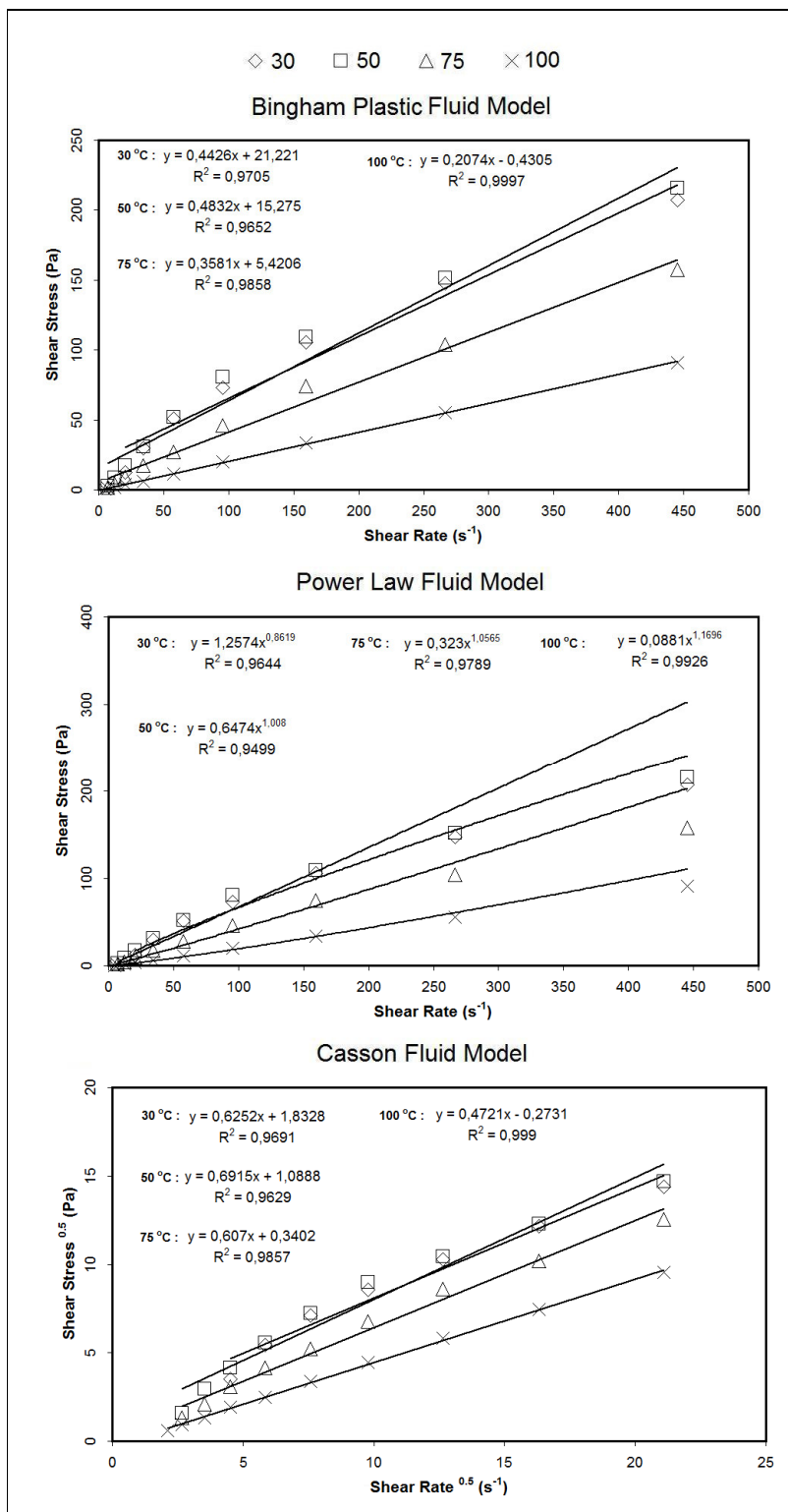


Figure A 15 Rheology of Çamurlu Crude oil after the addition of 1% Fe

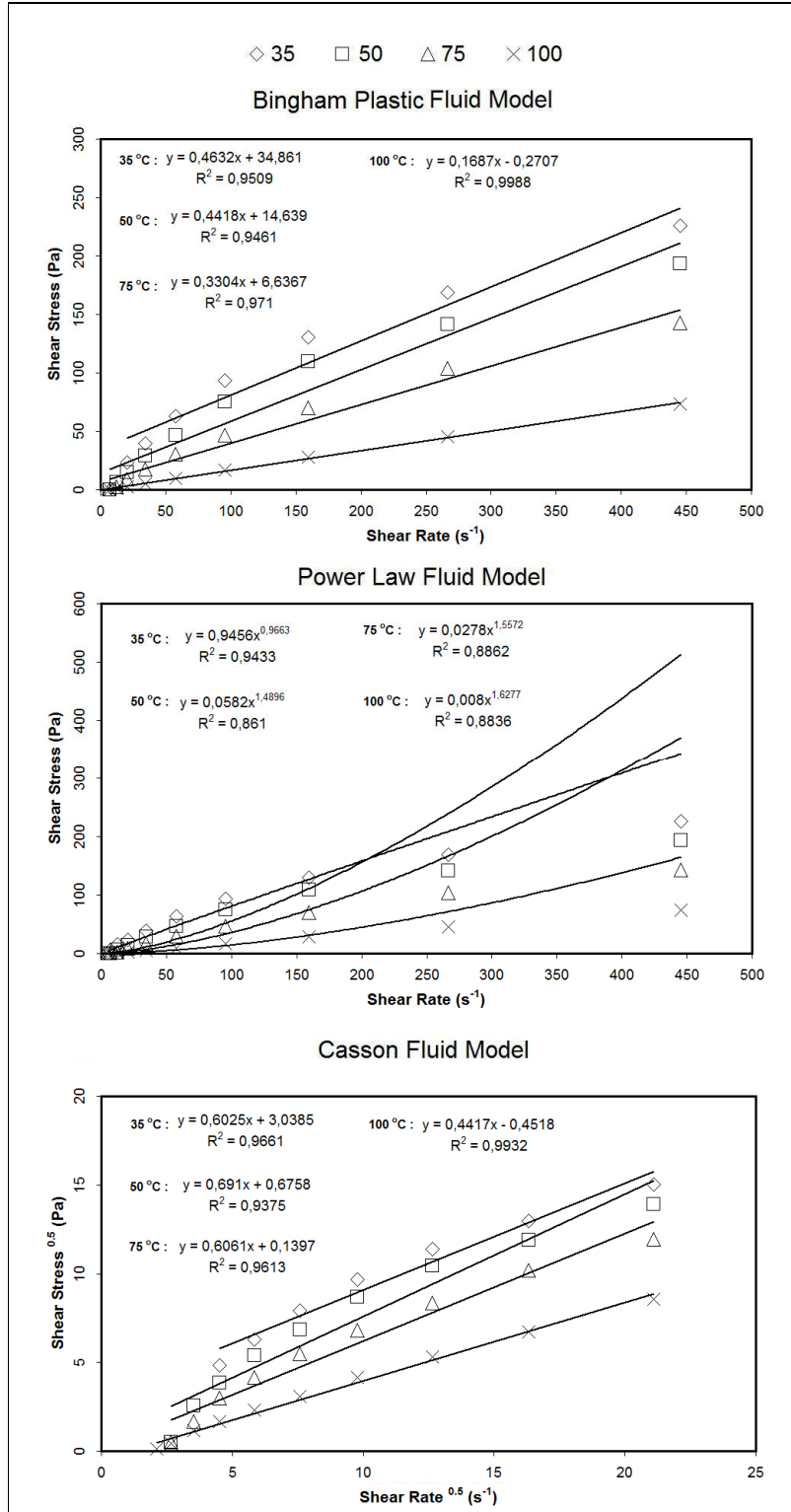


Figure A 16 Rheology of Çamurlu Crude oil after the addition of 0.1 % Fe<sub>2</sub>O<sub>3</sub>

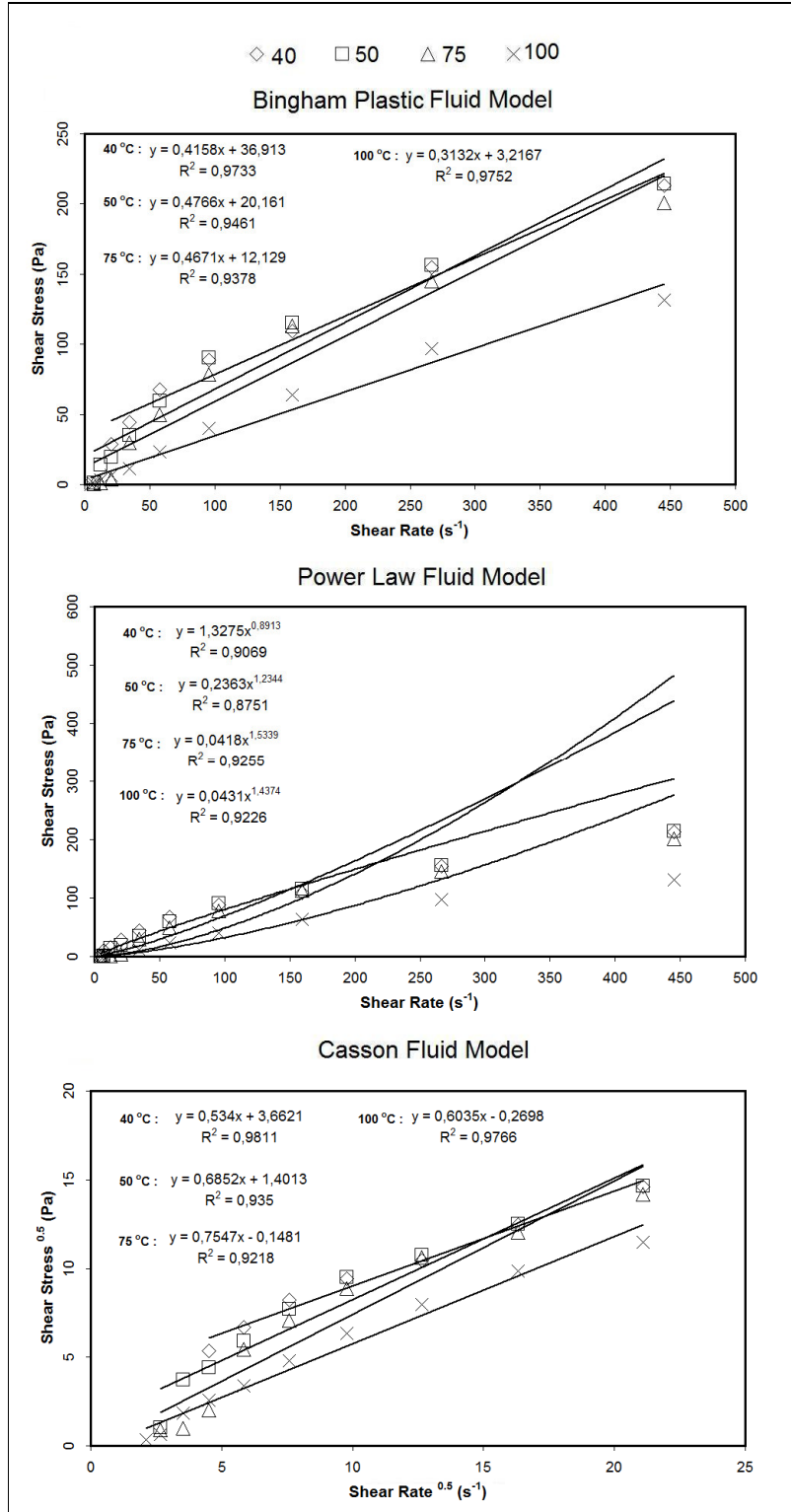


Figure A 17 Rheology of Çamurlu Crude oil after the addition of 0.5 % Fe<sub>2</sub>O<sub>3</sub>

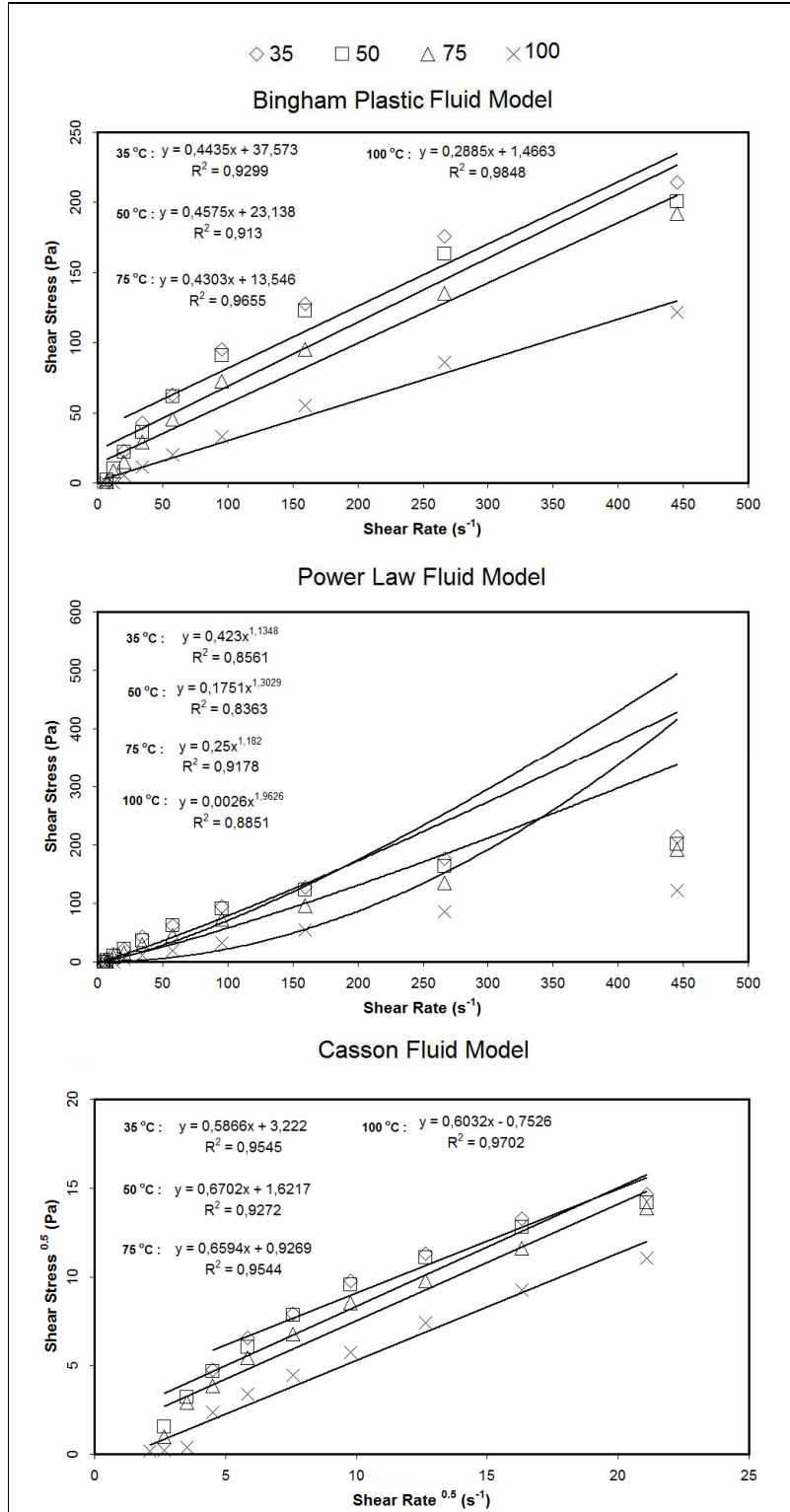


Figure A 18 Rheology of Çamurlu Crude oil after the addition of 1 % Fe<sub>2</sub>O<sub>3</sub>

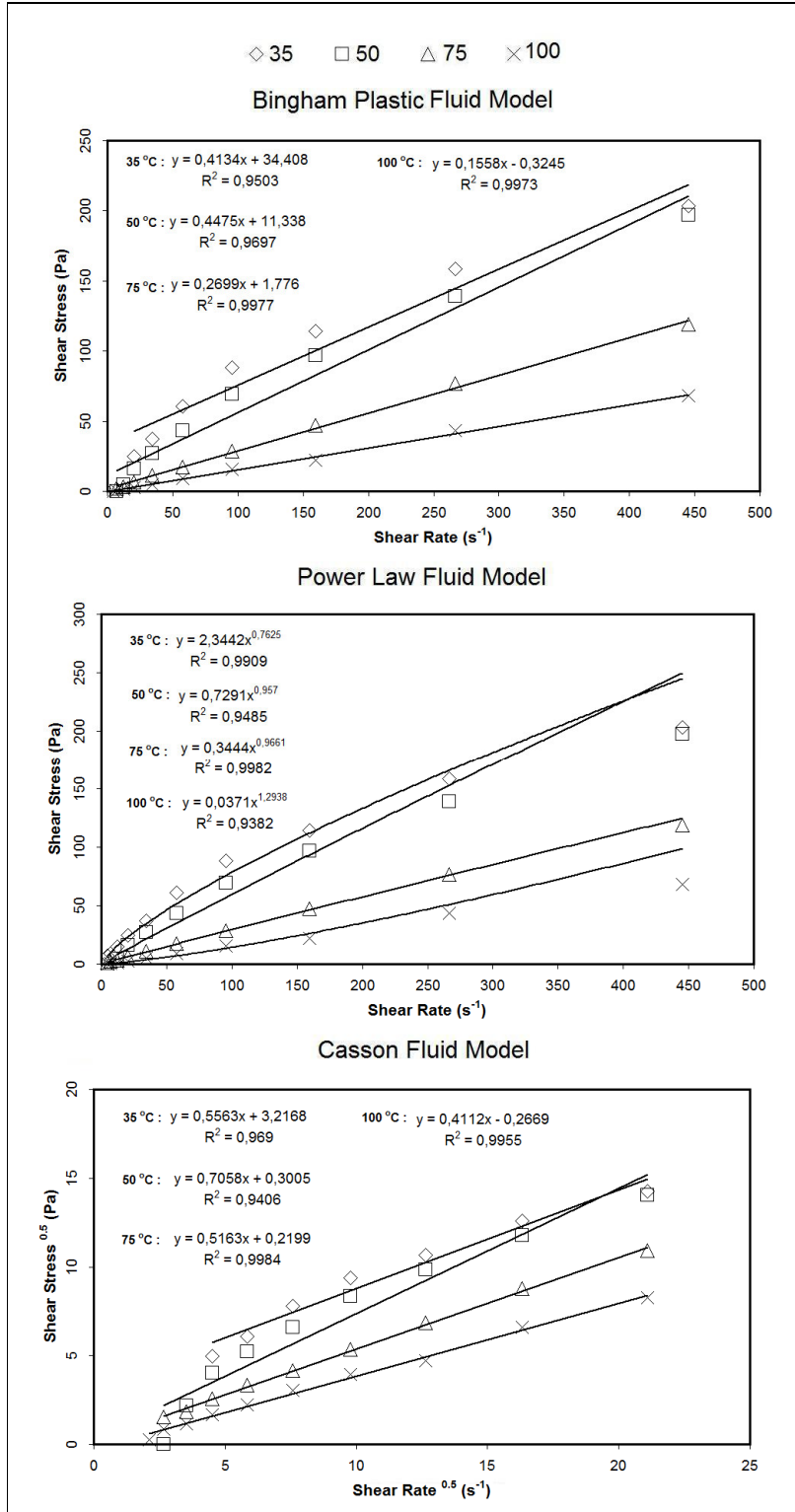


Figure A 19 Rheology of Çamurlu Crude oil after the addition of 0.1 % FeCl<sub>3</sub>

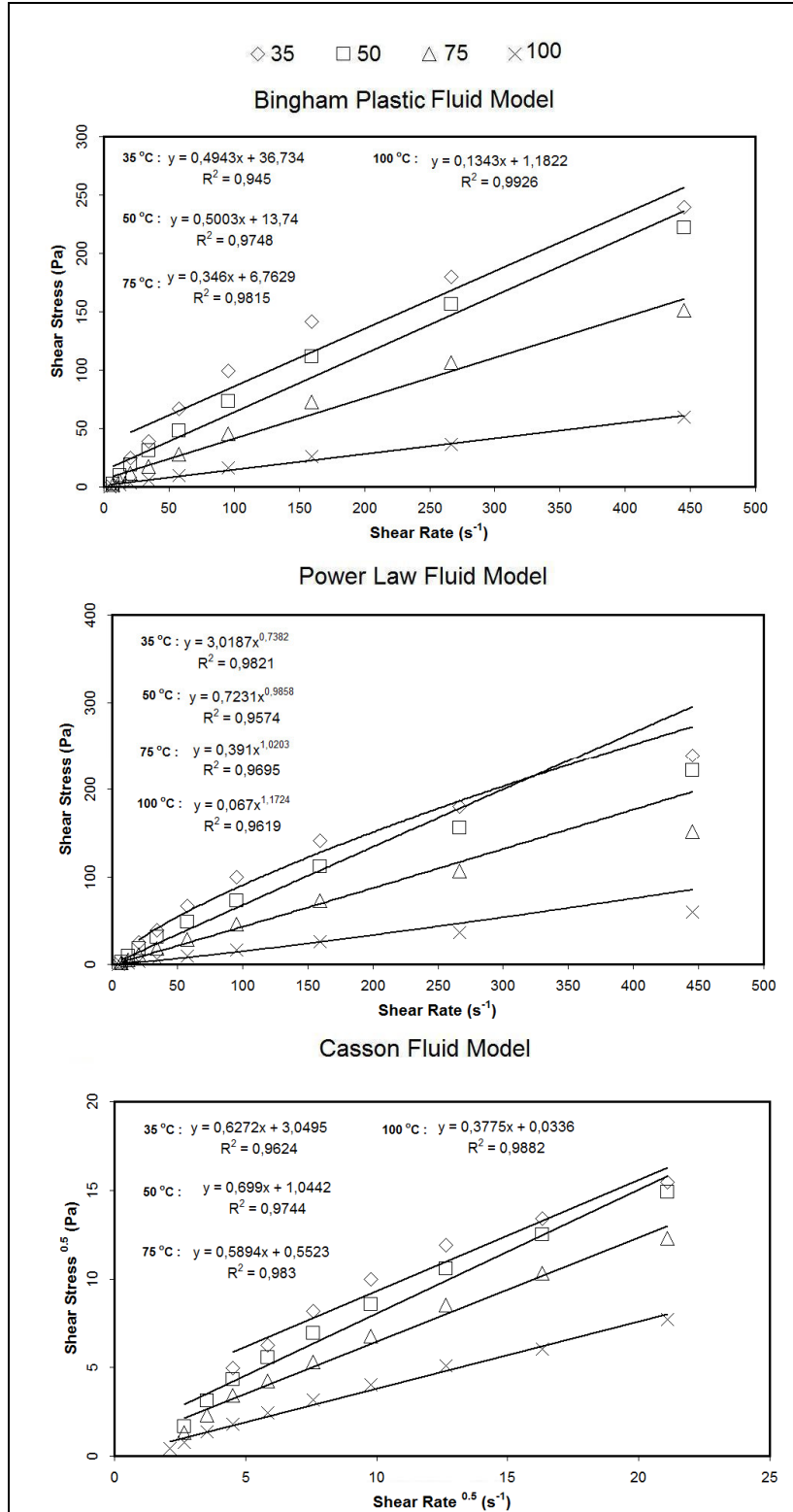


Figure A 20 Rheology of Çamurlu Crude oil after the addition of 0.5 % FeCl<sub>3</sub>

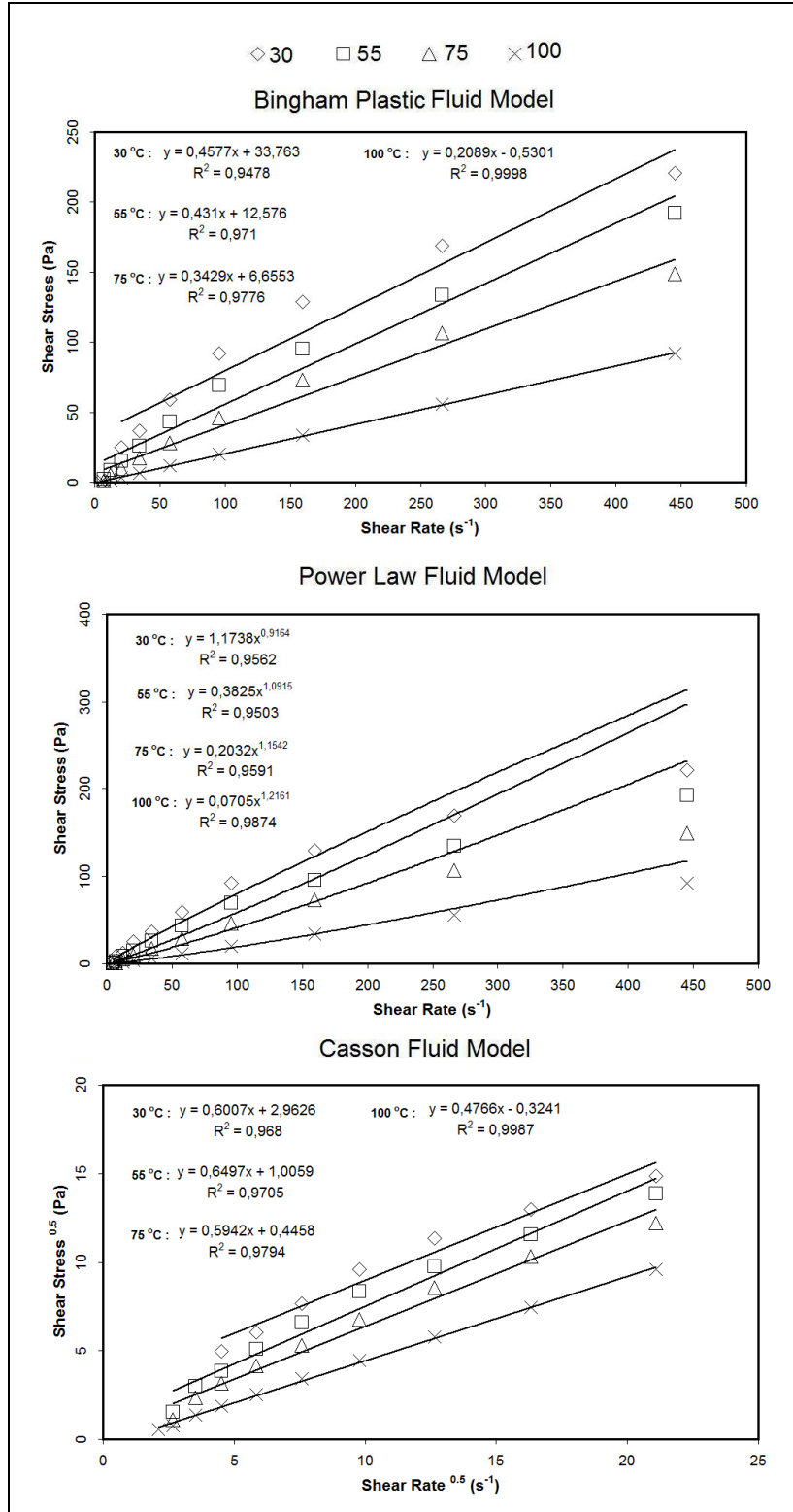


Figure A 21 Rheology of Çamurlu Crude oil after the addition of 1 % FeCl<sub>3</sub>

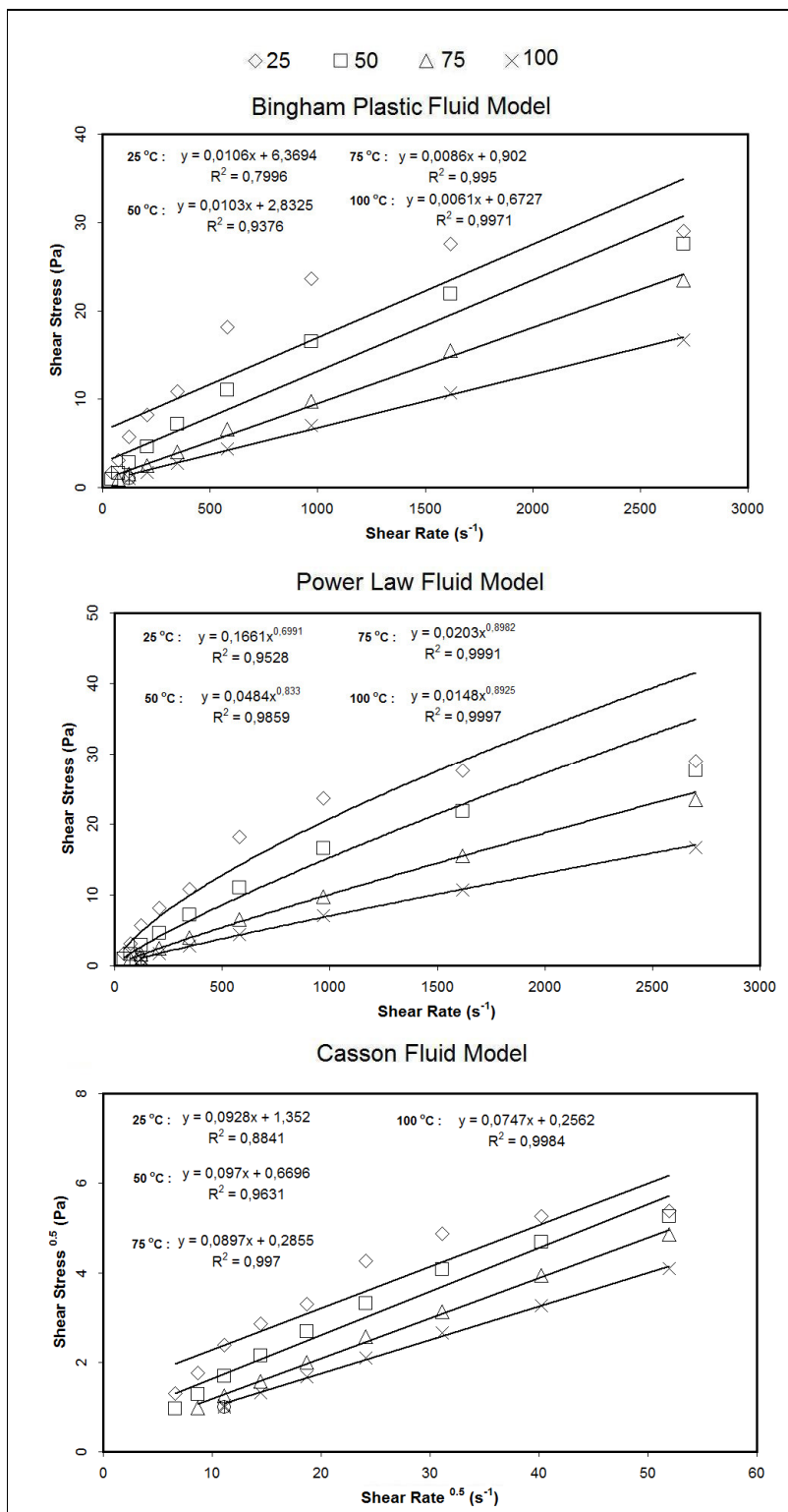


Figure A 22 Rheology of Dead Garzan Crude oil

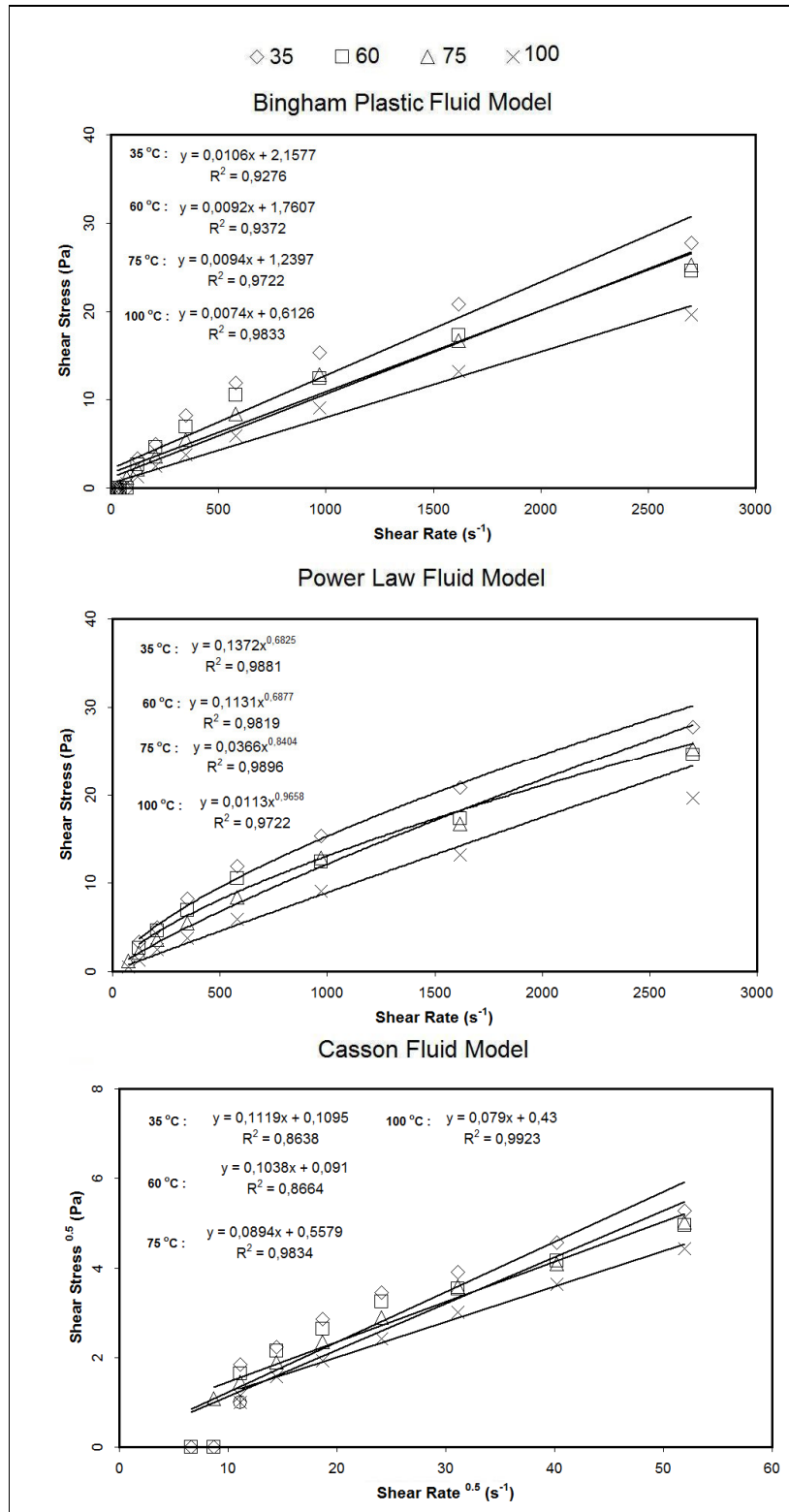


Figure A 23 Rheology of Garzan Crude oil after the addition of 0.1 % Fe

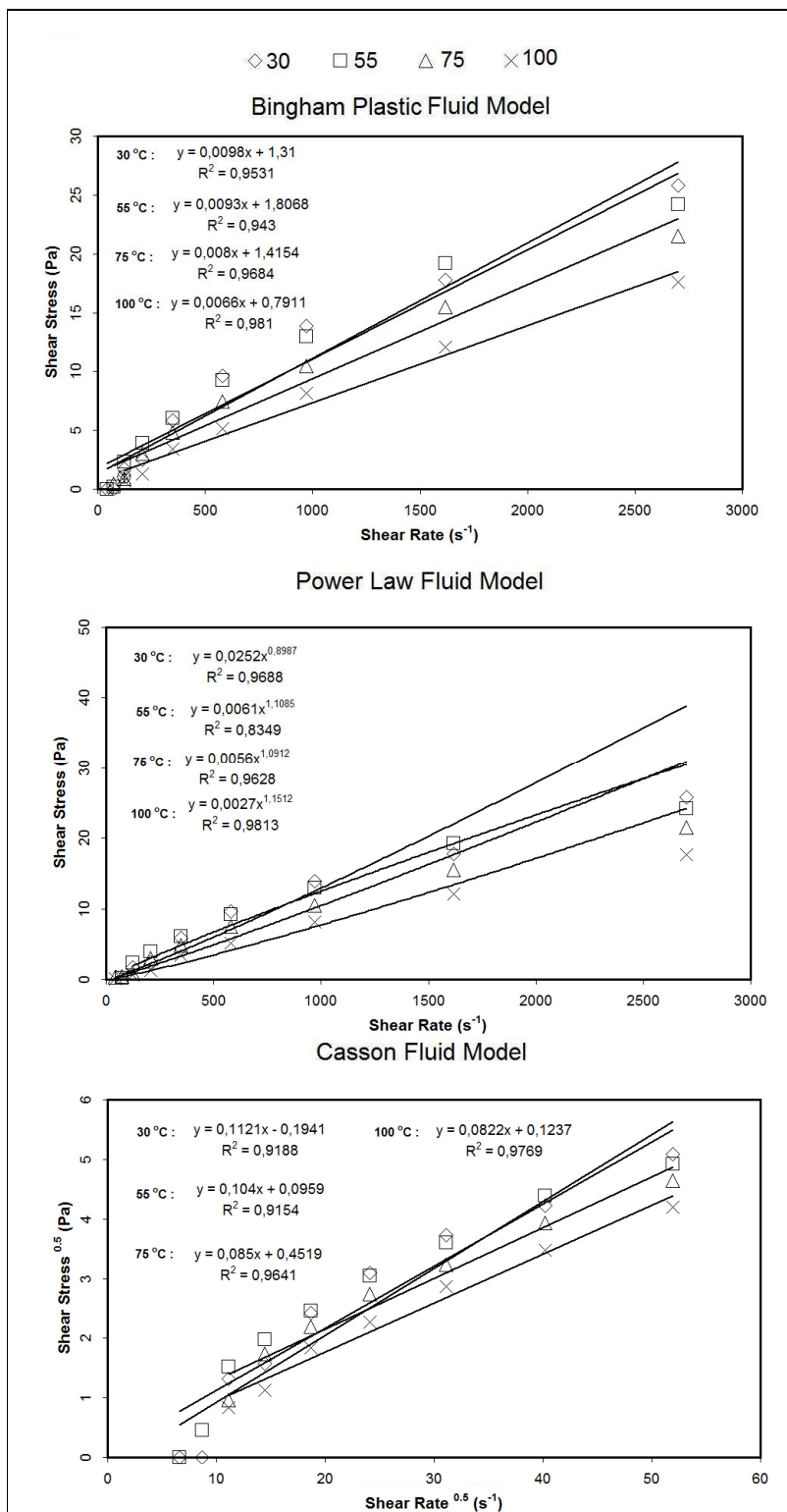


Figure A 24 Rheology of Garzan Crude oil after the addition of 0.5 % Fe

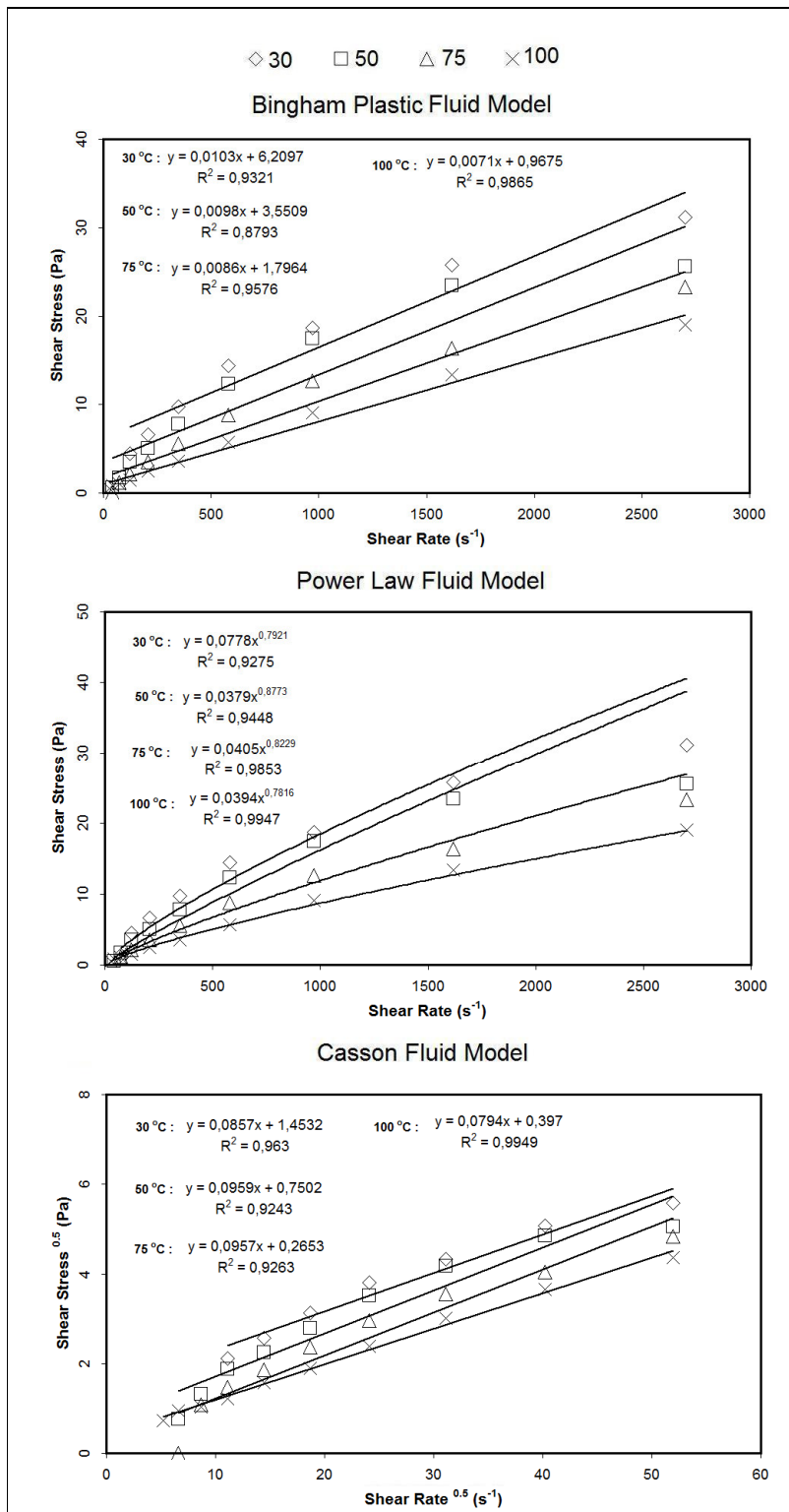


Figure A 25 Rheology of Garzan Crude oil after the addition of 1 % Fe

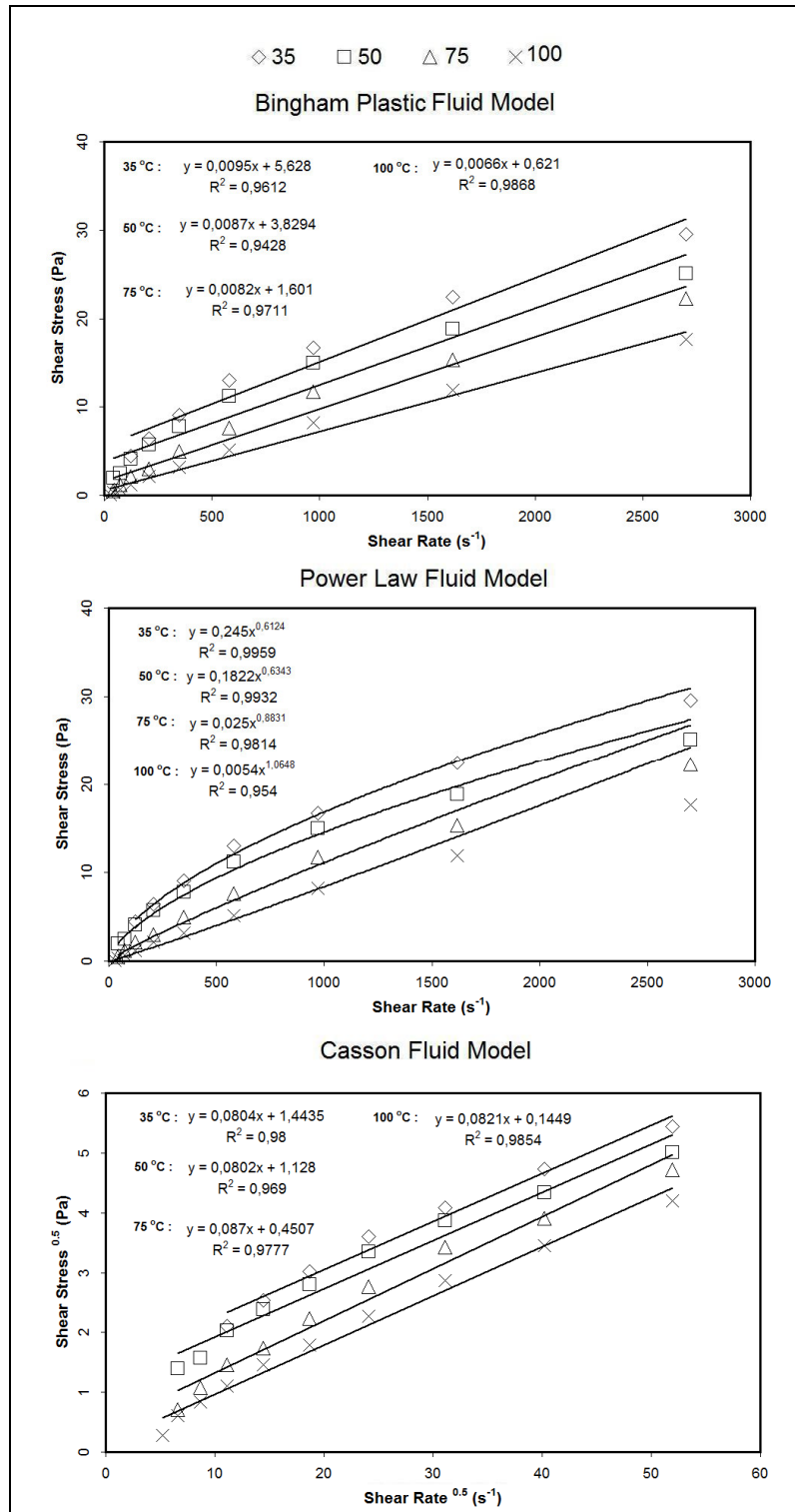


Figure A 26 Rheology of Garzan Crude oil after the addition of 0.1 % Fe<sub>2</sub>O<sub>3</sub>

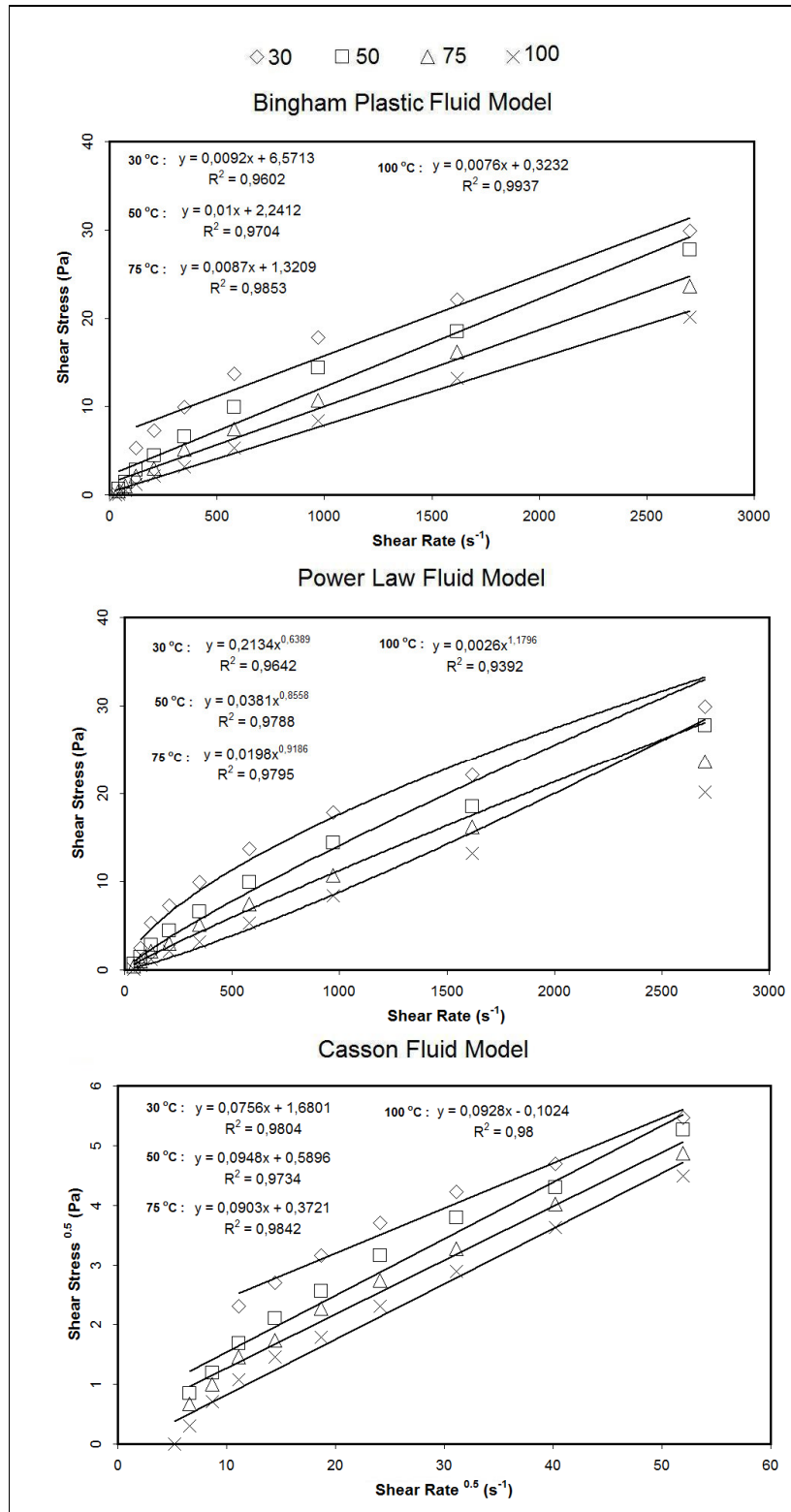


Figure A 27 Rheology of Garzan Crude oil after the addition of 0.5 % Fe<sub>2</sub>O<sub>3</sub>

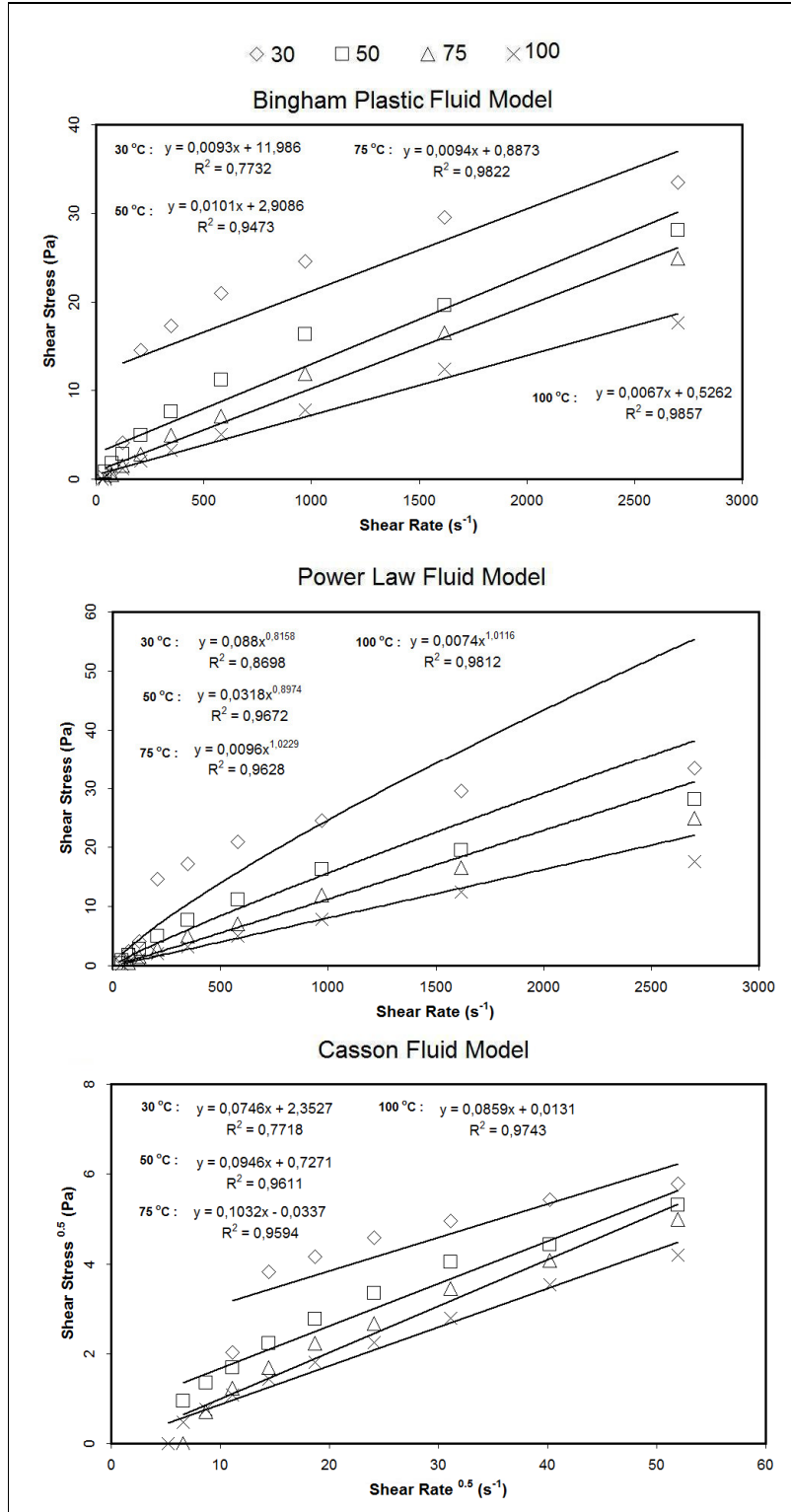


Figure A 28 Rheology of Garzan Crude oil after the addition of 1 % Fe<sub>2</sub>O<sub>3</sub>

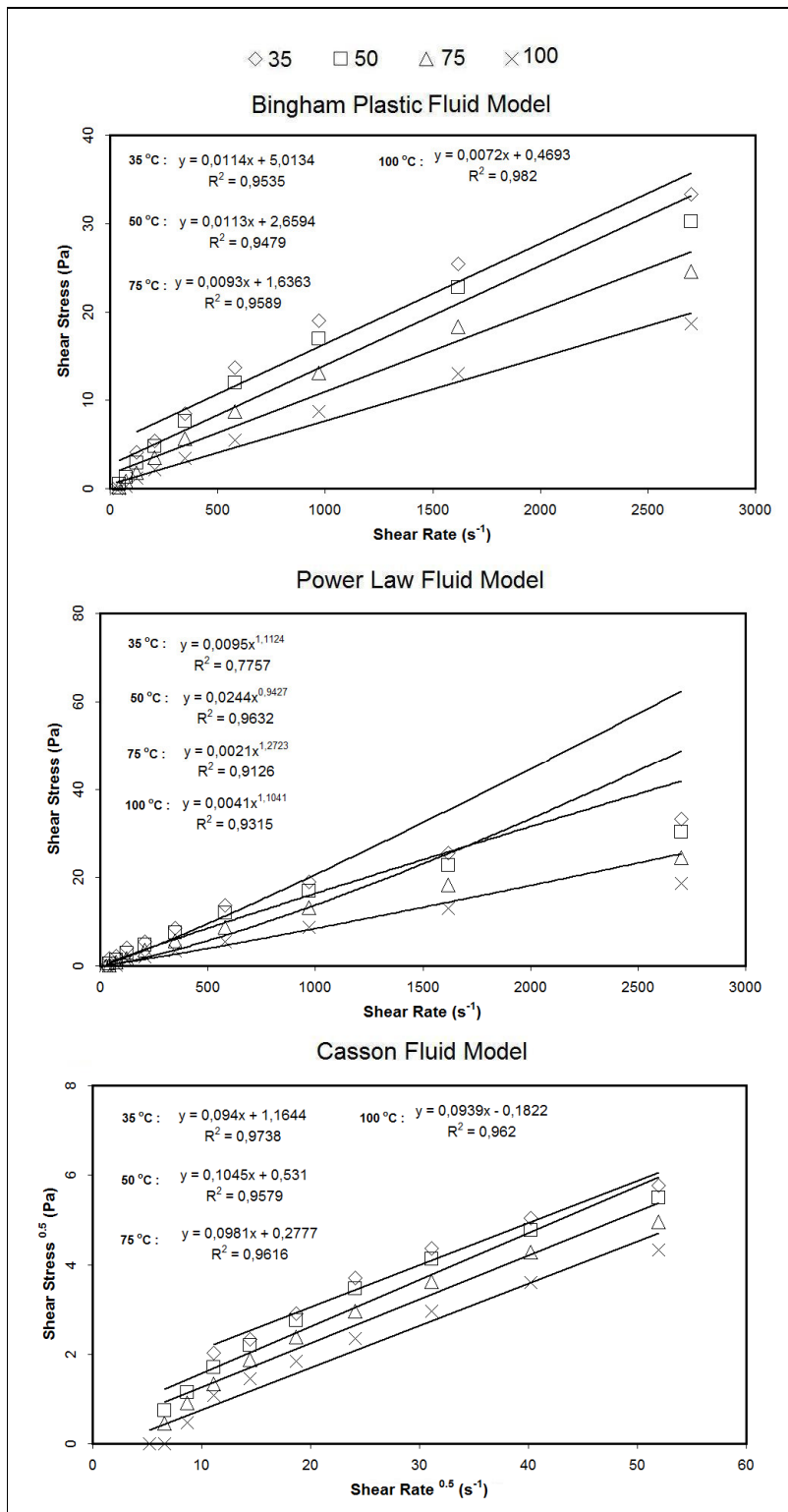


Figure A 29 Rheology of Garzan Crude oil after the addition of 0.1 % FeCl<sub>3</sub>

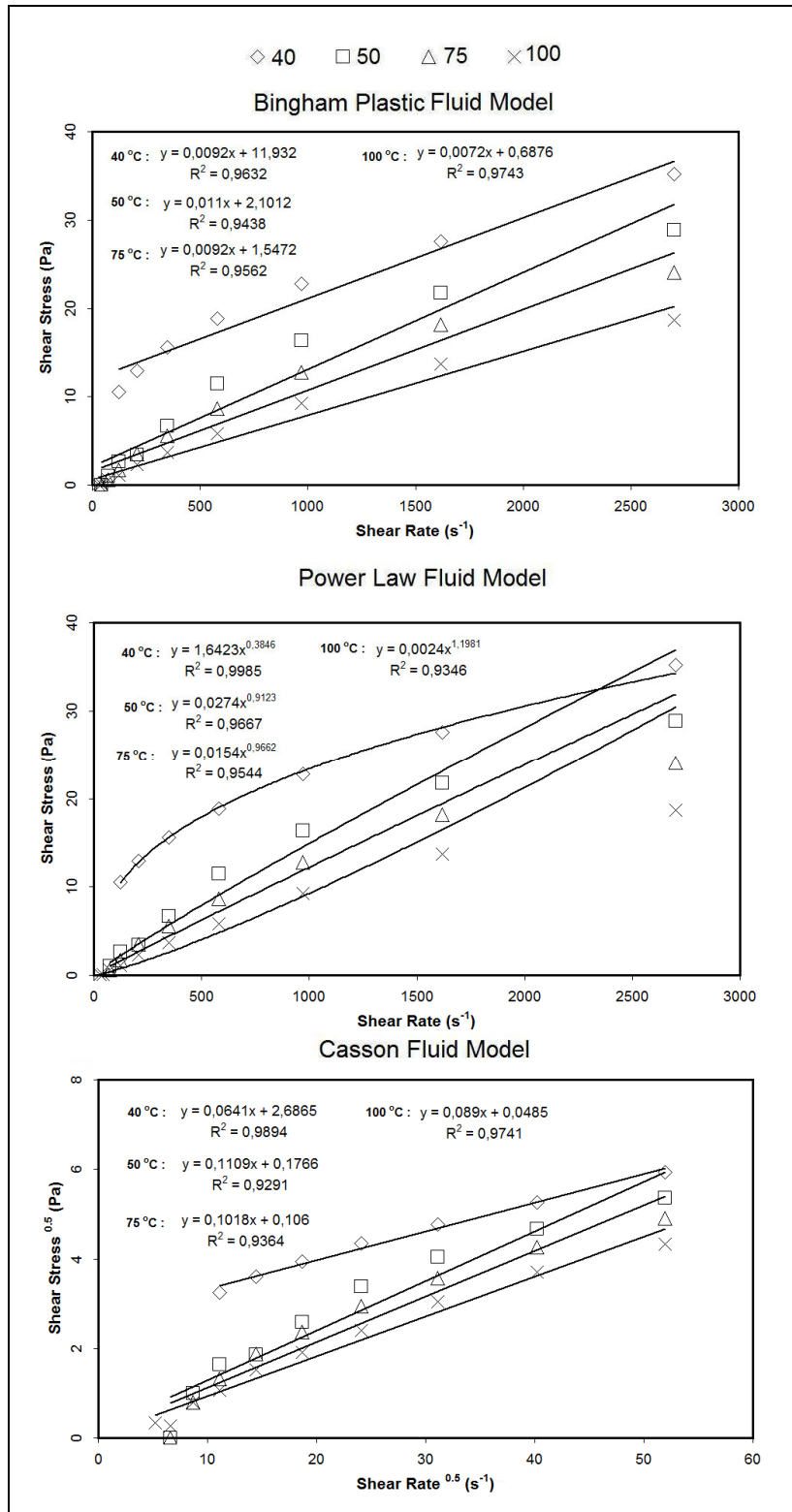


Figure A 30 Rheology of Garzan Crude oil after the addition of 0.5 % FeCl<sub>3</sub>

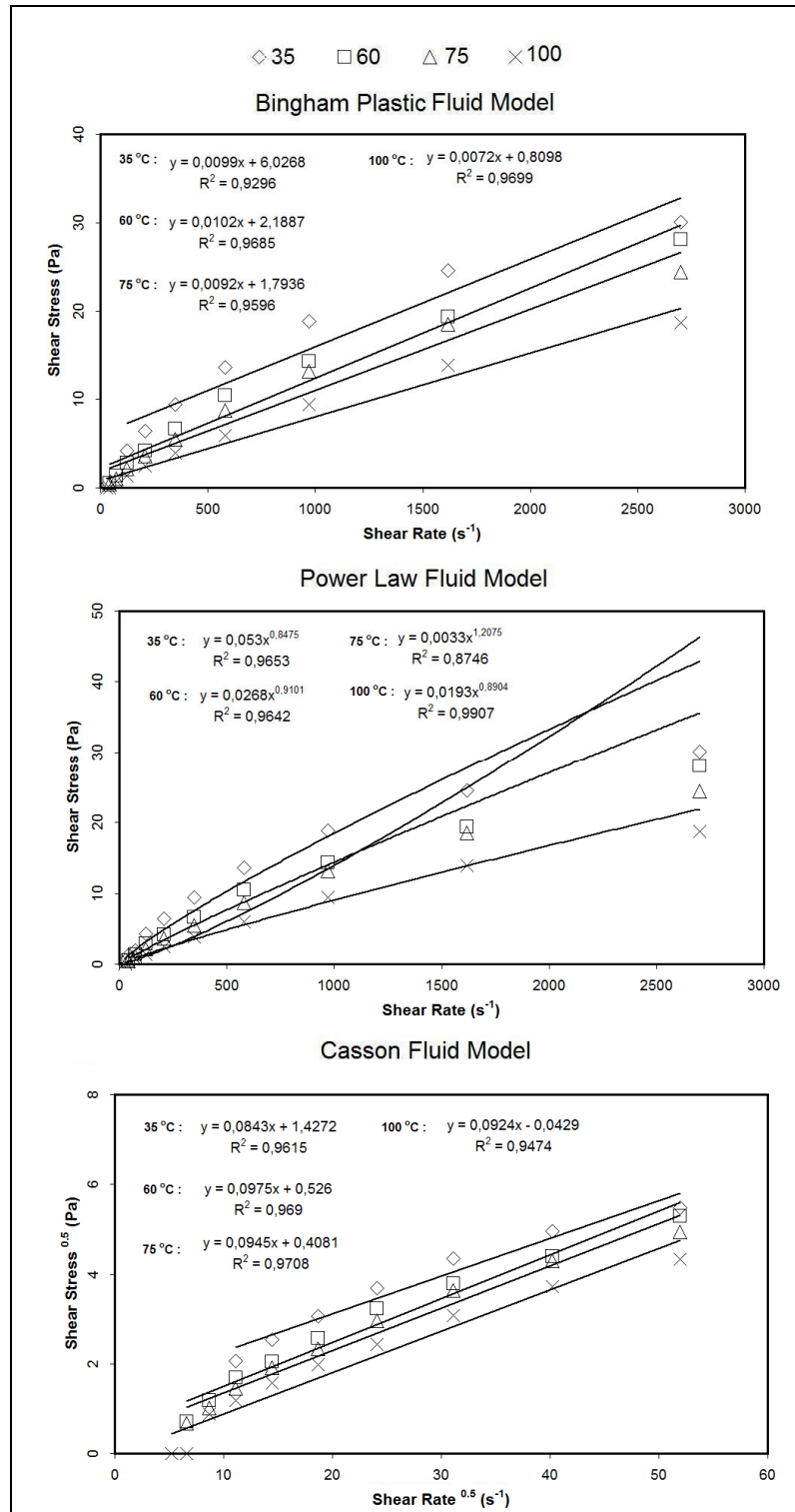


Figure A 31 Rheology of Garzan Crude oil after the addition of 1 % FeCl<sub>3</sub>

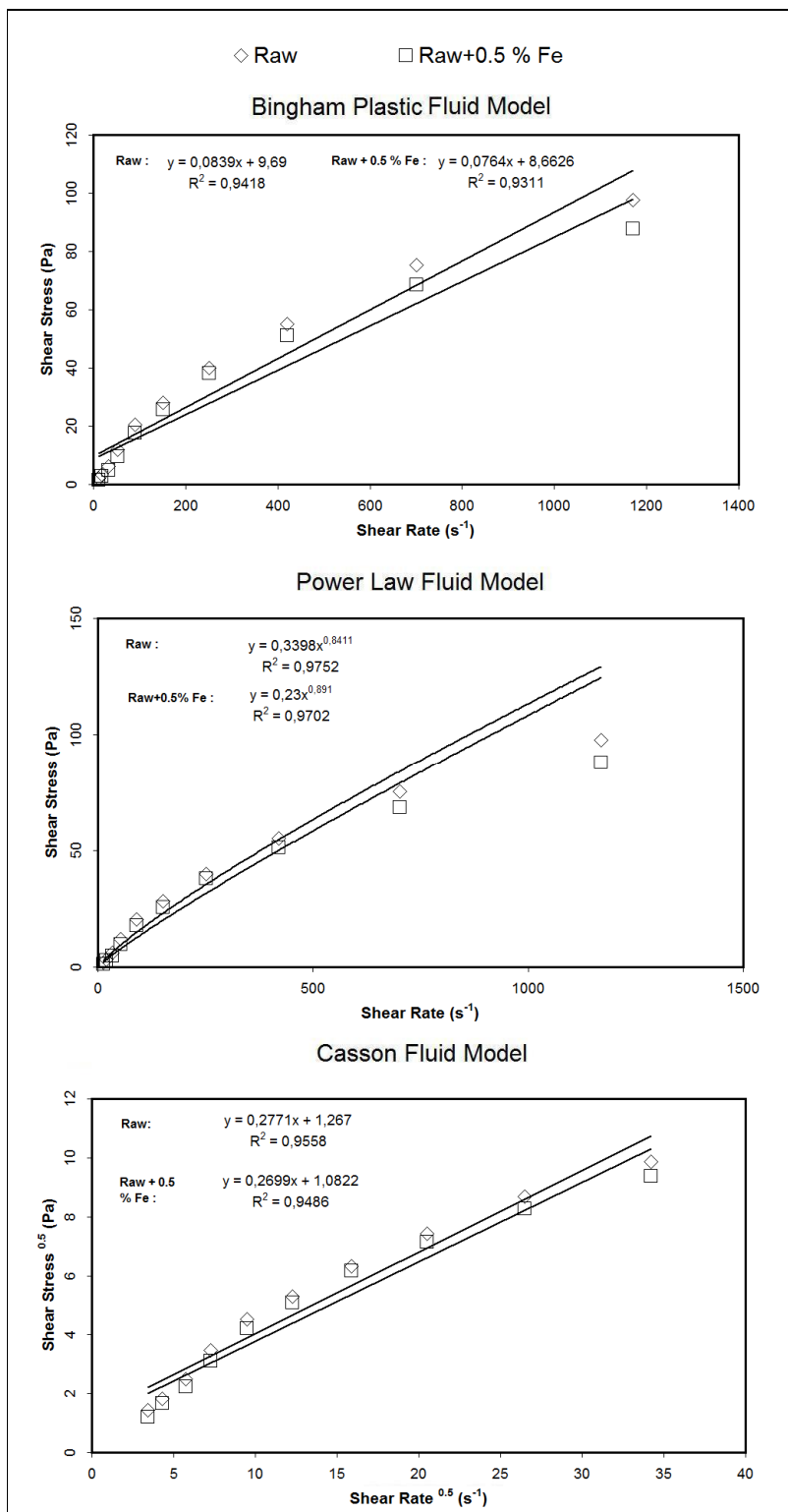


Figure A 32 Rheology of Bati Raman Crude oil after microwave irradiation

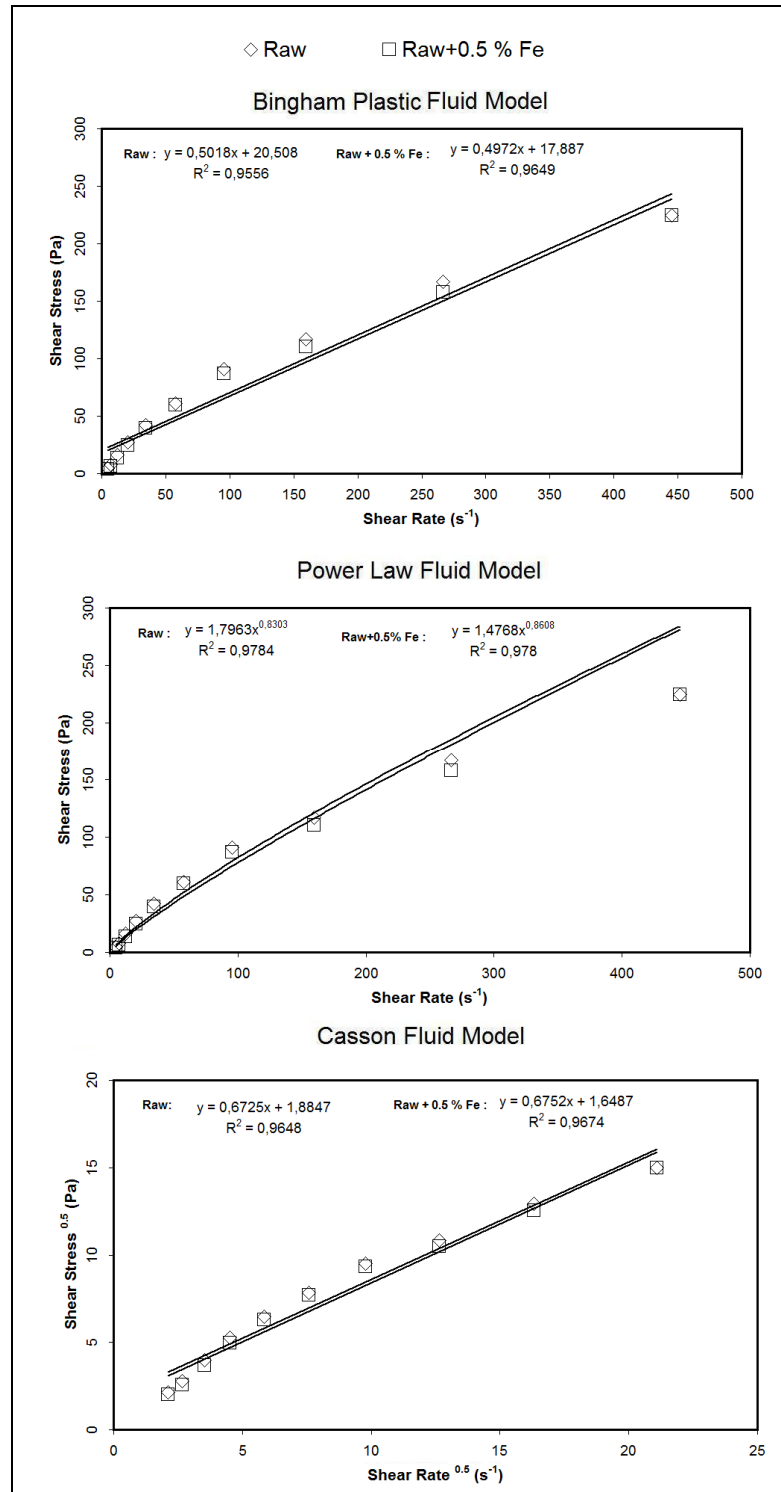


Figure A 33 Rheology of Çamurlu Crude oil after microwave irradiation

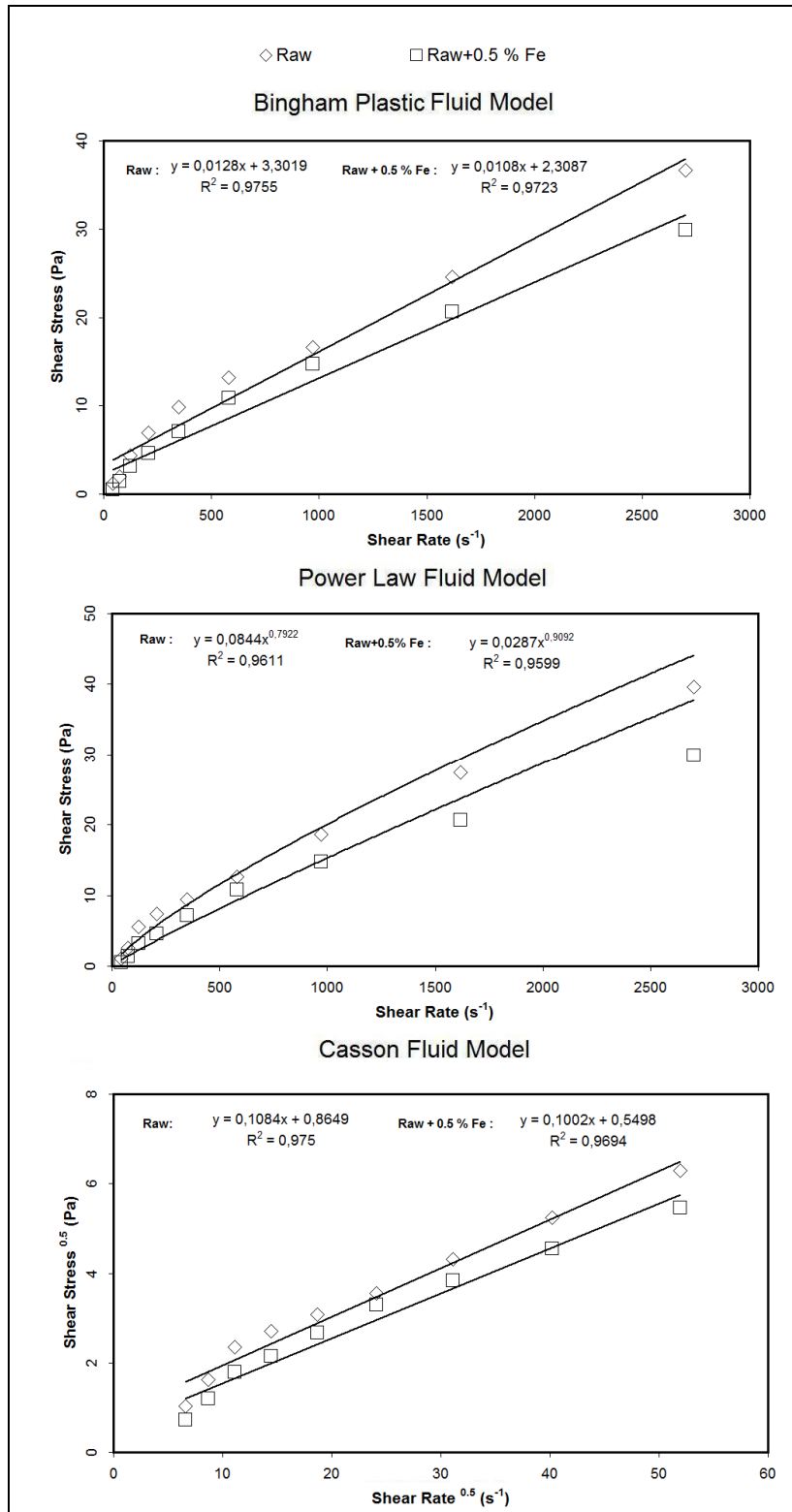


Figure A 34 Rheology of Garzan Crude oil after microwave irradiation

## APPENDIX B

### TEMPERATURE DISTRIBUTIONS AND GAS EMISSIONS

#### B.1. Temperature Distribution of Microwave Experiments

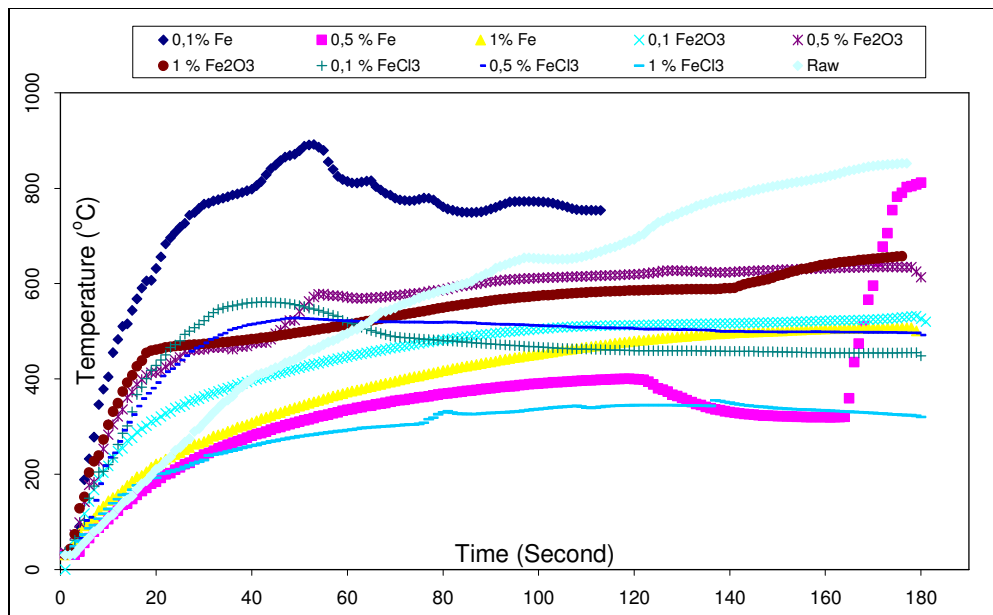


Figure B 1 Temperature distribution of Himmetoglu Oil Shale

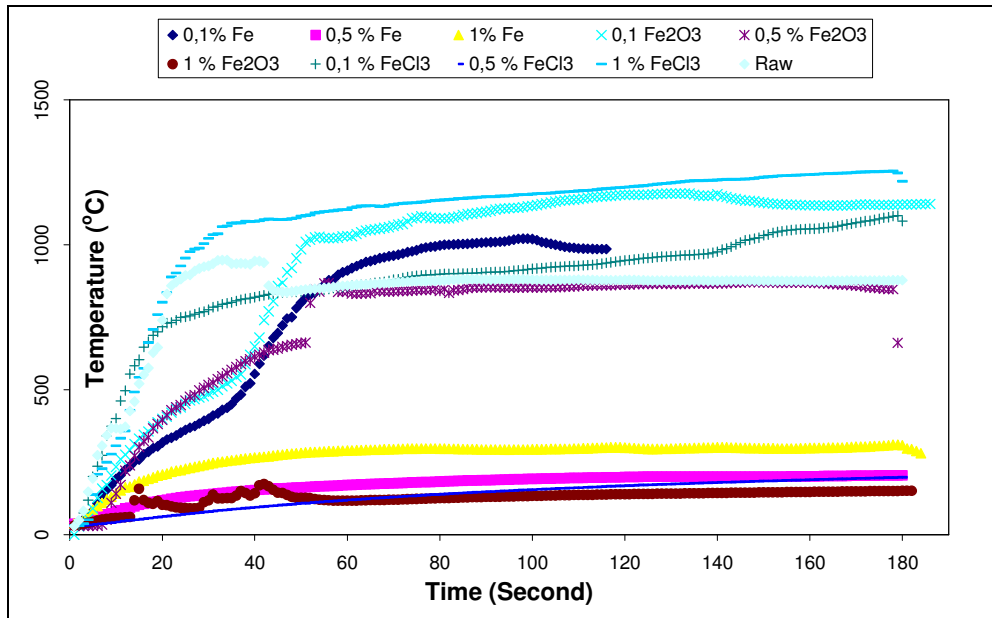


Figure B 2 Temperature distribution of Hatıldağ Oil Shale

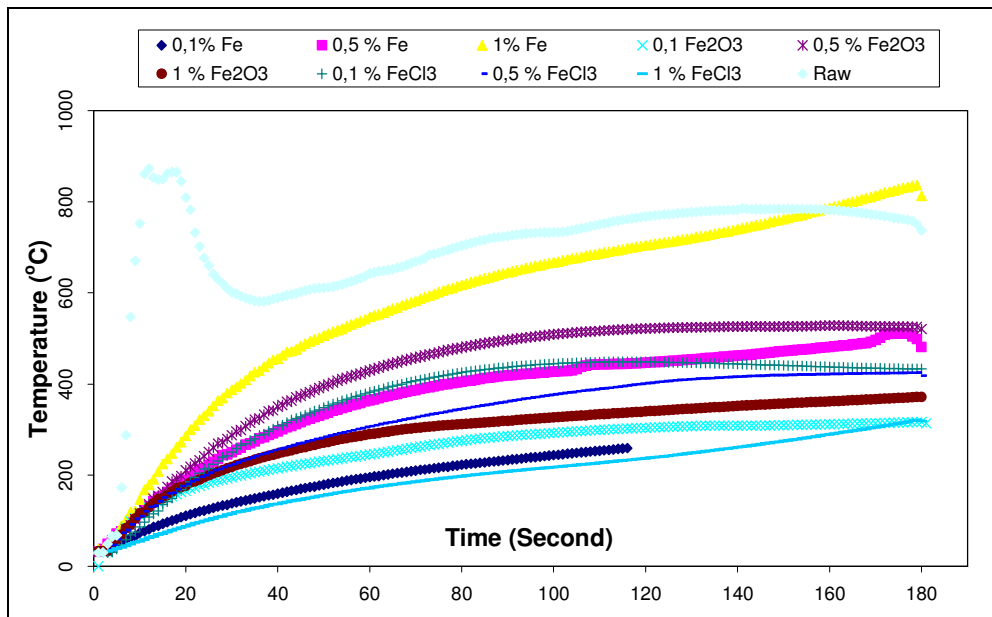


Figure B 3 Temperature distribution of Seyitömer Oil Shale

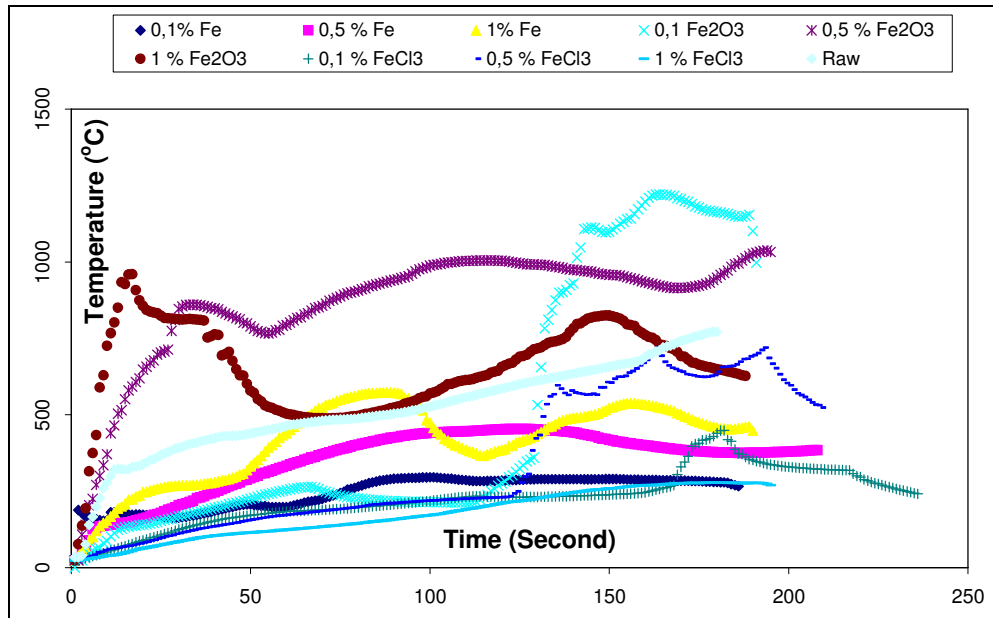


Figure B 4 Temperature distribution of Ulukışla Oil Shale

## B.2. Gas Emissions of Microwave Experiments

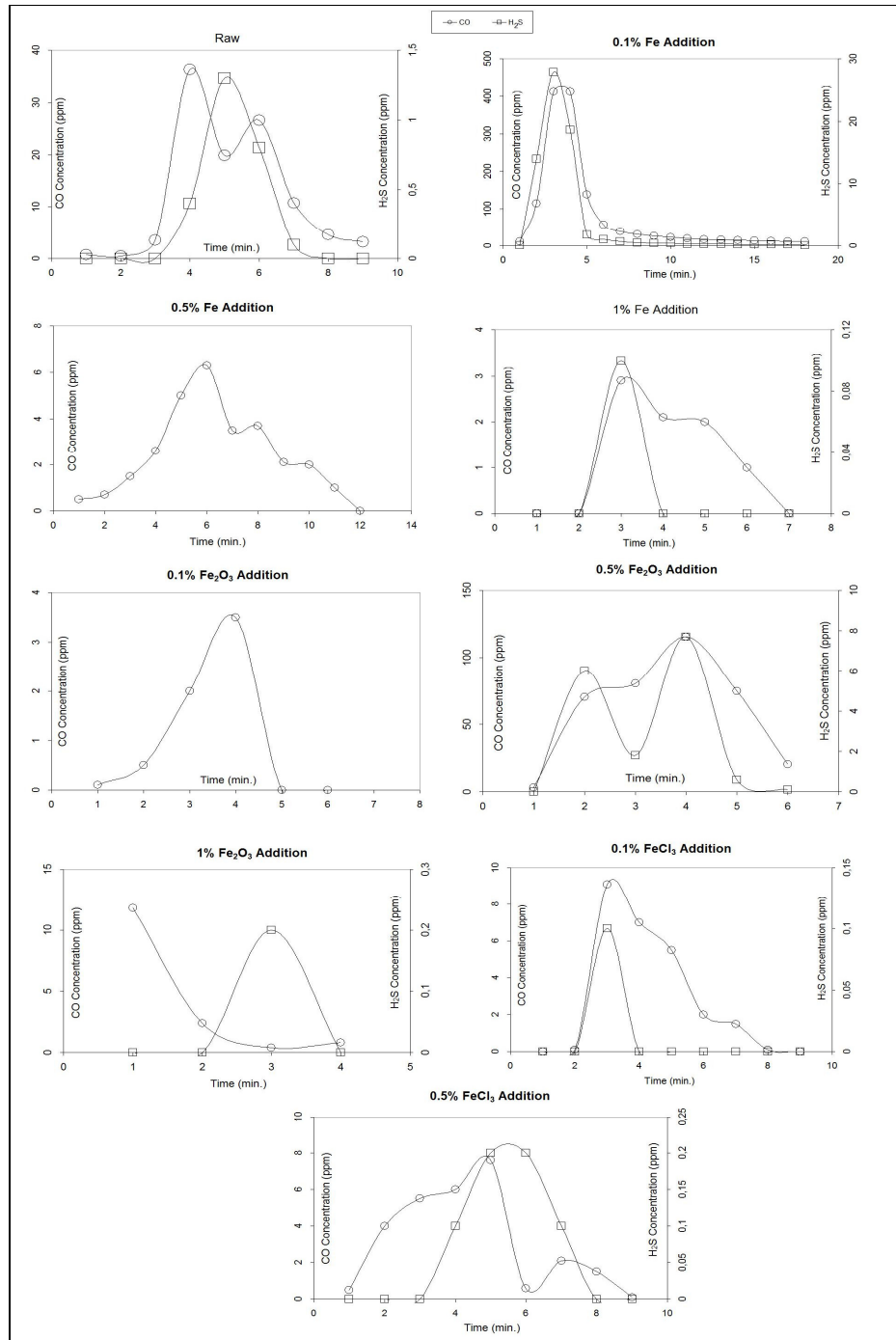


Figure B 5 Gas emissions for Himmetoglu oil shale after electromagnetic heating

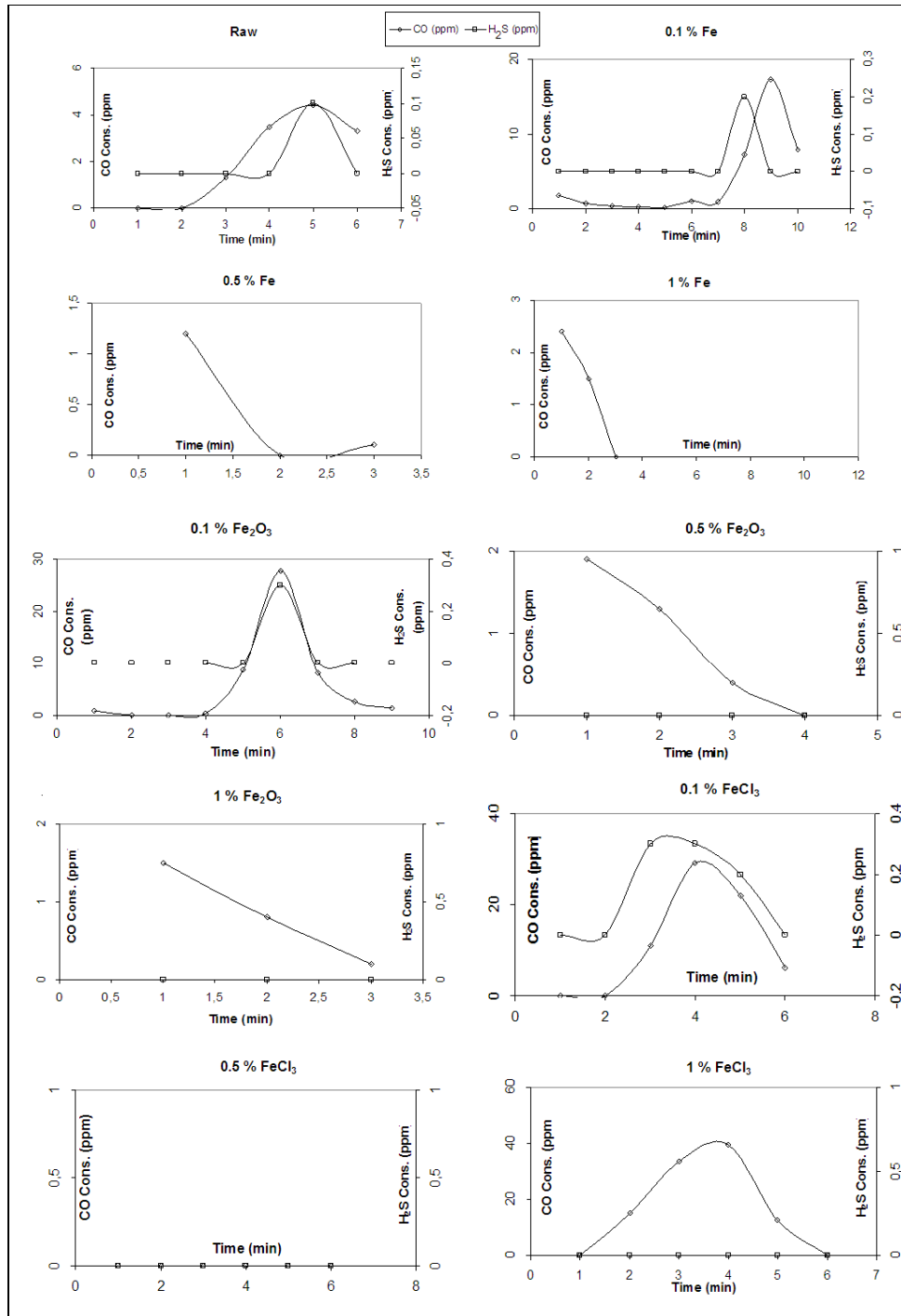


Figure B 6 Gas emissions for Hatıldağ oil shale after electromagnetic heating

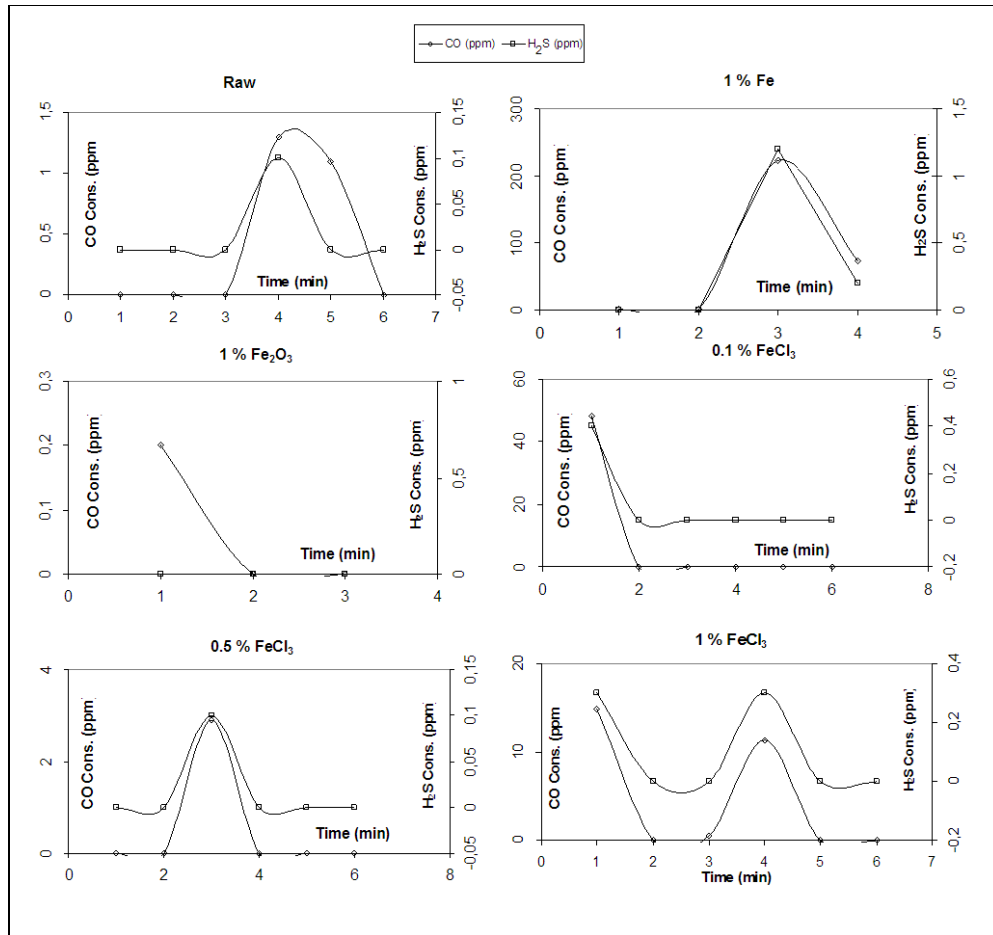


Figure B 7 Gas emissions for Seyitömer oil shale after electromagnetic heating

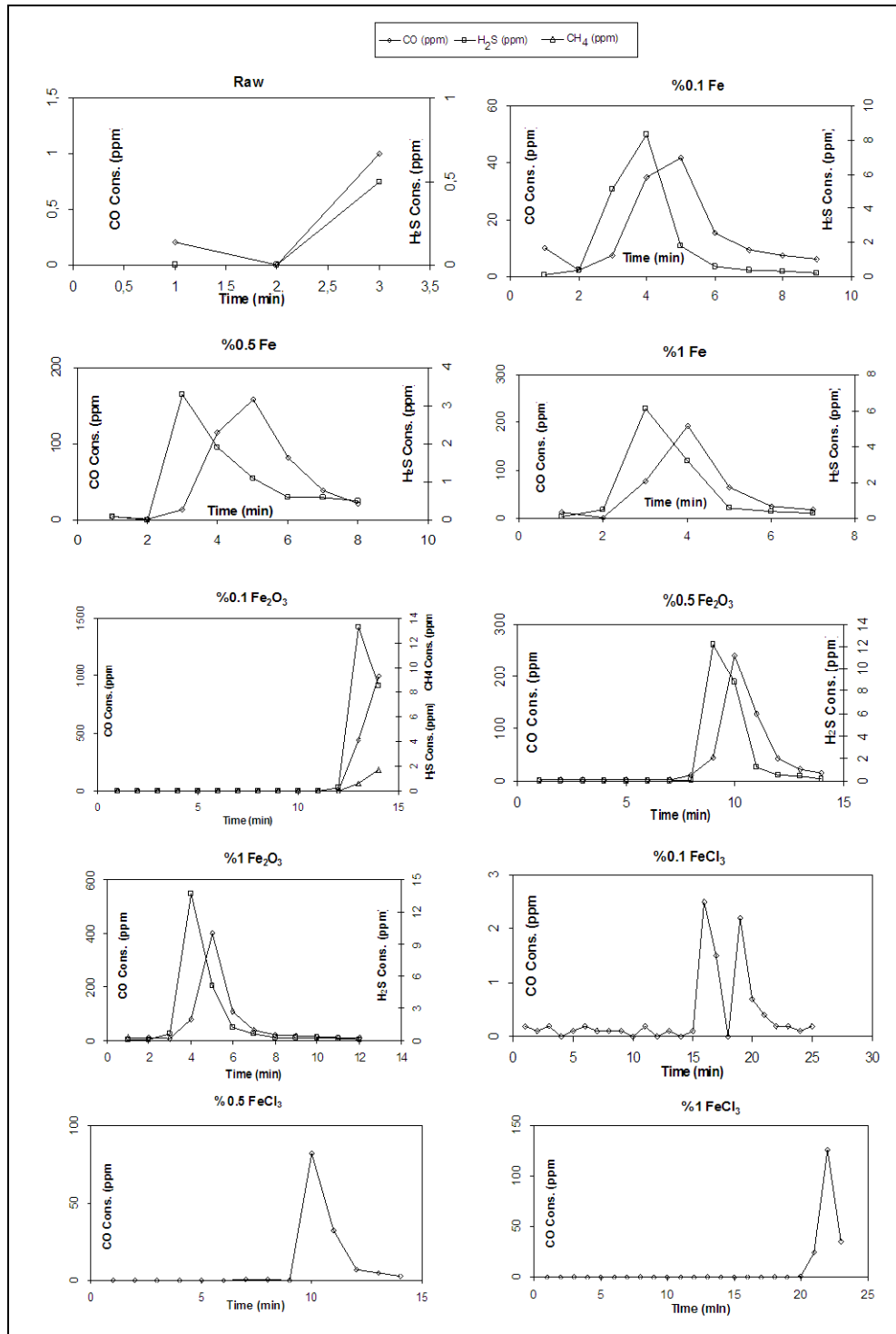


Figure B 8 Gas emissions for Ulukışla oil shale after electromagnetic heating

B.3. Temperature Distribution of Retort Experiments

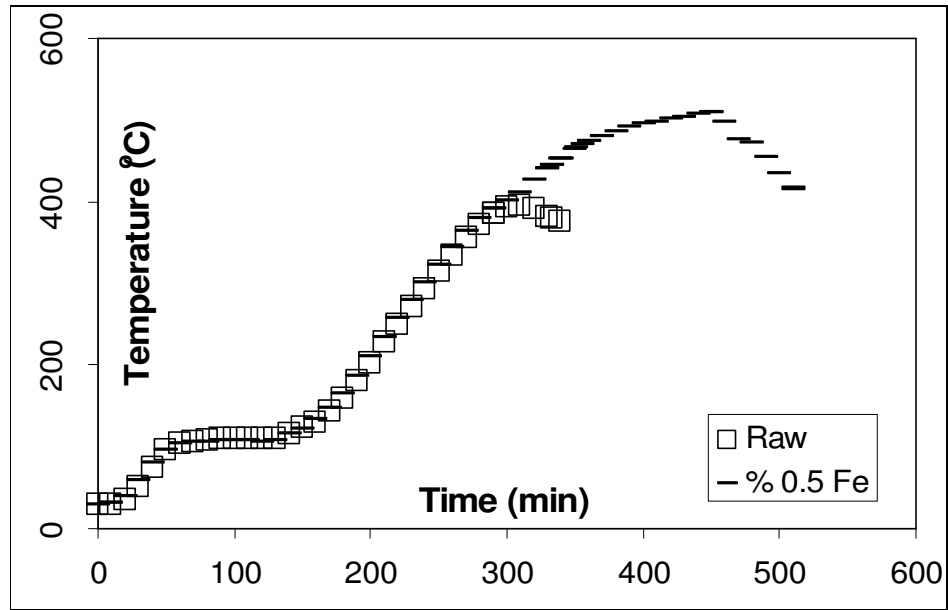


Figure B 9 Temperature distribution for Himmetoğlu oil shale

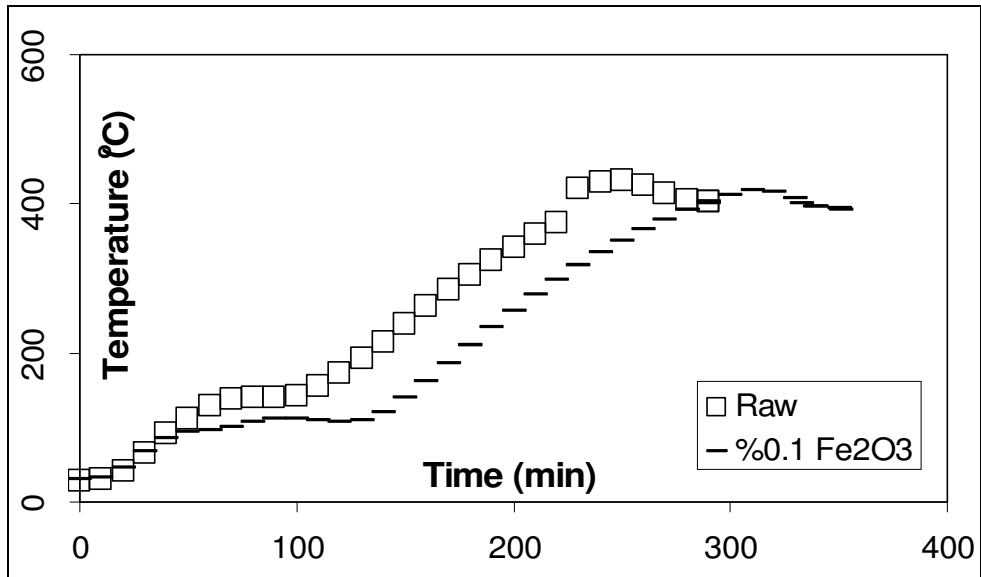


Figure B 10 Temperature distribution for Hatıldağ oil shale

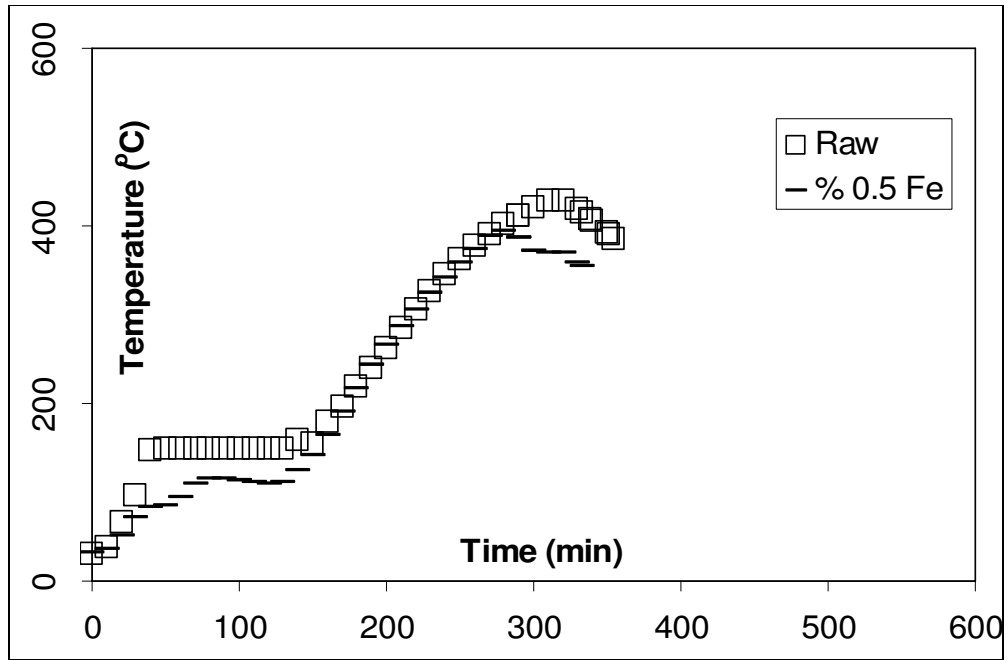


Figure B 11 Temperature distribution for Seyitömer oil shale

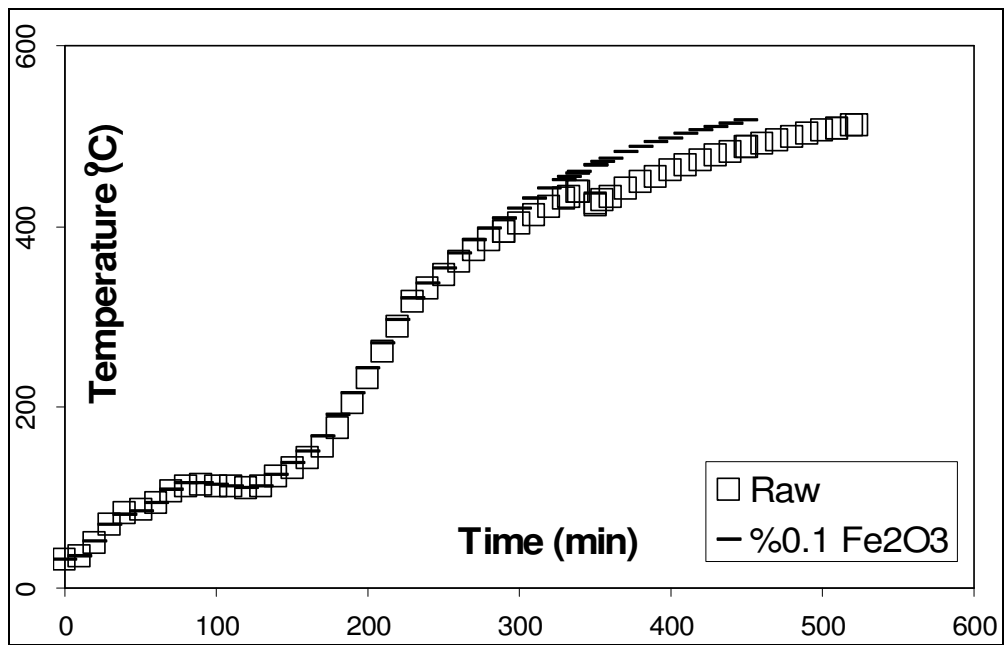


Figure B 12 Temperature distribution for Niğde-Ulukışla oil shale

B.4. Gas Emissions of Retort Experiments

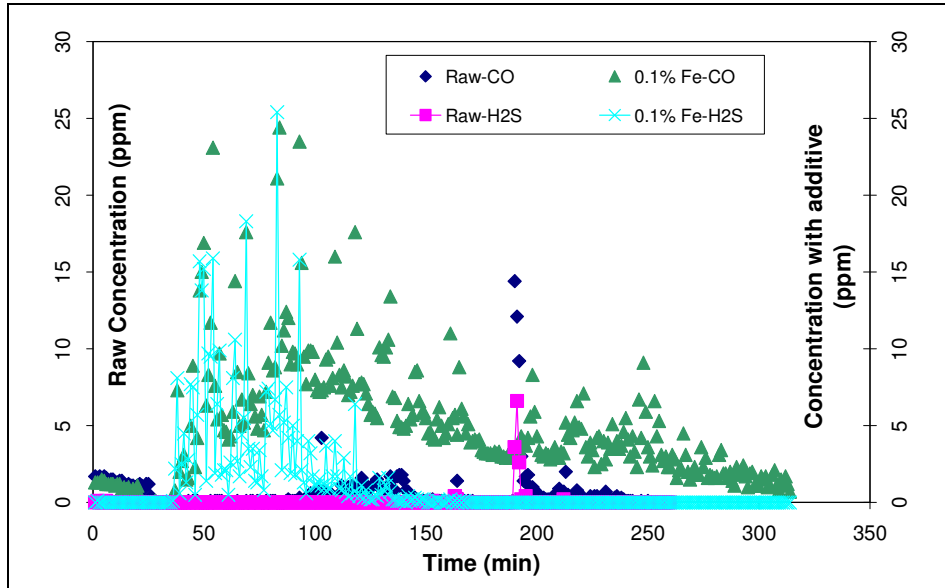


Figure B 13 Gas emissions for Himmetoğlu oil shale

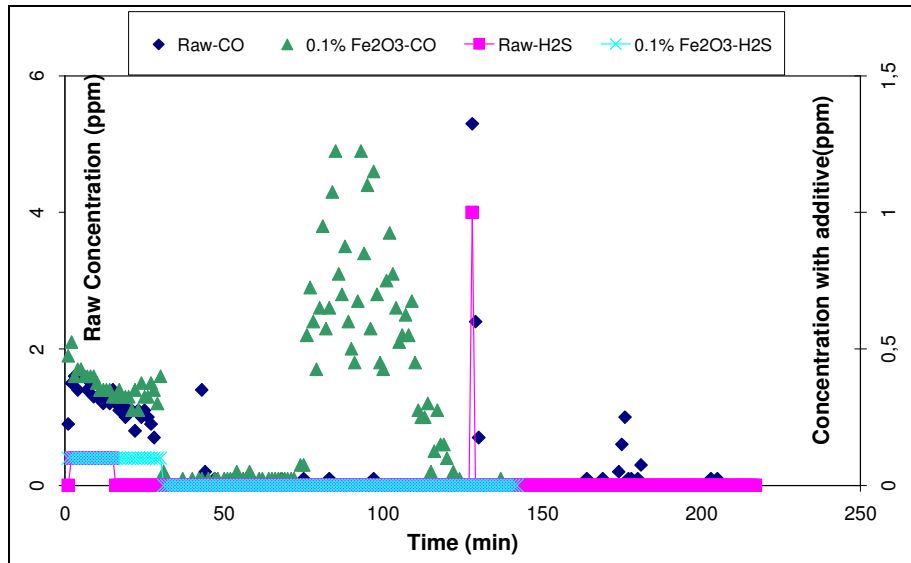


Figure B 14 Gas emissions for Hatıldağ oil shale

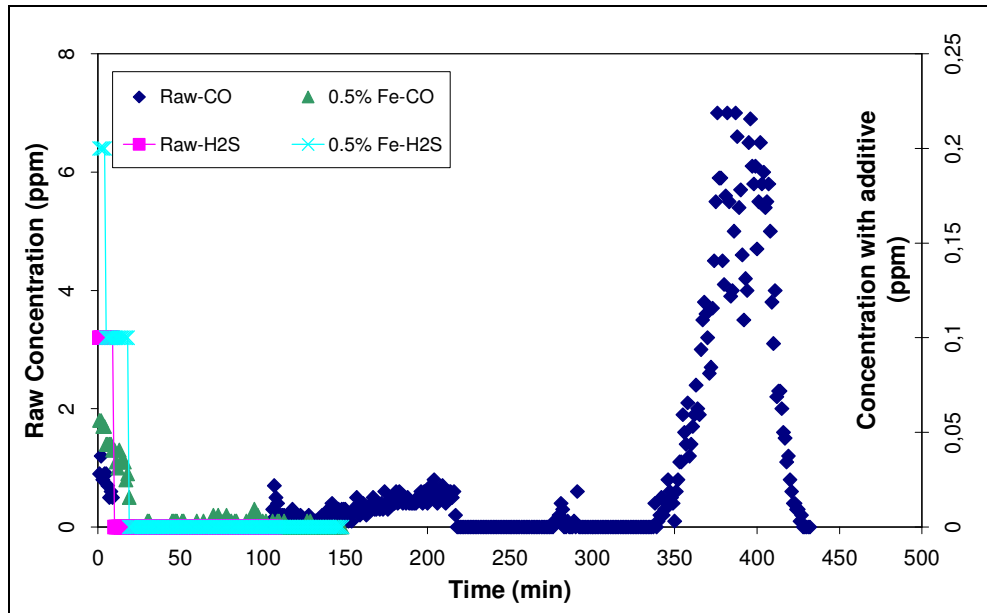


Figure B 15 Gas emissions for Seyitömer oil shale

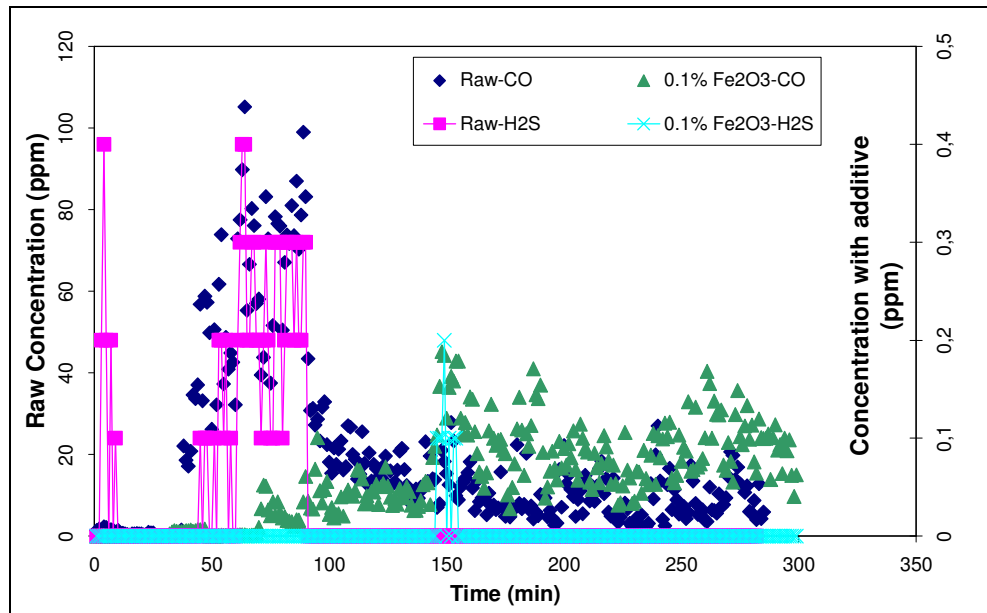


Figure B 16 Gas emissions for Ulukışla oil shale

## APPENDIX C

### NUMERICAL SIMULATIONS

#### C.1. Temperature Distributions of Oil Shale Samples

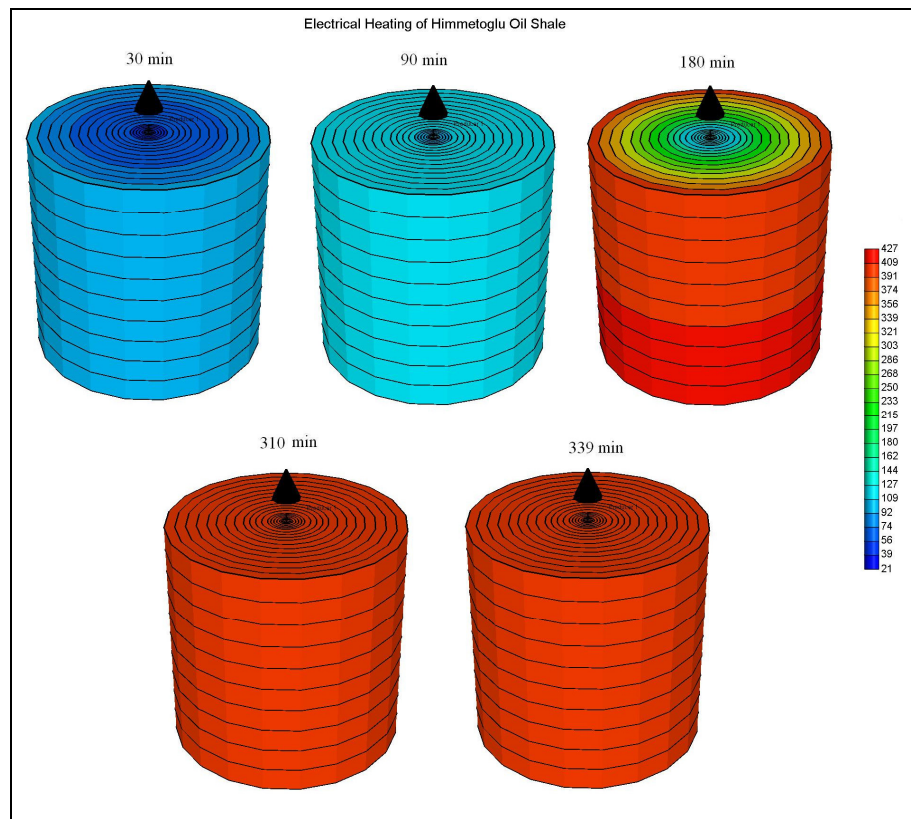


Figure C 1 Temperature distribution for Himmetoglu oil shale

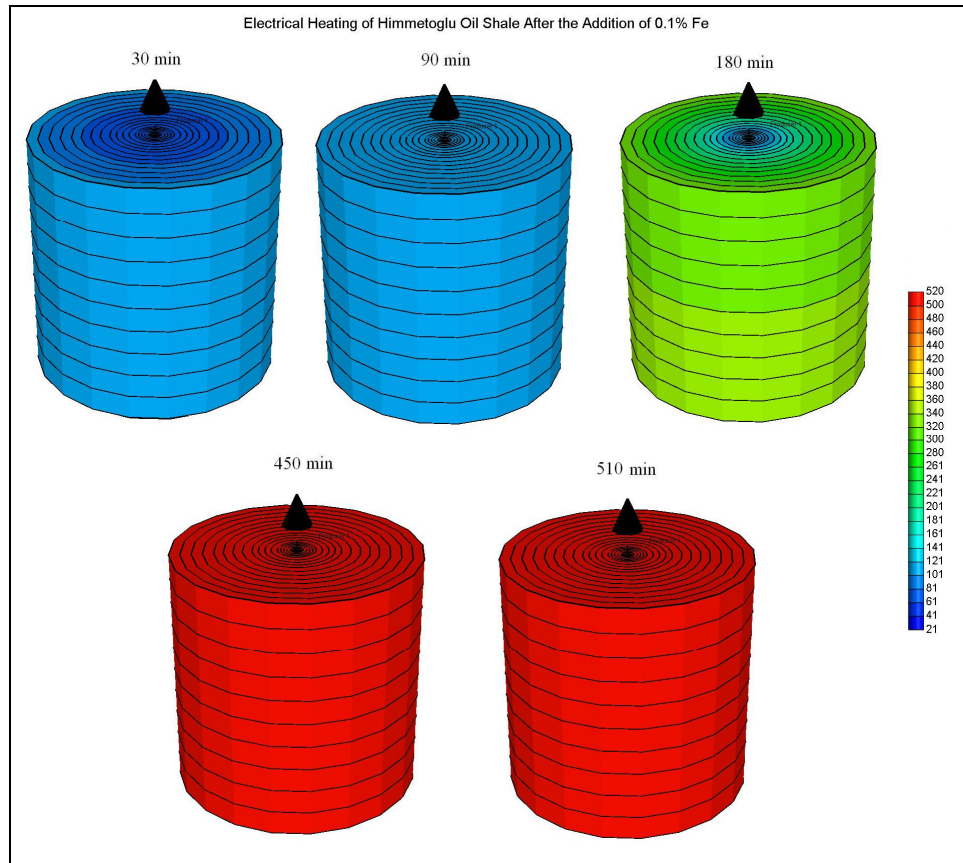


Figure C 2 Temperature distribution for Himmetoglu oil shale + 0.1% Fe

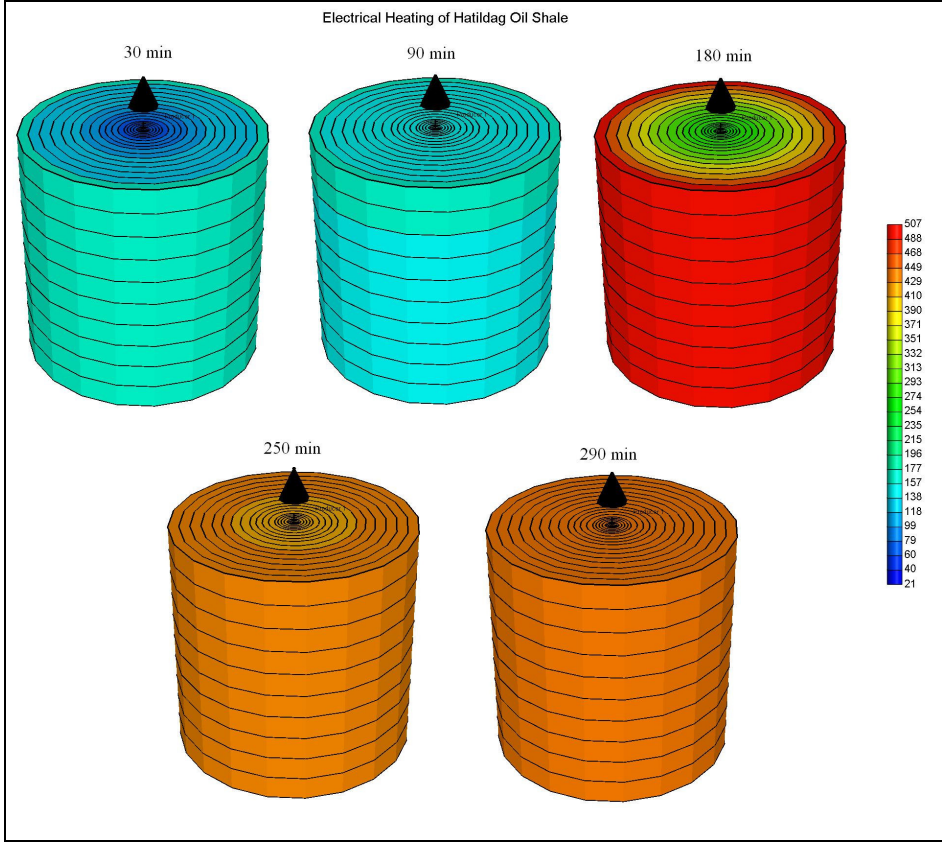


Figure C 3 Temperature distribution for Hatıldağ oil shale

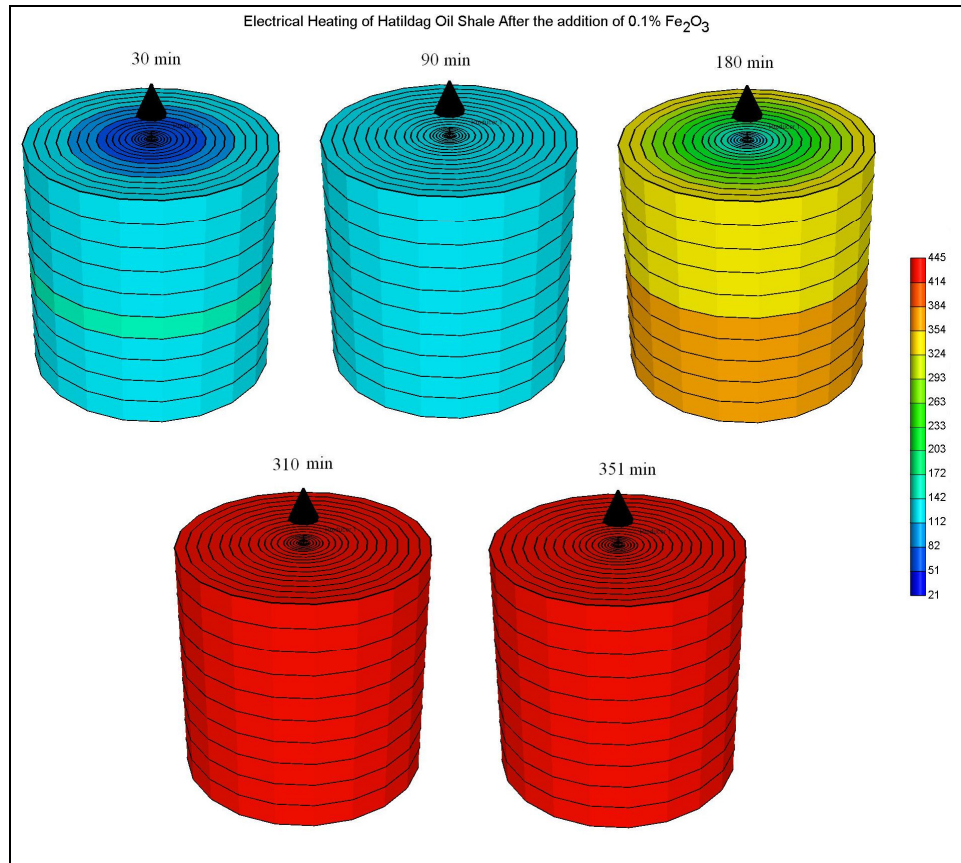


Figure C 4 Temperature distribution for Hatıldağ oil shale + 0.1 %  $\text{Fe}_2\text{O}_3$

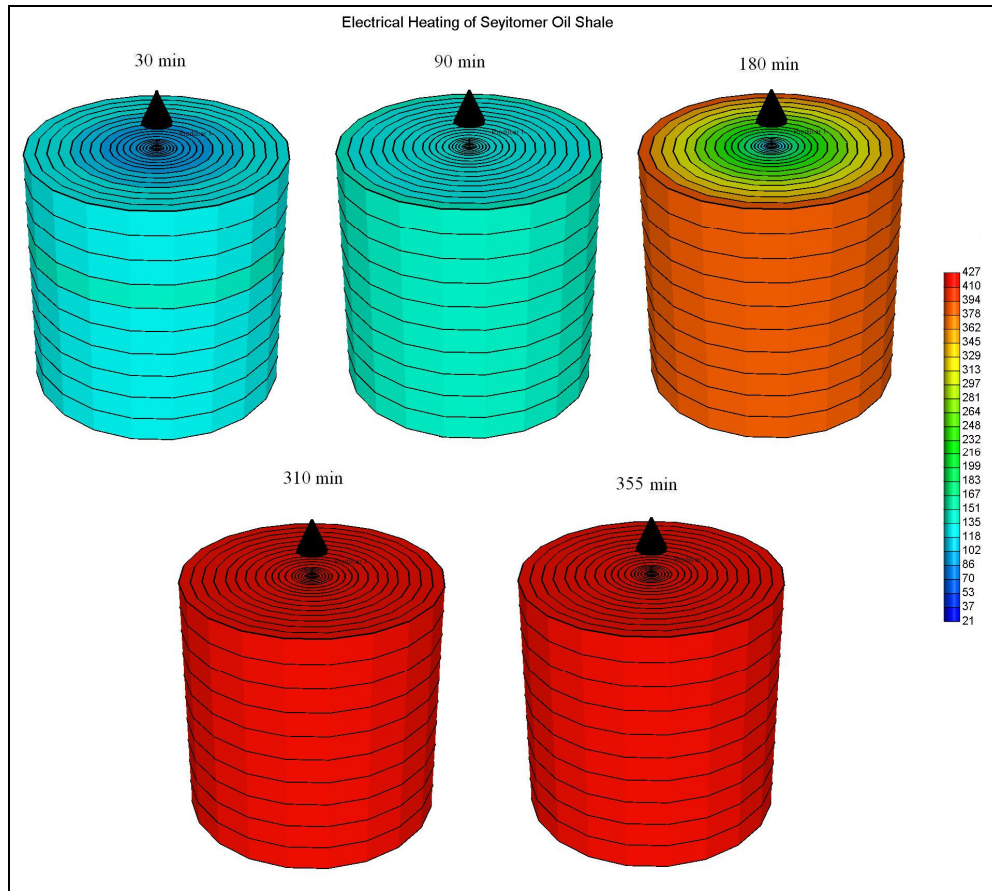


Figure C 5 Temperature distribution for Seyitömer oil shale

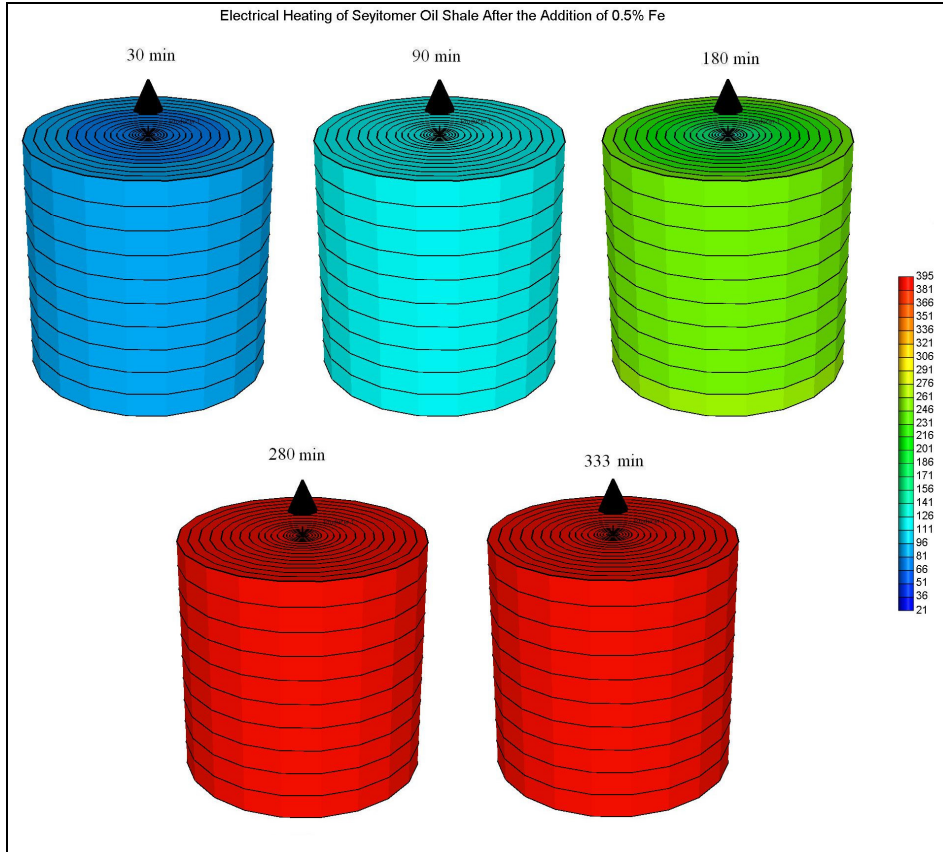


Figure C 6 Temperature distribution for Seyitömer oil shale +0.5 % Fe

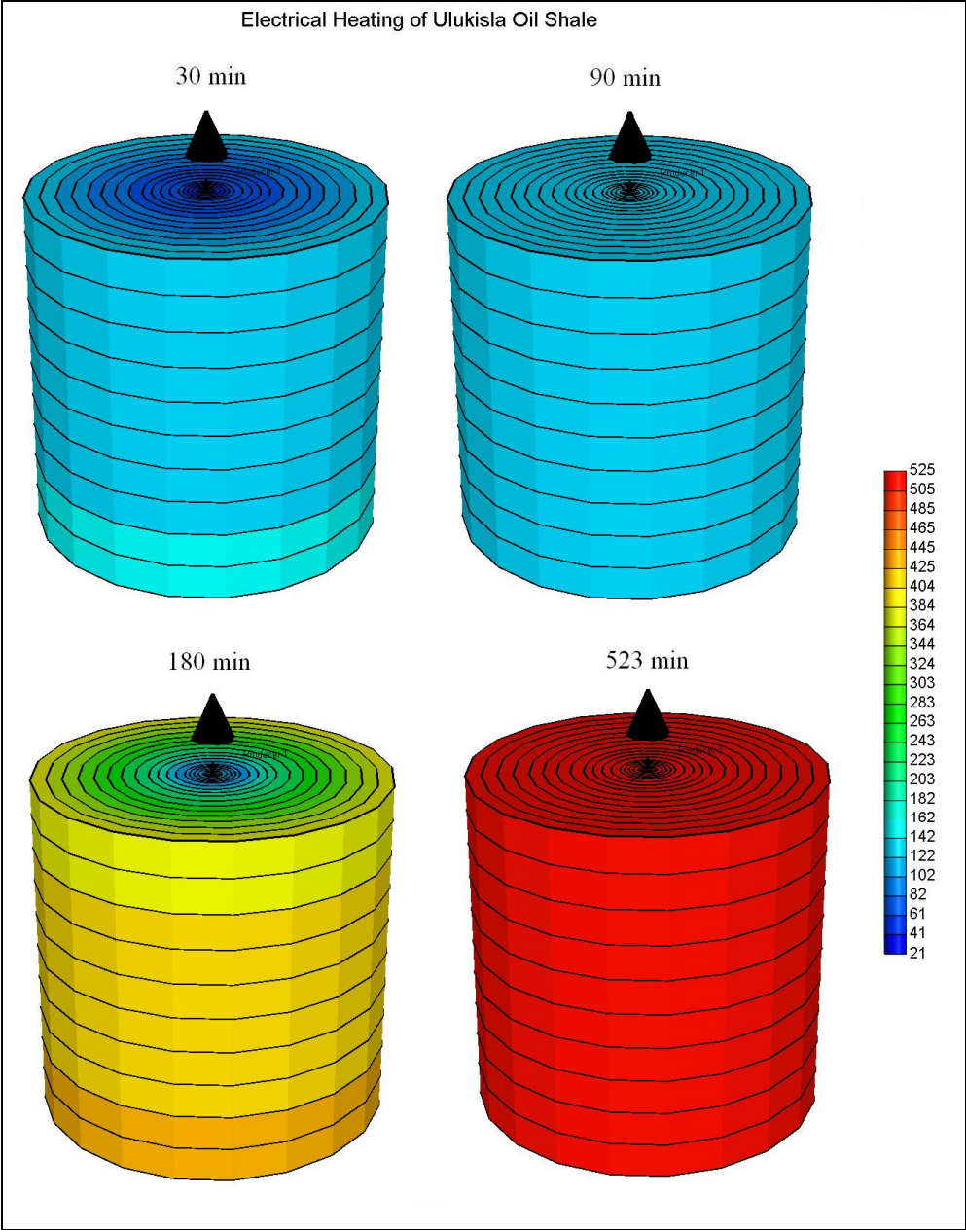


Figure C 7 Temperature distribution for Niğde-Ulukışla oil shale

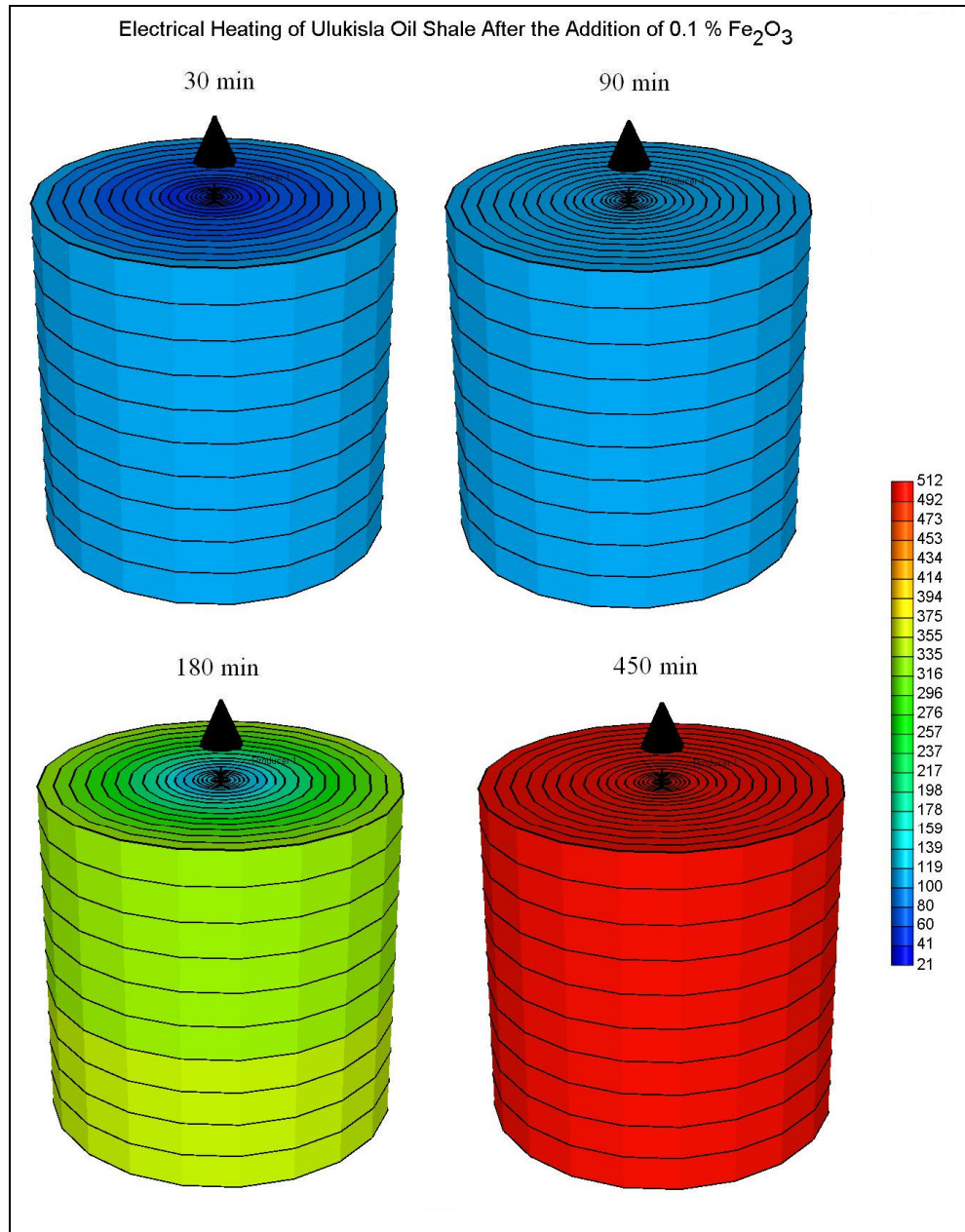


Figure C 8 Temperature distribution for Seyitömer oil shale + 0.1 %  $\text{Fe}_2\text{O}_3$

## **APPENDIX D**

### **ANALYTICAL MODEL**

#### **D.1. Crude Oil Samples**

##### **D.1.1. Batı Raman Crude oil**

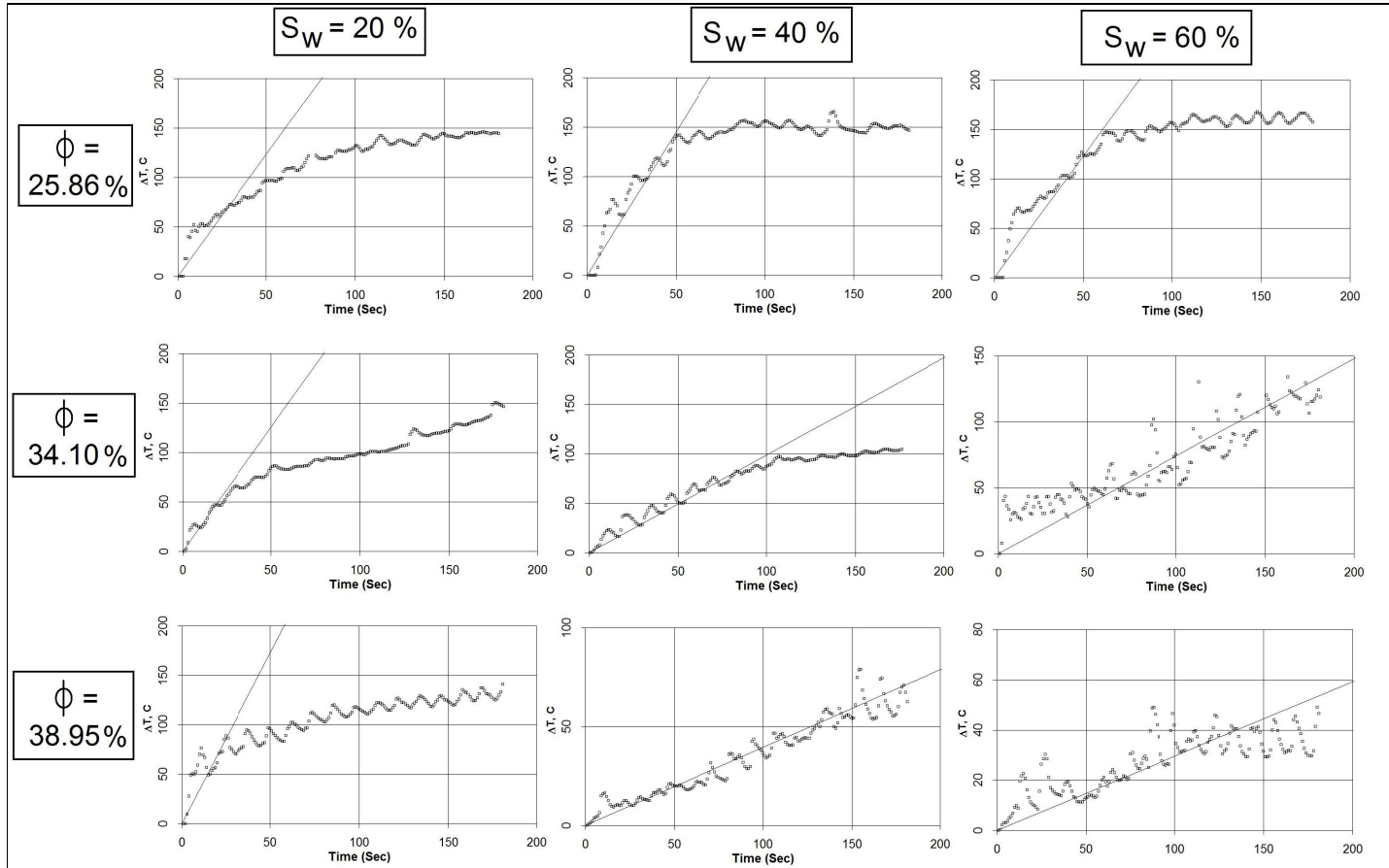


Figure D 1 Analytical modeling results for water wet condition

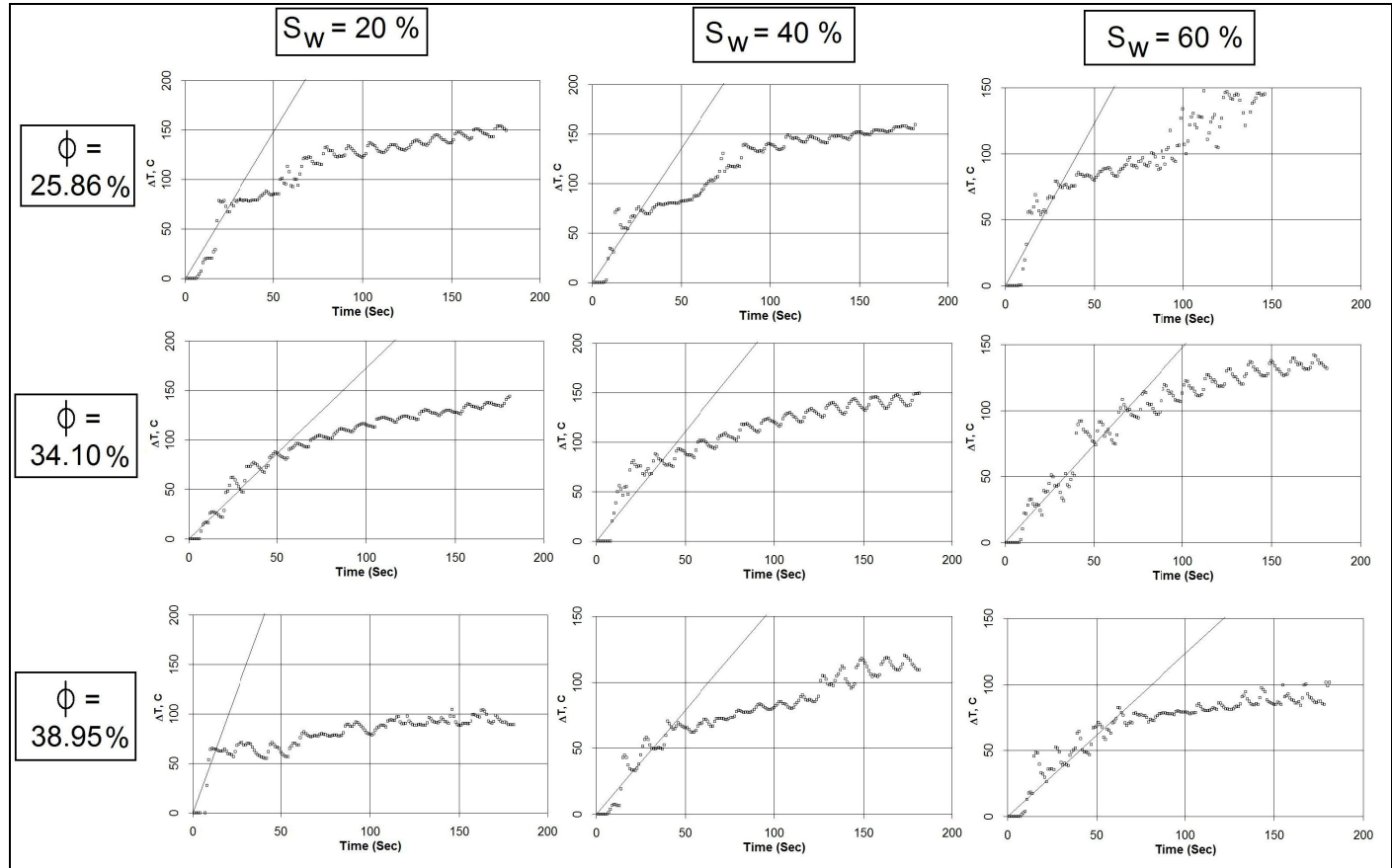


Figure D 2 Analytical modeling results for oil wet condition

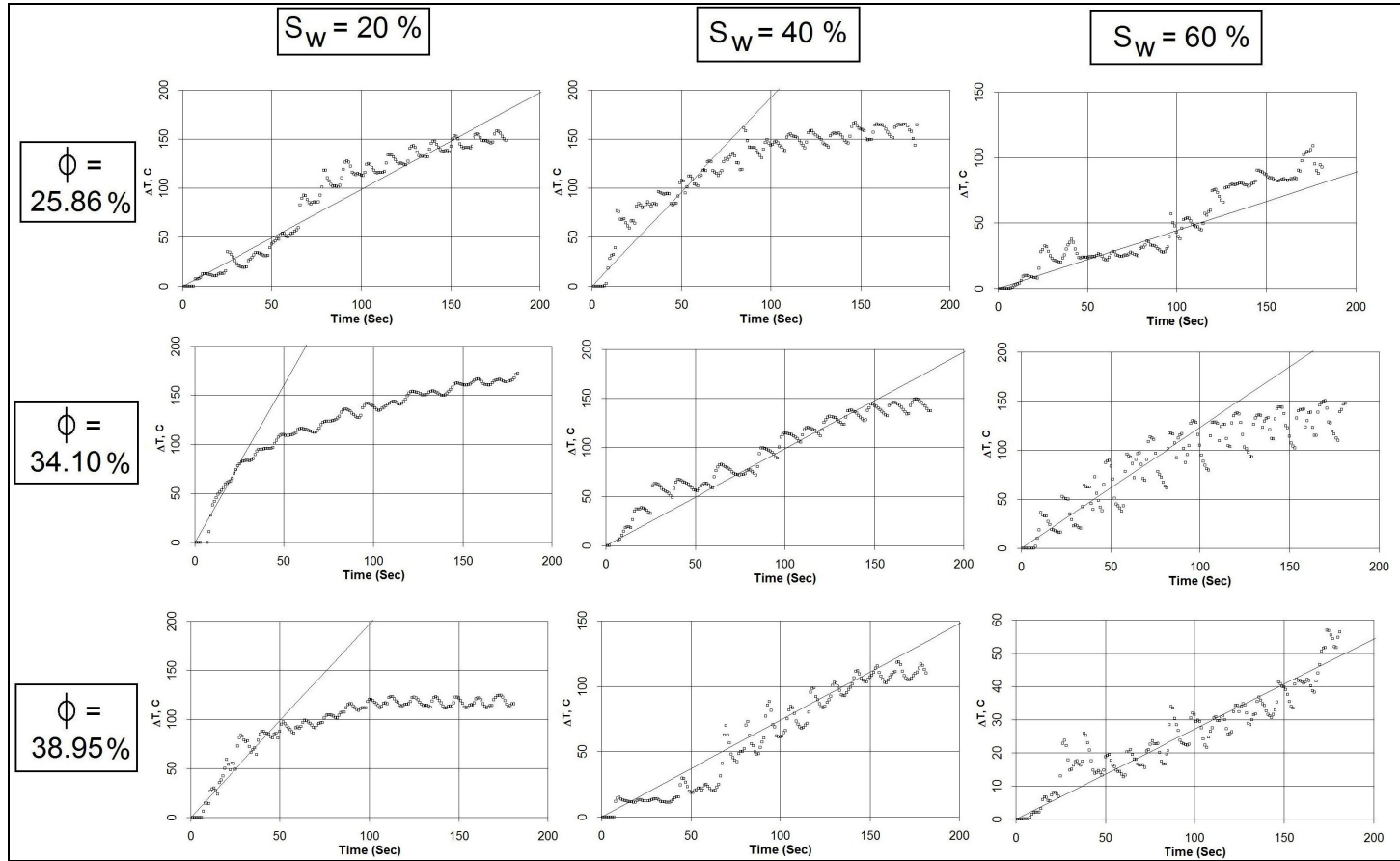


Figure D 3 Analytical modeling results for mixed wet condition

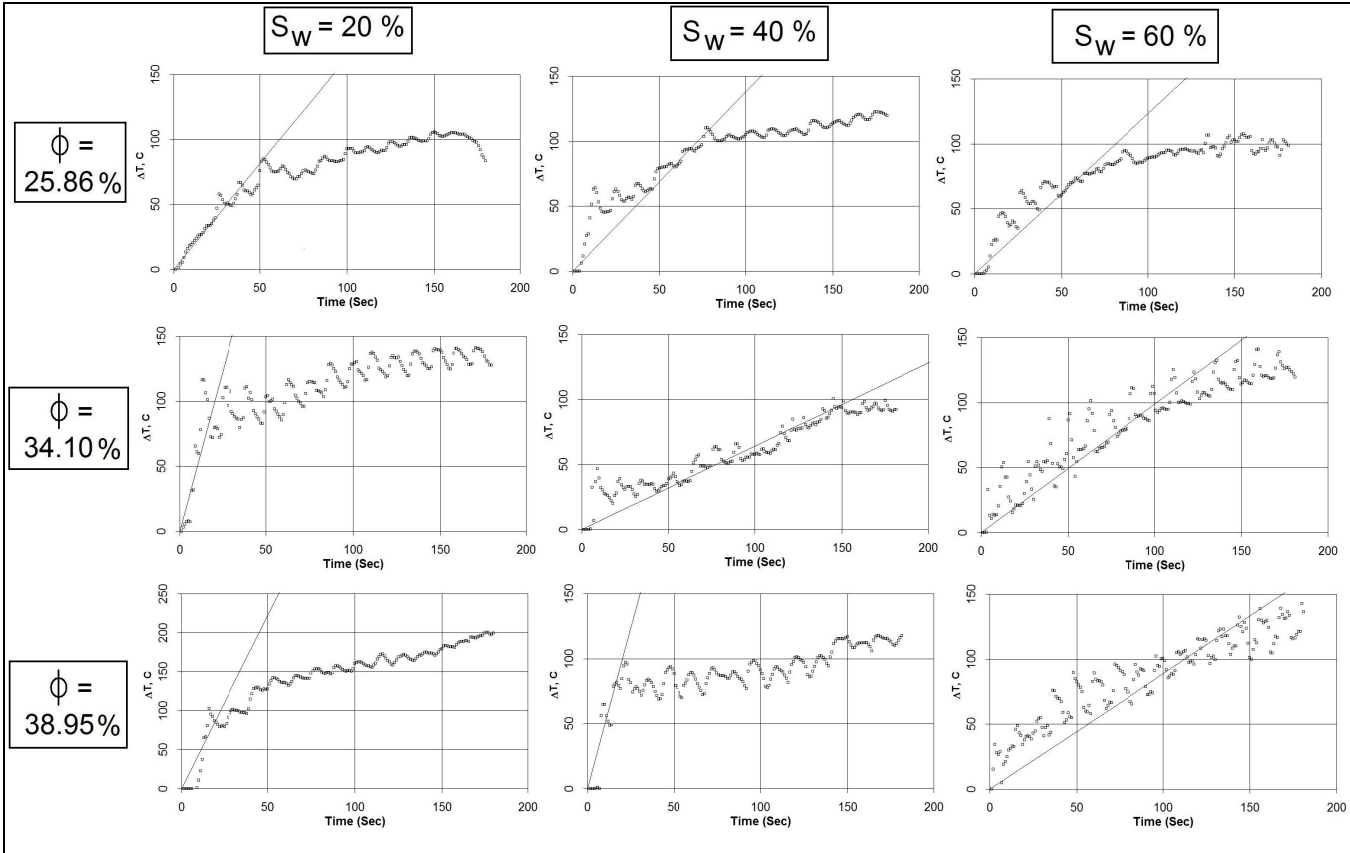


Figure D 4 Analytical modeling results for water wet condition

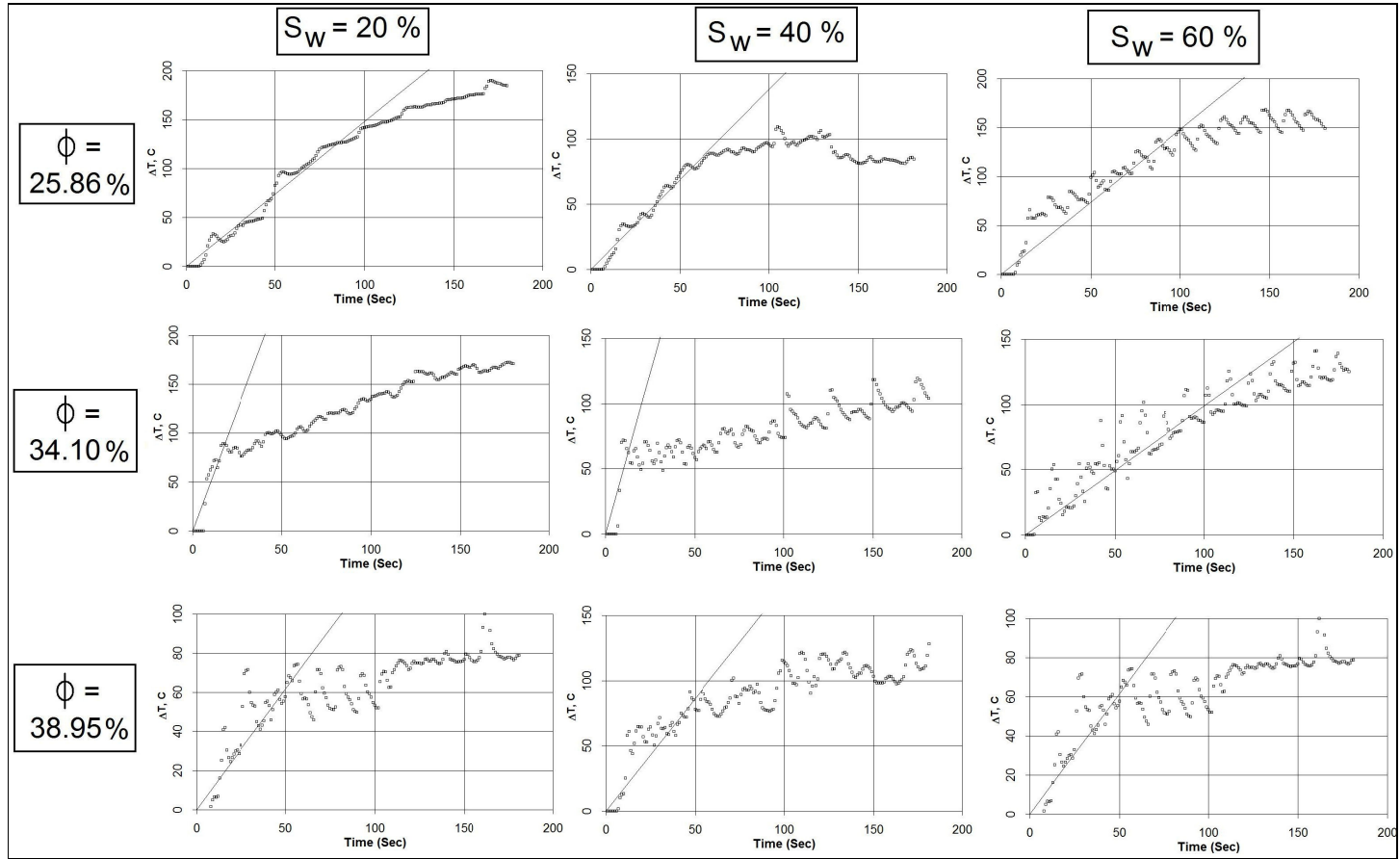


Figure D 5 Analytical modeling results for oil wet condition

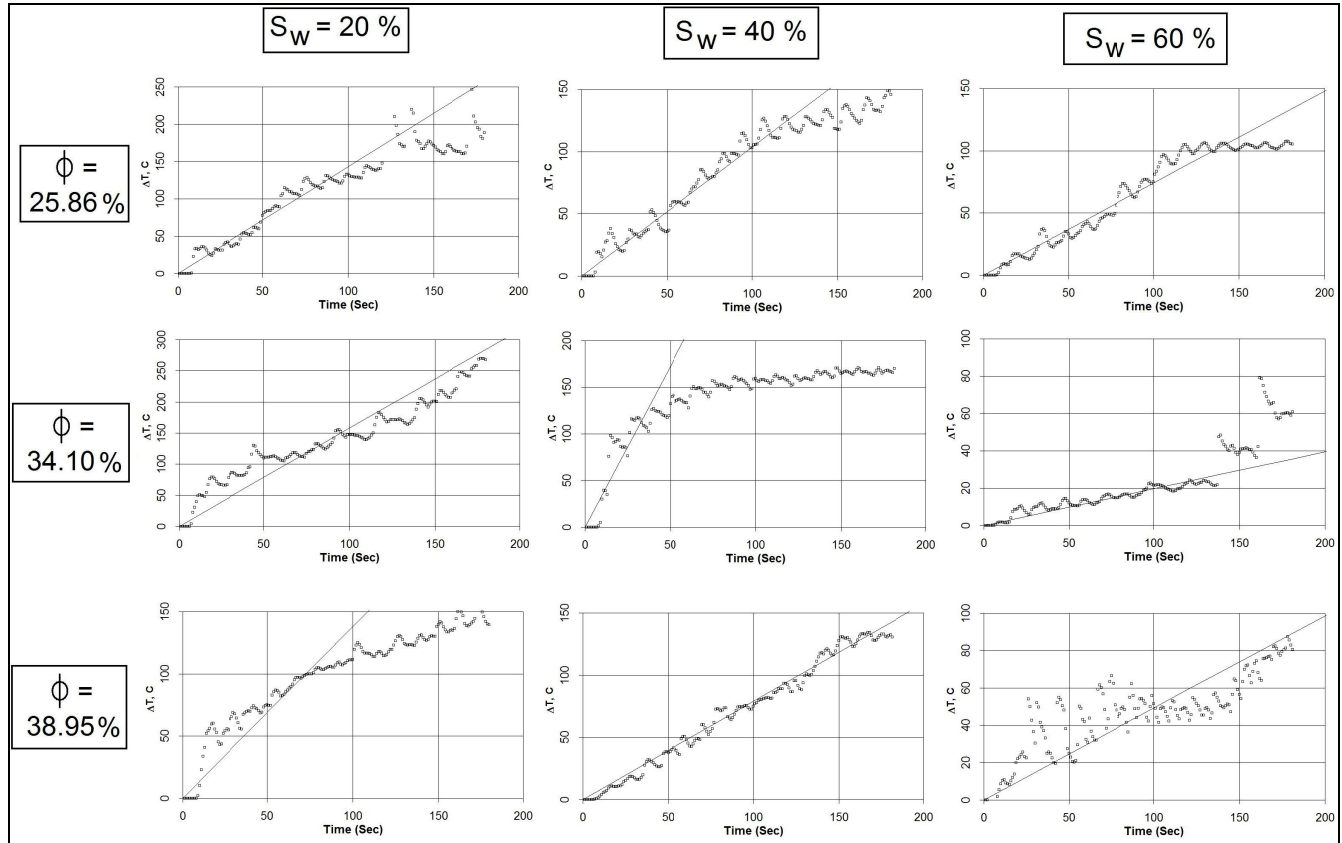


Figure D 6 Analytical modeling results for mixed wet condition

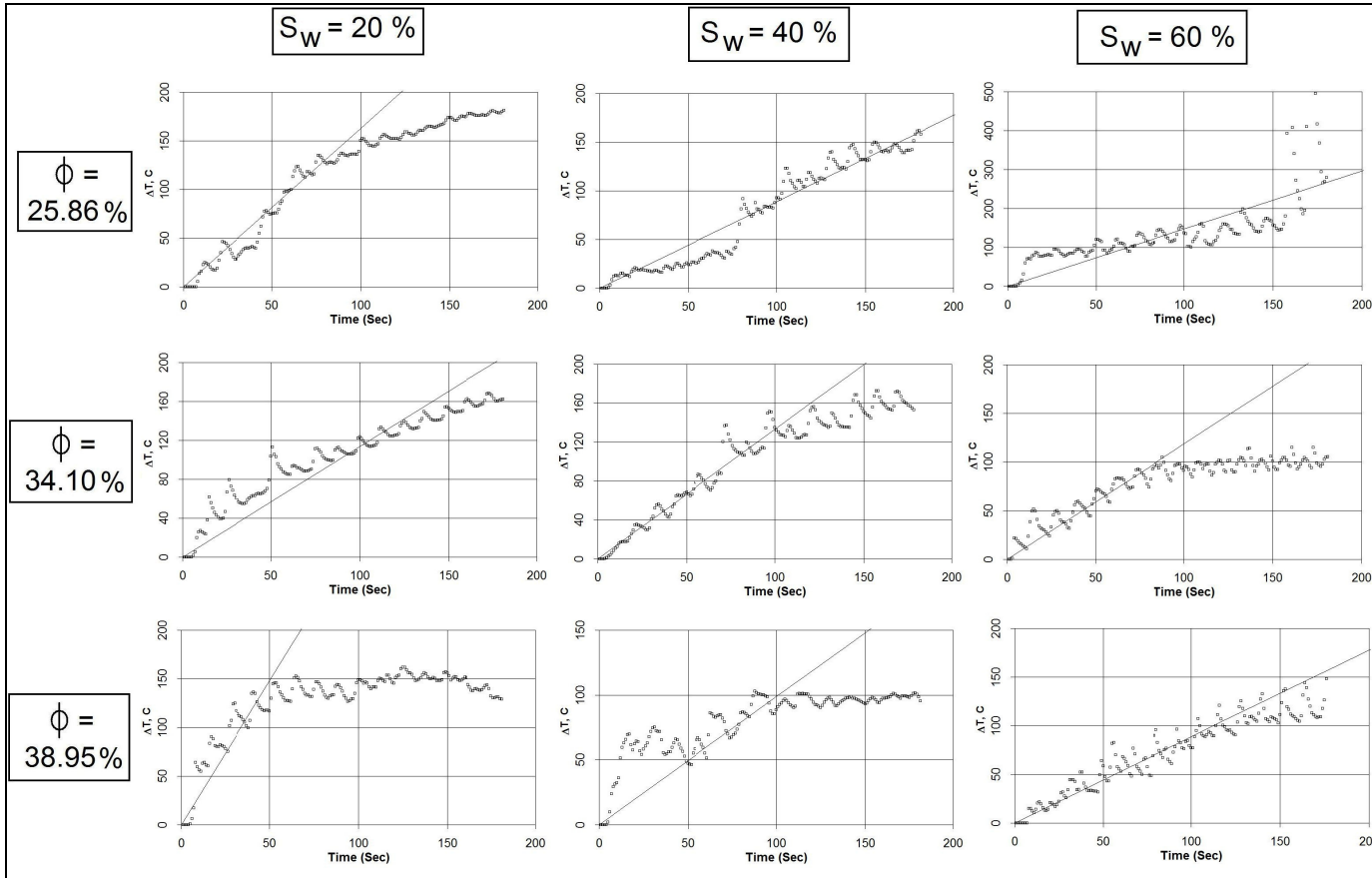


Figure D 8 Analytical modeling results for water wet condition

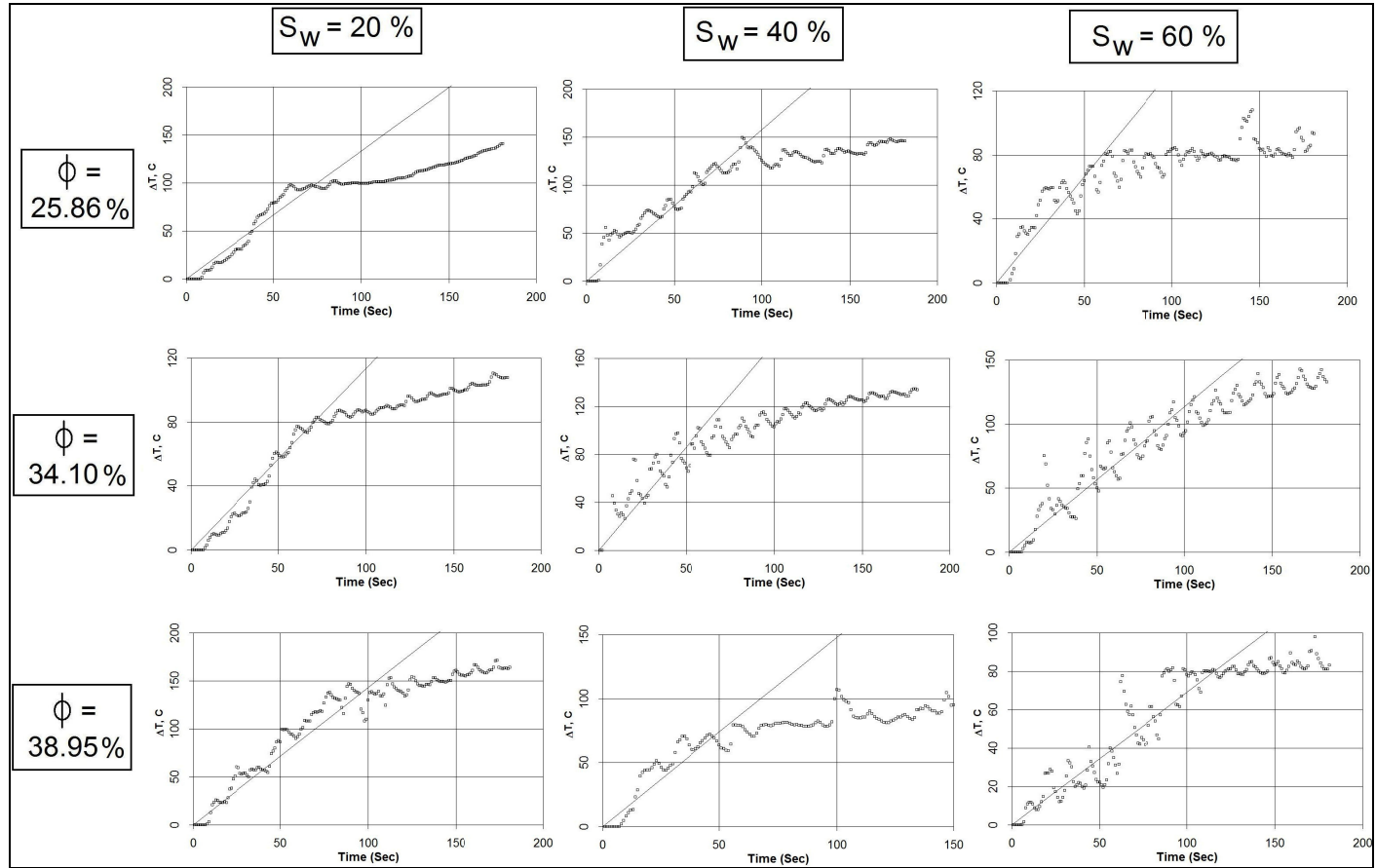


Figure D 9 Analytical modeling results for oil wet condition

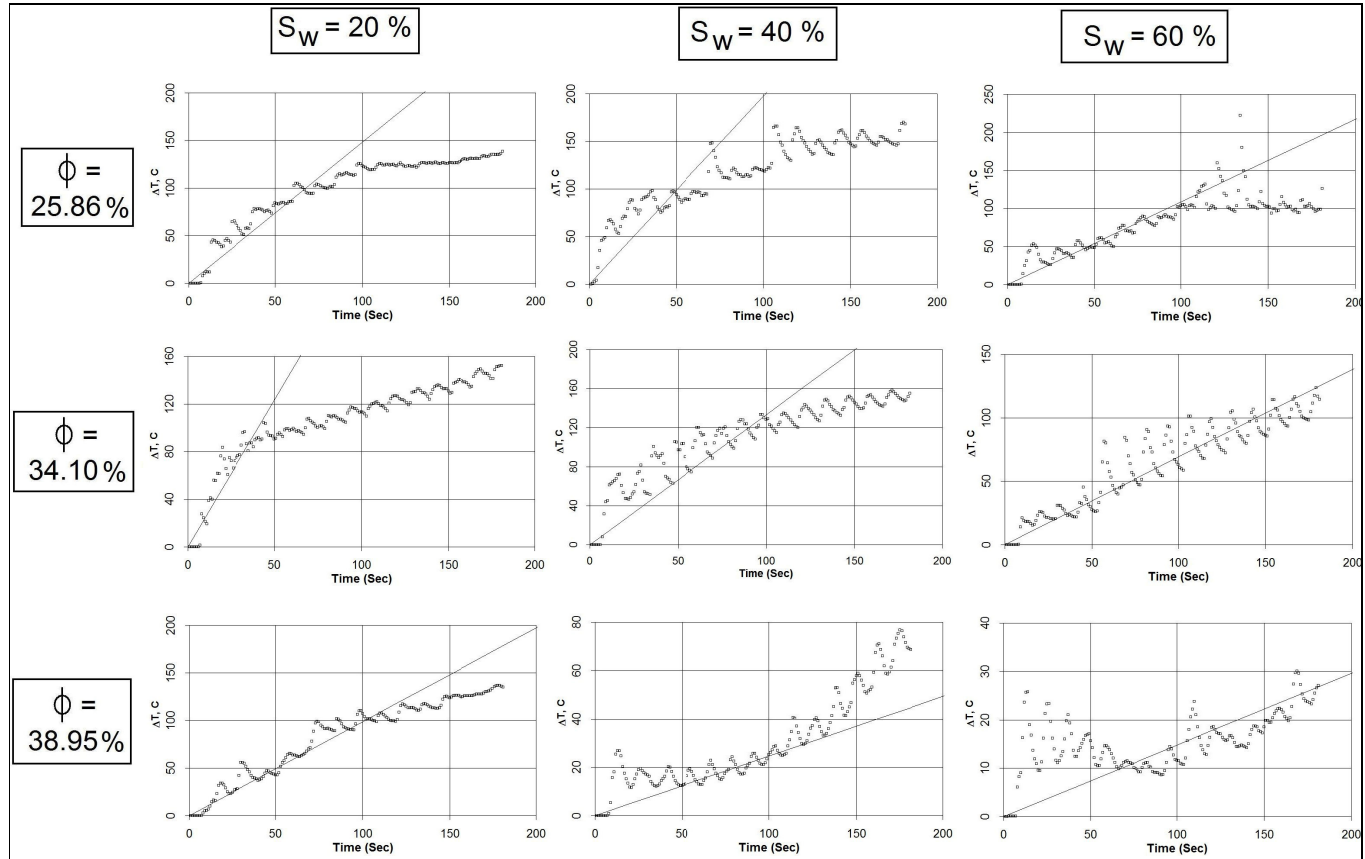


Figure D 10 Analytical modeling results for mixed wet condition

## D.2. Oil Shale Samples

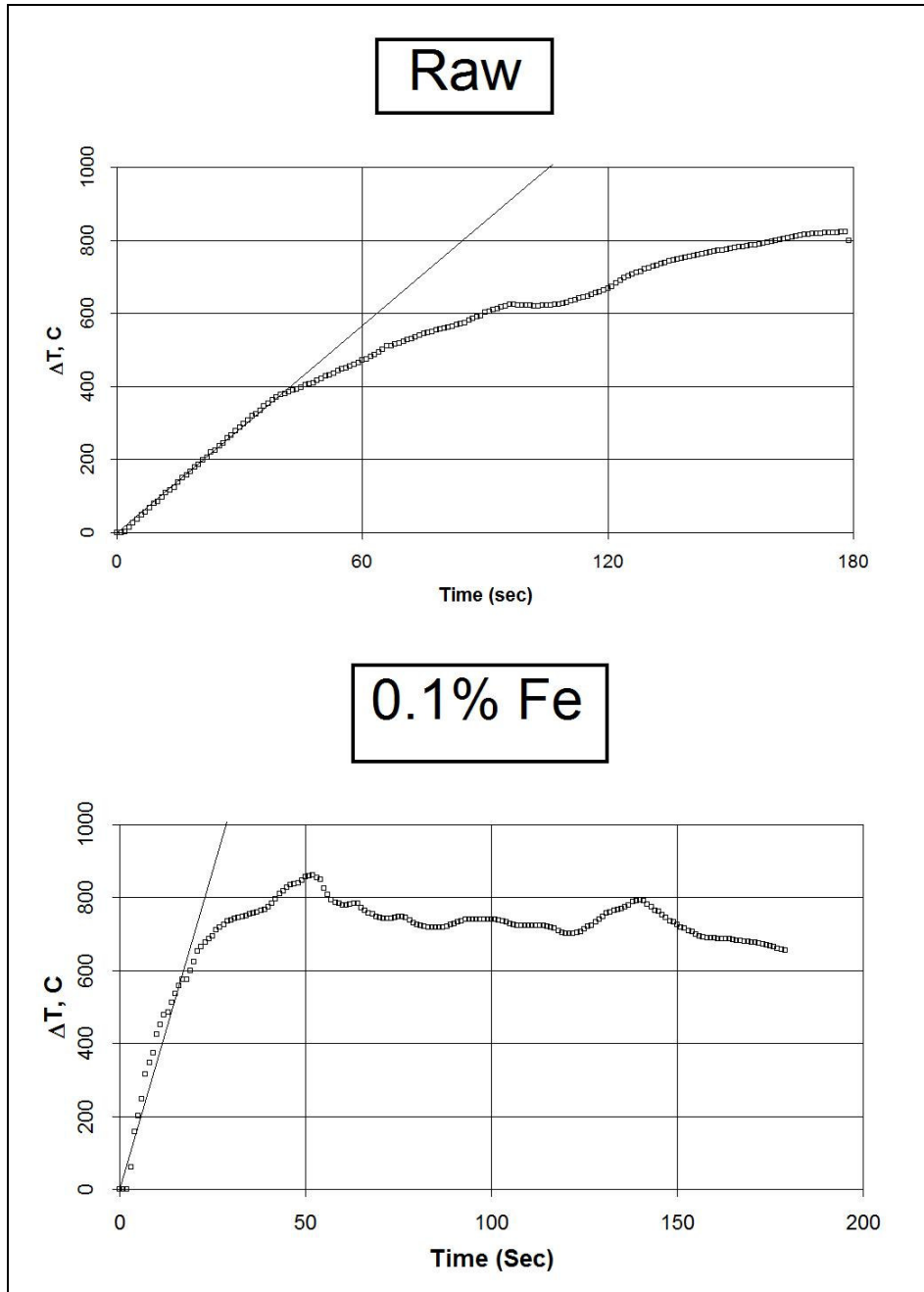


Figure D 11 Analytical modeling results for Himmetoğlu oil shale

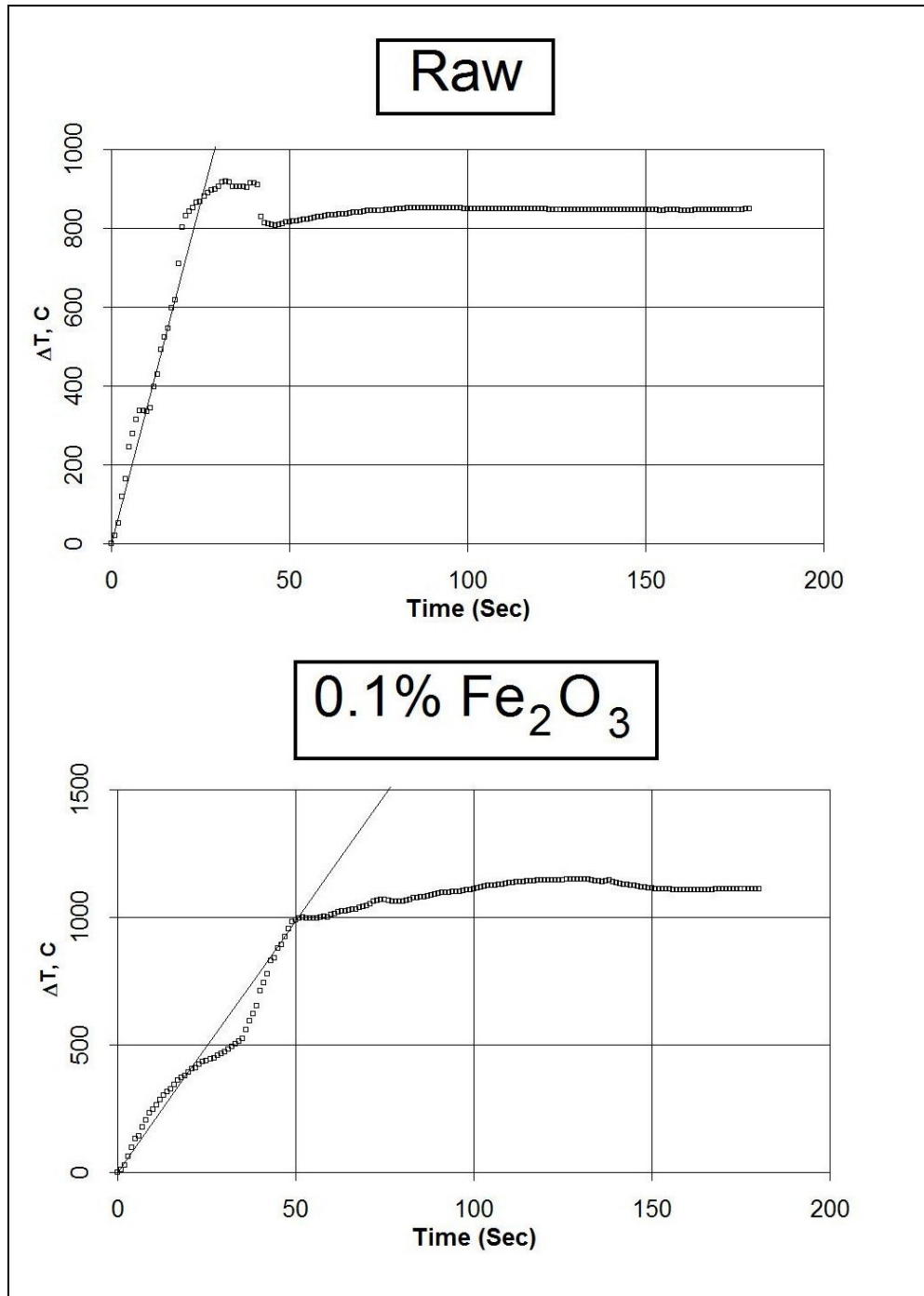


Figure D 12 Analytical modeling results for Hatıldağ oil shale

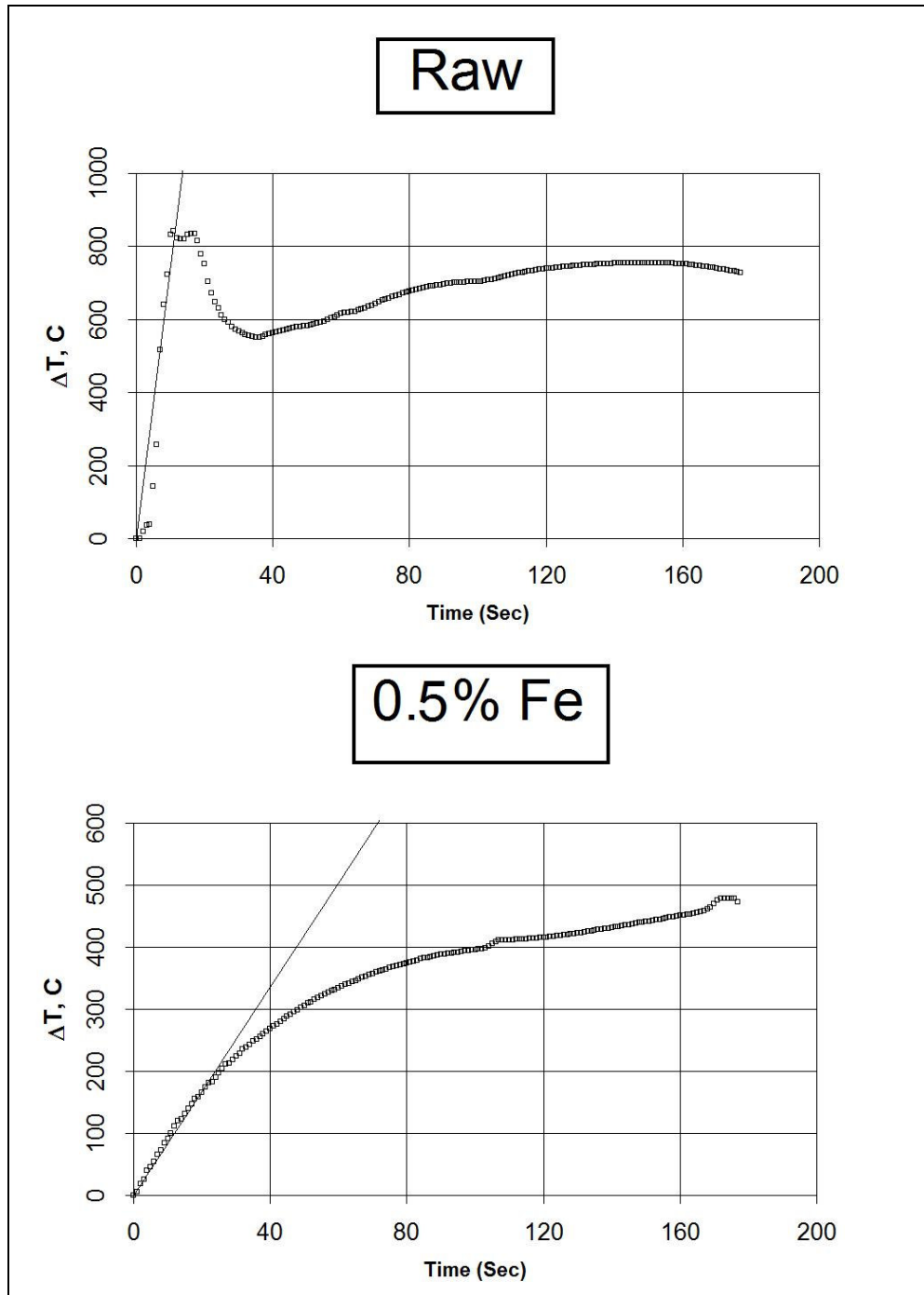


Figure D 13 Analytical modeling results for Seyitömeroil shale

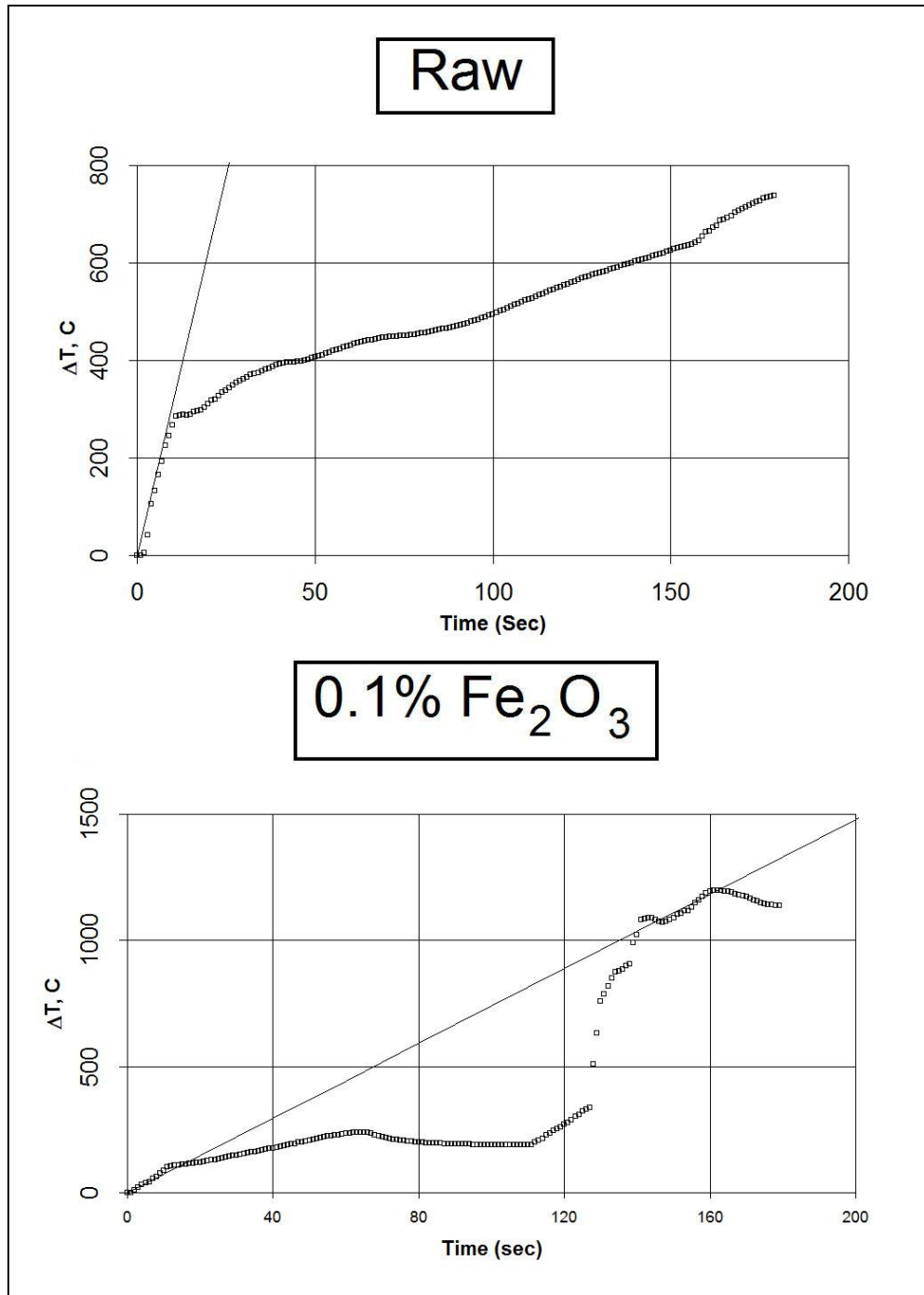


Figure D 14 Analytical modeling results for Ulukışla oil shale

## APPENDIX D

### ECONOMIC EVALUATION OF THE STUDY

Table E 1 Economic evaluation of microwave heating for water wet condition

Sample	Water Content (%)	Porosity (%)	Energy Consumed, kWh/kg	Cost of oil, \$/bbl		
				Morning	Prime Time	Night
Bati Raman	60	38,95%	15	186	326	99
		34,10%	54	659	1154	350
		25,86%	10	125	218	66
	40	38,95%	51	620	1086	330
		34,10%	39	474	830	252
		25,86%	12	149	262	79
	20	38,95%	141	1709	2992	909
		34,10%	50	610	1067	324
		25,86%	15	183	321	98
Çamurlu	60	38,95%	176	2182	3821	1161
		34,10%	192	2378	4164	1265
		25,86%	28	341	597	181
	40	38,95%	45	550	964	293
		34,10%	118	1457	2551	775
		25,86%	11	133	233	71
	20	38,95%	38	466	817	248
		34,10%	128	1581	2768	841
		25,86%	21	259	453	138
Garzan	60	38,95%	19	242	424	129
		34,10%	211	2722	4766	1448
		25,86%	11	137	240	73
	40	38,95%	12	160	281	85
		34,10%	60	770	1348	410
		25,86%	5	64	112	34
	20	38,95%	12	148	259	79
		34,10%	409	5271	9229	2804
		25,86%	6	78	136	41

Table E 2 Economic Evaluation of microwave heating

Sample	Porosity (%)	Sw (%)	Cost of oil \$/bbl		
			Water Wet	Oil Wet	Mixed Wet
Bati Raman	38,95%	60	225	304	100
	34,10%	60	976	832	353
	25,86%	60	293	183	67
	38,95%	40	366	211	332
	34,10%	40	366	732	254
	25,86%	40	92	225	80
	38,95%	20	169	225	915
	34,10%	20	586	473	327
	25,86%	20	87	140	98
Çamurlu	38,95%	60	221	146	1129
	34,10%	60	1439	959	1230
	25,86%	60	192	127	176
	38,95%	40	122	141	285
	34,10%	40	480	521	753
	25,86%	40	72	152	69
	38,95%	20	78	80	241
	34,10%	20	2878	157	818
	25,86%	20	65	56	134
Garzan	38,95%	60	67	44	110
	34,10%	60	874	771	1231
	25,86%	60	67	47	62
	38,95%	40	62	87	73
	34,10%	40	403	749	348
	25,86%	40	36	31	29
	38,95%	20	51	46	67
	34,10%	20	375	125	2384
	25,86%	20	27	27	35

## CURRICULUM VITAE

### PERSONAL INFORMATION

Surname, Name: Hasçakır, Berna  
Nationality: Turkish (TC)  
Date and Place of Birth: 14 October 1978, İzmir  
Phone: +90 312 210 48 84  
Fax: +90 312 210 48 83  
E-mail: hascakir@metu.edu.tr

### EDUCATION

Degree	Institution	Year of Graduation
Ph. D.	METU Petroleum and Natural Gas Engineering	2008
M. Sc.	DEU Environmental Engineering	2003
B. Sc.	DEU Environmental Engineering	2001
High School	Şirinyer Lisesi, İzmir	1996

### WORK EXPERIENCE

Year	Place	Enrollment
Feb-Aug 2003	Harmandali Waste Disposal Site, İzmir/TURKEY	Environmental Engineer
2001-2003	Center for Environmental Research and Development, (ÇEVMER), İzmir/TURKEY	Project Assistant
2002-2003	Mimar Kemalettin Elementary School, İzmir/TURKEY	Computer Instructor
2001-2002 2000, July	Altın Computer Course, İzmir/TURKEY Ministry of Environment Antalya Head Office /TURKEY	Computer Instructor Internship

### MEMBERSHIPS

2004- Petroleum Engineering Association  
2002- Chamber of Environmental Engineering  
2004- Society of Petroleum Engineers (SPE)  
2006- Clay Mineral Society

2005- Turkish National Committee of Clay Science

## **FOREIGN LANGUAGES**

Fluent English

## **PROFESSIONAL**

2004- 2008, Research Assistant;

Middle East Technical University (METU), Department of Petroleum and Natural Gas Engineering, Ankara, Turkey.

2007 September – 2008 March, Visiting Researcher;

University of Alberta, Department of Civil & Environmental Engineering, School of Mining and Petroleum Engineering, Edmonton, AB, Canada.

## **PUBLICATIONS**

### JOURNAL PAPER

1. Hascakir, B., Babadagli, T., and Akin, S., "Experimental and Numerical Simulation of Oil Recovery from Oil Shales by Electrical Heating", Energy and Fuel, Article in Press.

2. Hascakir, B., Dolgen, D., "Utilization of Clay Minerals in Wastewater Treatment: Organic Matter Removal with Kaolinite" Ecology, vol. 66-6, pp.47-54, 2008 (Turkish).

### CONFERENCE PAPER

3. Hascakir, B., Acar, C., Demiral, B., and Akin, S., "Microwave Assisted Gravity Drainage of Heavy Oils", International Petroleum Technology Conference held in Kuala Lumpur, Malaysia, 3–5 December 2008.

4. Hascakir, B., Babadagli, T., and Akin, S., "Experimental and Numerical Modeling of Heavy-Oil Recovery by Electrical Heating", SPE International Thermal Operations and Heavy Oil Symposium, Calgary, Alberta, CANADA, 21-23 October 2008.
5. Acar, C., Hascakir, B., Demiral, B., Akin, S., Karaca, H., and Kartal, O.E., "Microwave Heating of Heavy Oil Reservoirs: Effect of Wettability", 150 Years of Petroleum Industry: Tradition & Challenges, Bucharest, ROMANIA, October 2007.
6. Hascakir, B., Acar, C., Demiral, B., Akin, S., Karaca, H., and Kartal, O.E., "Heavy Oil Recovery from Thin Pay Zones by Microwave Heating", International Petroleum and Natural Gas Congress & Exhibition of Turkey, Ankara, TURKEY, May,2007(Turkish).
7. Hascakir, B., Akin S. "Effect of Metallic Additives on Upgrading Heavy Oil with Microwave Heating", First World Heavy Oil Conference (WHOC), Beijing, CHINA, November 2006.
8. Hascakir, B., Dolgen, D. "Investigation of Treatment Performance of Kaolinite onto Different Wastewater Types and Treatment Methods", Fourth Mediterranean Clay Meeting, Ankara, TURKEY, September 2006.
9. Hascakir, B., Dolgen, D., "Evaluation of Treatment Efficiencies of Kaolinite for Various Wastewater Samples", Bridging Clays, Ile d'Oléron, FRANCE, June 2006.
10. Hascakir, B., "Hydraulic Potential of Turkey", 3rd Aegean Energy Symposium, Mugla, TURKEY, May 2006 (Turkish).
11. Hascakir, B., Dolgen, D., "Chemical Treatment of Wastewaters Originated From Printing Processes of Corrugated Box Industries", 6th National Environmental Engineering Conference, Istanbul, TURKEY, November 2005 (Turkish).

12. Hascakir, B., Dolgen, D., "Utilization of Clay Minerals in Wastewater Treatment: Organic Matter Removal with Kaolin (China Clay)", 12th National Clay Conference, Van, September 2005 (Turkish).

13. Hascakir, B., Demiral, B., and Akin, S., "Experimental and Numerical Analysis of Oil Shale Production Using Retort Technique", 15th International Petroleum And Natural Gas Congress And Exhibition of Turkey, Ankara, TURKEY, May 2005.

14. Dolgen, D., Hascakir, B., and Akkus, M., "Application of Clay Minerals in the Environmental Engineering: Experiments with Domestic Wastewater", Ecology Congress, Denizli, TURKEY, 2004 (Turkish).

15. Hascakir, B., Dolgen, D., and Akkus, M., "Treatability of Corrugated Paperboard Industry Wastewater by Physicochemical Treatment Methods", 9th Industrial Contamination Congress, Istanbul, TURKEY, June 2004 (Turkish).

**SUMMER SCHOOLS:**

1. "European School of English" – Paceville / MALTA, 3 weeks
2. "International Summer School of Geothermal Exploration Prospecting-Reservoir- Engineering Monitoring " Izmir / TURKEY